Agata Poświata, MSc

The interactome of AXL receptor provides insights into its biological roles and intracellular trafficking

PhD thesis
Completed in the Laboratory of Cell Biology
of the International Institute of Molecular and Cell Biology
in Warsaw

SUPERVISOR:
Prof. dr hab. Marta Miączyńska

AUXILIARY SUPERVISOR:
dr Daria Zdżalik-Bielecka

Warsaw, 2022

The research leading to these results has received funding
from the National Science Centre, Poland (2015/19/D/NZ3/03270)

Acknowledgements

First and foremost I would like to thank my supervisor Professor Marta Miączyńska for giving me the opportunity to first perform an internship and then a PhD project in the Laboratory of Cell Biology. I am grateful for the support and guidance that I received at all stages of the project as well as for the critical review of this thesis.

I would like to acknowledge my auxiliary supervisor Dr. Daria Zdżalik-Bielecka who has introduced me into the AXL project and supported throughout my studies. I am grateful for her guidance, advice and time spent on scientific discussions. In addition, I would like to thank for the critical reading of this thesis.

I would like to also thank Dr. Tomasz Prószyński, a member of my Thesis Advisory Committee, for sharing scientific ideas and reagents during the project.

Many thanks to Kamila Kozik, a member of the 'AXL team', for her invaluable input to all AXL-related projects.

I would like to thank Dr. Kamil Jastrzębski for his help during my struggles with confocal microscopy and the MotionTracking software, Dr. Krzysztof Kolmus for the GO analysis performed in R software, as well as Monika Matuszczyk for her hard work, which makes our laboratory life easier.

Additionally, I would like to thank all present and past members of the Laboratory of Cell Biology that I had a pleasure to work with, namely Magdalena Banach-Orłowska, Noga Budick-Harmelin, Jarosław Cendrowski, Purevsuren Erdenebat, Malwina Grębowicz-Maciukiewicz, Marta Jakubik, Julia Kirylczuk, Katarzyna Kuźmicz, Małgorzata Maksymowicz, Agnieszka Mamińska, Michał Mazur, Agata Mieżaniec, Ranjana Maurya, Paulina Nowak, Karolina Romaniuk, Blair Stewig, Ewelina Szymańska, Patryk Ślusarczyk, Małgorzata Świątek, Karolina Wojciechowska, Lidia Wolińska-Nizioł, Marta Wróbel and Renata Wyszyńska for their cooperation, ideas, willingness to help and a pleasant atmosphere in the laboratory.

Special thanks to my Family and Friends for their presence, moral support and motivation for further work.

Thank you!

Table of contents

Abbreviations 7

Abstract 10

Streszczenie 12

1. Introduction 14

1.1 TAM – a subfamily of receptor tyrosine kinases 14

1.2 AXL 16

1.2.1 Regulation of *AXL* expression 16

1.2.2 Characterization and activation of AXL 16

1.3 Biological roles and functions of AXL 18

1.3.1 AXL in regulation of the immune system and autoimmune diseases 18

1.3.2 AXL role in cancer 19

1.3.2.1 AXL in cancer cell proliferation, survival and tumor angiogenesis 19

1.3.2.2 AXL migration and invasion of cancer cells – the role in epithelial-to-mesenchymal transition 20

1.3.2.3 AXL activation in resistance to conventional and targeted anti-cancer therapies 21

1.3.2.4 GAS6-AXL signaling in the regulation of immune responses in the tumor microenvironment 22

1.3.2.5 AXL targeting in anti-cancer therapies 22

1.3.3 AXL in viral entry 24

1.4 Endocytosis 25

1.4.1 Endocytic routes 26

1.4.1.1 Clathrin-mediated endocytosis 26

1.4.1.2 Clathrin-independent endocytosis (CIE) 27

1.4.1.2.1 Macropinocytosis 27

1.4.1.2.2 Caveolae-dependent endocytosis 28

1.4.1.2.3 Flotillin-dependent endocytosis 28

1.4.1.2.4 CLIC/GEEC 29

1.4.1.2.5 ARF6-dependent endocytosis 29

1.4.1.2.6 FEME 29

1.4.2 The role of endocytosis in regulation of RTK-mediated signaling 30

1.4.3 The role of endocytosis in cancer 31

2. Aims of the study 33

3. Materials and Methods 34

3.1 Materials 34
3.1.1 Cell lines 34
3.1.2 Cell culture media and supplements 34
3.1.3 Bacterial strains (*Escherichia coli*) 35
3.1.4 Bacteria culture media and supplements 35
3.1.5 Primary antibodies 35
3.1.6 Secondary antibodies 36
3.1.7 Transfection reagents 37
3.1.8 Other reagents 37
3.1.9 Commercial kits 38
3.1.10 Small interfering RNA oligonucleotides (siRNA) 39
3.1.11 Guide RNA oligonucleotides (gRNAs) used for CRISPR-Cas9-mediated gene inactivation 39
3.1.12 Primers used for real-time quantitative PCR (RT-qPCR) gene expression analysis 40
3.1.13 Plasmids 40
3.1.14 Commonly used buffers 40
3.2 Methods 42
3.2.1 Cloning of DNA fragments into plasmid vectors 42
3.2.2 Preparation of chemically competent bacteria 43
3.2.3 Bacteria transformation 43
3.2.4 Cell culture, freezing and thawing 43
3.2.5 Cell seeding 44
3.2.6 Generation of stable HEK293 cell line secreting GAS6-MycHis 44
3.2.7 Purification of GAS6-MycHis from the conditioned medium 44
3.2.8 Cell stimulation with the ligands and treatment with inhibitors 45
3.2.9 Production of lentiviruses and lentiviral transduction 45
3.2.10 Generation of HEK293 cells stably expressing BirA*-HA or AXL-BirA*-HA 46
3.2.11 Generation of LN229 cells stably expressing BirA*-HA or AXL-BirA*-HA 46
3.2.12 Proximity-dependent biotin identification (BioID) 46
3.2.13 Mass spectrometry analysis 47
3.2.14 Gene Ontology (GO) analysis of mass spectrometry data 48
3.2.15 Surface biotinylation assay 48
3.2.16 Generation of LN229 cells with CRISPR-Cas9-mediated knockout of *CAV1* or *FLOT1* 49

3.2.17 Transfection of cells with siRNA 50
3.2.18 Immunofluorescence (IF) staining and image analysis 50
3.2.19 Total internal reflection fluorescence (TIRF) microscopy live-cell microscopy 51
3.2.20 Protein electrophoresis and western blot (WB) 51
3.2.21 Real-time quantitative PCR (RT-qPCR) 52
3.2.22 Statistical analysis 52
4. Results 53
4.1 Identification of AXL proximity interactome 53
4.1.1 Purification of GAS6-Myc-His 53
4.1.2 Generation of cell lines for BioID 54
4.1.3 Proximity-dependent biotin identification (BioID) 57
4.1.4 Analysis of identified AXL proximity interactors 58
4.1.5 Proteins implicated in intracellular trafficking among identified AXL proximity interactors 61
4.2 Involvement of AXL and activation of its kinase domain in the internalization of GAS6-AXL complexes 67
4.2.1 The role of GAS6 in endocytosis of AXL 67
4.2.2 AXL - a primary receptor for GAS6 required for GAS6 internalization 68
4.2.3 The crucial role of AXL tyrosine kinase domain activation in AXL internalization 71
4.3 Characterization of the kinetics of AXL endocytosis 72
4.3.1 The kinetics of GAS6-induced internalization of GAS6-AXL complexes 72
4.3.2 The kinetics of AXL internalization in comparison to the uptake of other RTKs 73
4.4 Characterization of endocytic routes mediating AXL endocytosis 76
4.4.1 Clathrin-mediated endocytosis (CME) in AXL internalization 76
4.4.2 Clathrin-independent endocytosis (CIE) in the uptake of AXL 81
4.4.2.1 The involvement of macropinocytosis in AXL internalization 81
4.4.2.2 The influence of caveolin 1 or flotillin 1 depletion on AXL endocytosis 82
4.4.2.3 The contribution of the CLIC/GEEC pathway to GAS6-AXL endocytic uptake 83
4.4.2.4 The impact of downregulation of ARF6 for the uptake of GAS6-AXL complexes 85
4.5 The fate of internalized AXL receptor 86
4.5.1 Limited colocalization between AXL and EEA1 86
4.5.2 The colocalization between AXL, GAS6 or EGF with LAMP1 87
4.5.3 The protein level of AXL upon GAS6 stimulation 88

4.5.4 Prolonged phosphorylation of AKT upon GAS6-mediated activation of AXL.....89
5. Discussion.....91
5.1 BioID as a tool for characterization of biological processes regulated by AXL 92
5.2 Multitude of routes of GAS6-induced AXL internalization 94
5.3 The role of endocytosis in the regulation of the fate of internalized receptors.....96
5.4 The role of GAS6 in the activation of TAM receptors 99
5.5 Consequences of AXL endocytosis – the role in viral entry 99
6. Conclusions 101
7. Future prospects.....102
8. Literature 105
9. Publications by Agata Poświata 126
10. Supplementary materials 127

Abbreviations

AML	acute myeloid leukemia
ARF6	ADP-ribosylation factor 6
BAR	Bin/Amphiphysin/Rvs domain
BCL2	B-cell lymphoma 2
BioID	proximity-dependent biotin identification
CAV1	caveolin 1
CCV	clathrin-coated vesicle
CDR	circular dorsal ruffle
CHC	clathrin heavy chain
CIE	clathrin-independent endocytosis
CLC	clathrin light chain
CLIC/GEEC	clathrin-independent carriers/glycosylphosphatidylinositol-anchored proteins (GPI-AP)-enriched compartments
CME	clathrin-mediated endocytosis
CTxB	cholera toxin B subunit
DCs	dendritic cells
DMSO	dimethyl sulfoxide
ECM	extracellular matrix
EEA1	early endosome antigen 1
EGF	epidermal growth factor
EGFR	epidermal growth factor receptor
EMT	epithelial-to-mesenchymal transition
EPS15	epidermal growth factor receptor pathway substrate 15
EPS15L1	epidermal growth factor receptor pathway substrate 15 like 1
ERK	extracellular signal-regulated kinase
FAs	focal adhesions
FCHO	F-BAR domain-containing Fer/Cip4 homology domain-only protein
FEME	fast endophilin-mediated endocytosis
FGF	fibroblast growth factor
FGFR	fibroblast growth factor receptor
FLOT1	flotillin 1
FNIII	fibronectin type III
GAS6	growth arrest specific protein 6
GLA	glutamic acid

GO	Gene Ontology
GPCRs	G protein-coupled receptors
GPI-AP	glycosylphosphatidylinositol-anchored protein
GRAF1	GTPase regulator associated with focal adhesion kinase-1
gRNA	single-guide RNA
HEK293	human embryonic kidney 293 cells
HGF	hepatocyte growth factor
HNSCC	head and neck squamous cell carcinoma
IF	immunofluorescence
IFN	interferon
Ig	immunoglobulin
IGF1R	insulin-like growth factor 1 receptor
IL	interleukin
ITGβ1	integrin β1
KO	knockout
LAMP1	lysosomal-associated membrane protein 1
LB	Luria-Bertani broth
LDL	low-density lipoprotein
LG	laminin G
mAb	monoclonal antibodies
MAPK	mitogen-activated protein kinase
MET	mesenchymal epithelial transition factor receptor
MHC	major histocompatibility complex
MW	molecular weight
NF-κB	nuclear factor kappa-light-chain-enhancer of activated B cells
NGF	nerve growth factor
NK	natural killer cells
ns	non-significant
NSCLC	non-small cell lung cancer
PBS	phosphate buffered saline
PCR	polymerase chain reaction
PDGF	platelet-derived growth factor
PDGFR	platelet-derived growth factor receptor
PD-L1	programmed cell death ligand 1
PI3K	phosphoinositide 3-kinase

PICALM	phosphatidylinositol-binding clathrin assembly protein
PLC-γ	phospholipase C-γ
PM	plasma membrane
PROS1	protein S
PRs	peripheral ruffles
PtdSer	phosphatidylserine
RPE	retinal pigment epithelial cells
RT	room temperature
RT-qPCR	real-time quantitative PCR
RTK	receptor tyrosine kinase
SEM	standard error of the mean
siRNA	small interfering RNA
SNX	sorting nexin
SOCS	suppressor of cytokine signaling
STAT1	signal transducer and activator of transcription 1
Tf	transferrin
TGF-β	transforming growth factor-β
TIRF	total internal reflection fluorescence
TLR	Toll-like receptor
TNBC	triple negative breast cancer
TNF	tumor necrosis factor
TrkA	tropomyosin receptor kinase A
UNTR	untransfected
VEGFR	vascular growth factor receptor
WB	western blot
WT	wild type

Abstract

AXL is a receptor tyrosine kinase (RTK) which together with TYRO3 and MER constitutes the TAM receptor subfamily. TAMs participate in the regulation of the immune system, phagocytic clearance of apoptotic cells and tumorigenesis. AXL and its ligand GAS6 were shown to be overexpressed in many types of human cancers, which correlated with increased tumor progression, metastasis and acquired resistance to anti-cancer therapies. In addition, AXL acts as an important receptor for the cellular entry of viruses, including ZIKA and SARS-CoV-2. Therefore, AXL is a promising therapeutic target, both for cancer treatment and anti-viral therapy, and one of its inhibitors is currently being tested in clinical trials for the treatment of cancer and COVID-19.

Endocytosis facilitates uptake of fragments of the plasma membrane (PM) together with the extracellular content via endosomes. This process plays a crucial role in the regulation of RTK functions, since it may lead to degradation of RTKs in lysosomes or their recycling to the PM, which terminates or sustains RTK-mediated signaling, respectively.

Despite numerous studies reporting the involvement of AXL in carcinogenesis as well as virus infections, the molecular mechanisms underlying these processes have been poorly characterized and AXL-binding proteins remained practically unknown. Additionally, none of TAM receptors have been studied so far with respect to their endocytosis. Thus, the aim of this thesis was the identification of AXL-interacting partners and the characterization of AXL endocytosis.

To discover the interactome of AXL, the proximity-dependent biotin identification (BioID) was used. Its results showed that AXL interacted with proteins implicated in actin-related processes, axonogenesis, cell junction organization, signaling and endocytosis. The latter category indicated that intracellular trafficking is an important regulator of AXL function. Therefore, the mechanisms of AXL internalization have been examined in detail. It was demonstrated that, upon GAS6 stimulation, GAS6-AXL complexes were rapidly internalized into cells, and this uptake operated via multiple endocytic routes, both clathrin-mediated (CME) and clathrin-independent endocytosis (CIE). Interestingly, blocking a single endocytic route, except for clathrin-independent carriers/GPI-AP-enriched compartments (CLIC/GEEC) and ADP-ribosylation factor 6 (ARF6)-dependent endocytosis, was not sufficient to reduce endocytosis of GAS6-AXL complexes. In contrast, the inhibition of AXL kinase activity completely blocked internalization of the ligated receptor. These findings offer a mechanistic explanation for previous studies showing that AXL inhibitor treatment decreases AXL-mediated viral infections. They further provide a rationale for using pharmacological inhibition of AXL in anti-viral therapies.

Subsequent analyses concerning the kinetics of AXL internalization revealed that this process operated faster than the uptake of other RTKs, such as epidermal growth factor (EGFR) and platelet-derived growth factor receptor β (PDGFRβ). Moreover, in contrast to ligated EGFR, endocytosis of AXL did not lead to receptor degradation but most probably to its recycling back to the PM. The latter was associated with the prolonged phosphorylation of AXL and the sustained activation of its downstream effector AKT, which may contribute to AXL-driven cancer cell migration and invasion. Finally, the presented results revealed that depletion of AXL was sufficient to block GAS6 internalization, which supports a notion previously reported by our laboratory that AXL is a primary receptor for GAS6.

Altogether, this study provides the first comprehensive analysis of the AXL interactome as well as a detailed characterization of endocytosis of AXL, the first TAM receptor studied in this respect. The results presented here shed light on the molecular mechanisms regulating AXL and AXL-mediated processes on the cellular level that significantly extends our current understanding of the role of AXL in cancer progression and viral entry.

Streszczenie

AXL jest receptorową kinazą tyrozynową (RTK), która wraz z białkami TYRO3 i MER należy do rodziny TAM. Kinazy TAM uczestniczą w regulacji odpowiedzi układu odpornościowego, usuwaniu komórek apoptotycznych oraz biorą udział w nowotworzeniu. Badania wykazały, że kinaza AXL i jej ligand, białko GAS6, ulegają nadmiernej ekspresji w komórkach nowotworowych, co koreluje ze zwiększoną inwazyjnością, powstawaniem przerzutów oraz opornością nowotworów na terapie. Ponadto, AXL pośredniczy również w procesie wnikania wirusów do komórek, np. wirusa ZIKA oraz SARS-CoV-2. Dlatego też AXL stanowi potencjalny cel terapeutyczny, a jeden z inhibitorów jej aktywności kinazowej jest testowany w badaniach klinicznych pod kątem zastosowania w leczeniu nowotworów oraz COVID-19.

Endocytoza jest procesem, w którym fragmenty błony komórkowej wraz ze składnikami zewnątrzkomórkowymi są pobierane do komórek za pomocą endosomów. W przypadku RTK, proces ten pełni kluczową rolę w przekazywaniu sygnału, regulując degradację tych białek w lizosomach lub ich recykling do błony komórkowej.

Pomimo wielu doniesień naukowych wskazujących na ważną rolę AXL w powstawaniu nowotworów oraz wnikaniu wirusów do komórek, molekularne mechanizmy leżące u podstaw tych procesów ani białka oddziałujące z AXL nie były dobrze poznane. Co więcej, żadna kinaza z rodziny TAM nie była dotychczas badana pod kątem endocytozy. Dlatego też, celem niniejszej rozprawy doktorskiej było zidentyfikowanie białek oddziałujących z AXL oraz scharakteryzowanie mechanizmów endocytozy tej kinazy.

Wykorzystując metodę BioID (ang. proximity-dependent biotin identification) zidentyfikowano białka wchodzące w interakcje z AXL. Uzyskane wyniki wykazały, że AXL oddziałuje m. in. z białkami regulującymi cytoszkielet aktynowy, aksonogenezę, organizację połączeń międzykomórkowych i przekazywanie sygnału. Ponadto, zidentyfikowano wiele białek zaangażowanych w endocytozę, co wskazywało na kluczową rolę tego procesu w regulacji funkcji AXL. Dlatego też w kolejnych etapach projektu szczegółowo scharakteryzowano endocytozę AXL. Wykazano, że stymulacja komórek ligandem GAS6 powoduje szybkie pobieranie kompleksów GAS6-AXL do komórek, które zachodzi na drodze endocytozy zależnej oraz niezależnej od klatryny. Co więcej, pokazano, że spośród badanych ścieżek internalizacji, jedynie zablokowanie ścieżki CLIC/GEEC (ang. clathrin-independent carriers/GPI-AP-enriched compartments) oraz ścieżki zależnej od białka ARF6 powodowało zmniejszenie pobierania kompleksów GAS6-AXL, a całkowite zahamowanie endocytozy GAS6-AXL zaobserwowano wyłącznie po zablokowaniu aktywności domeny kinazowej AXL. Wyniki te stanowią mechanistyczne wyjaśnienie wcześniejszych badań pokazujących,

że stosowanie inhibitorów AXL hamuje wnikanie wirusów do komórek, co tym samym uzasadnia wykorzystanie tych inhibitorów w terapiach przeciwwirusowych.

W kolejnym etapie, analiza kinetyki endocytozy AXL wykazała, że w porównaniu do receptorów EGFR i PDGFRβ internalizacja AXL zachodzi szybciej. Stwierdzono także, że w przeciwieństwie do EGFR, pobieranie AXL nie prowadzi do degradacji tej kinazy, a najprawdopodobniej do jej recyklingu do błony komórkowej, co koreluje z długotrwałą fosforylacją i aktywacją AXL oraz białka AKT. Ta przedłużona aktywacja sygnalizacji może odgrywać rolę w zależnej od AXL migracji oraz inwazji komórek nowotworowych. Dodatkowo, przedstawione wyniki potwierdziły wcześniejsze obserwacje wskazujące, że GAS6 aktywuje przede wszystkim receptor AXL, a nie inne kinazy TAM.

Podsumowując, w niniejszej pracy przeprowadzono pierwszą kompleksową analizę białek oddziałujących z AXL oraz przedstawiono charakterystykę endocytozy AXL jako pierwszej kinazy z rodziny TAM badanej pod tym kątem. Zaprezentowane wyniki poszerzają wiedzę na temat molekularnych mechanizmów regulujących AXL i procesów regulowanych przez tę kinazę na poziomie komórkowym oraz przyczyniają się do lepszego zrozumienia roli AXL w progresji chorób nowotworowych i we wnikaniu wirusów do komórek.

1. Introduction

1.1 TAM – a subfamily of receptor tyrosine kinases

Receptor tyrosine kinases (RTKs) are plasma membrane receptors that transmit signals between cells and from an extracellular environment to cells. They bind and respond to ligands, which causes dimerization of receptors and activation of their kinase domains initiating signal transduction [1]. RTKs function as important regulators of various cellular processes such as cell growth, proliferation, differentiation or migration. Thus, their altered expression or mutations are correlated with many pathological conditions, including cancer [1].

AXL, TYRO3 and MER comprise the TAM receptor subfamily of RTKs. This family of receptors was one of the latest to appear in the evolution as the first TAM-like protein was identified in the genomes of prevertebrate urochordates, such as *Ciona intestinalis* [2, 3]. In contrast to other RTKs, such as epidermal (EGFR), fibroblast (FGFR) growth factor receptors or erythropoietin-producing human hepatocellular (Eph) receptors subfamilies, there are no TAM representatives in either *Drosophila melanogaster* or *Caenorhabditis elegans* genomes [4, 5]. In humans, TAM receptors are ubiquitously expressed in various cell types including cells of the immune, nervous, vascular and reproductive systems [6]. They participate in regulation of the immune system and tissue homeostasis through their role in phagocytic clearance of apoptotic cells. However, TAMs also play a role in cancer progression, promoting cancer cell survival and motility [7].

All three TAMs display a similar structure composed of an extracellular part containing two immunoglobulin (Ig)-like domains implicated in the ligand binding and two fibronectin type III (FNIII) repeats, followed by a single helix transmembrane region. The C-terminal fragment consists of a cytoplasmic tyrosine kinase domain containing a signature KW(I/L)A(I/L)ES sequence that distinguishes TAM receptors from other RTKs (Fig. 1.1A) [7, 8].

Up to date there are five known ligands activating TAM receptors: anticoagulant protein S (PROS1), growth arrest specific protein 6 (GAS6) [9], Tubby, Tubby-like protein 1 (TULP-1) [10] and galectin-3 [11]. However, the latter three proteins were poorly characterized in the context of TAMs activation and were only shown to modulate the function of MER [10, 11]. In turn, the role of PROS1 and GAS6 in activation of TAM receptors was extensively studied. Specifically, it was shown that PROS1 activates TYRO3 and MER, whereas GAS6 is able to bind all three TAMs with the highest affinity for AXL [12-14]. Both ligands are secreted glycoproteins that require vitamin K-dependent γ-

carboxylation to fully activate their cognate receptors [12, 13]. GAS6 and PROS1 share about 40% sequence identity and display a similar structural organization [9, 15]. Both proteins consist of an N-terminal glutamic acid (GLA)-rich domain, followed by four epidermal growth factor (EGF)-like domains and a C-terminal sex hormone-binding globulin (SHBG) domain composed of two laminin G (LG)-like domains (Fig. 1.1B) [14].

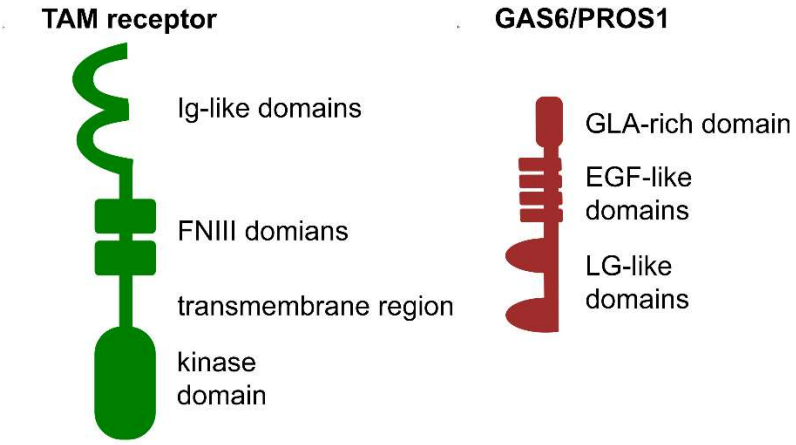

Fig. 1.1 Schematic representation of the domain composition of TAMs (TYRO3, AXL, MER) and their ligands (GAS6 and PROS1)
A TYRO3, AXL and MER consist of two N-terminal immunoglobulin (Ig)-like domains, two fibronectin type III (FNIII) repeats, a transmembrane domain and a C-terminal intracellular kinase domain. **B** GAS6 and PROS1 contain an N-terminal glutamic acid (GLA)-rich domain, four epidermal growth factor (EGF)-like domains and two laminin G (LG)-like domains at the C-terminus.

The activation of a TAM receptor is mediated by the interaction between the LG-like domains of the ligand and the Ig-like domains of the receptor (Fig 1.1) [7, 14]. In turn, the N-terminal, γ-carboxylated GLA-rich domains of the TAM ligands mediate binding to phosphatidylserine (PtdSer). This phospholipid is a component of an inner layer of the plasma membrane (PM) in eukaryotic cells, and becomes exposed on the cell surface upon apoptosis [16]. Extracellular PtdSer serves as a potent 'eat-me' signal, by which dead cells are recognized by phagocytes expressing TAM receptors. Therefore, GAS6 and PROS1 serve as bridging molecules linking TAM receptors on phagocytic cells and PtdSer exposed on apoptotic cells, which facilitates TAM-mediated efferocytosis - the phagocytic clearance of apoptotic cells [16-19]. Additionally, TAMs play an important role in the modulation of innate immune response by suppressing production of pro-inflammatory cytokines (e.g. interleukin-6 [IL-6], IL-12, tumor necrosis factor [TNF], type I interferons [IFNs]), promoting production of anti-inflammatory cytokines (e.g. IL-10, transforming growth factor-β [TGF-β], hepatocyte growth factor [HGF], IL-4) and regulating differentiation and maturation of natural killer (NK) cells [6, 13, 20, 21]. Overexpression and activation of TAMs was also reported in a variety of human cancers. However, they do not display an oncogenic potential themselves but rather promote survival, chemoresistance and motility of cancer cells [12, 13].

1.2 AXL

The gene encoding AXL is located on chromosome 19q13.2 and was initially discovered in 1988 as a transforming gene in chronic myelogenous leukemia (CML) [22]. Due to its transforming capacity in NIH3T3 cells, AXL was named after the Greek word 'anexelekto' which means “uncontrolled”, however in the literature a few alternative names exist, such as Ark, Tyro7 or Ufo [23, 24].

1.2.1 Regulation of *AXL* expression

AXL is expressed relatively late in embryogenesis and studies in mice showed that the initial expression of *AXL* appeared 12.5 days post fertilization [25, 26]. Additionally, in contrast to many RTKs, TAM receptors are dispensable for the embryonic development, as triple knockout (KO) mice of all three TAMs are viable [27]. However, they develop a severe lymphoproliferative disorder accompanied by broad-spectrum autoimmunity and abnormalities in the nervous and reproductive systems [28].

AXL gene expression is regulated on multiple levels. Several transcription factor complexes were described to promote the expression of AXL gene: Fos and Jun – components of activator protein 1 (AP1), specificity protein 1 and 3 (SP1/SP3), Yes-associated protein (YAP)/ transcriptional coactivator with PDZ-binding motif (TAZ)/TEA domain family member (TEAD), hypoxia inducible factor (HIF) and myeloid zinc finger 1 protein (MZF-1) [24, 29]. On the other hand, *AXL* transcription can be negatively regulated via microRNAs, miR-34a and miR-199a/b, which bind to the 3’-UTR region of the *AXL* gene [24, 29]. Additionally, AXL mRNA synthesis depends on the epigenetic changes in histone acetylation and histone/DNA methylation [24].

1.2.2 Characterization and activation of AXL

The full length AXL consists of 894 amino acids and encodes a protein of predicted molecular weight (MW) around 98 kDa, however the actual MW varies between 100-140 kDa due to posttranslational modifications including glycosylation, phosphorylation and ubiquitination [23]. As for typical RTKs, binding of the ligand, GAS6, causes dimerization of the receptor and autophosphorylation of tyrosine residues within its kinase domain. Six tyrosine phosphorylation sites have been identified in the AXL kinase domain. Among them three are considered as putative autophosphorylation sites: Tyr698, Tyr702, Tyr703, required for activation of the receptor. The other three (Tyr779, Tyr821, Tyr866) are docking sites for downstream adaptor proteins involved in the activation of various signaling pathways such as phosphoinositide 3-kinase (PI3K)/AKT, phospholipase C-γ (PLC-γ) and mitogen-activated

protein kinase (MAPK)/extracellular signal-regulated kinases (ERK), leading to various cellular responses such as migration, proliferation or cell survival (Fig. 1.2) [26, 29].

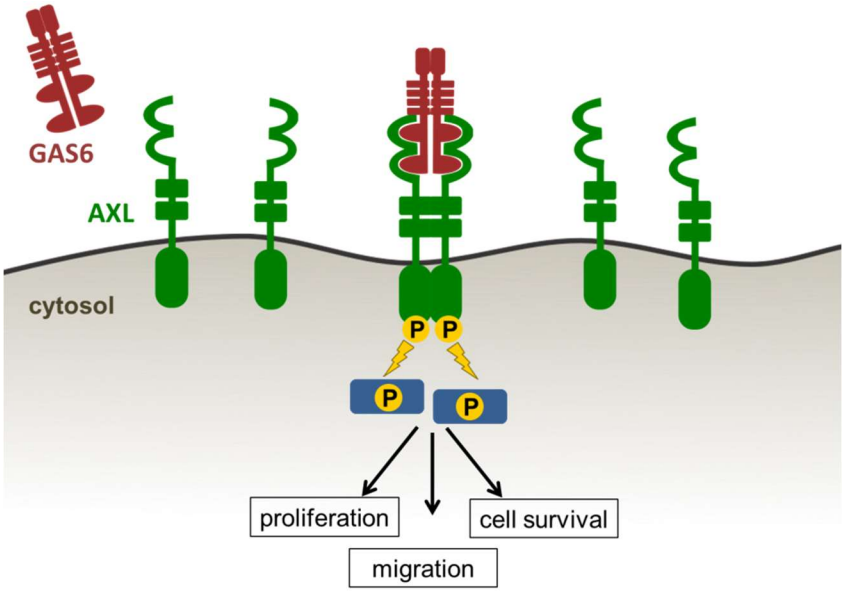

Fig. 1.2 Schematic representation of GAS6-induced phosphorylation of AXL and activation of its downstream effectors
GAS6 binding promotes dimerization of AXL receptor which promotes autophosphorylation of tyrosine residues within its kinase domain and activation of various downstream signaling pathways that promote proliferation, migration and cell survival.

GAS6 is the only ligand with proven activity for AXL, and the crystal structure of a minimal AXL-GAS6 complex has been determined with 3.3Å resolution. The study revealed that AXL-GAS6 complex displays 2:2 stoichiometry, in which the two Ig-like domains of the AXL extracellular domain are crosslinked by the first LG-like domain of GAS6, with no direct AXL-AXL or GAS6-GAS6 contacts observed [30].

AXL activation can also occur by ligand-independent mechanisms [24]. Firstly, AXL overexpression leads to homophilic binding of extracellular domains on opposite cells or ligand-independent homodimerization [31, 32]. Secondly, AXL may be activated in response to hydrogen peroxide which was also shown to prevent its ubiquitination and subsequent degradation in lysosomes [26, 33, 34]. Moreover, cross-phosphorylation and heterodimerization between AXL and other TAMs [35, 36] as well as non-TAM RTKs such as FGFR [37], EGFR [38, 39] and mesenchymal epithelial transition factor receptor (MET) [39, 40] have been postulated.

1.3 Biological roles and functions of AXL

1.3.1 AXL in regulation of the immune system and autoimmune diseases

Together with other TAMs, AXL was proposed to play a role in regulation of the immune system and maintenance of tissue homeostasis, by modulation of inflammation and efferocytosis [6]. Efferocytosis is predominantly mediated by macrophages or dendritic cells (DCs), considered as professional phagocytes. However, in a tissue-specific context, phagocytic clearance of apoptotic cells can be also facilitated by other cells, such as Sertoli cells in testis or retinal pigment epithelial (RPE) cells in eyes [41]. Importantly, the lack of TAM receptors in Sertoli cells resulted in impaired spermatogenesis and male infertility in mice [27], whereas KO of MER in RPE cells led to degradation of photoreceptors which resulted in blindness [42, 43].

Despite the fact that the role of TAMs in efferocytosis was predominantly attributed to MER, the participation of AXL in this processes was also described [44, 45]. Studies by Seitz *et al.* showed that all three TAMs participate in macrophage-mediated phagocytosis *in vitro*, albeit to different degrees [36]. In line with previous observations, downregulation of MER completely inhibited this process, however depletion of AXL (and/or TYRO3) caused >50% decrease, indicating that these receptors also play a role [17, 36]. In contrast, MER was dispensable for apoptotic cell clearance mediated by DCs, which relied predominantly on AXL and TYRO3 [36]. These differences may result from different expression patterns of *MER* and *AXL* in these cell types, since Zagórska *et al.* showed that *MER* was more prominently expressed in macrophages, whereas expression of *AXL* was higher in DCs [44].

In DCs, AXL was additionally shown to act as a suppressor of inflammatory response mediated by Toll-like receptors (TLRs). In response to a pathogen (an immune stimulus) TLRs promoted a signaling cascade involving activation of interferon-α/β receptor (IFNAR) and signal transducer and activator of transcription 1 (STAT1), which stimulated cytokine production and inflammation, as well as induced expression of *AXL* mRNA. In turn, AXL activation promoted expression of genes encoding suppressor of cytokine signaling (SOCS) proteins, which inhibit TLR-mediated signaling and cytokine secretion, thus inhibiting an immune response [20].

AXL, as the other TAMs, was also described to contribute to NK cell maturation and differentiation. These bone marrow-derived lymphocytes have an important role in the innate immune system providing a rapid response to pathogens and tumors. NK cells from AXL KO mice displayed up to 90% impairment of their cytotoxic activity, in comparison to cells isolated from wild type animals [21]. Additionally, blocking GAS6-AXL signaling

diminished the number of NK cells derived from $CD34^+$ hematopoietic progenitor cells and downregulated IFN-γ production [46].

Taken together, AXL and other TAM receptors play very important roles in maintaining tissue homeostasis and inhibition of the innate immune system. Thus, their loss leads to various types of chronic inflammatory pathologies and autoimmune responses [45]. These diseases include rheumatoid arthritis (RA) [47], systemic lupus erythematosus (SLE) [48], sepsis [49, 50] or multiple sclerosis (MS) [51], among others. Therefore, modulation of AXL signaling may serve as a potential therapeutic strategy for multiple immune diseases.

1.3.2 AXL role in cancer

Despite its involvement in variety of inflammatory pathologies, AXL is predominantly studied in the context of tumorigenesis. Its overexpression and signaling were correlated with pathogenesis of many types of human cancers, including gliomas, melanomas, lung, colorectal, ovarian, pancreatic or breast cancer, and were shown to associate with poorer prognosis and increased invasiveness [24]. In addition, GAS6-mediated AXL activation was described to promote tumor progression via multiple mechanisms, such as increased proliferation and survival of cancer cells, epithelial-to-mesenchymal transition (EMT), metastasis and resistance to anti-cancer therapies, which altogether confirm its oncogenic potential (Fig. 1.3) [13, 24, 29, 52].

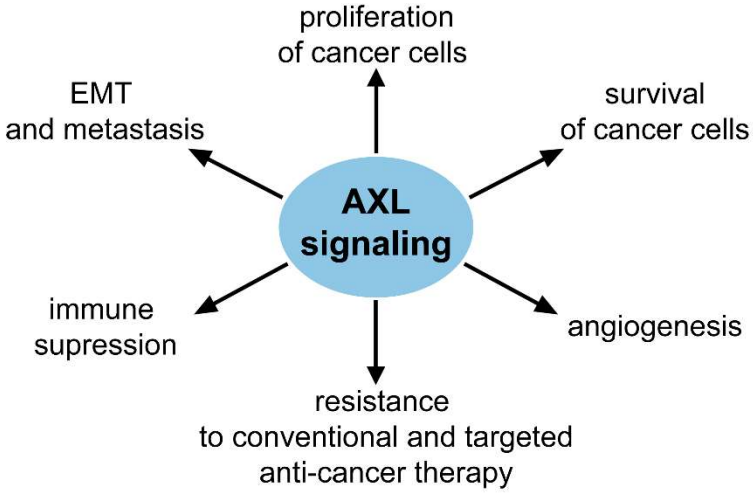

Fig. 1.3 The role of GAS6-AXL signaling in tumor growth
AXL activation promotes proliferation and survival of cancer cells, supports formation of blood vessels in a growing tumor, suppresses anti-cancer immune responses, promotes epithelial-to-mesenchymal transition (EMT) and metastasis and confers resistance to conventional and targeted anti-cancer therapies. Modified after Rankin *et al.* [52].

1.3.2.1 AXL in cancer cell proliferation, survival and tumor angiogenesis

GAS6-AXL was shown to activate various signaling pathways promoting cell proliferation and survival, such as MAPK/ERK, JAK/STAT or PI3K/AKT [24, 29]. In line with that, AXL was reported to promote tumor growth, and its downregulation reduced

proliferative potential of glioblastoma [53], osteosarcoma [54] or prostate [55, 56] cancer cells. Moreover, GAS6-AXL signaling contributed to the activation of an anti-apoptotic response. GAS6-AXL-dependent AKT activation was shown to facilitate nuclear translocation of nuclear factor kappa-light-chain-enhancer of activated B cells (NF-κB), which in turn induced the expression of anti-apoptotic markers such as survivin, B-cell lymphoma 2 (BCL2) and B-cell lymphoma-extra large (BCL-XL). Simultaneously, the activity of pro-apoptotic proteins such as BCL2-associated agonist of cell death (BAD) or caspase-3 was reduced, which altogether prevented apoptosis of cancer cells [24, 57-59]. Consequently, AXL inhibition induced cancer cell apoptosis, through the inhibition of PI3K/AKT as well as MAPK/ERK pathways [60, 61]. Additionally, AXL was shown to support an immunosuppressive phenotype in the tumor immune microenvironment, therefore allowing immune evasion and promoting tumorigenesis [62].

Increased proliferation of cancer cells resulting in growth of a tumor mass requires formation of new blood vessels, in the process called angiogenesis, to provide oxygen and nutrients essential for tumor cell growth [63]. Angiogenesis contributes to expansion of a tumor and several studies suggested that AXL signaling, together with vascular growth factor (VEGF), fibroblast growth factor (FGF) or platelet-derived growth factor (PDGF) receptors plays a role in this process [24]. Autocrine or paracrine GAS6-mediated AXL activation was shown to promote proliferation and migration of vascular smooth muscle cells [64]. Similarly, activation of GAS6-AXL signaling in human umbilical vein endothelial cells (HUVECs) promoted growth and migration of these cells, as well as tube formation in the co-culture of HUVECs and pulmonary artery smooth muscle cells, which was inhibited upon AXL downregulation [65].

1.3.2.2 AXL migration and invasion of cancer cells – the role in epithelial-to-mesenchymal transition

Several studies, both *in vitro* and *in vivo*, pointed towards participation of AXL signaling in tumor invasiveness and metastasis, and AXL expression was shown to increase during cancer progression [24, 29, 52]. It was reported that an elevated AXL expression is crucial for all steps of metastatic process in highly invasive breast cancer cells including intravasation, extravasation and growth of metastatic lesions in distant tissues [66].

To migrate and invade, cancer cells need to detach from a tumor mass and degrade extracellular matrix (ECM) components. These processes are connected with the loss of an epithelial phenotype and acquisition of mesenchymal properties by cancer cells in a process called epithelial-to-mesenchymal transition (EMT) [67, 68]. EMT requires intense phenotypic changes in cells reflected by reduced levels of epithelial markers, such as E-cadherin or

cytokeratins, and induced production of mesenchymal proteins, e.g. N-cadherin or vimentin [24, 68], along with profound cytoskeleton rearrangements [69].

Multiple studies reported the involvement of AXL in EMT, however its specific role in this process is still under debate as it is not fully established whether AXL acts as a regulator or effector of EMT [52]. It was shown that TGF-β-induced EMT resulted in upregulated AXL protein level which was important for maintenance of a mesenchymal phenotype of cells and supported their migratory and invasive properties [66, 70, 71]. On the other hand, AXL was also reported to act as an EMT inducer, since it regulated expression of genes encoding EMT-related transcription factors such as SNAI1/2, TWIST1/2 or SLUG [72, 73]. Importantly, AXL downregulation was sufficient to reverse EMT and reduced invasive properties of cancer cells *in vitro* and metastasis *in vivo* [66, 71, 72, 74, 75].

1.3.2.3 AXL activation in resistance to conventional and targeted anti-cancer therapies

Drug resistance is one of major obstacles in the cancer treatment, which leads to disease recurrence and poor patient survival. Several examples of AXL association with this process were described in case of both conventional, as well as targeted anti-cancer therapy [24, 52]. For instance, AXL-mediated chemotherapy resistance was reported in acute myeloid leukemia (AML) [59], esophageal [76], triple negative breast (TNBC) and non-small cell lung cancer (NSCLC) [70], whereas radiotherapy resistance occurred for head and neck squamous cell carcinoma (HNSCC) [77]. In case of targeted therapies, AXL upregulation was observed in cancer cells resistant to inhibitors of EGFR [78, 79], BRAF [80], PI3Kα [81] and ALK [82].

In most cases, one of the hallmarks of AXL-associated drug resistance is AXL overexpression linked with an EMT-like phenotype, and numerous studies showed that cells which had undergone EMT revealed a higher degree of resistance [67, 68]. Thus, AXL-mediated mesenchymal phenotype of cancer cells followed by their decreased proliferation can altogether explain an observed resistance to commonly used anti-proliferative drugs [29, 67, 68, 83]. Another example of a mechanism underlying AXL-induced drug resistance includes the crosstalk between AXL and other RTKs, such as EGFR or HER2 [66, 81]. In HNSCC cells resistant to PI3Kα inhibition, heterodimerization of AXL and EGFR activated PLCα/ protein kinase C (PKC)/ mammalian target of rapamycin (mTOR) signaling pathway that further supported tumor growth [81]. Consequently, AXL downregulation reversed a pro-survival phenotype and resensitized cancer cells to therapy [81].

1.3.2.4 GAS6-AXL signaling in the regulation of immune responses in the tumor microenvironment

Immune evasion is one of the crucial steps of cancer progression, and cancer cells exploit several mechanisms to avoid activation of the immune system in the tumor microenvironment. Several studies showed that a tumor immunosuppressive phenotype was correlated with AXL expression and signaling, both in tumor as well as stromal cells [62].

AXL-mediated immunosuppressive phenotype is maintained by reduced secretion of pro-inflammatory cytokines and induced production of immunosuppressive cytokines and SOCS proteins, which altogether dampen inflammation and tissue damage, therefore promoting cancer cell growth and proliferation [20, 62]. Additionally, to avoid immune system activation, cancer cells express immune checkpoint molecules, e.g. programmed cell death ligand 1 (PD-L1), which was also shown to correlate with AXL expression [84, 85]. Binding of PD-L1 by its cognate receptor PD-1 on the surface of T-cells abolished T-cell activation and prevented immune-mediated cancer cell death [86]. Importantly, AXL depletion in TNBC cell line MDA-MB-231 reduced the expression and PM level of PD-L1 [85] and similar results were observed in lung adenocarcinoma cell lines treated with AXL inhibitor R428 [87].

1.3.2.5 AXL targeting in anti-cancer therapies

Since AXL contributes to tumor growth via multiple mechanisms, its targeting is a promising strategy to develop anti-cancer therapy [24, 88]. AXL depletion or inhibition was described to suppress migration and invasion of cancer cells and promote their apoptosis [89, 90]. Therefore, several strategies dampening the GAS6-AXL system are tested in preclinical and clinical studies including tyrosine kinase inhibitors, non-tyrosine kinase inhibitors, monoclonal anti-AXL antibodies, GAS6-neutralizing antibodies, soluble receptors and nucleotide aptamers (Fig. 1.4) [24, 88].

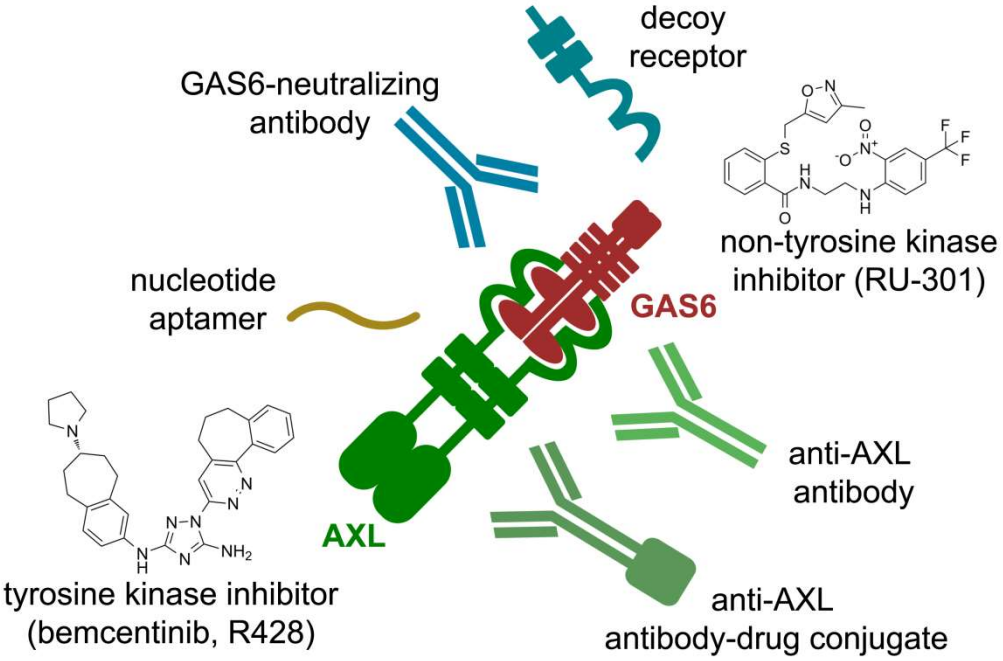

Fig. 1.4 Different approaches to target GAS6-AXL signaling
Examples of strategies dampening GAS6-AXL signaling from preclinical and clinical studies described in detail in chapter 1.3.2.5. Chemical structures of RU-301 and R428 from https://www.medchemexpress.com/. Scheme modified from Di Stasi *et al.* [88].

Promising preclinical results of small molecule AXL tyrosine kinase domain inhibitors in cancer treatment allowed their implementation in clinical trials [91-95]. Besides multikinase inhibitors targeting AXL e.g. bosutinib, crizotinib, gilteritinib, a selective AXL inhibitor bemcentinib (R428) is currently being tested in the I/II phase of several clinical trials against glioblastoma (ClinicalTrials.gov identifier: NCT03965494), melanoma (NCT02872259), NSCLC (NCT02424617, NCT02922777), AML (NCT02488408) and TNBC (NCT03184558) [24, 88, 96, 97].

Preventing GAS6-AXL binding serves as an alternative strategy to abolish tumorigenic AXL signaling, and multiple approaches have been developed to block GAS6-induced AXL activation [24, 88]. Developing non-tyrosine kinase inhibitors targeting AXL extracellular domain is one example. Studies by Kimani *et al.* showed that small molecule inhibitors, RU-301 and RU-302, blocked binding between an LG-like domain of GAS6 and an Ig-like domain of AXL, which in turn abolished GAS6-induced cancer cell motility and suppressed lung cancer tumor growth in a mouse xenograft model [98]. Another approach includes targeting AXL extracellular region by nucleotide aptamers, which are short, structured, single-stranded RNAs or DNAs able to bind their targets. The RNA aptamer GL21.T and its corresponding DNA aptamer were shown to efficiently decrease AXL signaling *in vitro* and *in vivo*, preventing tumor growth in NSCLC and ovarian cancer models [99, 100]. Additionally, removing GAS6 by neutralizing proteins, such as anti-GAS6

antibodies or a decoy receptor containing AXL extracellular domain, inhibited tumor growth of pancreatic adenocarcinoma or ovarian and breast cancer, respectively [101, 102].

Another promising AXL-targeting strategy is based on the generation of anti-AXL monoclonal antibodies (mAb), which prevent GAS6-AXL signaling. Anti-cancer efficacy was shown for anti-AXL YW327.6S2, DAXL-88 or 20G7-D9 antibodies, among others, and was validated in mouse and patient-derived xenograft models [103-105]. In addition, very efficient anti-cancer activity was reported for antibody-drug conjugate targeting AXL, AXL107-MMAE (enapotamab vedotin, AXL107 IgG1 mAb conjugated with microtubule-disrupting agent monomethyl auristatin E) in the NSCLC model [106]. AXL107-MMAE is currently being tested in clinical trials against ovarian, cervical, endometrial, thyroid cancer, NSCLC, melanoma and sarcoma (NCT02988817) [88, 96].

1.3.3 AXL in viral entry

A growing body of evidence reveals that GAS6-AXL complexes mediate entry of several viruses e.g. dengue virus [107], Lassa virus [108], Ebola virus [109], Zika virus [110] and SARS-CoV-2 [111]. In the process called “apoptotic mimicry”, enveloped viruses were shown to expose PtdSer on their surface (similarly to apoptotic cells) and bind AXL using GAS6 as a bridging molecule, which promoted viral entry [107, 112, 113]. Additionally, AXL signaling during viral infection attenuated innate immune and inflammatory responses, which facilitated viral infection and immune evasion. Specifically, virus binding promoted activation of AXL signaling and phosphorylation of STAT1/2, which in turn stimulated expression of genes encoding AXL and SOCS1/3. The latter inhibited virus-induced activation of TLR3 and prevented production of pro-inflammatory cytokines [114, 115].

Moreover, AXL depletion or inactivation of its kinase domain were shown to prevent viral infection of Ebola virus or Zika virus [109, 116, 117]. Accordingly, AXL constitutes a promising target for anti-viral treatment, and one of its inhibitors, R428 (bemcentinib) is currently being tested in the second phase of a clinical trial for the treatment of COVID-19 patients under the ACCORD programme (The Accelerating COVID-19 Research & Development Platform) [118-120].

1.4 Endocytosis

Endocytosis is a process by which cells take up a fragment of PM together with transmembrane proteins and the content of extracellular milieu. Internalized material is enclosed in vesicles of different sizes varying from 60 nm up to 10 µm in diameter, which subsequently fuse with early endosomes [121, 122]. The latter serve as sorting platforms from where cargo is distributed to various cellular compartments. By modulating the composition of proteins on the PM e.g. receptors, transporters, channels, and regulating the fate of internalized cargo, endocytosis was shown to control the responsiveness of cells to various extracellular stimuli. In addition, endocytosis contributes to uptake of nutrients, and facilitates cellular entry of toxins and pathogens, including viruses [121, 123, 124].

Endocytosis is an important regulator of RTK functions, and RTKs were described to undergo constitutive or ligand-induced endocytosis, which mediates their availability at the cell surface, half-life and signaling [124-126]. Specifically, several studies revealed that internalized and ubiquitinated receptors can be sorted for lysosomal degradation, which terminates their signaling and decreases the number of receptors on the PM (Fig. 1.5). Alternatively, internalized RTKs can be targeted for recycling back to the PM. This increases the number of receptors on the cell surface accessible for ligand binding and activation, and in turn sustains and/or enhances RTK-mediated signaling (Fig. 1.5) [121, 125, 127].

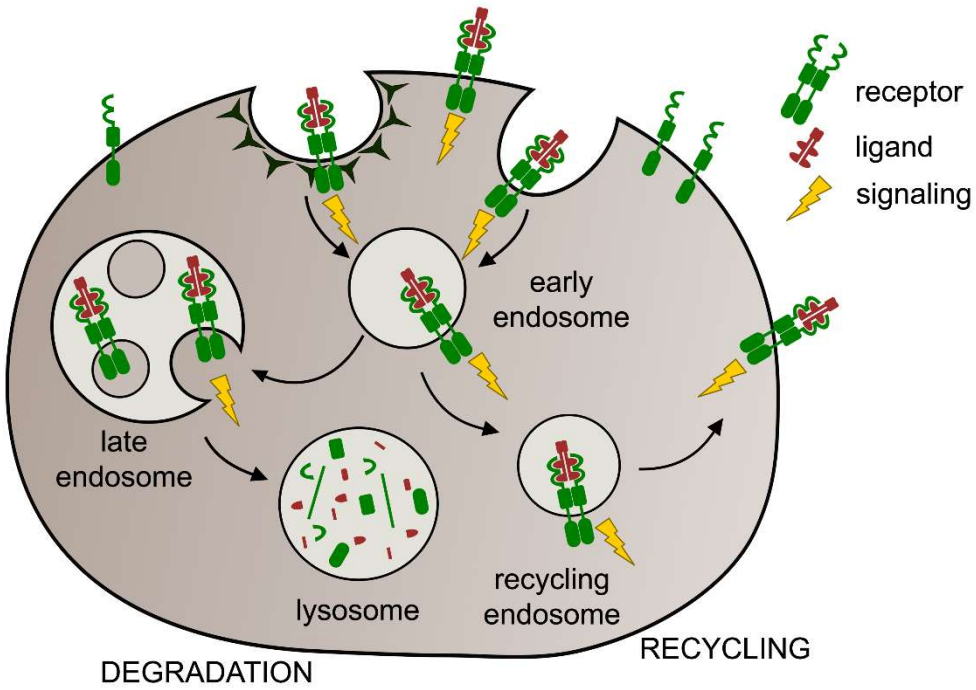

Fig. 1.5 Schematic representation of receptor-mediated endocytosis and possible fates of internalized receptors
Upon ligand stimulation receptors undergo endocytosis and reach early endosomes. The latter serve as sorting platforms from where internalized proteins are directed towards degradation or recycling.

1.4.1 Endocytic routes

Cellular entry of receptors was shown to be facilitated by several mechanisms, which are typically divided into clathrin-mediated (CME) and clathrin-independent (CIE) endocytosis. The latter can be further divided into multiple distinct pathways, characterized by the involvement of different effector proteins and the morphology of formed membrane carriers (Fig 1.6) [121, 126].

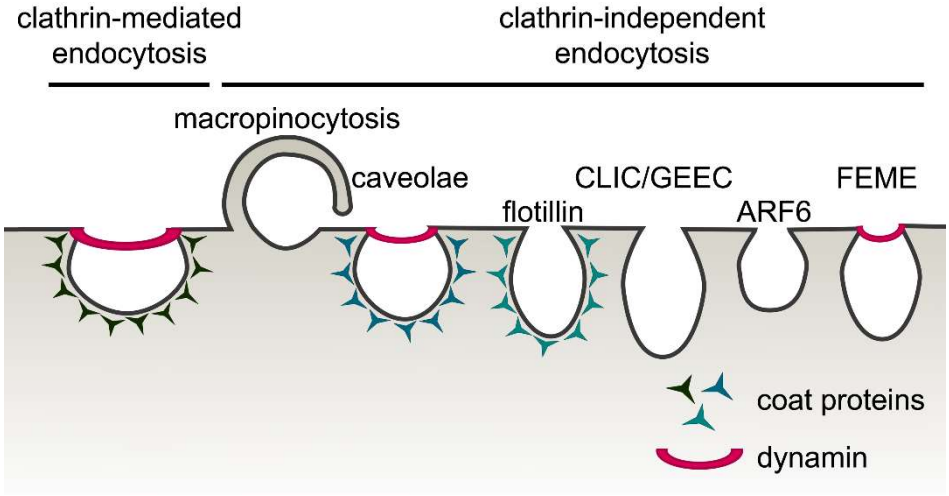

Fig. 1.6 Schematic representation of endocytic routes operating in cells
Endocytosis is mediated via multiple pathways typically divided into clathrin-mediated (CME) and clathrin-independent (CIE) endocytosis. Clathrin-independent endocytosis can be further divided into caveolae- or flotillin-mediated endocytosis, the CLIC/GEEC pathway – clathrin-independent carriers (CLIC)/ glycosylphosphatidylinositol-anchored proteins (GPI-AP)-enriched compartments (GEEC), ARF6-dependent endocytosis or FEME – fast endophilin-mediated endocytosis.

1.4.1.1 Clathrin-mediated endocytosis

CME is the best characterized endocytic route and was named after its key component, the coat protein clathrin discovered in 1975 [128]. This pathway was described to play a pivotal role in the uptake of several receptors including G protein-coupled receptors (GPCR), RTKs, transferrin (Tf) or low-density lipoprotein (LDL) receptor. The latter two were shown to be almost exclusively internalized through CME, thus Tf receptor is considered as a typical cargo of this pathway [129].

Internalization of cargo through CME can be divided into several, partially overlapping steps: initiation, cargo recruitment, coat assembly, scission and uncoating (Fig. 1.7) [129-131]. The process starts with binding of Fer/Cip4 homology domain-only (FCHO) proteins to the PM, which induces membrane curvature and marks the place for vesicle formation [132]. Next, heterotetrameric AP2 adaptor protein complex or monomeric adaptors and scaffolding proteins such as epsins, phosphatidylinositol-binding clathrin assembly protein (PICALM), epidermal growth factor receptor pathway substrate 15 (EPS15),

epidermal growth factor receptor pathway substrate 15 like 1 (EPS15L1), NUMB or intersectins interact with PM lipids and cargo molecules [130, 131, 133-136]. This in turn allows clathrin recruitment and clathrin coat assembly resulting in the formation of clathrin-coated pits (CCP). Clathrin coat assembly together with actin filament polymerization provide force for efficient PM bending and eventually for vesicle scission [126, 130, 131, 137]. The latter step is mediated by the large GTPase dynamin supported by Bin/Amphiphysin/Rvs (BAR)-domain containing proteins such as amphiphysin, endophilin or sorting nexin 9 (SNX9) which participate in membrane constriction and fission at the neck of budding vesicles [130, 131, 138-141]. As a consequence, clathrin-coated vesicles (CCVs) are released from the PM. Finally, CCVs undergo uncoating, which leads to the disassembly of coat and adaptor proteins and release of a matured vesicle [130, 131].

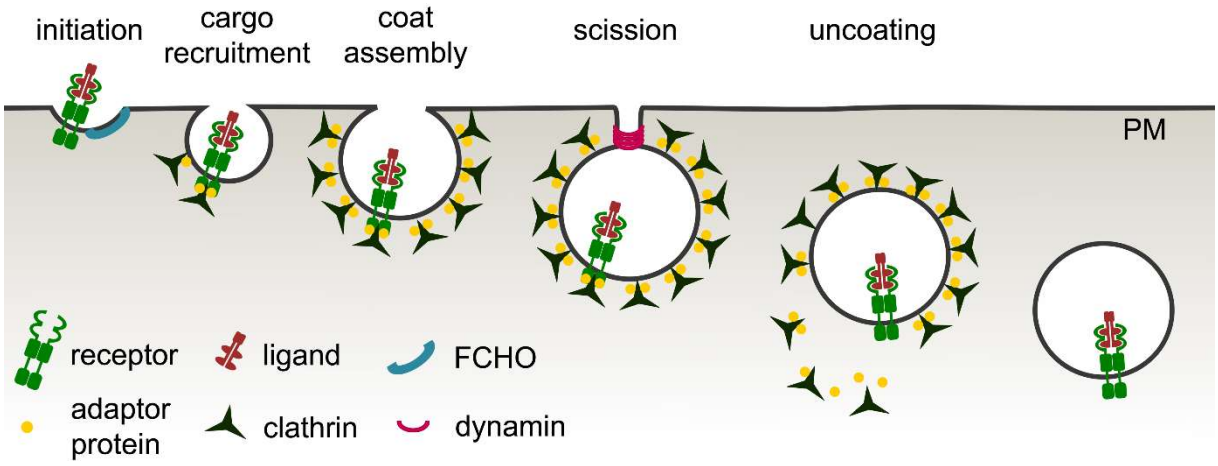

Fig. 1.7 Schematic representation of the formation of clathrin-coated vesicle (CCV)
CCV formation can be divided into five steps: initiation, cargo recruitment, coat assembly, scission and uncoating.

1.4.1.2 Clathrin-independent endocytosis (CIE)

CIE defines the group of various endocytic routes that do not require clathrin, but strongly rely on actin remodeling [126, 142]. They are further divided based on the carrier morphology (e.g. macropinocytosis), transported cargo (e.g. GPI-AP), PM markers (e.g. caveolins, flotillins), the speed of the process (e.g. FEME) or involved GTPase regulators (e.g. ARF6, RhoA) (Fig. 1.6). However, since some of the regulators are shared between different pathways and the same cargo can be internalized via multiple routes, this classification remains under debate [126, 143-145].

1.4.1.2.1 Macropinocytosis

Macropinocytosis mediates non-selective uptake of extracellular fluids and soluble compounds. This process requires actin polymerization, activation of PI3K and RAS GTPases, and occurs via closure of actin-rich membrane protrusions, which results in the

formation of large vesicles, up to 10 μm in diameter, called macropinosomes [122, 146]. Macropinocytosis was shown to be induced by signaling mediated by various receptors, such as RTKs or TLRs, or to be constitutively active in cells deficient of PTEN and expressing mutated RAS or PI3K [143, 146-149]. Importantly, a growing body of evidence suggests that such constitutive macropinocytic uptake of proteins or cell debris provides nutrients required for cancer cell growth, especially under nutrient-deprived conditions [147-149].

Macropinocytosis was described to mediate uptake of RTKs, such as EGFR or PDGFR upon stimulation by their cognate ligands [150, 151]. Additionally, several studies revealed that macropinocytosis facilitates cellular entry of viruses, e.g. vaccinia virus, Ebola virus or Lassa virus, and bacteria e.g. several species of *Legionella*, *Salmonella* or *Shigella* genera [152, 153].

1.4.1.2.2 Caveolae-dependent endocytosis

Caveolae are cholesterol- and sphingolipid-rich flask-shaped PM invaginations of 60-80 nm in diameter [154]. They are formed by association of cholesterol-binding proteins caveolins and cytoplasmic proteins cavins, which altogether form a coat of caveolae. Among 3 isoforms of caveolins and 4 isoforms of cavins, caveolin 1, 3 and cavin 1 are required for the assembly of caveolae [155-157]. Additionally, their formation depends on the presence of PM cholesterol and its depletion by e.g. methyl-β-cyclodextrin leads to caveolae disassembly [143, 154, 158]. Similarly to CME, budding caveolae may undergo scission by GTPase dynamin, which results in the formation of vesicles [154, 158].

Caveolae were shown to mediate uptake of several cargos, e.g. SV40 virus [159], cholera [160] and tetanus [161] toxins, RTKs [162, 163] and tumor necrosis factor receptor 1 (TNFR1) [164]. Moreover, besides participating in endocytosis, caveolae provide mechanoprotection of cells, reflected by caveolae flattening in response to stretching [165].

1.4.1.2.3 Flotillin-dependent endocytosis

Flotillin-dependent endocytosis is mediated by PM proteins flotillin 1 and 2 [166, 167], whose co-assembly results in formation of microdomains and induces PM curvature [168, 169]. Involvement of dynamin in this process is still under debate, since there are studies in favor of as well as against this hypothesis [168, 170, 171]. Flotillin-mediated endocytosis was described to mediate internalization of GPI-AP CD59 [168], cholera toxin B subunit (CTxB) [168], EGFR [172] or LDL receptor-related protein 6 [173]. Moreover, a recent study showed that flotillin-mediated fluid phase endocytosis enhances cellular uptake of cytotoxic drugs, such as cisplatin, revealing a new possible drug delivery route for cancer treatment [174].

1.4.1.2.4 CLIC/GEEC

CLIC/GEEC is an abbreviation for clathrin-independent carriers (CLIC)/ glycosylphosphatidylinositol-anchored proteins (GPI-AP)-enriched compartments (GEEC) and is a clathrin- and dynamin-independent endocytic route [126, 144]. This pathway requires presence of cholesterol and sphingolipids on the PM and activation of actin polymerization that generates pulling forces for CLICs formation. The latter is regulated by small GTPase CDC42 and GTPase regulator associated with focal adhesion kinase-1 (GRAF1) [126, 175-177]. The CLIC/GEEC route is responsible for internalization of GPI-APs, CTxB [178], CD44, β1-integrin (ITGβ1) [179], galectin-3 [180] or RTKs e.g. PDGFRβ [181], but also mediates macropinocytosis-independent fluid phase uptake [143]. Interestingly, galectin-3 was also shown to initiate PM invagination for CLIC formation by clustering of glycosylated proteins e.g. CD44 or integrins in a glycosphingolipid-dependent manner [179, 180]. In fibroblasts, CLIC/GEEC-mediated rapid turnover of PM at the leading edges of cells was shown to be implicated in redistribution of adhesion molecules and cell migration [179].

1.4.1.2.5 ARF6-dependent endocytosis

ARF6 belongs to the ADP-ribosylation factor family of small GTPases, which was described to mediate various cellular functions including lipid metabolism, motility, apoptosis, transcription and membrane trafficking [182, 183]. The role of ARF6 in endocytosis has been initially attributed to endocytic recycling [184], however further studies showed that it can be also implicated in the internalization of several PM proteins such as major histocompatibility complex (MHC) class I, interleukin 2 receptor alpha subunit [185], glucose transporter 1 (GLUT1), CD44, CD55, CD98, CD147 and intercellular adhesion molecule 1 (ICAM1) [186]. ARF6-dependent endocytosis was shown to be dynamin-independent and sensitive to cholesterol depletion [187]. Despite sharing similarities with the CLIC/GEEC pathway, these two endocytic routes are considered separate since ARF6 does not play a role in CLIC/GEEC-mediated cargo internalization [188], and perturbation of GRAF1 affected CLIC/GEEC-mediated dextran uptake but not MHC class I internalization [177].

1.4.1.2.6 FEME

FEME stands for fast endophilin-mediated endocytosis, and is a recently discovered dynamin- and actin-dependent endocytic route [189]. Markers and main effectors of this pathway are endophilins A, BAR domain-containing proteins, which were previously described to function in CME [189, 190]. Three endophilin A proteins were identified in mammalian cells, with ubiquitously expressed endophilin A2 and tissue specific A1 and A3

[191]. FEME carriers are formed upon stimulation of cargo receptors by their cognate ligands, which leads to the formation of small (~1 μm), tubulo-vesicular endophilin-positive assemblies (EPAs) at the leading edges of migrating cells [189, 191]. Unlike CME, where a clathrin coat assembles after cargo recruitment, FEME requires pre-enrichment of endophilins on the PM prior to cargo internalization [192]. This pathway mediates transport of GPCRs, RTKs [189] and bacterial CTxB and Shiga toxins [193], and is negatively regulated by GSK3β and CDK5 [194]. Additionally, a recent study by Genet *et al.* characterized the SLIT-ROBO pathway as a critical regulator of cargo uptake through FEME. In the presence of SLIT-ROBO signaling, vascular endothelial growth factor receptor 2 (VEGFR2) was specifically directed for internalization through FEME, which further induced polarized migration of endothelial cells [195].

1.4.2 The role of endocytosis in regulation of RTK-mediated signaling

Nowadays, endocytosis is believed to regulate not only the duration of RTK-mediated signaling by downregulation of PM levels of receptors but also to affect their signaling outcomes. Therefore, endocytosis acts as an important organizer of RTK-mediated signaling and endosomes are considered as organelles which serve as platforms for signal propagation [125, 196].

A growing body of evidence suggests that signaling from RTKs is not restricted to the PM, but activated and internalized receptors signal also from endosomes [125, 196, 197]. The idea of signaling endosomes arose from studies on activated EGFR and tropomyosin receptor kinase A (TrkA), which were detected within endocytic compartments together with their downstream effectors [198, 199]. Similarly, endosomal activation of PDGFR was shown to recruit several signaling proteins such as GRB2, SHC, PLC-γ, p85α subunit of PI3K [200]. Subsequent studies on EGFR showed that the inhibition of its internalization by overexpression of dominant negative mutant of dynamin 2 (dynamin 2 K44A mutant) resulted in reduced ERK1/2 signaling. The latter suggested that receptor endocytosis was required for the full activation of specific signaling pathways [201]. Importantly, EGFR activated on endosomes was shown to be able to induce normal signaling responses [202].

Several studies provided evidence that endosomes participate also in transport and delivery of RTK-mediated signaling effectors from one cellular compartment to another. It was shown that endosomes carrying nerve growth factor (NGF)-activated TrkA and associated signaling effectors were transported from axon to the cell body in neurons, providing efficient signal transduction from cell periphery to the nucleus [125, 203]. Additionally, endosomal delivery of activated receptors to perinuclear regions appeared to be

crucial for amplification of weak signals. Such regulation was demonstrated for HGF-induced STAT3 activation. It was shown that STAT3 phosphorylation and its nuclear translocation was observed only if HGF-activated MET localized to the perinuclear endosomal compartment [125, 204]. Finally, an endosomal system provides also compartmentalization of signaling since particular subpopulations of endosomes differ in their functions or lipid and protein composition, therefore providing different environments for signal transduction [125, 197]. For example, APPL endosomes, a subpopulation of early endosomes [205], was shown to participate in activation of AKT and ERK effectors upon EGF or NGF stimulation [206, 207].

Internalization of RTKs via different endocytic routes may also affect signaling outcomes and cellular responses mediated by these receptors. One of the mechanisms regulating the choice of an internalization pathway relies on the concentration of a ligand [125]. It was shown that low concentration of EGF (~1 ng/ml) stimulated uptake of EGFR mainly through CME, which resulted in receptor recycling. This led to sustained and prolonged EGFR-mediated signaling. In contrast, high EGF concentration (>20 ng/ml) induced clathrin-independent uptake of EGFR, which caused receptor degradation and termination of signaling [208, 209]. Activation of different signaling effectors in response to low or high ligand concentrations was also reported for PDGFR. Low PDGF concentration (1 ng/ml) was proposed to induce PDGFR internalization through CME, which preferentially promoted cell migration. In contrast, at high PDGF concentration (>5 ng/ml), PDGFR was internalized via CIE, which resulted in cell proliferation [210]. However, studies from our laboratory showed that in normal human fibroblasts (CCD-1070Sk cells), stimulation with high PDGF-BB concentration induced both CME and CIE of PDGFRβ, and inhibition of both mechanisms of internalization resulted in reduced STAT3 phosphorylation and cell proliferation [181]. These data suggest that signaling outcomes and cellular responses induced by various doses of ligands activating RTKs can be cell type-specific.

1.4.3 The role of endocytosis in cancer

RTKs play an important role in cancer progression and since endocytosis regulates their signaling outcomes, aberrant RTK trafficking can support tumorigenesis [211]. In cancer cells, RTKs are frequently mutated or overexpressed, which correlates with their constitutive activation. The latter very often results from abnormal endocytic trafficking of RTKs manifested by their impaired degradation, which leads to sustained signaling [212, 213]. Mechanisms responsible for such phenotypes include mutations in RTKs leading to loss of sorting signals for internalization or ubiquitination, thereby maintaining their signaling

activity at the PM [212]. An example of such mutated receptor is EGFRvIII, which evades c-CBL-mediated degradation due to the lack of phosphorylation of tyrosine 1045, a docking site for c-CBL ubiquitin ligase [214].

Enhanced recycling is another mechanism underlying prolonged activation and signaling of RTKs in cancer [213]. A characteristic feature of some types of cancer is increased expression of small GTPases (e.g. RAB25 or RAB35) that regulate endocytic recycling. They were shown to facilitate transport of internalized RTKs back to the PM for further signaling, which in turn promoted cancer cell migration and invasion [215]. Elevated recycling of RTKs was also reported in cells with oncogenic mutations in p53, which together with RAS are major drivers of human cancers [212]. In line with that, cells expressing mutated p53 displayed reduced degradation and enhanced recycling of EGFR and MET [216, 217]. On the other hand, G12V mutation in H-Ras was shown to promote tumor progression by upregulation of PDGFRβ signaling, resulting from its internalization by macropinocytosis [151]. Additionally, activated RAS was shown to induce macropinocytosis in pancreatic cancer cells, thus stimulating uptake of extracellular proteins, that served as a source of amino acids indispensable for cancer cell proliferation [148].

Finally, endocytosis was shown to contribute to the migration and invasion of cancer cells due to its involvement in adhesion molecule turnover [212]. For example, increased recycling of integrins, transmembrane receptors facilitating contacts between cell-cell and cell-ECM, was correlated with invasion and metastasis [216]. Furthermore, internalization and lysosomal targeting of E-cadherin downregulated cell-cell adhesions and supported EMT and cell migration [218].

2. Aims of the study

AXL, a member of the TAM (TYRO3, AXL, MER) receptor tyrosine kinase (RTK) family, and its ligand GAS6 are associated with pathogenesis of many types of human cancers [7]. AXL overexpression was shown to correlate with poorer prognosis, metastasis and resistance to conventional and targeted cancer therapies [52]. Additionally, a growing body of evidence demonstrates that AXL is also implicated in viral infections and together with GAS6 serves as a cofactor for cellular entry of several viruses including Zika virus or SARS-CoV-2 [110, 111]. However, the exact biological processes regulated by the GAS6-AXL pathway remained largely unexplored, and data concerning proteins that interact with AXL were almost completely lacking. Moreover, up to date, neither AXL nor other TAM receptors have been studied in the context of endocytosis, which is nowadays considered as an important regulator of RTK function. Thus, the general aim of this dissertation was to characterize an interactome and endocytic trafficking of AXL.

The specific aims of this study included:

1. Generation of tools for proximity-dependent biotin identification assay (BioID).
2. Identification of AXL proximity interactome by BioID.
3. Evaluation of the contribution of AXL and other TAM receptors to the uptake of the ligand GAS6.
4. Assessing the involvement of AXL kinase domain activity in the ligand-induced AXL endocytosis.
5. Characterization of the kinetics of GAS6-AXL internalization.
6. Identification of endocytic pathways involved in the internalization of GAS6-AXL complexes.
7. Characterization of the population of endosomes involved in the endocytic trafficking of AXL.
8. Determination of the intracellular fate of internalized AXL receptor.

3. Materials and Methods

3.1 Materials

3.1.1 Cell lines

Table 3.1 List of cell lines used in the project

Cell line	Description	Source	Medium
HEK293	human embryonic kidney	ATCC	DMEM
HEK293T	highly transfectable, HEK293-derived cells, containing the SV40 T-antigen	ATCC	DMEM
LN229	glioblastoma	ATCC	DMEM
CCD-1070Sk	normal human foreskin fibroblasts	ATCC	MEM
LN229-gNT#1	NT- non-targeting gRNA	Laboratory of Cell Biology	DMEM
LN229-gNT#2	NT- non-targeting gRNA		
LN229-gAXL#1	LN229 cells with CRISPR-Cas9-mediated KO of *AXL*	Laboratory of Cell Biology	DMEM
LN229-gAXL#2			
LN229-gTYRO3#1	LN229 cells with CRISPR-Cas9-mediated KO of *TYRO3*	Laboratory of Cell Biology	DMEM
LN229-gTYRO3#2			
LN229-gNUMB#1	LN229 cells with CRISPR-Cas9-mediated KO of *NUMB*	Laboratory of Cell Biology	DMEM
LN229-gNUMB#2			
LN229-gEPS15#1	LN229 cells with CRISPR-Cas9-mediated KO of *EPS15*	Laboratory of Cell Biology	DMEM
LN229-gEPS15#2			
LN229-gEPS15L1#1	LN229 cells with CRISPR-Cas9-mediated KO of *EPS15L1*	Laboratory of Cell Biology	DMEM
LN229-gEPS15L1#2			
LN229-gCAV1#1	LN229 cells with CRISPR-Cas9-mediated KO of *CAV1*	Generated in this thesis	DMEM
LN229-FLOT1#1	LN229 cells with CRISPR-Cas9-mediated KO of *FLOT1*	Generated in this thesis	DMEM
LN229-FLOT1#2			

3.1.2 Cell culture media and supplements

Table 3.2 List of products used for cell culture

Product	Source	Cat. No.
Dulbecco's Modified Eagle's Medium (DMEM) high glucose	Sigma-Aldrich	D5671
Minimum Essential Medium (MEM)	Sigma-Aldrich	M2279
Fetal bovine serum (FBS)	Sigma-Aldrich	F7524
L-glutamine	Sigma-Aldrich	G7513

3.1.3 Bacterial strains (*Escherichia coli*)

Table 3.3 List of bacterial strains used in the project

Strain	Genotype	Source
DH5α	fhuA2 Δ(argF-lacZ)U169 phoA glnV44 φ80Δ(lacZ)M15 gyrA96 recA1 relA1 endA1 thi-1 hsdR17	Thermo Fisher Scientific
Stbl3	F-mcrB mrrhsdS20(rB-, mB-) recA13 supE44 ara-14 galK2 lacY1 proA2 rpsL20(StrR) xyl-5 λ-leumtl-1	Thermo Fisher Scientific

3.1.4 Bacteria culture media and supplements

Table 3.4 List of products used for bacteria culture

Product	Source	Cat. No.
LB Broth Lennox	Bio Shop	LBL405.1
LB Agar Lennox	Bio Shop	LBL406.1
Ampicilin – selective antibiotic	Sigma-Aldrich	A9518
Kanamycin – selective antibiotic	Sigma-Aldrich	K4000

3.1.5 Primary antibodies

Table 3.5 List of primary antibodies used in the project. WB – western blot, IF - immunofluorescence

Antigen	Origin	Application/Dilution	Cat. No.	Source
AKT	mouse	WB 1:2000	2920	Cell Signaling Technology
AXL	goat	IF 1:400	sc-1096	Santa Cruz Biotechnology
AXL	rabbit	WB 1:1000, IF 1:200	sc-20741	Santa Cruz Biotechnology
AXL	goat	WB 1:1000	AF154	R&D Systems
biotin	rabbit	WB 1:1000	ab53494	Abcam
Caveolin 1	rabbit	WB 1:1000, IF 1:500	PA1-064	Thermo Fisher Scientific
CD44 (agonistic antibody)	mouse	Cell stimulation 1:100	338802	BioLegend
CDC42	rabbit	WB 1:1000	sc-87	Santa Cruz Biotechnology
clathrin heavy chain (CHC)	mouse	WB 1:5000	610499	BD Biosciences
c-Myc	mouse	IF 1:100	sc-40	Santa Cruz Biotechnology
EEA1	rabbit	IF 1:1000	ALX-210-239	Enzo Life Sciences
EGFR	rabbit	WB 1:1000	ab52894	Abcam
EPS15	mouse	WB 1:1000	sc-390259	Santa Cruz Biotechnology
EPS15L1	rabbit	WB 1:1000	ab76004	Abcam
ERK1/2	mouse	WB 1:1000	9107	Cell Signaling

				Technology
Flotillin 1	mouse	WB 1:1000	sc-74566	Santa Cruz Biotechnology
HA	rabbit	WB 1:1000, IF 1:200	sc-805	Santa Cruz Biotechnology
LAMP1	rabbit	IF 1:200	L-1418	Sigma-Aldrich
NUMB	rabbit	WB 1:1000	2756	Cell Signaling Technology
P-AKT (Ser 473)	rabbit	WB 1:1000	4060	Cell Signaling Technology
P-AXL (Tyr702)	rabbit	WB 1:1000	5724	Cell Signaling Technology
PDGFRβ	rabbit	WB 1:1000, IF 1:200	sc-432	Santa Cruz Biotechnology
P-EGFR (Tyr1173)	mouse	WB 1:1000	558382	BD Biosciences
P-ERK1/2 (Thr202/Tyr204)	rabbit	WB 1:1000	4370	Cell Signaling Technology
TYRO3	rabbit	WB 1:1000	5585	Cell Signaling Technology
α-tubulin	mouse	WB 1:10000	T5168	Sigma-Aldrich
β-actin	mouse	WB 1:5000	A5441	Sigma-Aldrich

3.1.6 Secondary antibodies

Table 3.6 List of secondary antibodies used in the project. WB – western blot, IF - immunofluorescence

Type	Origin	Application/Dilution	Cat. No.	Source
Alexa Fluor 488-conjugated anti-mouse	donkey	IF 1:500	A-21202	Thermo Fisher Scientific
Alexa Fluor 555-conjugated anti-mouse	donkey	IF 1:500	A-31570	Thermo Fisher Scientific
Alexa Fluor 647-conjugated anti-mouse	donkey	IF 1:500	A-31571	Thermo Fisher Scientific
Alexa Fluor 488-conjugated anti-rabbit	donkey	IF 1:500	A-21206	Thermo Fisher Scientific
Alexa Fluor 555-conjugated anti-rabbit	donkey	IF 1:500	A-31572	Thermo Fisher Scientific
Alexa Fluor 647-conjugated anti-rabbit	donkey	IF 1:500	A-31573	Thermo Fisher Scientific
Alexa Fluor 488-conjugated anti-goat	donkey	IF 1:500	A-11055	Thermo Fisher Scientific
Alexa Fluor 555-conjugated anti-goat	donkey	IF 1:500	A-21432	Thermo Fisher Scientific
Alexa Fluor 647-conjugated anti-goat	donkey	IF 1:500	A-21447	Thermo Fisher Scientific

Horseradish peroxidase (HRP)-conjugated anti-mouse	goat	WB 1:10000	115-035-062	Jackson ImmunoResearch Labs
Horseradish peroxidase (HRP)-conjugated anti-rabbit	goat	WB 1:10000	111-035-144	Jackson ImmunoResearch Labs
Horseradish peroxidase (HRP)-conjugated anti-goat	bovine	WB 1:10000	805-035-180	Jackson ImmunoResearch Labs
Anti-mouse IRDye 800CW	donkey	WB 1:10000	926-32212	LI-COR Biosciences
Anti-rabbit IRDye 680CW	donkey	WB 1:10000	926-68023	LI-COR Biosciences
Anti-goat IRDye 800CW	donkey	WB 1:10000	926-32214	LI-COR Biosciences

3.1.7 Transfection reagents

Table 3.7 List of transfection reagents used in the project

Reagent	Source	Cat. no.
Lipofectamine® RNAiMAX	Thermo Fisher Scientific	13778150
Lipofectamine® 2000	Thermo Fisher Scientific	11668019

3.1.8 Other reagents

Table 3.8 List of other reagents used in the project

Product	Source	Cat. No.
BamHI restriction enzyme	Thermo Fisher Scientific	ER0051
Biotin	Sigma-Aldrich	B4501
Bovine serum albumin (BSA)	BioShop	ALB001
BsmBI restriction enzyme	Thermo Fisher Scientific	ER0452
Calf intestinal alkaline phosphatase (CIAP)	Thermo Fisher Scientific	18009019
CO_2-independent medium	Thermo Fisher Scientific	18045070
Cycloheximide (CHX)	Carl Roth GmbH	8682.1
DAPI	Sigma-Aldrich	D9542
Dimethyl sulfoxide (DMSO)	BioShop	DMS666.100
DNase I	Sigma-Aldrich	10104159001
dNTP	Thermo Fisher Scientific	R0193
Dynabeads™ MyOne™ Streptavidin C1	Thermo Fisher Scientific	65002
EGF	PeproTech	AF-100-15
EGF-Alexa-Fluor-555	Thermo Fisher Scientific	E35350
EZ-Link™ Sulfo-NHS-SS-biotin	Thermo Fisher Scientific	21328
Geneticin® Selective Antibiotic (G418)	Sigma-Aldrich	11811031
HEPES	Sigma-Aldrich	H3375-100G
LDC1267	MedChemExpress	HY-12494
MluI restriction enzyme	Thermo Fisher Scientific	ER0561

NeutraVidin™ Agarose	Thermo Fisher Scientific	29200
M-MLV Reverse Transcriptase	Sigma-Aldrich	M1302
NheI restriction enzyme	Thermo Fisher Scientific	ER0971
Ni-NTA Agarose	Qiagen	30210
Oligo(dT)$_{23}$, Anchored	Sigma-Aldrich	O4387
Opti-MEM	Sigma-Aldrich	11058021
PageRuler Prestained Protein Ladder	Thermo Fisher Scientific	26617
PDGF-BB	PeproTech	100-14B
Phalloidin-Atto 390	Sigma-Aldrich	50556
Phosphatase inhibitor cocktail 2 (PIC2)	Sigma-Aldrich	P5726
Phosphatase inhibitor cocktail 3 (PIC3)	Sigma-Aldrich	P0044
Phusion™ High-Fidelity DNA Polymerase	Thermo Fisher Scientific	F530L
Puromycin	Toku-e	P001
PvuI restriction enzyme	Thermo Fisher Scientific	ER0621
R428	MedChemExpress	HY-15150
Random Nonamers	Sigma-Aldrich	R7647
T4 DNA ligase	Thermo Fisher Scientific	EL0011
T4 Polynucleotide Kinase (T4PNK)	Thermo Fisher Scientific	EK0031
Taq DNA Polymerase	Thermo Fisher Scientific	EP0401
Transferrin-Alexa-Fluor-647	Thermo Fisher Scientific	T23366
Trypsine	VWR	MDTC25-052-CV
Vitamin K$_1$	Carl Roth GmbH	3804.1
XbaI restriction enzyme	Thermo Fisher Scientific	ER0681
XhoI restriction enzyme	Thermo Fisher Scientific	ER0691

3.1.9 Commercial kits

Table 3.9 List of commercial kits used in the project

Product	Source	Cat. No.
Clarity Western ECL Substrate	Bio-Rad	1705061
High Pure RNA Isolation Kit	Roche Diagnostics	11828665001
KAPA SYBR FAST qPCR Master Mix (2X) Universal Kit	KapaBiosystem	KK4618
MinElute Reaction Cleanup Kit	Qiagen	28204
Pierce BCA Protein Assay	Thermo Fisher Scientific	23225
Plasmid Screening Kit	Syngen	SY103000
QIAquick Gel Extraction Kit	Qiagen	28706X4

3.1.10 Small interfering RNA oligonucleotides (siRNA)

Ambion Silencer Select siRNAs were from Thermo Fisher Scientific. Non-specific Silencer Select siRNA oligonucleotides (siCTR#1 and siCTR#2) were used as a negative control.

Table 3.10 List of siRNA oligonucleotides used in the project

Name	Cat. no.	Sequence (5'-3')
siCTR#1	4390846	Sequence not provided by the supplier.
siCTR#2 (custom selected)	4390828	UACGACCGGUCUAUCGUAGtt
siARF6#1	s1565	GUCUCAUCUUCGUAGUGGAtt
siARF6#2	s1567	CCAAGGUCUCAUCUUCGUAtt
siAXL#1	s1845	GGAACUGCAUGCUGAAUGAtt
siAXL#2	s1846	GGGUGGAGGUUAUCCUGAAtt
siAXL#3	s1847	AGCGAGAUUUAUGACUAUtt
siCDC42#1	s2765	UGGUGCUGUUGGUAAAACAtt
siCDC42#2	s2767	CAGUUAUGAUUGGUGGAGAtt
siCLTC#1	s475	GGUUGCUCUUGUUACGGAUtt
siCLTC#2	s476	CGGUUGCUCUUGUUACGGAtt
siGRAF1#1	s23013	GAGCAAGGGCUGUAUCGAAtt
siGRAF1#2	s23015	GGAUACGGAUGAUUGAGAAtt
siTYRO3#1	s14544	GAGCUUUACUUGUCUGCGAtt
siTYRO3#1	s14546	CAAGCGACAUUGAAGAGUUtt
siTYRO3#2	s14545	CAGUGACUGUCGGUACAUAtt

3.1.11 Guide RNA oligonucleotides (gRNAs) used for CRISPR-Cas9-mediated gene inactivation

Two 20-bp-long single-guide RNA (gRNAs) were selected from the Brunello library [219] and appropriate pairs of DNA oligonucleotides were designed as described in chapter 3.2.16.

Table 3.11 List of gRNAs used in the project. F – forward primer, R – reverse primer

gRNA name	Oligonucleotide name	Sequence (5'-3')
gCAV1#1	gCAV1#1-F	CACCGGCACACCAAGGAGATCGACC
	gCAV1#1-R	AAACGGTCGATCTCCTTGGTGTGCC
gFLOT1#1	gFLOT1#1-F	CACCGAGACGTTAGAGGGCCACCAG
	gFLOT1#1-R	AAACCTGGTGGCCCTCTAACGTCTC
gFLOT1#2	gFLOT1#2-F	CACCGAAAGGTTTACACTCGCCATG
	gFLOT1#2-R	AAACCATGGCGAGTGTAAACCTTTC

3.1.12 Primers used for real-time quantitative PCR (RT-qPCR) gene expression analysis

Table 3.12 List of RT-qPCR primers used in the project. F – forward primer, R – reverse primer

Gene name	Sequence (5'-3')
ACTB	F- CAGGTCATCACCATTGGCAAT
	R- TCTTTGCGGATGTCCACGT
AFR6	F- ATGGGGAAGGTGCTATCCAAAATC
	R- GCAGTCCACTACGAAGATGAGACC
ARHGAP26 (GRAF1)	F- TAAGAATGCTTCCAGGACCACTC
	R- GCTGTAACATCTGCCGATTTTTC

3.1.13 Plasmids

Table 3.13 List of plasmids used in the project

Name	Source
pEGFP-N2	Clontech
pcDNA3.1-BirA*-HA	Addgene plasmid #36047 pcDNA3.1-MCSBirA(R118G)-HA
pmRFP-CLC	Kind gift from Dr. K.O. Schink (Institute for Cancer Research, Oslo University Hospital, Oslo, Norway)
pmCherry-N1-PICALM	Kind gift from Dr. K.O. Schink (Institute for Cancer Research, Oslo University Hospital, Oslo, Norway)
pLenti-CMV-MCS-GFP-SV-puro	Addgene plasmid #73582
LentiCRISPRv2	Addgene plasmid #52961
psPAX2	Addgene plasmid #12260
pMD2.G	Addgene plasmid #12259
pcDNA3.1-GAS6-MycHis	Laboratory of Cell Biology
LentiCRISPRv2-gCAV1#1	Generated in this thesis, see chapter 3.2.16.
LentiCRISPRv2-gFLOT1#1	Generated in this thesis, see chapter 3.2.16.
LentiCRISPRv2-gFLOT1#2	Generated in this thesis, see chapter 3.2.16.
pcDNA3.1-AXL-BirA*-HA	Generated in this thesis, see chapter 3.2.10.
pLenti-CMV-MCS-BirA*-HA	Generated in this thesis, see chapter 3.2.11.
pLenti-CMV-MCS-AXL-BirA*-HA	Generated in this thesis, see chapter 3.2.11.
pEGFP-N2-AXL	Generated in this thesis, see chapter 3.2.19.

3.1.14 Commonly used buffers

Table 3.14 List and the composition of commonly used buffers

Name	Composition
CLAAP	0.6 µg/ml chymostatin, 0.5 µg/ml leupeptin, 10 µg/ml antipatin, 2 µg/ml aprotinin, 0.7 µg/ml pepstatin, 10 µg/ml APMSF
2xHBS buffer	280 mM NaCl, 50 mM HEPES, 1.5 mM Na_2HPO_4, 10 mM KCl, 12 mM sucrose, pH 7.5
Laemmli buffer	50 mM Tris pH 6.8, 100 mM DTT, 2% SDS, 10% glycerol, 0.05% bromophenol blue

Mowiol	100 mM Tris pH 8.5, 25% glycerol, 10% polyvinyl alcohol
Paraformaldehyde (PFA)	3.6% paraformaldehyde, 0.12 mM $CaCl_2$, 0.12 mM $MgCl_2$
Phosphate buffered saline (PBS)	0.13 M NaCl, 2.7 mM KCl, 4.2 mM Na_2HPO_4, 1.4 mM KH_2PO_4, pH 7.4
PBST	0.1% Tween-20 in PBS
RIPA lysis buffer	150 mM NaCl, 1% NP-40, 0.5% deoxycholic acid, 0.1% SDS, 50 mM Tris pH 8.0, 0.5 mM EDTA
Running buffer	25 mM Tris pH 8.5, 0.19 M glycine, 1% SDS
Saponin solution I in PBS	0.1% saponin, 0.2% gelatin, 5 mg/ml BSA
Saponin solution II in PBS	0.01% saponin, 0.2% gelatin
TAE buffer	40 mM Tris, 20 mM acetic acid, 1 mM EDTA
TBST	0.05% Tween-20, 10 mM Tris, 150 mM NaCl
Transfer buffer	20 mM Tris pH 8.3, 0.15 M glycine, 20% methanol
WB blocking buffer	5% non-fat dry milk in TBST

3.2 Methods

3.2.1 Cloning of DNA fragments into plasmid vectors

To generate required plasmids, appropriate DNA sequences were amplified by polymerase chain reaction (PCR) using Phusion™ High-Fidelity DNA Polymerase according to the manufacturer's protocol. Reaction mix contained the following reagents (final volume 50 µl): 10 µl of HF reaction buffer (5x concentrated), 200 µM of each dNTP, 0.5 µM of each primer (forward and reverse), 50 ng of DNA template, 1 U of Phusion™ High-Fidelity DNA Polymerase and H_2O up to 50 µl. The presence and proper size of amplified DNA fragment was assessed via DNA electrophoresis in agarose gels. After PCR, amplified DNA fragment was purified with MinElute Reaction Cleanup Kit and next, together with an appropriate plasmid, was incubated at 37 °C with dedicated restriction enzymes. Products of reactions were run on agarose gels, purified with QIAquick Gel Extraction Kit and ligated for 16 h with T4 DNA ligase at 22 °C to generate a plasmid with a given insert. Ligation was terminated by 5 min incubation at 70 °C. Ligation mix contained the following reagents (final volume 20 µl): 2 µl of T4 DNA ligase buffer (10x concentrated), 50 ng of digested plasmid, an appropriate amount of the insert calculated according to the molar vector-to-insert ratio 1:3 (calculated with http://www.insilico.uni-duesseldorf.de/Lig_Input.html ligation calculator), 0.5 mM ATP, 1 U of T4 DNA ligase and H_2O up to 20 µl.

Next, chemically competent bacteria of the DH5α *E. coli* strain were transformed with the products of ligation. For selection of transformed bacteria, they were seeded on LB agar plates with ampicillin (final concentration 100 µg/ml) or kanamycin (final concentration 50 µg/ml) and incubated overnight at 37 °C. Selected colonies of bacteria were next screened for the presence of plasmids by colony PCR. Colony PCR mix contained the following reagents (final volume 50 µl): 5 µl of Taq DNA Polymerase buffer, 200 µM of each dNTP, 0.5 µM of each primer (forward and reverse), 1.5 mM $MgCl_2$, 1 U of Taq DNA Polymerase (recombinant) and H_2O up to 50 µl. A single colony of bacteria was used as DNA template. The presence of amplified DNA fragment was checked via DNA electrophoresis in an agarose gel. Subsequently, bacteria colonies carrying generated plasmids were inoculated in 4 ml of liquid LB medium supplemented with appropriate antibiotic and incubated overnight at 37 °C with shaking (180 rpm, STUART orbital incubator SI500). Plasmid DNA was next isolated with Plasmid Screening Kit, DNA concentration was measured with NanoDrop 8000 Spectrophotometer (Thermo Fisher Scientific) and the cloned sequences were verified by sequencing (performed by Genomed Warsaw).

3.2.2 Preparation of chemically competent bacteria

A single colony of the DH5α or Stbl3 *E. coli* strains was incubated in 10 ml of LB medium overnight at 37 °C. The following day, the bacteria culture was added to 1 l of LB and grown until reaching the optical density (measured at 600 nm) between 0.3 and 0.5. Next, bacteria were incubated on ice for 10 min and centrifuged at 1500 g for 10 min at 4 °C. The pellet was suspended in 100 ml of cold TF1 buffer (10 mM MES pH 5.8, 45 mM $MnCl_2$, 10 mM $CaCl_2$, 100 mM RbCl) and kept on ice for 5 min. After that, bacteria were again centrifuged as described above, resuspended in 20 ml of TF2 buffer (10 mM PIPES pH 6.5, 50 mM $CaCl_2$, 10 mM RbCl, 15% glycerol) and incubated on ice for 20 min. Competent bacteria were aliquoted, immediately frozen on dry ice and stored at -80 °C.

3.2.3 Bacteria transformation

Chemically competent DH5α of Stbl3 bacteria was thawed on ice. Next, plasmid DNA or ligation mixture was added to the competent bacteria, mixed and incubated on ice for 30 min. After that, cells were transferred to 42 °C for 1 min (heat shock) and moved back to ice for 2 min. One ml of warm LB medium was added to bacteria which were subsequently grown for 1 h at 37 °C with shaking. Then, bacteria were plated on pre-warmed agar plates with LB medium supplemented with appropriate antibiotic and incubated overnight at 37 °C.

3.2.4 Cell culture, freezing and thawing

HEK293, HEK293T, wild type (WT) and CRISPR-Cas9-mediated knockout (KO) LN229 cells were maintained in DMEM, whereas CCD-1070Sk cells in MEM medium. All media were supplemented with 10% FBS and 2 mM L-glutamine (full medium) and cells were cultured in 10 cm diameter dishes in an incubator with 5% CO_2 at 37 °C. Cells that reached 80% confluency were washed twice with PBS, detached from the dish by incubation with trypsin at 37 ºC, diluted to a desired density (HEK293, HEK293T 1:20, WT and KO LN229 1:6-1:10, CCD-1070Sk 1:6) and transferred to a new dish.

In order to be frozen, cells were detached from dishes with trypsin and centrifuged at 200 g for 5 min. Cell pellets were suspended in FBS supplemented with 10% dimethyl sulfoxide (DMSO), transferred to cryotubes, slowly frozen at -80 °C and moved to liquid nitrogen for long time storage.

For thawing, cells were quickly defrosted at 37 °C in a water bath and suspended in appropriate medium pre-heated up to 37 °C. To remove DMSO, cells were centrifuged at 200 g for 5 min, resuspended in fresh medium and plated on the dish for further culture.

3.2.5 Cell seeding

To seed a desired number of cells, 10 µl of cell suspension was mixed with 10 µl of Trypan blue, moved to EVE^{TM} cell counting slides (NanoEntek, cat. no. EVS-050) and cell density was analyzed in EVE^{TM} Automated Cell Counter (NanoEntek, cat. no. EVE-MC). Next, cells were diluted and seeded accordingly:

- 5×10^4 cells/well or 2×10^4 cells/well (for siRNA transfection experiments) of LN229 cells and 5×10^4 cells/well of CCD-1070Sk cells on 12-mm coverslips in 24-well plates for immunofluorescence (IF),
- 3×10^5 cells/well or 1.5×10^5 cells/well (for siRNA transfection) of LN229 cells in 6-well plates for western blot (WB).

3.2.6 Generation of stable HEK293 cell line secreting GAS6-MycHis

To generate HEK293 cells expressing GAS6-MycHis recombinant protein, pcDNA3.1-GAS6-MycHis plasmid, linearized with PvuI restriction enzyme was used for transfection of HEK293 cells. Transfection was performed using Lipofectamine® 2000 transfection reagent, according to manufacturer's instructions. Next, cells were cultured with G418 for 2 weeks to select transfected cells and single clones were isolated from G418-resistant population. GAS6-MycHis secretion to the medium was verified via western blot. Single clones were obtained by culturing 500 cells in 10 cm dishes for 2 weeks, followed by transfer of the formed colonies to 24-well plates by scratching cells with sterile 200 µl pipette tips. Clones expressing high levels of GAS6-MycHis were selected for the production of conditioned medium.

3.2.7 Purification of GAS6-MycHis from the conditioned medium

For GAS6-Myc-His purification from the conditioned medium, HEK293 expressing recombinant GAS6 were cultured for 72 h in serum-free medium, supplemented with 10 µg/ml vitamin K1. Next, the conditioned medium with GAS6-MycHis was collected, filtered through 0.2 µm filters and dialyzed twice against 50 mM phosphate buffer, pH 7.4, with 300 mM NaCl and 10 mM imidazole for 24 h. Next, GAS6-MycHis was captured on Ni-NTA Agarose and eluted with 50 mM phosphate buffer pH 7.4 containing 300 mM NaCl and 150 mM imidazole. Protein purity and yield were assessed by 10% SDS-PAGE followed by Coomassie Brilliant Blue (R-250) staining of the gel. GAS6-MycHis-containing fractions were pooled and dialyzed against PBS using Amicon Ultra-15 Centrifugal Filter Unit (Millipore). The purified GAS6-MycHis concentration was measured with Pierce™ BCA Protein Assay Kit (Thermo Fisher Scientific). Finally, purified GAS6-MycHis was diluted to the concentration of 0.2 mg/ml and kept at -80 °C for long time storage.

3.2.8 Cell stimulation with the ligands and treatment with inhibitors

Sixteen hours before stimulation cell culture medium was exchanged to FBS-free medium (starvation medium). On the day of LN229 cell stimulation, 1 M HEPES pH 7.5 was added to the medium to the final concentration of 20 mM. Subsequently, cells were incubated with 400 ng/ml GAS6-MycHis, 400 ng/ml EGF-Alexa-Fluor-555, 400 ng/ml EGF or 5 µg/ml anti-CD44 antibodies for the indicated time periods at 37 °C outside of the CO_2 incubator.

For CCD-1070Sk cell stimulation, the medium was exchanged to ice-cold CO_2-independent medium supplemented with 2 mM L-glutamine. To allow ligand binding, serum-starved cells were incubated with 400 ng/ml GAS6 and 50 ng/ml PDGF-BB on ice for 30 min. To remove unbound ligands, cells were next washed twice with ice-cold CO_2-independent medium and incubated in warm CO_2-independent medium for the indicated time periods at 37 °C to allow endocytosis.

For inhibitor treatment, cells were incubated with 10 µg/ml of cycloheximide, 5 µM R428 or LDC1267 for 30 min at 37 °C prior to stimulation with GAS6. In control samples, the same volume of DMSO was added.

3.2.9 Production of lentiviruses and lentiviral transduction

To produce lentiviruses used for transduction of LN229 cells for recombinant protein expression or CRISPR-Cas9-mediated knockout of genes, 8×10^5 cells/well HEK293T cells were seeded into a 6-well plate. The following day, a 100 µl mix of 4 µg of pLenti-CMV-MCS-BirA*-HA or pLenti-CMV-MCS-AXL-BirA*-HA (for BirA*-HA or AXL-BirA*-HA protein expression, respectively) or LentiCRISPRv2 with cloned appropriate gRNA (see chapter 3.1.11), together with pMD2.G (1 µg) and psPAX2 (3 µg) packaging plasmids and $CaCl_2$ (250 mM) was diluted twice by adding it dropwise into 2xHBS buffer. The obtained transfection mixes were incubated for 15 min and added to HEK293T cells for lentiviral production. The next day, medium was exchanged for 1.1 ml fresh full DMEM medium to concentrate the virus. Forty eight hours after transfection medium was collected, filtered through sterile 0.45 µm filters and used for transduction of LN229 cells.

For lentiviral transduction 3×10^5 cells/well of LN229 cells were seeded into a 6-well plate. One day later, the medium was exchanged to 1 ml fresh full DMEM and 1 ml of virus-containing media to infect cells. After 48 h, medium from LN229 cells was exchanged to fresh full DMEM supplemented with puromycin (final concentration 1 µg/ml) for selection of transduced cells. Expression of recombinant proteins or knockout of genes was verified via WB and/or IF.

3.2.10 Generation of HEK293 cells stably expressing BirA*-HA or AXL-BirA*-HA

HEK293 cells expressing BirA*-HA or AXL-BirA*-HA were generated using pcDNA3.1-BirA*-HA or pcDNA3.1-AXL-BirA*-HA, respectively. pcDNA3.1-AXL-BirA*-HA plasmid was generated by amplification of *AXL* coding sequence from pcDNA3.1-AXL with forward primer 5'-TGTTCTGCTAGCATGGCGTGGCGGTGCCCCAG-3', containing NheI restriction site and reverse primer 5'-GTGCTTGGATCCGGCACCATCCTCCTGCCCTG-3' containing BamHI restriction site and its subcloning into pcDNA3.1-BirA*-HA vector.

HEK293 cells were transfected with PvuI restriction enzyme-linearized pcDNA3.1-BirA*-HA or pcDNA3.1-AXL-BirA*-HA plasmids. Transfection was performed using Lipofectamine® 2000 Transfection Reagent according to the manufacturer's protocol. Subsequently, cells were grown for 2 days, and transfected cells were selected by culturing in medium supplemented with G418 (final concentration 1 mg/ml). Expression of BirA*-HA or AXL-BirA*-HA was checked using WB and IF. Since the obtained G418-resistant population of cells was heterogeneous with respect to BirA*-HA and AXL-BirA*-HA expression, single clones were obtained as described in chapter 3.2.6.

3.2.11 Generation of LN229 cells stably expressing BirA*-HA or AXL-BirA*-HA

LN229 cells stably expressing BirA*-HA or AXL-BirA*-HA were generated by lentiviral transduction as described in chapter 3.2.9. For generation of pLenti-CMV-MCS-BirA*-HA plasmid, BirA*-HA coding sequence was amplified from pcDNA3.1-BirA*-HA using forward primer 5'-TGTTCTTCTAGAGCTAGCGCTTAAGGCCTGTTAAC-3' (containing XbaI restriction site) and reverse primer 5'-GTGCTTACGCGTCTATGCGTAATCCGGTACATC-3' (containing MluI restriction site) and subcloned into pLenti-CMV-MCS-GFP-SV-puro.

pLenti-CMV-MCS-AXL-BirA*-HA plasmid was generated by amplification of AXL-BirA*-HA coding sequence from pcDNA3.1-AXL-BirA*-HA using forward primer 5' TGTTCTGCTAGCATGGCGTGGCGGTGCCCCAG-3' (containing NheI restriction site) and reverse primer 5'-GTGCTTACGCGTCTATGCGTAATCCGGTACATC-3' (containing MluI restriction site) and subcloning into pLenti-CMV-MCS-GFP-SV-puro.

3.2.12 Proximity-dependent biotin identification (BioID)

The BioID protocol was adapted from Roux *et al.* [220] and experiments were performed in 3 biological repeats. 1×10^6 HEK293 or LN229 cells expressing BirA*-HA or AXL-BirA*-HA protein were seeded in 10 cm dish in full medium. HEK293 cells were then incubated for 24 h with 50 μM biotin in the presence or absence of 400 ng/ml GAS6. In

case of LN229 cells, they were washed with PBS and starved for 16 h in medium without FBS before biotin and GAS6 treatment.

After incubation with biotin, cells were washed two times with PBS and lysed using lysis buffer (50 mM Tris-Cl, pH 7.4, 500 mM NaCl, 0.2% SDS) supplemented with 1 mM DTT, CLAAP (diluted 1:500) and phosphatase inhibitor cocktails 2 and 3 (diluted 1:100). Next, 60 µl Triton X-100 was added to lysates to the final concentration of 2%. Lysates were subsequently sonicated twice with 20 pulses, using a Badelin Ultrasonic Homogenizer HD 2070, at 20% duty cycle, and an output level of 2. After that, 540 µl of pre-chilled 50 mM Tris-Cl, pH 7.4 was added to each sample. Samples were then centrifuged at 16500 g for 15 min at 4 °C, 150 µl of each sample was kept for WB (input) and the rest was incubated overnight on the rotator with 100 µl of streptavidin-coated magnetic beads (Dynabeads™ MyOne™ Streptavidin C1) at 4 °C. Before incubation, beads were equilibrated in 0.75 ml of lysis buffer and 0.75 ml of 50 mM Tris-Cl pH 7.4 at room temperature (RT).

The next day, samples were washed twice with 1.5 ml of wash buffer I (2% SDS in H_2O), once with 1.5 ml of wash buffer II (0.1% deoxycholic acid, 1% Triton X-100, 1 mM EDTA, 500 nM NaCl, 50 mM HEPES pH 7.5) and 1.5 ml of wash buffer III (0.5% deoxycholic acid, 0.5% NP-40, 1 mM EDTA, 250 mM LiCl, 10 mM Tris-Cl pH 7.4) for 8 min. After that, beads were resuspended in 1.5 ml 50 mM Tris-Cl pH 7.4 and 10% of each sample was kept for WB analysis. All samples were subsequently centrifuged for 5 min at 2000 g at 4 °C. The supernatants were removed and beads were resuspended in 50 µl of water or Laemmli buffer (output samples) for mass spectrometry or WB analysis, respectively. Prior to mass spectrometry analyses, protein biotinylation status in the input and output samples was assessed by WB.

3.2.13 Mass spectrometry analysis

Mass spectrometry analyses were performed by the Laboratory of Mass Spectrometry at the Institute of Biochemistry and Biophysics, Polish Academy of Sciences in Warsaw. Biotinylated proteins bound to streptavidin-coated magnetic beads underwent a standard procedure for qualitative mass spectrometry, which included reduction and alkylation of protein disulfide bonds and trypsin digestion for peptide generation [221]. Peptide mixtures were next analyzed by liquid chromatography coupled to tandem mass spectrometry (LC-MS/MS) using Nano-Acquity (Waters Corporation) UPLC system and LTQ-FT-Orbitrap (Thermo Scientific) mass spectrometer. Acquired raw data were processed by Mascot Distiller followed by Mascot Search (Matrix Science, London, UK, on-site license) against the SwissProt database restricted to human sequences. The mass spectrometry proteomics

data have been deposited to the ProteomeXchange Consortium via the PRIDE [222] partner repository with the dataset identifier PXD017933.

3.2.14 Gene Ontology (GO) analysis of mass spectrometry data

Lists of hits obtained from mass spectrometry analysis of AXL-BirA*-HA samples (with or without GAS6) were compared to the ones obtained from BirA*-HA expressing cells considered as control samples. Proteins identified in at least 2 out of 3 experiments, with ≥ 2 peptides at least in one experiment, and having sum of Mascot scores in AXL-BirA*-HA samples three times higher in comparison to control, were considered as AXL proximity interactors.

AXL interactors underwent GO analysis of biological processes, molecular functions and cellular components using the clusterProfiler package (version 3.6.0; [223] and enrichGO function. All enrichment p-values in GO analysis were corrected for multiple testing using the Benjamini–Hochberg method, and only proteins with adjusted p-value < 0.05 were considered significant. The minimal and maximal sizes of protein clusters were set to 10 and 500, respectively. Redundant terms were removed by means of the simplify function with cutoff 0.65. Calculations were performed in R version 3.6.1 (https://www.R-project.org) by Dr. Krzysztof Kolmus (Laboratory of Cell Biology, IIMCB Warsaw).

3.2.15 Surface biotinylation assay

LN229 cells were seeded at the density of 3×10^5 cells/well in a 6-well plate. The following day medium was exchanged, and cells were serum-starved for 16 h. After starvation, cells were stimulated with EGF (400 ng/ml) or GAS6 (400 ng/ml) for the indicated time periods, cooled down on ice, washed twice with ice-cold PBS and incubated with EZ-Link™ Sulfo-NHS-SS-biotin (0.33 mg/ml in PBS) for 45 min at 4 °C with gentle agitation. Next, cells were washed 3 times with cold quenching buffer (40 mM glycine, 0.4% BSA, 0.5 mM $MgCl_2$, 1 mM $CaCl_2$ in TBS), twice with cold TBS supplemented with 0.5 mM $MgCl_2$, 1 mM $CaCl_2$ and lysed in 200 µl of RIPA buffer. Lysates were then centrifuged at 15000 g for 15 min at 4 °C, supernatants were transferred to new tubes and protein concentration was assessed with Pierce BCA Protein Assay. For pull-down of biotinylated proteins, the same amount of proteins from each condition was diluted in 200 µl of RIPA buffer, and 10% of each sample was kept as a whole cell lysate control. The rest was incubated for 16 h with 30 µl/sample of NeutraVidin™ Agarose at 4 °C with rotation. Before incubation, NeutraVidin™ Agarose was diluted in RIPA buffer, centrifuged at 3200 g for 3 min at RT and washed further 2 times with RIPA buffer. After overnight incubation, samples were centrifuged at 3200 g for 3 min at 4 °C and washed with 500 µl of RIPA buffer. The washing step was

repeated 3 times. Finally, beads were resuspended in 50 µl Laemmli buffer and samples were analyzed using WB.

3.2.16 Generation of LN229 cells with CRISPR-Cas9-mediated knockout of *CAV1* or *FLOT1*

To establish KO LN229 cell lines, gRNA sequences targeting *CAV1 or FLOT1* were selected from the Brunello library [219] and appropriate oligonucleotides with added cloning overhangs (shown below in red) were ordered from Sigma-Aldrich. The used oligonucleotides are listed in chapter 3.1.11.

gRNA-F 5' – CACCG XXXXXXXXXXXXXXXXXXX – 3'

gRNA-R 3' – C XXXXXXXXXXXXXXXXXXX CAAA – 5'

Pairs (forward and reverse) of corresponding nucleotides were next phosphorylated and annealed by incubation with T4 Polynucleotide Kinase (T4PNK) for 30 min at 37 °C, heating up to 95 °C for 2 min and subsequent cooling down to RT. Reaction mix contained the following reagents (final volume 10 µl): 1 µl of reaction buffer A (10x concentrated), 2 µM oligonucleotide mix (forward and reverse), 0.5 mM ATP, 5 U of T4PNK and H_2O up to 10 µl.

LentiCRISPRv2 vector was linearized for 4 h with BsmBI restriction enzyme. The following reagents were used for the vector linearization (final volume 30 µl): 3 µl of Tango Buffer (10x concentrated), 5 µg of LentiCRISPRv2 vector, 1 µl of BsmBI restriction enzyme and H_2O up to 30 µl. Subsequently, linearized LentiCRISPRv2 vector was dephosphorylated by addition of 1 µl of calf intestinal alkaline phosphatase (CIAP) to the reaction mix. After that, vector was run on 0.5% agarose gel, cut out from the gel and purified using QIAquick Gel Extraction Kit. Then, linearized LentiCRISPRv2 was ligated for 16 h with annealed phosphorylated oligonucleotides with gRNA sequences diluted 20x in buffer A, using T4 DNA ligase at 22 °C. Ligation mix contained the following reagents (final volume 10 µl): 1 µl of T4 DNA ligase buffer (10x concentrated), 50 ng of linearized LentiCRISPRv2 vector, 0.5 µl of annealed oligonucleotides, 1 mM ATP, 2.5 U of T4 DNA ligase and H_2O up to 10 µl. Reaction was terminated by incubation of samples at 70 °C for 5 min. Next, samples were cooled down on ice, and products of ligation were transformed into Stbl3 *E. coli* strain (chapter 3.2.3). Transformed bacteria were selected with ampicillin (final concentration 100 µg/ml), plasmid DNA was isolated, and the presence of cloned oligonucleotides was verified by sequencing (Genomed Warsaw).

The obtained plasmids with appropriate gRNAs, together with psPAX2 and pMD2.G packaging plasmids, were used for production of lentiviruses and LN229 cells with CRISPR-

Cas9-mediated knockout of *CAV1* or *FLOT1* were generated by lentiviral transduction (described in chapter 3.2.9).

3.2.17 Transfection of cells with siRNA

Cells were seeded in appropriate plates 24 h before transfection. On the day of transfection, siRNAs were diluted in Opti-MEM medium to a final concentration of 10 nM. Cells were transfected with Lipofectamine® RNAiMAX transfection reagent according to the manufacturer's protocol and analyzed 72 h post transfection, unless stated otherwise. Silencing efficiency was controlled by WB or RT-qPCR (chapter 3.2.20 and 3.2.21, respectively). Sequences of the used Ambion Silencer Select siRNAs are listed in chapter 3.1.10.

For efficient *CLTC* silencing the protocol was modified as follows, 2.5×10^5 LN229 cells/well were seeded in 6-well plates and after 24 h cells were transfected with control siRNA or siRNAs against *CLTC*. Next, 48 h after transfection, 4×10^4 cells/well were re-plated on 12 mm coverslips in 24-well plates and 24 h later transfected again with the same siRNAs. Cells were analyzed 72 h after second transfection and silencing efficiency was controlled by WB. Experiments with *CLTC* silencing were performed together with Kamila Kozik, master student in the Laboratory of Cell Biology.

3.2.18 Immunofluorescence (IF) staining and image analysis

After stimulation, cells were transferred to ice, washed twice with ice-cold PBS for 5 min and fixed with 3.6% paraformaldehyde in PBS for 10 min at RT. Next, cells were washed twice with PBS and either stained directly or kept at 4 °C for later staining. Cells stimulated with anti-CD44 antibodies were additionally incubated for 5 min with ice-cold buffer containing 0.5% acetic acid and 0.5 M NaCl and washed twice with ice-cold PBS prior fixation.

For staining, cells were incubated in saponin solution I for 10 min to permeabilize the PM. Next, cells on coverslips were incubated in droplets of primary antibodies diluted in saponin solution II in a humid chamber for 1 h at RT. After that, cells were washed twice with saponin solution II, and incubated with fluorescent secondary antibodies diluted in saponin solution II for 30 min in a humid chamber at RT. To stain actin or nuclei, Phalloidin-Atto 390 (diluted 1:500) or DAPI (diluted 1:1000), respectively, were added during the incubation with secondary antibodies. Then, cells on coverslips were washed twice in PBS, briefly soaked in water and attached to glass slides using Mowiol.

Cells were imaged using LSM 710 confocal microscope (Zeiss) with EC-Plan-Neofluar 40×/1.3 oil immersion objective, and ZEN 2009 software (Zeiss) was used

for acquisition. For each experimental condition at least ten 12-bit images with resolution 1024×1024 pixels were acquired. Integral fluorescence intensity, number of vesicles and colocalization were calculated using the MotionTracking software (http://motiontracking.mpi-cbg.de) [224, 225]. Pictures were assembled in Photoshop (Adobe) with only linear adjustments of brightness and contrast.

3.2.19 Total internal reflection fluorescence (TIRF) microscopy live-cell microscopy

For TIRF live-cell imaging, LN229 cells were transfected with pEGFP-N2-AXL together with pmRFP-CLC or pmCherry-N1-PICALM using Lipofectamine® 2000 transfection reagent according to the manufacturer's protocol. Next, cells expressing AXL-EGFP and mRFP-CLC or AXL-EGFP and mCherry-PICALM were imaged using a Deltavision OMX V4 (GE Healthcare) with a 60× TIRF objective. Images were acquired every 20 s up to 10 min after the ligand administration and were further deconvolved as described elsewhere [226]. Experiments were performed by Dr. Daria Zdżalik-Bielecka during realization of her EMBO Short Term Fellowship at the Institute for Cancer Research, Oslo University Hospital, Norway.

For the generation of pEGFP-N2-AXL plasmid, *AXL* coding sequence was amplified from pcDNA3.1-AXL using forward primer 5'-TGTTCTCTCGAGATGGCGTGGCGGTGCCCCAG-3' containing XhoI restriction site and reverse primer 5'- GTGCTTGGATCCAGGCACCATCCTCCTGCCCTG-3' containing BamHI restriction site and subcloned into pEGFP-N2 vector (Clontech).

3.2.20 Protein electrophoresis and western blot (WB)

For protein analyses, cells were transferred to ice, washed 2 times with ice-cold PBS and lysed in RIPA buffer containing CLAAP (diluted 1:500), phosphatase inhibitor cocktail 2 and 3 (diluted 1:100), and DNase I (1 µg/ml). Lysates were centrifuged at 15000 g for 15 min at 4 °C and supernatants were kept for further analyses. Protein concentration was assessed with Pierce BCA Protein Assay, and samples were denatured by adding Laemmli buffer and incubated at 95 °C for 5 min.

Electrophoretic separation of proteins was performed under denaturing conditions (SDS-PAGE) on 10-15% polyacrylamide gels. Protein samples together with molecular weight marker were loaded on gels and resolved in running buffer at 60 V for 30 min, and next voltage was increased up to 100 V. After electrophoresis, proteins were transferred onto nitrocellulose membrane (GE Healthcare, cat. no. GE10600002) at 100 V for 1.5 h in transfer buffer at 4 °C. Membranes were then blocked in 5% milk (or BSA for BioID samples) in TBST for 1 h and incubated for 16 h at 4 °C with primary antibodies, diluted as described in

chapter 3.1.5. Next, membranes were washed 3 times with TBST and incubated for 1 h at RT with appropriate secondary antibodies (conjugated with HRP or infrared fluorescent dyes, listed in chapter 3.1.6). After that, membranes were washed 3 times with TBST, and signals were detected with Clarity Western ECL blotting substrate using the ChemiDoc Touch Imaging System (Bio-Rad) if HRP-conjugated secondary antibodies used, or the Odyssey infrared imaging system (LI-COR Biosciences) for secondary antibodies conjugated with infrared fluorescent dyes. Figures were assembled in Photoshop (Adobe) with only linear adjustments of brightness and contrast. Densitometric analysis of detected bands (Fig. 4.31B) was performed with Image Lab Software (Bio-Rad).

3.2.21 Real-time quantitative PCR (RT-qPCR)

For RT-qPCR total RNA was isolated using High Pure RNA Isolation Kit according to the manufacturer's protocol and the concentration of isolated RNA was assessed by NanoDrop 8000 Spectrophotometer (Thermo Fisher Scientific). One µg of isolated RNA diluted in 10 µl of H_2O was used for cDNA synthesis. First, a denaturation step was performed for 10 min at 70 °C and the denaturation mix contained the following reagents (final volume 13 µl): 10 µl diluted RNA (100 ng/µl), 1 µl of dNTP mix (10 mM), 1 µl of Random Nonamers (50 µM) and 1 µl of Oligo$(dT)_{23}$ (70 µM). After that, samples were cooled down on ice and reverse transcription was performed. Reaction mixes contained: 13 µl of denaturation mix (from the previous step), 2 µl of M-MLV reverse transcriptase buffer, 1 µl M-MLV reverse transcriptase and 4 µl of H_2O (final volume 25 µl). The prepared samples were incubated for 10 min at RT, followed by 50 min incubation at 37 °C, and finally 10 min at 90 °C. The obtained cDNA was diluted 4 times in H_2O before further analysis by RT-qPCR.

RT-qPCR was performed with a KAPA SYBR FAST qPCR Master Mix (2X) Universal Kit using a 7900HT fast real-time PCR system (Applied Biosystems). The primers used for RT-qPCR are listed in chapter 3.1.12. Data were quantified using Data Assist v2.0 software (Applied Biosystems) and the expression of target genes were normalized to the level of *ACTB* mRNA.

3.2.22 Statistical analysis

Quantitative data for statistical analysis were shown as means ± SEM (displayed as an error bar) from at least three independent experiments, unless stated otherwise. Statistical analyses were calculated in GraphPad Prism version 8 software using the Student's one sample t-test. The significance of mean comparisons was annotated as follows: ns, non-significant ($p>0.05$), *$p\leq0.05$, **$p<0.01$, and ***$p\leq0.001$, ****$p\leq0.0001$.

4. Results

4.1 Identification of AXL proximity interactome

To provide the first comprehensive analysis of AXL interactome, proximity-dependent biotin identification (BioID) was performed. BioID is based on a fusion of a mutated biotin ligase BirA-R118G (BirA*) from *Escherichia coli* to the protein of interest. Addition of biotin to the culture medium of cells expressing BirA*-tagged proteins activates the biotin ligase and induces proximity-dependent biotinylation of proteins that are near-neighbors of the fusion protein [227]. Next, biotinylated proteins are isolated by affinity capture and identified by mass spectrometry (Fig. 4.1). Given this, BioID allows identification of weak and transient interactions but also proteins which are located in close proximity of the tested protein.

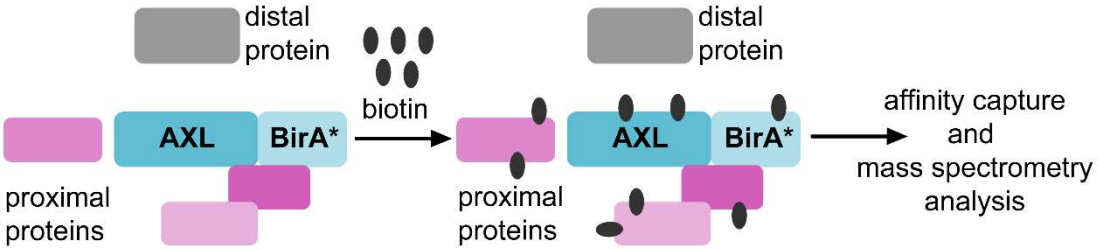

Fig. 4.1 Schematic representation of the BioID method

4.1.1 Purification of GAS6-Myc-His

To identify AXL interactome under basal and ligand-stimulated conditions, C-terminally-modified Myc-His-tagged version of human GAS6 was purified from culture supernatants. To this end, HEK293 cells were transfected with plasmid pcDNA3.1-GAS6-Myc-His containing the GAS6-Myc-His coding sequence preceded with the secretion signal from the V-J2-C region of the mouse Ig kappa-chain (Fig. 4.2A). The latter allows secretion of GAS6-Myc-His to the culture media for its subsequent purification. To ensure efficient production of a recombinant protein, the clonal selection of transfected cells was performed. As shown in Fig. 4.2B, secretion of GAS6-Myc-His differed between clones, and the highest level of secreted ligand was detected in the culture medium of clone 1, therefore it was further used for the production of conditioned medium and the purification of GAS6-Myc-His (Fig. 4.2C). The purified GAS6-Myc-His (hereafter called GAS6) was biologically active, since it induced phosphorylation of AXL in a dose-dependent manner in glioblastoma LN229 cells (Fig. 4.2D).

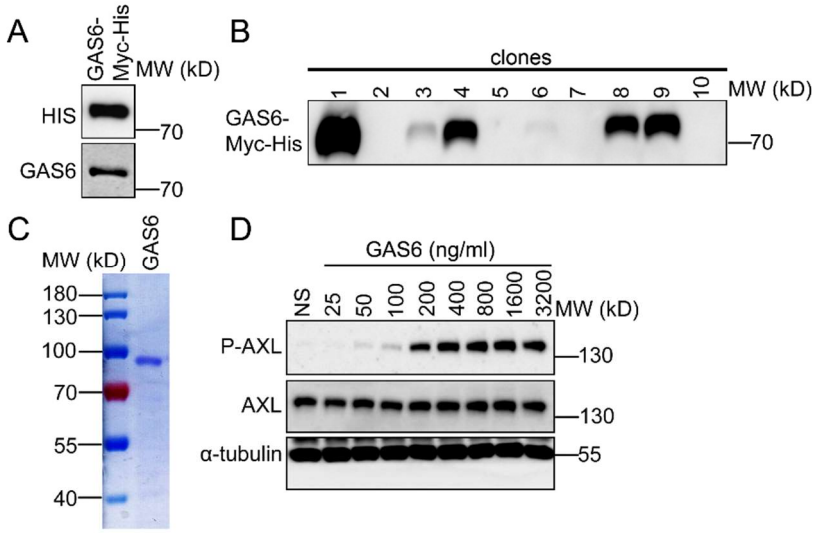

Fig. 4.2 Dose-dependent phosphorylation of AXL by purified Gas6
A Western blot showing expression of GAS6-Myc-His in HEK293 cells after transient transfection with pcDNA3.1-GAS6-Myc-His plasmid. Antibodies recognizing HIS tag or GAS6 were used for immunodetection of proteins. **B** Western blot showing the level of GAS6-Myc-His in the culture supernatant of clonally selected, stably transfected HEK293 cells. Antibodies recognizing GAS6 were used for immunoblotting. **C** A Coomassie stained gel of GAS6-Myc-His (GAS6) purified from culture medium collected from clone 1 of HEK293 cells expressing GAS6-Myc-His. **D** Western blot showing phosphorylation of AXL (P-AXL, Y702) after stimulation of LN229 cells with increasing concentration of GAS6. Serum-starved LN229 cells were incubated with the ligand for 10 min and immunoblotted against the indicated proteins. α-tubulin served as a loading control. NS- non-stimulated cells.

4.1.2 Generation of cell lines for BioID

HEK293 cells, which do not express AXL and AXL-expressing LN229 cells were used to determine AXL proximity interactome (Fig. 4.3A). HEK293 cells were selected since they are routinely used in the BioID assay [227-229], and LN229 cells as they represent a cancer relevant model to investigate cellular functions of AXL.

To perform proximity-dependent biotin identification, HA-tagged, mutated biotin ligase BirA-R118G-HA (hereafter denoted as BirA*-HA) was fused to the C-terminal part of AXL, generating AXL-BirA*-HA fusion protein (Fig. 4.3B). To this end, *AXL* coding sequence was subcloned into pcDNA3.1-BirA*-HA vector to generate pcDNA3.1-AXL-BirA*-HA plasmid. Next, both plasmids were used for transfection of HEK293 cells. The expression of BirA*-HA, which further served as a control for BioID, and AXL-BirA*-HA was verified by WB in HEK293 cells (Fig. 4.3C). To check the functionality of AXL-BirA*-HA fusion protein, its activation was analyzed upon GAS6 stimulation. As shown in Fig. 4.3D, GAS6 triggered phosphorylation of AXL-BirA*-HA, which confirmed that AXL-BirA*-HA fusion protein was biologically active. Additionally, the immunofluorescence (IF) analysis showed that AXL-BirA*-HA fusion protein localized properly to the plasma membrane (Fig. 4.3E).

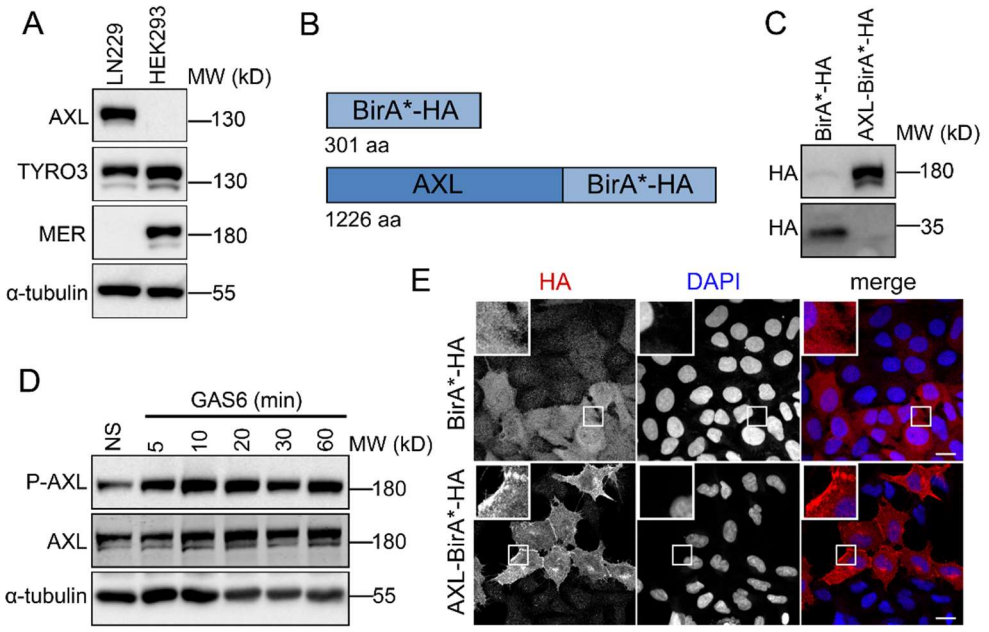

Fig. 4.3. Generation and validation of tools for BioID
A Western blot showing expression of AXL, TYRO3 and MER (TAM receptors) in LN229 and HEK293 cells. Cells were lysed and immunoblotted against the indicated proteins. α-tubulin served as a loading control. **B** Schematic representation of BirA*-HA and AXL-BirA*-HA proteins generated for the purpose of the BioID analysis. **C** Western blot showing expression of BirA*-HA and AXL-BirA*-HA in HEK293 cells after transient transfection with pcDNA3.1-BirA*-HA or pcDNA3.1-AXL-BirA*-HA plasmids, respectively. Antibodies recognizing HA were used for immunodetection of proteins. **D** Western blot showing the phosphorylation of AXL-BirA*-HA protein (P-AXL, Y702) upon stimulation with GAS6. Serum-starved HEK293 cells expressing AXL-BirA*-HA were stimulated with GAS6 for the indicated time periods, lysed and immunoblotted against the indicated proteins. α-tubulin was used as a loading control. NS- non-stimulated cells. **E** Confocal images showing expression of BirA*-HA and AXL-BirA*-HA in HEK293 cells after transient transfection with pcDNA3.1-BirA*-HA or pcDNA3.1-AXL-BirA*-HA plasmids, respectively. Cells were fixed and stained with antibodies recognizing HA (red), DAPI was used to visualize nuclei (blue). Insets show magnified views of boxed regions in the main images. Scale bars: 20 μm.

However, since the obtained population of cells was heterogeneous with respect to BirA*-HA or AXL-BirA*-HA expression (Fig. 4.3E), a clonal selection was performed. The presence of BirA*-HA or AXL-BirA*-HA proteins in the generated clones was verified by WB and IF. The latter additionally allowed confirming their proper cellular localization. As shown in Fig. 4.4A, among 27 clones tested, AXL-BirA*-HA was detected only in six of them (clones 3, 6, 7, 15, 22, 24). The highest level of AXL-BirA*-HA protein was detected for clone 15, nevertheless this population of cells was still heterogeneous, and only around 60% of cells expressed AXL-BirA*-HA (Fig. 4.4B). Therefore, yet another round of clonal selection was applied.

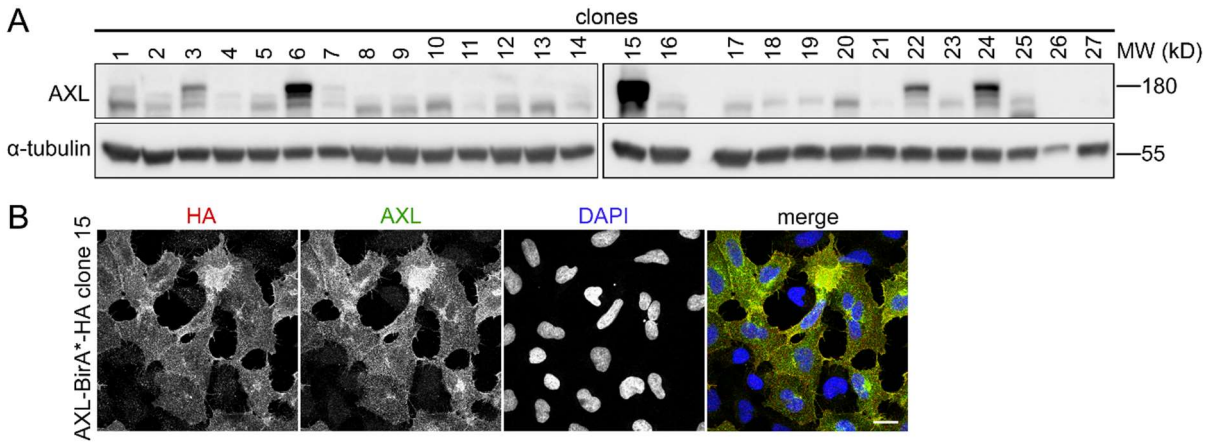

Fig. 4.4 Generation of HEK293 cell line stably expressing AXL-BirA*-HA fusion protein
A Western blot analyses of AXL-BirA*-HA protein level in clones generated from AXL-BirA*-HA-expressing HEK293 cells. Cells were lysed and immunoblotted against AXL. α-tubulin was used as a loading control. **B** Confocal images showing expression of AXL-BirA*-HA in HEK293 cells after clonal selection. Cells of HEK293 AXL-BirA*-HA clone 15 were fixed and stained with anti-HA (red), anti-AXL (green) antibodies and DAPI was used to visualize nuclei (blue). Scale bar: 20 μm.

The second clonal selection was sufficient to generate HEK293 cell line in which AXL-BirA*-HA was detected in almost all cells (Fig. 4.5). Of note, only one round of clonal selection was required for generation of BirA*-HA-expressing HEK293 cell line (Fig. 4.5).

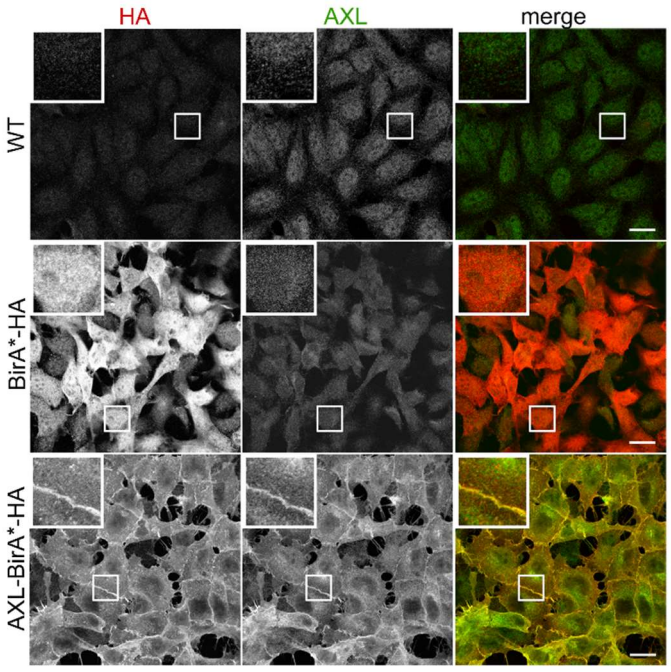

Fig. 4.5 HEK293 cell lines stably expressing BirA*-HA or AXL-BirA*-HA proteins
Confocal images of HEK293 cells stably expressing BirA*-HA or AXL-BirA*-HA showing the localization of ectopically expressed proteins. Cells were fixed and stained with anti-HA (red) and anti-AXL (green) antibodies. Insets show magnified views of boxed regions in the main images. WT- wild type HEK293 cells. Scale bars: 20 μm.

The same strategy was initially used for the generation of LN229 cells stably expressing BirA*-HA or AXL-BirA*-HA. Unfortunately, this method was largely ineffective

in case of this cell line, because of low transfection efficiency, and after double clonal selection cells were still largely heterogenous with respect to AXL-BirA-HA* expression (Fig. 4.6A). Therefore, the sequences encoding BirA*-HA and AXL-BirA*-HA were subcloned into pLenti-CMV-MCS-GFP-SV-puro plasmid and lentiviral transduction was used to establish LN229 cells expressing BirA*-HA or AXL-BirA*-HA. This method allowed generating desired cell lines without subsequent clonal selection, since BirA*-HA or AXL-BirA*-HA was detected in almost all LN229 cells after lentiviral transduction followed by antibiotic selection (Fig. 4.6B).

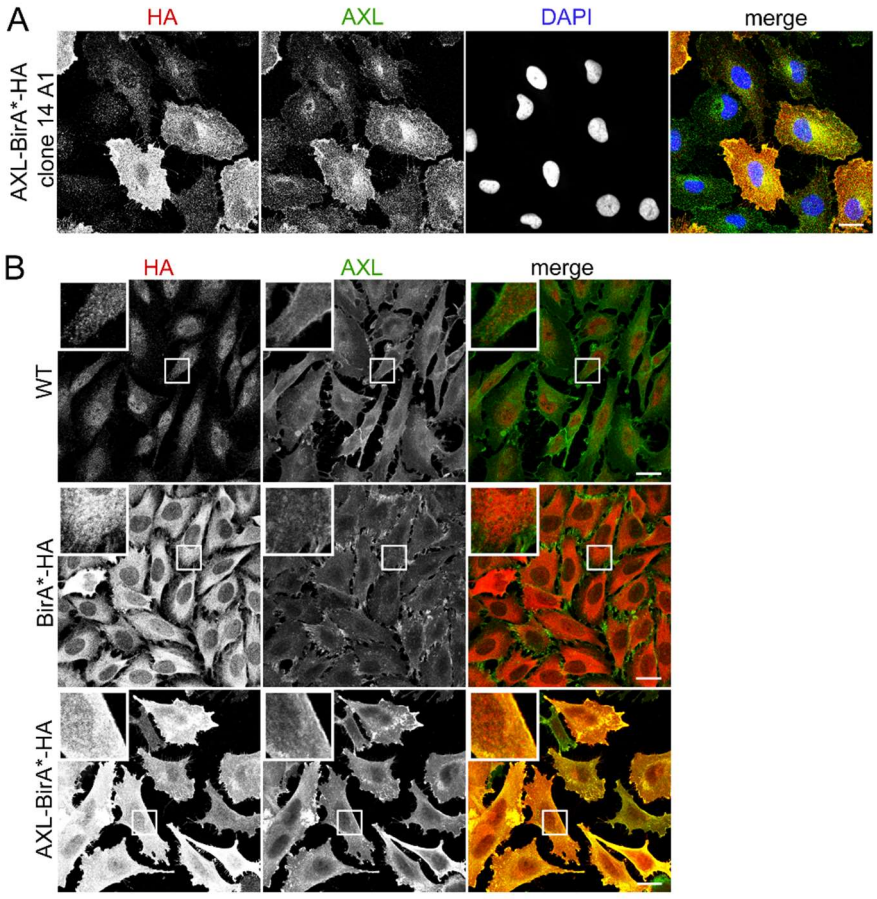

Fig. 4.6 Generation of LN229 cell lines stably expressing BirA*-HA or AXL-BirA*-HA proteins
A Confocal images of LN229 cells expressing AXL-BirA*-HA after transfection and double clonal selection. Cells were transfected with pcDNA3.1-AXL-BirA*-HA plasmid, fixed and stained with anti-HA (red), anti-AXL (green) antibodies and DAPI was used to stain nuclei (blue). Insets show magnified views of boxed regions in the main images. Scale bar: 20 µm. **B** Confocal images of LN229 stably expressing BirA*-HA or AXL-BirA*-HA. Cells were transduced with lentiviruses, fixed and stained with anti-HA (red) and anti-AXL (green) antibodies. Insets show magnified views of boxed regions in the main images. WT- wild type LN229 cells Scale bars: 20 µm.

4.1.3 Proximity-dependent biotin identification (BioID)

The generated HEK293 and LN229 cells expressing BirA*-HA or AXL-BirA*-HA proteins were next used for the BioID assay. To ensure efficient protein biotinylation, LN229 AXL-BirA*-HA cells were incubated with biotin for various time periods and the

biotinylation of proteins was assessed by WB (Fig. 4.7A). In line with the literature [227] and our data, 24 h of biotin incubation was selected for further experiments as it ensured the most efficient protein biotinylation. Thus, HEK293 and LN229 cell lines stably expressing BirA*-HA or AXL-BirA*-HA were incubated with biotin for 24 h in the presence or absence of GAS6. Following cell lysis, biotinylated proteins were isolated using streptavidin-coated magnetic beads. Prior to mass spectrometry analysis, samples before (input) and after (output) streptavidin-mediated pull-down were analyzed by WB. The results showed significant enrichment of biotinylated proteins in the output samples, in comparison to the input, both in HEK293 and LN229 cells (Fig. 4.7B and C). Therefore, mass spectrometry analysis was performed to identify biotinylated AXL proximity interactors.

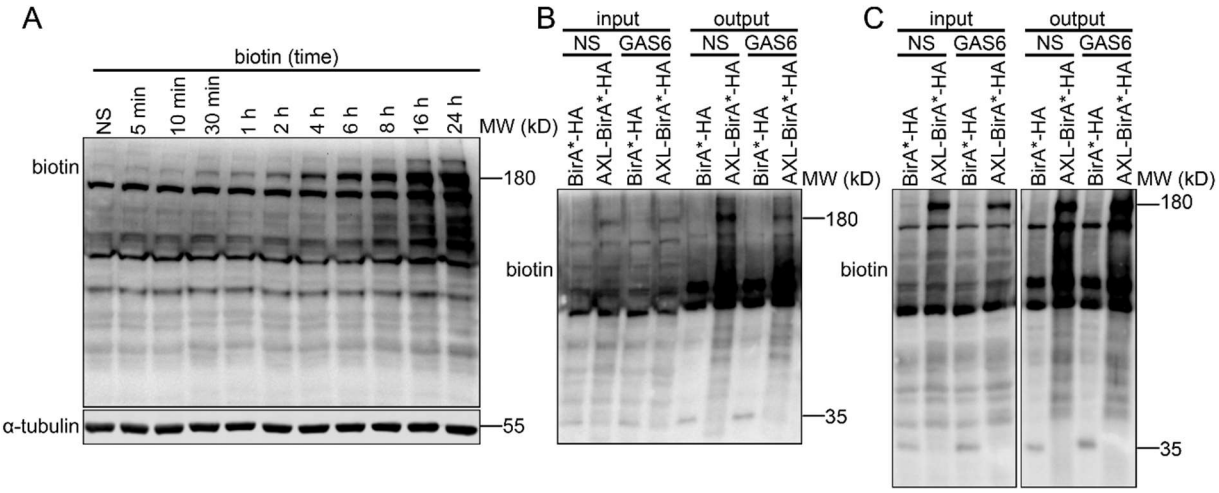

Fig. 4.7 Proximity-dependent biotin identification (BioID)
A Western blot showing protein biotinylation in LN229 AXL-BirA*-HA cells incubated with biotin for increasing time periods. Antibodies against biotin were used for immunoblotting. α-tubulin served as a loading control. **B, C** Western blot showing the biotinylation of proteins in HEK293 (B) and LN229 (C) cells expressing BirA*-HA or AXL-BirA*-HA before (input) and after (output) pull-down with streptavidin-coated magnetic beads. Cells were serum-starved and incubated with biotin for 24 h in the presence or absence of GAS6. Antibodies recognizing biotin were used for immunoblotting. NS- non-stimulated cells, GAS6- GAS6-stimulated cells.

4.1.4 Analysis of identified AXL proximity interactors

To distinguish AXL proximity interactors from false positive hits, the lists of proteins identified in cells expressing AXL-BirA*-HA fusion protein +/-GAS6 were compared to the ones found in control cells expressing BirA*-HA. The following criteria were applied to consider a protein as an AXL proximity interactor: i) identification in at least 2 out of 3 experiments, ii) with ≥ 2 peptides at least in one experiment, iii) with three times higher sum of Mascot scores in AXL-BirA*-HA samples in comparison to the control.

In HEK293 cells, 116 and 151 proteins fulfilling the criteria were found in non-stimulated (NS) and GAS6-treated samples, respectively (Fig. 4.8A, Table S1 in supplementary materials). Similarly, in LN229 cells 114 proteins in non-stimulated samples

and 147 in samples from GAS6-stimulated cells were identified (Fig. 4.8B, Table S2 in supplementary materials). In general, more proteins were identified in GAS6-stimulated than in non-stimulated cells. Among hits identified in HEK293 cells, 26 proteins were unique for non-stimulated cells, 61 for GAS6-stimulated cells and 90 proteins were common for both conditions (Fig. 4.8A, Table S1 in supplementary materials). In case of proteins identified in LN229 cells, 21 and 64 were unique for non-stimulated and GAS6-stimulated conditions, respectively, while 93 proteins were common for both groups (Fig. 4.8B, Table S2 in supplementary materials).

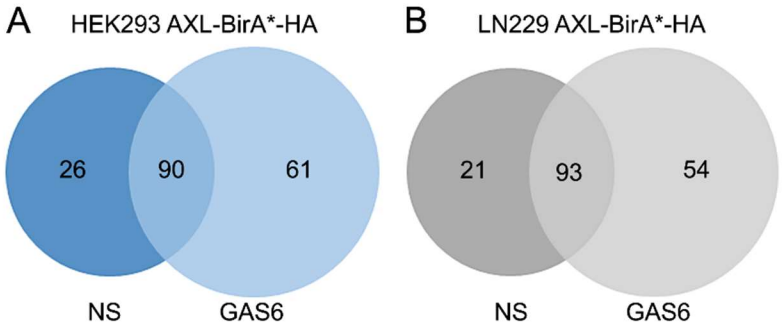

Fig. 4.8 Venn diagrams showing the number of identified AXL interactors in HEK293 and LN229 cells

A, B Analysis of the number of identified AXL proximity interactors in non-stimulated and GAS6-stimulated HEK293 (A) and LN229 (B) cells expressing AXL-BirA*-HA fusion protein. NS- non-stimulated cells, GAS6- GAS6-stimulated cells.

Next, the identified AXL proximity interactors underwent the Gene Ontology (GO) analysis of biological processes. As shown in Fig. 4.9, this analysis indicated the enrichment of proteins implicated in axonogenesis, cell junction organization, several actin-related processes, supramolecular fiber organization and angiogenesis among AXL interactors, both in non-stimulated and GAS6-stimulated samples. Additionally, in GAS6-stimulated cells, AXL was found to interact with proteins involved in receptor-mediated endocytosis and endosomal transport, signaling, positive regulation of GTPase activity, cell-substrate adhesion and positive regulation of migration, among others (Fig. 4.9).

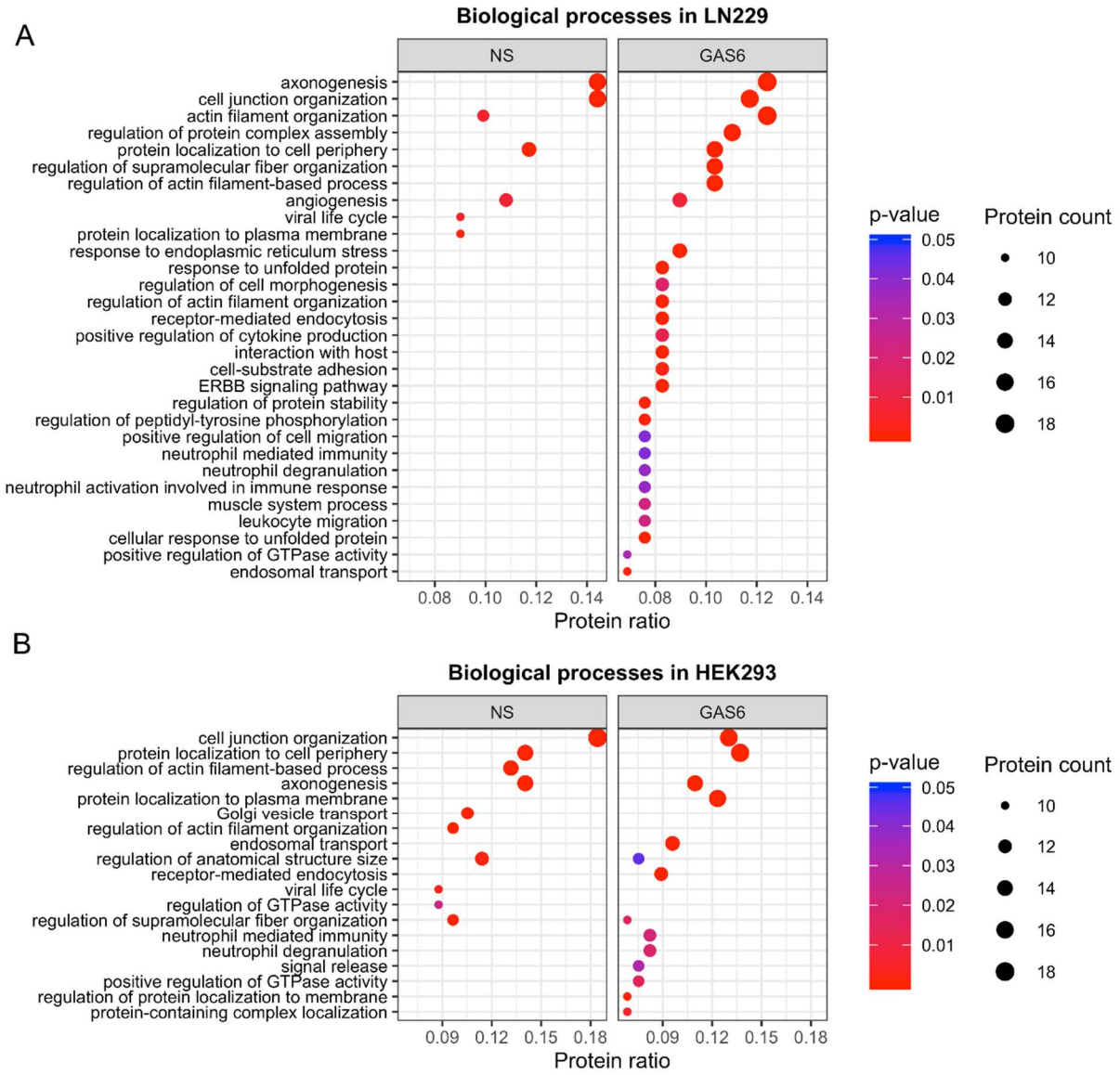

Fig. 4.9 The Gene Ontology analyses of biological processes of the identified AXL interactors

A, B The Gene Ontology (GO) analyses of biological processes among the identified AXL proximity interactors in LN229-AXL-BirA*-HA (A) and HEK293-AXL-BirA*-HA (B) cells. NS- non-stimulated cells, GAS6- GAS6-stimulated cells.

Similarly to the GO analysis of biological processes, the GO analysis of molecular functions highlighted that AXL proximity interactors were components of cytoskeleton and were involved in actin binding (Fig. 4.10A). Additionally, they were implicated in binding of cadherins, phosphatidylinositols, phospholipids or small GTPases and functioned as kinase activity regulators (Fig. 4.10A). The GO analysis of cellular components revealed that AXL proximity interactors localized to cell-cell and cell-substrate junctions, focal adhesions (FAs), leading edge and lamellipodium, among others (Fig. 4.10B). Altogether, the performed GO analyses linked AXL with processes and structures involving actin cytoskeleton, its regulation and rearrangements (Fig. 4.9 and 4.10). These processes were investigated in a separate study

in the Laboratory of Cell Biology [89], while this thesis focused on AXL proximity interactors linked with intracellular trafficking.

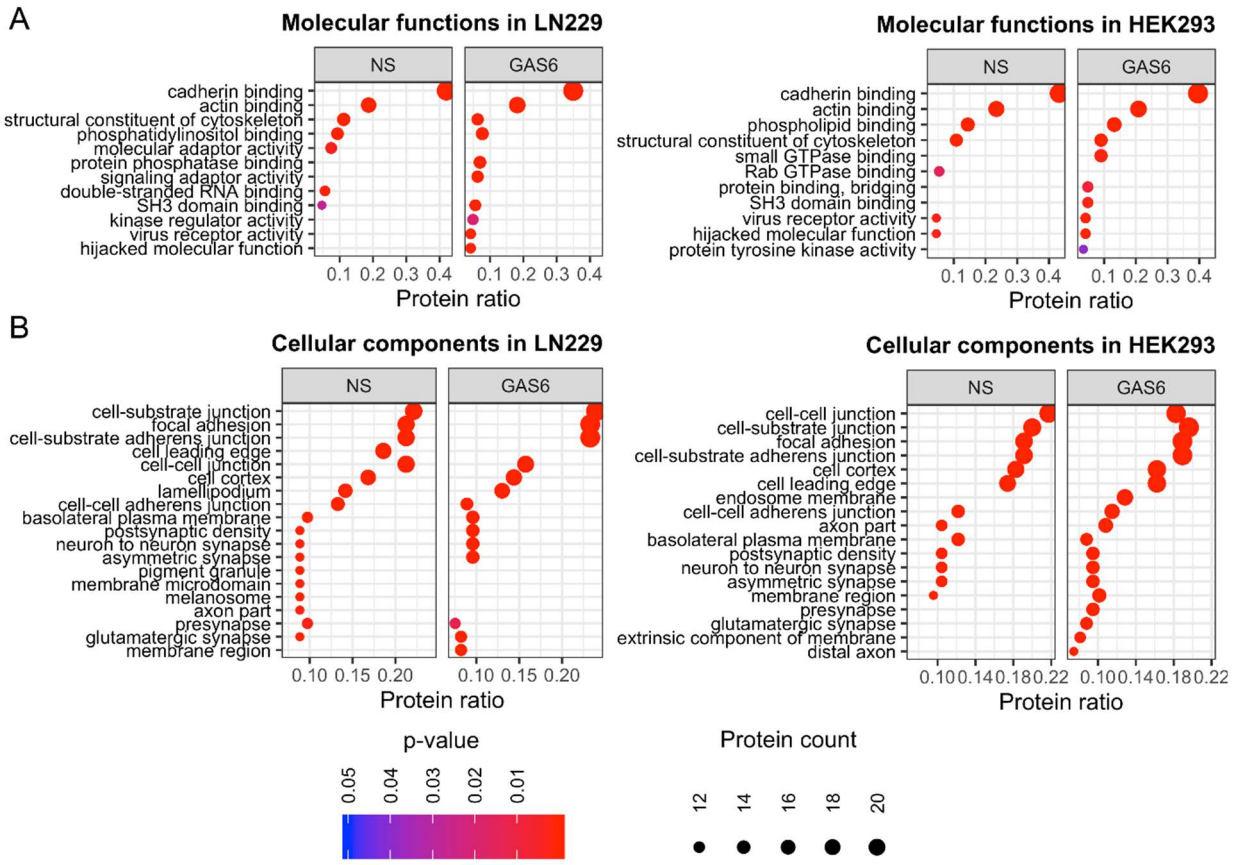

Fig. 4.10 The Gene Ontology analyses of molecular functions and cellular components of the identified AXL interactors

A, B The Gene Ontology (GO) analyses of molecular functions (A) and cellular components (B) among the identified AXL proximity interactors in LN229-AXL-BirA*-HA and HEK293-AXL-BirA*-HA cells. NS- non-stimulated cells, GAS6- GAS6-stimulated cells.

4.1.5 Proteins implicated in intracellular trafficking among identified AXL proximity interactors

Manual annotations of AXL proximity interactors based on GeneCards (https://www.genecards.org) and UniProt (https://www.uniprot.org/) databases as well as literature search showed that many AXL proximity interactors mediated various stages of vesicular trafficking starting from the internalization via various types of endocytosis, both CME and CIE, intracellular transport between endosomes, ER-to-Golgi or Golgi-to-endosomes transport, endosomal recycling, secretion and exocytosis (Fig. 4.11, Table 4.1, Table S1 and S2 in supplementary materials).

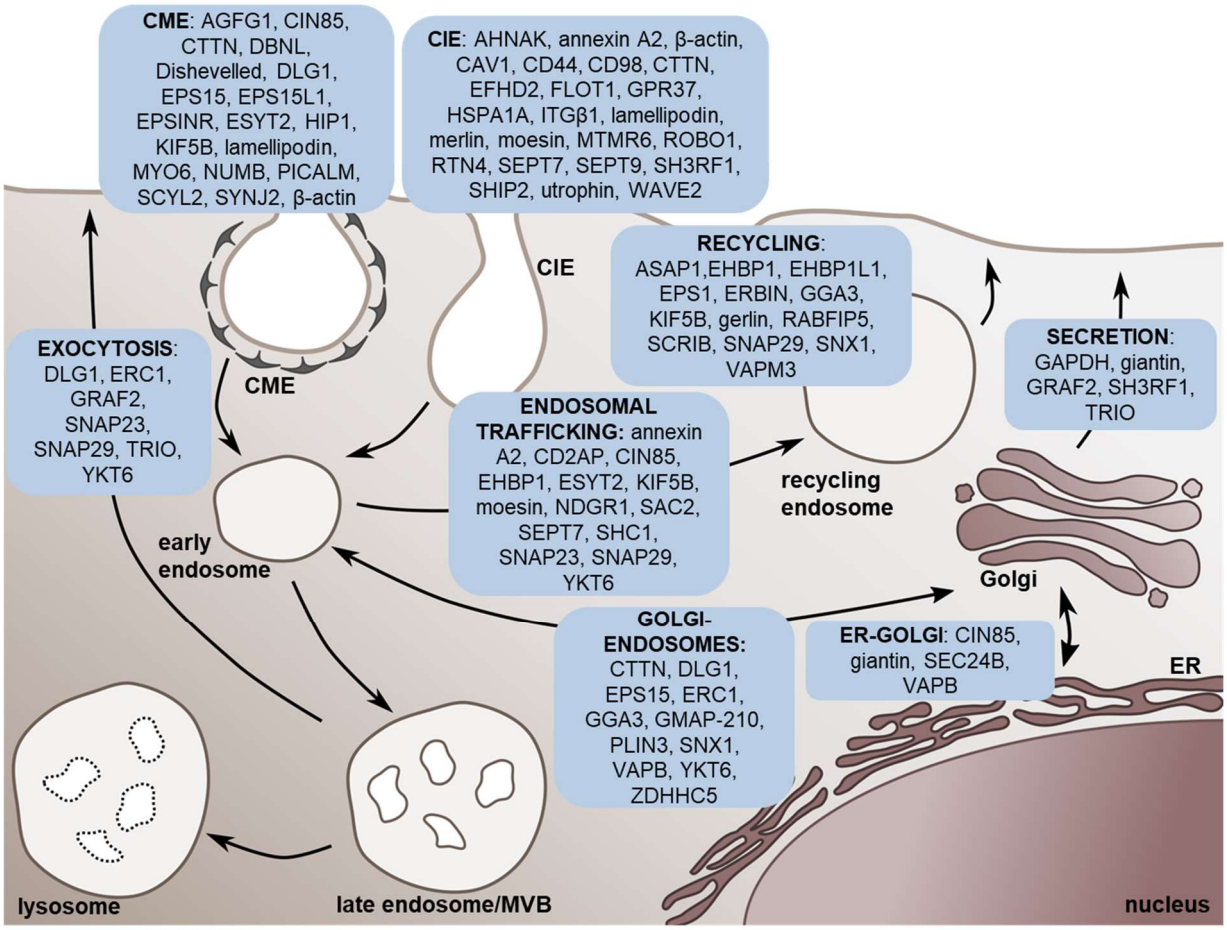

Fig. 4.11 Scheme of AXL proximity interactors involved in intracellular trafficking in LN229 cells

Table 4.1. AXL proximity interactors implicated in intracellular trafficking

No	Gene Symbol	Protein Name	Accession	Role in endocytosis	HEK293		LN229		References
					NS	GAS6	NS	GAS6	
1.	ACTB	β-Actin	P60709	Clathrin-mediated and -independent endocytosis	-	+	+	-	[137, 230]
2.	AGFG1	AGFG1	P52594	Clathrin-mediated endocytosis	-	+	-	+	[231, 232]
3.	AHNAK	AHNAK	Q09666	Clathrin-independent endocytosis	+	+	+	+	[179]
4.	ANKS1A	ANKS1A	Q92625	Endocytic recycling, endoplasmic reticulum-to-Golgi transport	-	+	-	-	[233, 234]
5.	ANXA1	Annexin 1	P04083	Multivesicular body biogenesis	-	+	-	-	[235]
6.	ANXA2	Annexin 2	P07355	Endocytic trafficking	+	+	+	-	[236, 237]
7.	AP3D1	AP3D1	O14617	Post-Golgi trafficking, secretion	-	+	-	-	[238-240]
8.	ARHGAP10	ARHGAP10	A1A4S6	Clathrin-independent endocytosis	-	-	-	+	[188]
9.	ARHGAP21	ARHGAP21	Q5T5U3	Endocytic trafficking, actin polymerization	+	-	-	-	[241]
10.	ARL13B	ARL13B	Q3SXY8	Endocytic recycling	+	-	-	-	[242]
11.	ASAP1	ASAP1	Q9ULH1	Endocytic recycling, autophagy	-	-	-	+	[243, 244]
12.	CAV1	Caveolin 1	Q03135	Clathrin-independent endocytosis	-	-	+	+	[154, 245]
13.	CBL	CBL	P22681	Receptor-mediated endocytosis, degradation	-	+	-	-	[246-248]
14.	CCDC88A	Girdin	Q3V6T2	Clathrin-mediated endocytosis	+	-	-	-	[249]
15.	CD2AP	CD2AP	Q9Y5K6	Endocytic trafficking	+	+	+	+	[250-252]
16.	CD44	CD44	P16070	Clathrin-independent endocytosis	-	-	+	+	[143, 179]
17.	CLINT1	EpsinR	Q14677	Clathrin-mediated endocytosis	+	+	-	-	[253-255]
18.	COPG1	COPI	Q9Y678	Endoplasmic reticulum-to-Golgi transport	+	+	-	-	[256, 257]
19.	COPG2	COPG2	Q9UBF2	Endoplasmic reticulum-to-Golgi transport	+	+	-	-	[258, 259]
20.	CTNND1	Catenin delta-1	O60716	Endocytosis of the dynamic E-cadherin-Bazooka complex	+	+	+	+	[260]
21.	CTTN	CTTN	Q14247	Clathrin-mediated and -independent endocytosis	+	+	-	+	[261, 262]
22.	DBNL	DBNL	Q9UJU6	Clathrin-mediated endocytosis	-	-	+	+	[263, 264]
23.	DLG1	DLG1	Q12959	Endocytic trafficking	+	+	+	+	[265]
24.	DVL2	Dishevelled	O14641	Clathrin-mediated endocytosis	-	+	-	-	[266]

25.	DYM	Dymeclin	Q7RTS9	Endoplasmic reticulum-to-Golgi transport	+	-	-	-	[267]
26.	EFHD2	Swiprosin-1	Q96C19	Clathrin-independent endocytosis	-	-	-	+	[268]
27.	EHBP1	EHBP1	Q8NDI1	Endocytic recycling, actin reorganization	+	+	+	+	[269-271]
28.	EHBP1L1	EHBP1L1	Q8N3D4	Endocytic recycling	-	-	+	+	[272]
29.	EMD	Emerin	P50402	Autophagy	-	+	-	-	[273]
30.	EPS15	EPS15	P42566	Clathrin-mediated endocytosis, post-Golgi trafficking, endocytic recycling	-	+	-	+	[274, 275]
31.	EPS15L1	EPS15L1	Q9UBC2	Clathrin-mediated endocytosis	+	+	+	+	[135, 276]
32.	ERBIN	Erbin	Q96RT1	Endocytic recycling	+	+	+	+	[277]
33.	ERC1	RAB6IP2, ERC1	Q8IUD2	Endosome-to-Golgi transport, exocytosis, secretion	-	-	+	+	[278-281]
34.	ESYT2	Extended synaptotagmin-2	A0FGR8	Clathrin-mediated endocytosis	-	-	+	+	[282]
35.	FAM129A	FAM129A	Q9BZQ8	Autophagy	-	-	+	+	[283]
36.	FLOT1	Flotillin 1	O75955	Clathrin-independent endocytosis	-	-	+	+	[168, 169]
37.	FLOT2	Flotillin 2	Q14254	Clathrin-independent endocytosis, endocytic recycling	+	+	-	-	[169, 284]
38.	GGA3	GGA3	Q9NZ52	Endocytic recycling	-	+	-	+	[285, 286]
39.	GAPDH	GAPDH	P04406	Endoplasmic reticulum-to-Golgi transport, intracellular trafficking	-	-	-	+	[287, 288]
40.	GOLGB1	Giantin	Q14789	Secretion	+	+	-	+	[289]
41.	GPR37	GPR37	O15354	Clathrin-independent endocytosis	-	-	+	-	[179]
42.	HIP1	HIP1	O00291	Clathrin-mediated endocytosis	-	+	-	-	[290, 291]
43.	HSPA1A	HSPA1A	P0DMV8	Clathrin-independent endocytosis	-	+	-	+	[292]
44.	INPP5F	INPP5F, SAC2	Q9Y2H2	Clathrin-mediated and -independent endocytosis	-	-	-	+	[293]
45.	INPPL1	SHIP2	O15357	Clathrin-independent endocytosis	-	+	+	+	[192, 294]
46.	KIF5B	KIF5B	P33176	Clathrin-mediated endocytosis, phagocytosis	-	+	+	-	[295, 296]
47.	LRBA	LRBA	P50851	Endocytic trafficking, recycling, autophagy	-	+	-	-	[297]
48.	MARCKS	MARCKS	P29966	Endocytic trafficking	+	+	+	+	[298, 299]
49.	MICALL1	MICALL1	Q8N3F8	Endocytic trafficking and recycling	+	+	-	-	[300-302]

50.	MSN	Moesin	P26038	Clathrin-mediated endocytosis, multivesicular body biogenesis	-	-	+	-	[303-305]
51.	MTMR6	MTMR6	Q9Y217	Clathrin-independent endocytosis, autophagy	-	-	-	+	[306, 307]
52.	MYO1B	MYO1B	O43795	Membrane invagination during post-Golgi vesicle formation	+	+	-	-	[308, 309]
53.	MYO6	MYO6	Q9UM54	Clathrin-mediated endocytosis	-	+	-	+	[310, 311]
54.	NDGR1	NDGR1	Q92597	Endocytic trafficking	-	+	+	+	[312]
55.	NF1	NF1	P21359	Clathrin-independent endocytosis	+	+	-	-	[313, 314]
56.	NF2	Merlin	P35240	Endocytic trafficking and recycling, clathrin-independent endocytosis	+	-	-	+	[315-317]
57.	NUMB	NUMB	P49757	Clathrin-mediated endocytosis	+	+	-	+	[136, 318]
58.	NUMBL	NUMBL	Q9Y6R0	Clathrin-mediated endocytosis	+	-	-	-	[319, 320]
59.	OCLN	Occludin	Q16625	Endocytic trafficking and secretion	+	+	-	-	[321, 322]
60.	PICALM	PICALM	Q13492	Clathrin-mediated endocytosis	+	+	-	-	[134, 323]
61.	PLIN3	Perilipin 3	O60664	Endosome-to-Golgi transport	-	-	+	+	[324, 325]
62.	PTPN11	SHP2	Q06124	Endocytic trafficking	-	-	-	+	[326, 327]
63.	RAB11FIP1	RAB11FIP1	Q6WKZ4	Endocytic recycling, endosome-to-Golgi transport, secretion	+	+	-	-	[328-330]
64.	RAB11FIP2	RAB11FIP2	Q7L804	Endocytic recycling	-	+	-	-	[331, 332]
65.	RAB11FIF5	RAB11FIP5	Q9BXF6	Endocytic recycling, secretion	-	+	-	+	[333-335]
66.	RAPH1	Lamellipodin	Q70E73	Clathrin-mediated and -independent endocytosis	-	-	+	+	[192, 336]
67.	ROBO1	ROBO1	Q9Y6N7	Clathrin-independent endocytosis	-	-	+	+	[195]
68.	RTN4	Reticulon-4	Q9NQC3	Clathrin-independent endocytosis	-	-	-	+	[179]
69.	SCRIB	SCRIB	Q14160	Regulation of retromer localization and cargo sorting; endocytic recycling	+	+	+	+	[337, 338]
70.	SCYL2	SCYL2	Q6P3W7	Clathrin-mediated endocytosis	-	+	-	-	[339]
71.	SEC24B	SEC24B	O95487	Endoplasmic reticulum-to-Golgi transport	+	+	-	+	[340, 341]
72.	SEPT7	Septin 7	Q16181	Endocytic trafficking	+	+	+	+	[342, 343]
73.	SEPT9	Septin 9	Q9UHD8	Endosomal sorting	+	+	+	+	[343, 344]

74.	SH3KBP1	CIN85	Q96B97	Endosomal sorting, clathrin-mediated endocytosis, degradation	-	-	+	+	[246, 345, 346]
75.	SH3RF1	SH3RF1	Q7Z6J0	Clathrin-independent endocytosis, secretion	-	-	-	+	[347, 348]
76.	SLC3A2	CD98	P08195	Clathrin-independent endocytosis	+	+	+	+	[179]
77.	SLITRK5	SLITRK5	O94991	Endocytic trafficking	+	-	-	-	[349]
78.	SNAP23	SNAP23	O00161	Endocytic trafficking	+	+	+	+	[350-352]
79.	SNAP29	SNAP29	O95721	Endocytic trafficking and recycling	+	+	+	+	[353-355]
80.	SNX1	SNX1	Q13596	Endocytic trafficking and recycling	+	+	+	+	[356-358]
81.	SNX2	SNX2	O60749	Endocytic trafficking and recycling	-	+	-	-	[357, 359]
82.	SNX6	SNX6	Q9UNH7	Endocytic recycling, endosome-to-Golgi transport	-	+	-	-	[360-362]
83.	SYNJ2	Synaptojanin 2	O15056	Clathrin-mediated endocytosis	-	+	-	+	[363]
84.	TRIO	TRIO	O75962	Post-Golgi trafficking	-	+	-	+	[364]
85.	TRIP11	GMAP-210	Q15643	Secretion	+	+	-	+	[365]
86.	UTRN	Utrophin	P46939	Caveolae-mediated endocytosis	+	+	+	+	[366]
87.	VAMP3	VAMP3	Q15836	Endocytic recycling	-	+	-	+	[367, 368]
88.	VAPB	VAPB	O95292	Endoplasmic reticulum-to-Golgi, endosome-to-Golgi transport	-	-	+	+	[369, 370]
89.	WASF2	WAVE2	Q9Y6W5	Clathrin-independent endocytosis	-	-	-	+	[371, 372]
90.	YKT6	YKT6	O15498	Endocytic trafficking, secretion	+	+	+	+	[373-375]
91.	ZDHHC5	ZDHHC5	Q9C0B5	Endosome-to-Golgi transport	+	+	+	+	[376]
92.	ZFYVE16	Endofin	Q7Z3T8	Clathrin-mediated endocytosis	-	+	-	-	[377]

NS- non-stimulated cells, GAS6- GAS6-stimulated cells

+ protein was identified as AXL proximity interactor in a given sample
- protein was not identified as AXL proximity interactor in a given sample

4.2 Involvement of AXL and activation of its kinase domain in the internalization of GAS6-AXL complexes

Since endocytosis is an important regulator of RTK function [124, 126], the broad representation of proteins involved in intracellular trafficking among AXL proximity interactors implies that it may also regulate the biology of AXL. Thus, as the endocytic trafficking of AXL and other TAM receptors has not been studied, the characterization of this process was undertaken.

4.2.1 The role of GAS6 in endocytosis of AXL

LN229 cells were selected as the main cellular model to study AXL endocytosis, as they display high endogenous level of the receptor (Fig. 4.3A) and were used for the identification of AXL interactome (Fig. 4.7-4.10). To check whether GAS6 triggered internalization of AXL, the level of plasma membrane AXL was analyzed by the surface biotinylation assay. As a positive control of the experiment, the surface level of EGFR was analyzed upon stimulation with its ligand EGF. Thus, serum-starved LN229 cells were stimulated with GAS6 or EGF and subsequently incubated on ice with EZ-Link™ Sulfo-NHS-SS-biotin to allow biotin labelling of surface proteins. Next, cells were lysed and incubated with NeutraVidin™ agarose resin to capture biotinylated proteins. After pull-down, samples were analyzed by WB. As shown in Fig. 4.12A, EGF stimulation decreased PM level of EGFR, which reflected ligand-induced endocytosis of EGFR and served as a control. Similarly, stimulation of cells with GAS6 reduced the surface level of AXL (Fig. 4.12A), which suggested that AXL was also internalized into the cells after ligand stimulation.

Next, tools and protocols for visualization of AXL endocytosis were generated and optimized. To this end, serum-starved LN229 cells were stimulated with GAS6, fixed and stained with anti-Myc and anti-AXL antibodies to label the ligand and the receptor, respectively. Confocal microscopy revealed that GAS6 stimulation triggered the formation of intracellular vesicles positive for both GAS6 and AXL. Additionally, siRNA-mediated silencing of *AXL* showed that AXL staining was specific, as receptor-positive vesicles disappeared in cells depleted of AXL (Fig. 4.12B). Efficient *AXL* silencing was confirmed by WB (Fig. 4.12C).

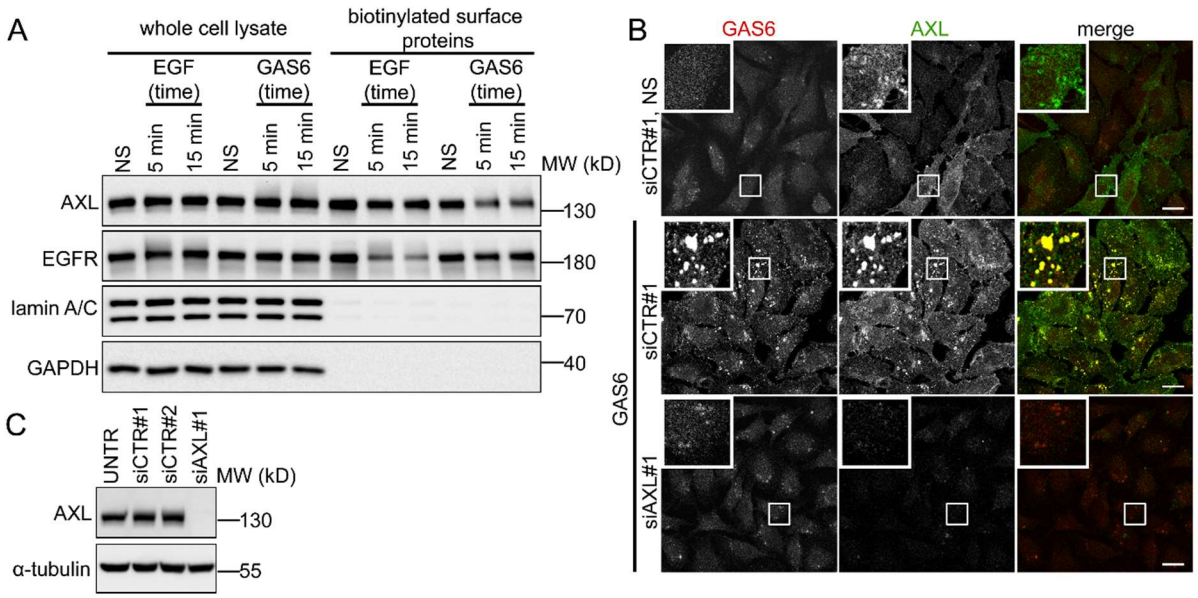

Fig. 4.12 The role of GAS6 in AXL internalization
A Western blot showing levels of AXL and EGFR after stimulation with GAS6 or EGF, respectively, and biotinylation with EZ-Link™ Sulfo-NHS-SS-biotin. Cells were lysed, and 10% of each sample was collected as a whole cell lysate control. The remaining samples were incubated with NeutraVidin™ agarose resin to isolate biotinylated surface proteins. Next, samples were immunoblotted with antibodies recognizing AXL and EGFR. Lamin A/C and GAPDH served as technical controls of the experiment. **B** Confocal images showing GAS6-mediated endocytosis of GAS6-AXL complexes. LN229 cells were transfected with non-targeting (siCTR#1) and *AXL*-targeting (siAXL#1) siRNA. Next, 72 h after transfection, serum-starved cells were stimulated for 5 min, fixed and stained with anti-Myc (red) to visualize GAS6 and anti-AXL (green) antibodies, to visualize ligand and receptor, respectively. Insets show magnified views of boxed regions in the main images. Scale bars: 20 µm. NS- non-stimulated cells, GAS6- GAS6-stimulated cells. **C** Western blot showing the efficiency of *AXL* silencing. LN229 cells were transfected as described in B, lysed and immunoblotted against AXL. UNTR- non-transfected cells. α-tubulin was used as a loading control.

4.2.2 AXL - a primary receptor for GAS6 required for GAS6 internalization

As shown in Fig. 4.3A, LN229 cells express two TAM receptors, AXL and TYRO3. Thus, since GAS6 was postulated to activate all three TAMs [9, 378-381], the involvement of AXL and TYRO3 in GAS6 endocytosis was investigated. CRISPR-Cas9-mediated *AXL* or *TYRO3* knockout (KO) LN229 cells were used to discriminate which of the two receptors was involved in GAS6 internalization. Endosomal accumulation of GAS6 and AXL, represented by a number or integral fluorescence intensity of vesicles, in wild-type (WT) and KO cells was measured after 5 min (Fig. 4.13A-C) and 10 min (Fig. 4.13D-F) of GAS6 stimulation. Early endosome antigen 1 (EEA1) immunostaining was used to mark early endosomes. The obtained results revealed that depletion of AXL but not of TYRO3 inhibited the endocytosis of GAS6 (Fig. 4.13).

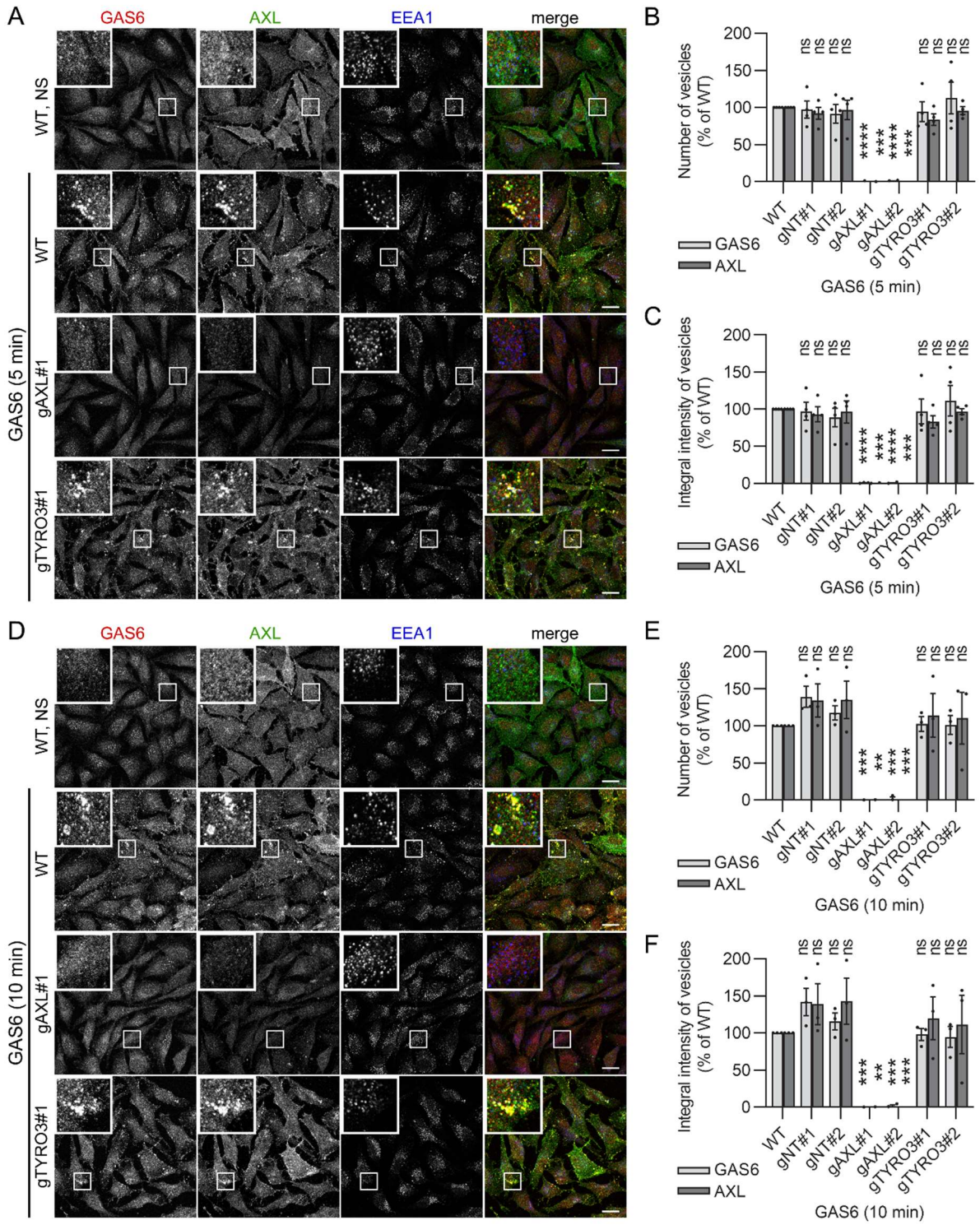

Fig. 4.13 Indispensable role of AXL in GAS6 internalization

A, D Confocal images showing uptake of GAS6-AXL complexes in wild type (WT) and AXL- or TYRO3-depleted LN229 cells. Two gRNAs targeting *AXL* (gAXL#1 and gAXL#2) and targeting *TYRO3* (gTYRO3#1 and TYRO3#2) were used to generate CRISPR-Cas9-edited cell lines. LN229 cells modified with two non-targeting gRNA (gNT#1 and gNT#2) served as controls. Serum-starved cells were stimulated with GAS6 for 5 min (A) or 10 min (D), fixed and stained with anti-Myc (red) to visualize GAS6, anti-AXL (green) and anti-EEA1 (blue) antibodies. Insets show magnified views of boxed regions in the main images. Scale bars: 20 μm. NS- non-stimulated cells, GAS6- GAS6-stimulated cells. **B, C, E, F** Quantification of number (B, E) and integral fluorescence intensity (C, F) of GAS6- and AXL-positive vesicles in AXL- or TYRO3-depleted LN229 cells stimulated with GAS6 for 5 min (B, C; representative confocal images shown in A), or 10 min (E, F; representative

confocal images shown in D) n=4. Student's one sample t-test, **p≤0.01, ***p≤0.001, ****p≤0.0001, ns - non-significant (p>0.05). Each dot represents data from one independent experiment whereas bars represent the means ± SEM from n experiments.

To further confirm the contribution of AXL to the internalization of GAS6, siRNA-mediated silencing of *AXL* or *TYRO3* was performed. Similarly to the results obtained in knockout cells, siRNA-induced depletion of AXL but not of TYRO3 abolished the endocytosis of GAS6 (Fig. 4.14A-C). The silencing efficiency of the siRNA used was verified by WB (Fig. 4.14D).

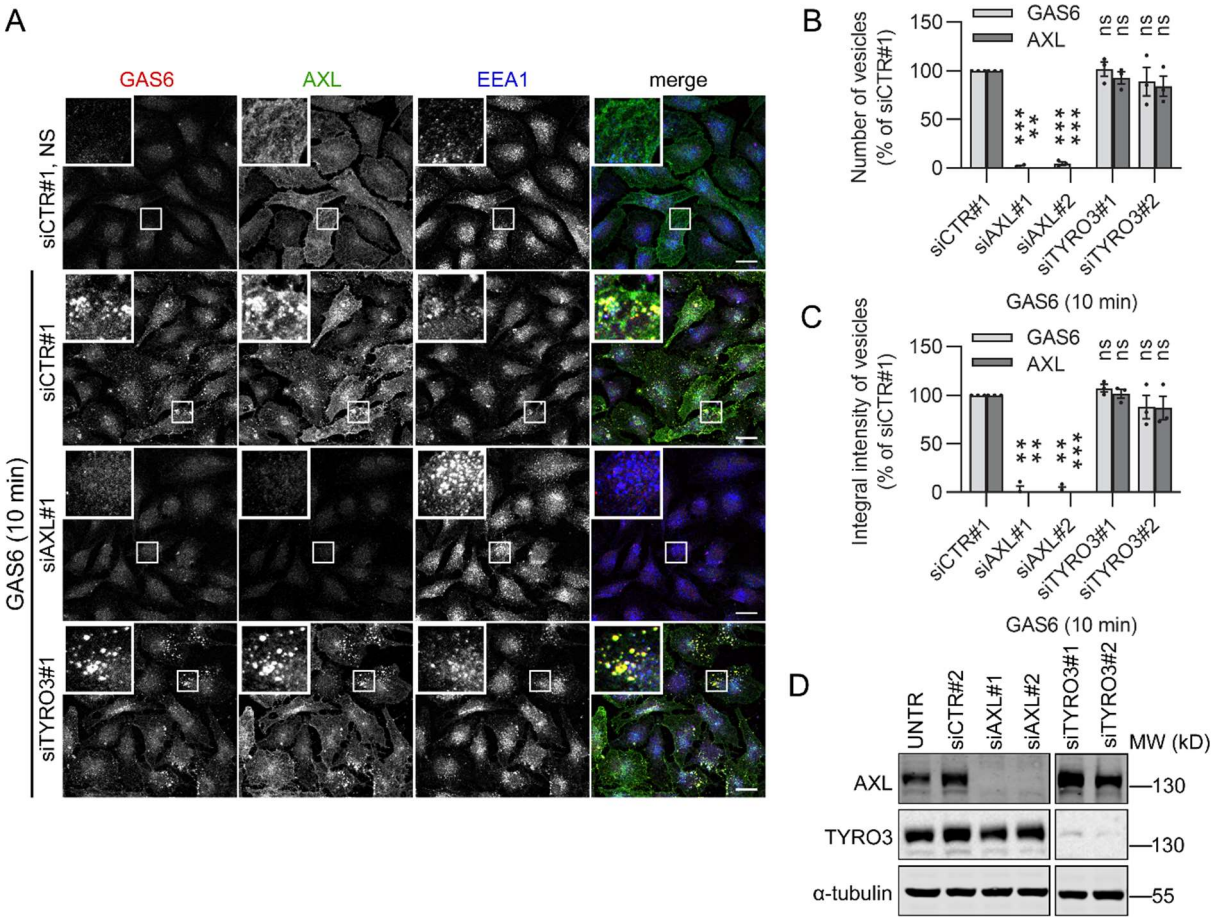

Fig. 4.14 Inhibition of GAS6 internalization upon *AXL* silencing
A Confocal images showing uptake of GAS6-AXL complexes after silencing of *AXL* (siAXL#1 and siAXL#2) or *TYRO3* (siTYRO3#1 and siTYRO3#2) in LN229 cells. Cells transfected with non-targeting siRNA (siCTR#1) were used as control. Seventy two h after transfection serum-starved LN229 cells were stimulated with GAS6 for 10 min, fixed and stained with anti-Myc (red) to visualize GAS6, anti-AXL (green) and anti-EEA1 (blue) antibodies. Insets show magnified views of boxed regions in the main images. Scale bars: 20 µm. NS- non-stimulated cells, GAS6- GAS6-stimulated cells. **B, C** Quantification of number (B) and integral fluorescence intensity (C) of GAS6- and AXL-positive vesicles in LN229 cells after silencing of *AXL* or *TYRO3*, n=3 (representative confocal images shown in A). Each dot represents data from one independent experiment whereas bars represent the means ± SEM from n experiments. Student's one sample t-test, **p≤0.01, ***p≤0.001, ns – non-significant (p>0.05). **D** Western blot showing the efficiency of AXL or TYRO3 depletion. LN229 cells were transfected as described in A, lysed and immunoblotted against AXL and TYRO3. UNTR- non-transfected cells. α-tubulin was used as a loading control.

Altogether, the presented data indicate that AXL is a primary receptor for GAS6 since depletion of AXL but not TYRO3 (achieved using two independent experimental methods) blocked the uptake of GAS6 in LN229 cells.

4.2.3 The crucial role of AXL tyrosine kinase domain activation in AXL internalization

The contribution of the activation of a tyrosine kinase domain of RTKs, such as PDGFR or EGFR, to their internalization is still under debate [382-384]. Therefore, the involvement of the activation of AXL tyrosine kinase domain in the uptake of GAS6-AXL was subsequently determined.

To this end, LN229 cells were pretreated with AXL inhibitors, R428 or LDC1267, and stimulated with GAS6. The obtained results showed that the treatment of cells with inhibitors blocked phosphorylation of AXL (Fig. 4.15A), which further resulted in the inhibition of GAS6-AXL endocytosis (Fig. 4.15 B-D). Thus, it corroborated that the activation of the tyrosine kinase domain of AXL is necessary for its ligand-induced internalization since the pharmacological inhibition of AXL phosphorylation blocked the uptake of GAS6-AXL complexes.

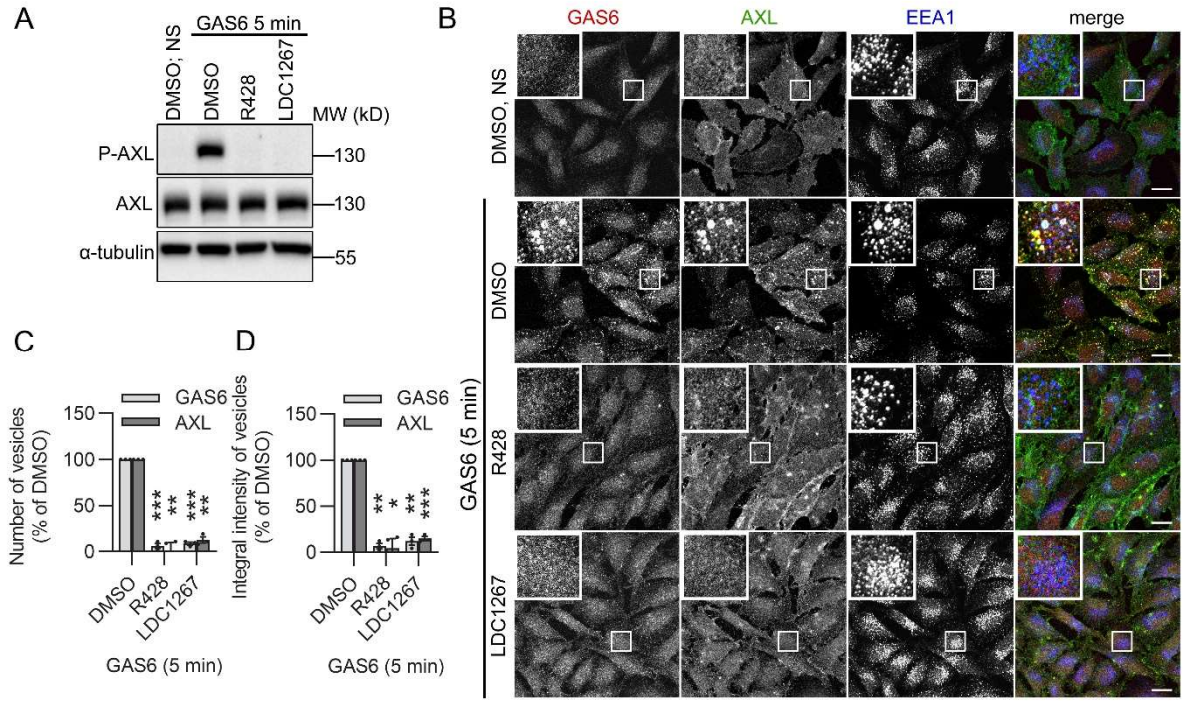

Fig. 4.15 Essential role of AXL tyrosine kinase domain activation in GAS6-induced AXL internalization

A Western blot showing phosphorylation of AXL after treatment with AXL inhibitors. Serum-starved LN229 cells were pretreated with R428 or LDC1267 for 30 min prior to GAS6 stimulation. α-tubulin was used as a loading control. DMSO- solvent control, NS- non-stimulated cells, GAS6- GAS6-stimulated cells. **B** Confocal images showing uptake of GAS6 and AXL after treatment with AXL inhibitors, R428 or LDC1267. Serum-starved LN229 were pretreated with inhibitors, stimulated with GAS6 for 5 min, fixed and stained with anti-Myc (red) to visualize GAS6, anti-AXL (green) and anti-EEA1 (blue) antibodies. Insets in confocal images show magnified views of boxed regions in the main images. Scale bars: 20

μm. DMSO- solvent control, NS- non-stimulated cells, GAS6- GAS6-stimulated cells. **C, D** Quantification of number (C) and integral fluorescence intensity (D) of GAS6- and AXL-positive vesicles in LN229 cells after treatment with R428 and LDC1267 (representative confocal images shown in B), n=3. DMSO- solvent control, GAS6- GAS6-stimulated cells. Each dot represents data from one independent experiment whereas bars represent the means ± SEM from n experiments. Student's one sample t-test, *p≤0,05, **p≤0.01, ***p≤0.001.

Cumulatively, the obtained results showed that GAS6 triggers endocytosis of AXL, which results in the accumulation of GAS6- and AXL-positive intracellular vesicles. Additionally, the presented data revealed that AXL is the primary receptor for GAS6 and the activation of its kinase domain is necessary for internalization of GAS6-AXL complexes.

4.3 Characterization of the kinetics of AXL endocytosis

4.3.1 The kinetics of GAS6-induced internalization of GAS6-AXL complexes

To study the kinetics of AXL endocytosis, serum-starved LN229 cells were incubated with GAS6 for increasing time periods. As shown in Fig. 4.16A, GAS6 triggered rapid accumulation of GAS6 and AXL on endosomal structures, since the number and integral intensity of fluorescence of GAS6- and AXL-positive vesicles peaked after 5 min of stimulation. At later time points the level of internalized GAS6-AXL complexes declined (Fig. 4.16B-C), however, a complete disappearance of GAS6-AXL endosomal accumulation was not observed. Additionally, up to 55% of AXL-positive vesicles colocalized with GAS6-containing endosomes, which suggested that a substantial fraction of AXL traffics inside the cell in the ligand-bound state (Fig. 4.16D).

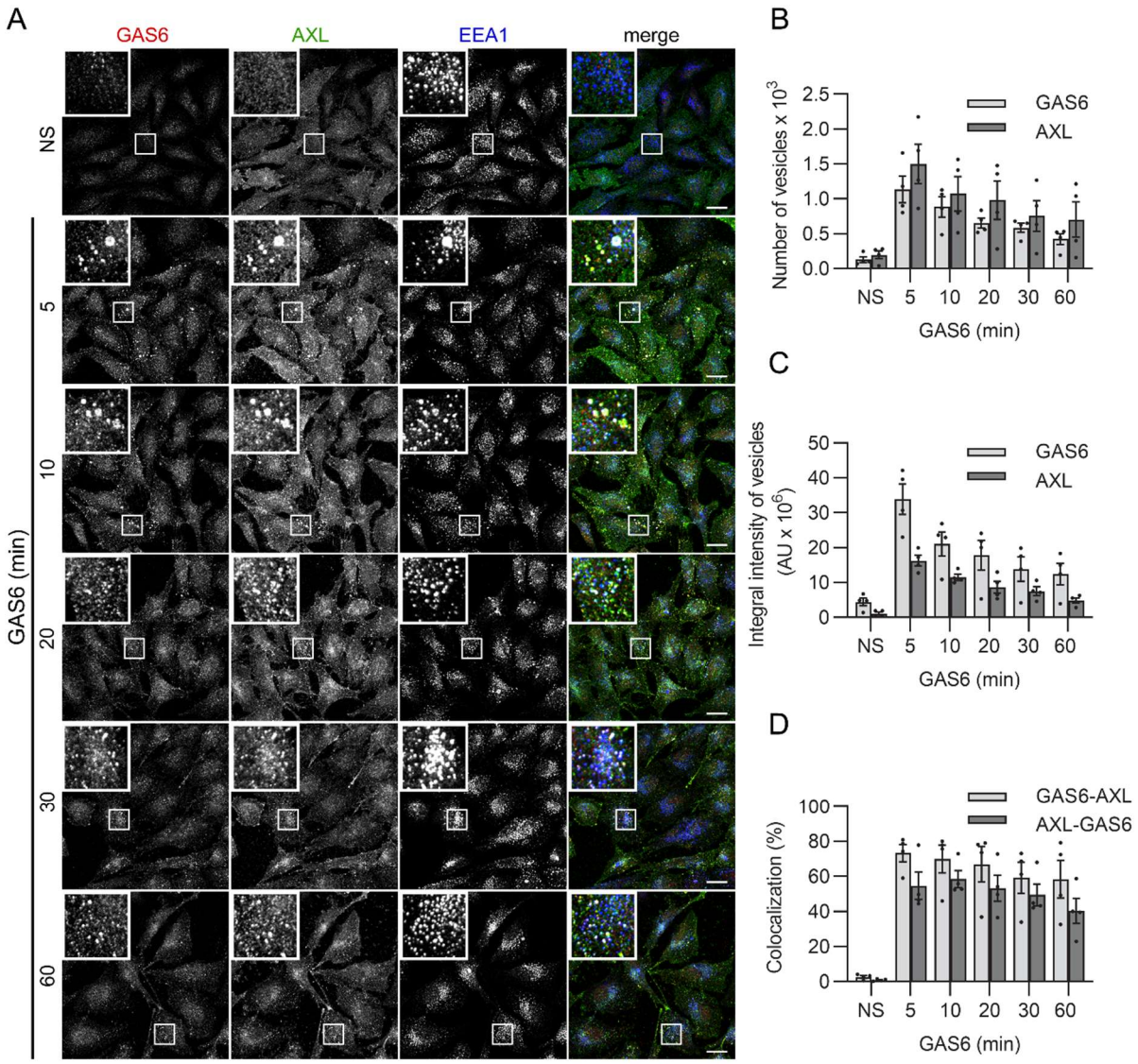

Fig. 4.16 Kinetics of AXL endocytosis

A Confocal images showing GAS6-induced accumulation of GAS6- and AXL- positive vesicles. Serum-starved LN229 cells were stimulated with the ligand for increasing time periods, fixed and stained with anti-Myc (red) to visualize GAS6, anti-AXL (green) and anti-EEA1 (blue) antibodies. Insets in confocal images show magnified views of boxed regions in the main images. Scale bars: 20 µm. NS- non-stimulated cells, GAS6- GAS6-stimulated cells. **B, C, D** Quantification of number (B) and integral fluorescence intensity (C) of GAS6- and AXL-positive vesicles and the colocalization between GAS6 and AXL (D) in LN229 cells after stimulation with GAS6 (representative confocal images shown in A), n=4. GAS6-AXL- percentage of GAS6-positive vesicles overlapping with AXL-positive vesicles, AXL-GAS6- percentage of AXL-positive vesicles overlapping with GAS6-positive vesicles. Each dot represents data from one independent experiment whereas bars represent the means ± SEM from n experiments. NS- non-stimulated cells, GAS6- GAS6-stimulated cells, AU- arbitrary units.

4.3.2 The kinetics of AXL internalization in comparison to the uptake of other RTKs

Since EGFR is a prototypical RTK, well-characterized in terms of endocytosis, and it was identified in BioID as one of AXL interactors, the kinetics of internalization of these two receptors was compared. To this end, LN229 cells were stimulated with fluorescently-tagged EGF, a ligand for EGFR, and the endosomal accumulation of EGF was calculated. The

obtained results showed that, in contrast to internalization of GAS6-AXL complexes, which peaked after 5 min of ligand stimulation (Fig. 4.16A-C), the maximal endosomal accumulation of EGF was observed after 15 min of stimulation, and gradually dropped at later time points (Fig. 4.17A-C). Additionally, GAS6 and AXL displayed limited colocalization with EGF (<25%), which may have resulted from different endocytic kinetics of AXL and EGFR (Fig. 4.17D).

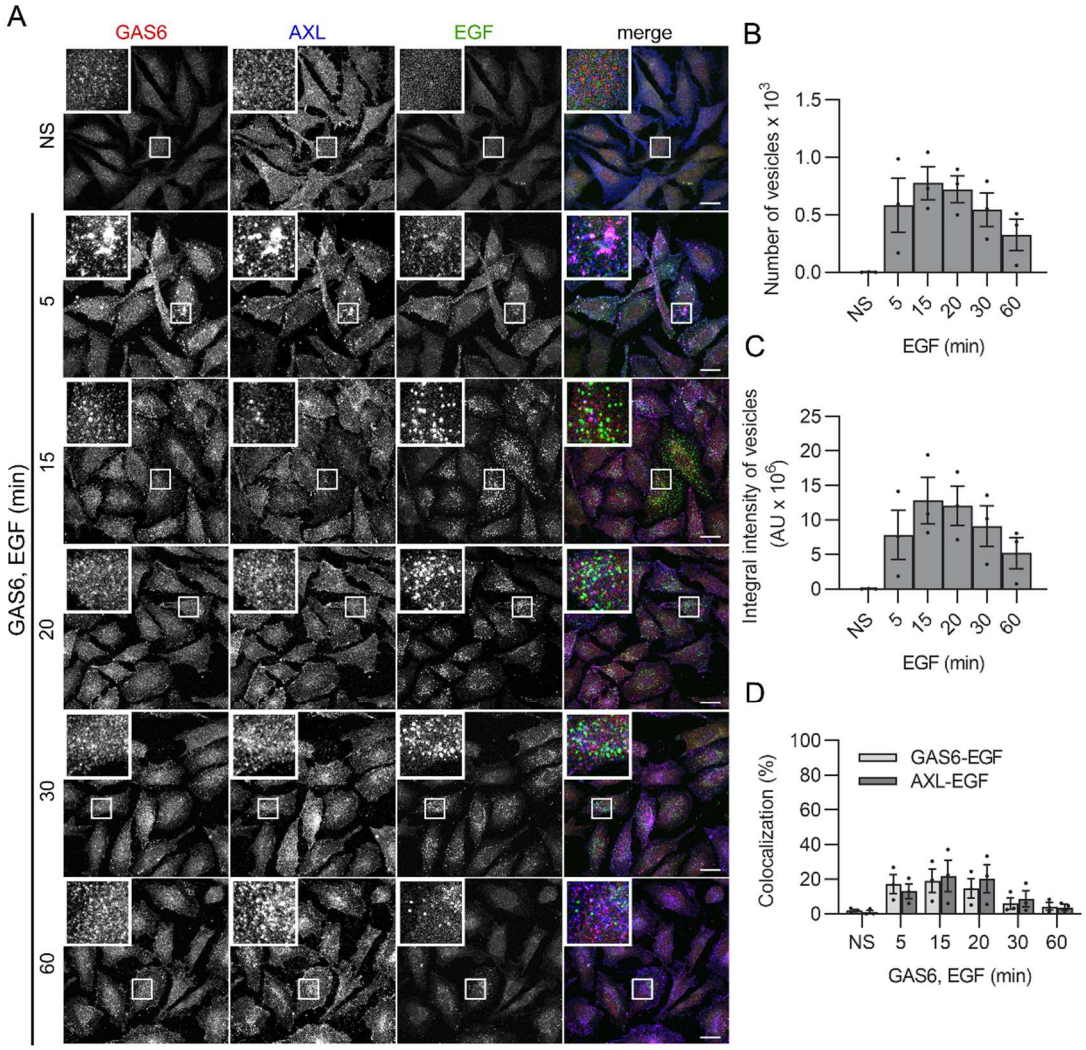

Fig. 4.17 Kinetics of EGF internalization

A Confocal images showing accumulation EGF- or AXL-positive vesicles. Serum-starved LN229 cells were stimulated with fluorescently-labelled EGF (green) and GAS6 for increasing time periods, fixed and stained with anti-Myc (red) to visualize GAS6 and anti-AXL (blue) antibodies. Insets in confocal images show magnified views of boxed regions in the main images. Scale bars: 20 µm. NS- non-stimulated cells, GAS6, EGF- GAS6 and EGF-stimulated cells. **B, C, D** Quantification of number (B) and integral fluorescence intensity (C) of EGF-positive vesicles in LN229 cells after stimulation with EGF and GAS6, and colocalization between AXL, GAS6 and EGF (D) (representative confocal images shown in A), n=3. Each dot represents data from one independent experiment whereas bars represent the means ± SEM from n experiments. NS- non-stimulated cells, EGF- EGF-stimulated cells, GAS6, EGF- GAS6 and EGF-stimulated cells, AU- arbitrary units.

Next, the endocytic kinetics of AXL and PDGFRβ was measured in human fibroblasts CCD-1070Sk. Cells were stimulated with GAS6 and PDGF-BB to induce the endocytosis of AXL and PDGFRβ, respectively. Similarly to the results obtained for AXL and EGF in LN229 cells (Fig. 4.16 and 4.17), the maximum of AXL internalization was observed after 5 min of GAS6 stimulation, whereas uptake of PDGFRβ peaked after 15 min of stimulation with PDGF-BB (Fig. 4.18A-C). Of note, these results also showed that AXL endocytosis is a fast process both in cancer (LN229) (Fig. 4.16A-C) as well as normal (CCD-1070Sk) human cells (Fig. 4.18A-C).

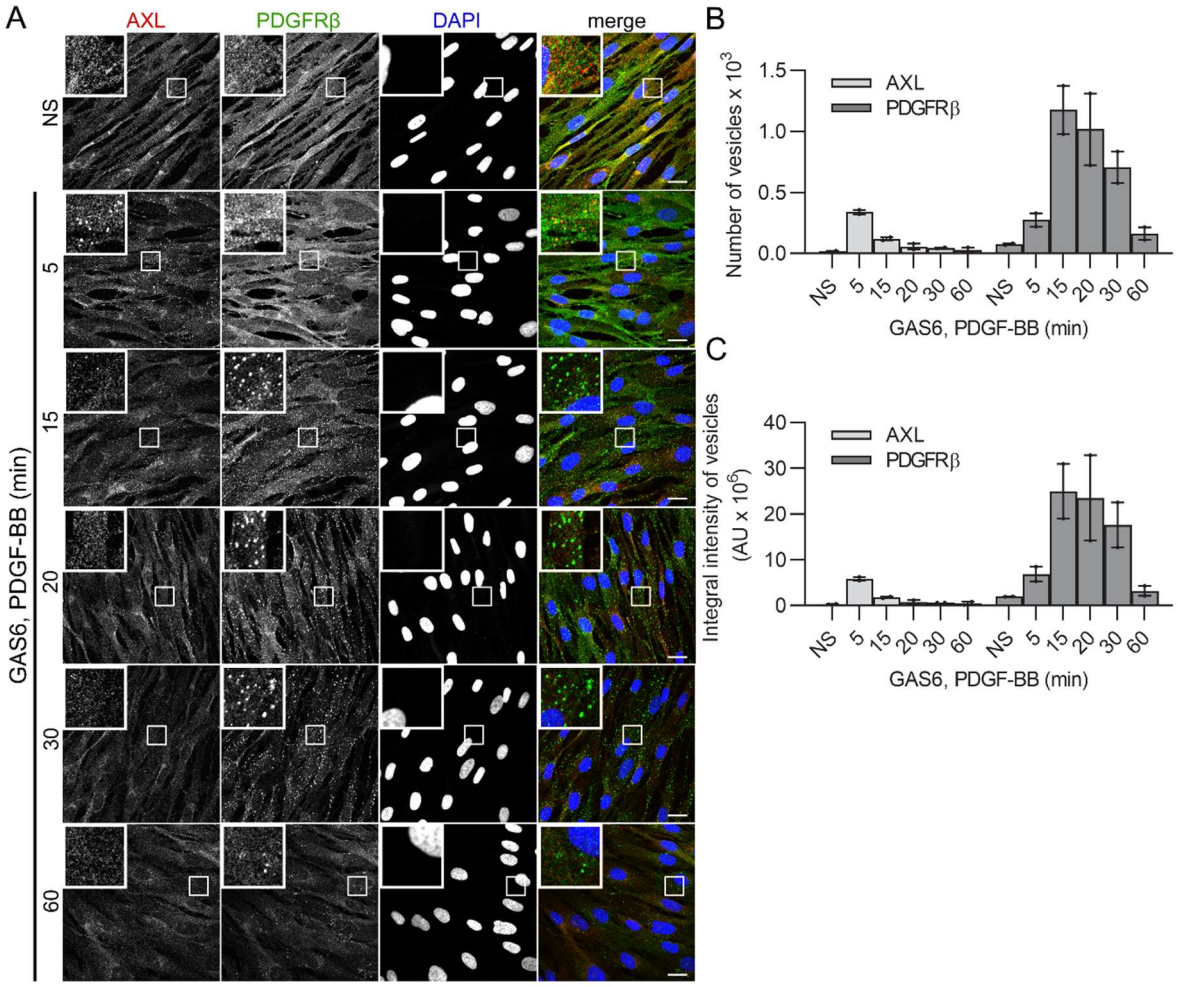

Fig. 4.18 Kinetics of PDGFRβ internalization

A Confocal images showing accumulation PDGFRβ- or AXL-positive vesicles. Serum-starved CCD-1070Sk cells were stimulated with PDGF-BB and GAS6 for increasing time periods, fixed and stained with anti-AXL (red) and anti- PDGFRβ (green) antibodies, and DAPI was used to stain nuclei (blue). Insets in confocal images show magnified views of boxed regions in the main images. Scale bars: 20 µm. NS- non-stimulated cells, GAS6- GAS6-stimulated cells, PDGF-BB- PDGF-BB-stimulated cells. **B, C** Quantification of number (B) and integral fluorescence intensity (C) of AXL- and PDGFRβ-positive vesicles in CCD-1070Sk cells after stimulation with PDGF-BB and GAS6 (representative confocal images shown in A), n=2. Bars represent the means ± SEM from n experiments. NS- non-stimulated cells, GAS6, PDGF-BB- GAS6- and PDGF-BB-stimulated cells, AU- arbitrary units.

Cumulatively, these data showed that after stimulation AXL is rapidly internalized into the cells. This fast internalization is unique in comparison to endocytic rates of other RTKs, such as EGFR and PDGFRβ, both in cancer cells (LN229) as well as in normal human fibroblasts (CCD-1070Sk). Specifically, the maximum of AXL internalization was observed after 5 min of GAS6 stimulation, whereas the highest endosomal accumulation of EGFR or PDGFRβ was observed after 15 min of ligand stimulation.

4.4 Characterization of endocytic routes mediating AXL endocytosis

As described in the Introduction, endocytosis can operate via various mechanisms, and both clathrin-mediated and -independent pathways were shown to function in the internalization of RTKs, such as EGFR or PDGFRβ [384, 385]. Several proteins implicated in CME and CIE were identified among AXL interactors, which suggests that AXL may also be internalized via multiple endocytic routes (Fig. 4.19, Table 4.1, Table S1 and S2 in supplementary materials).

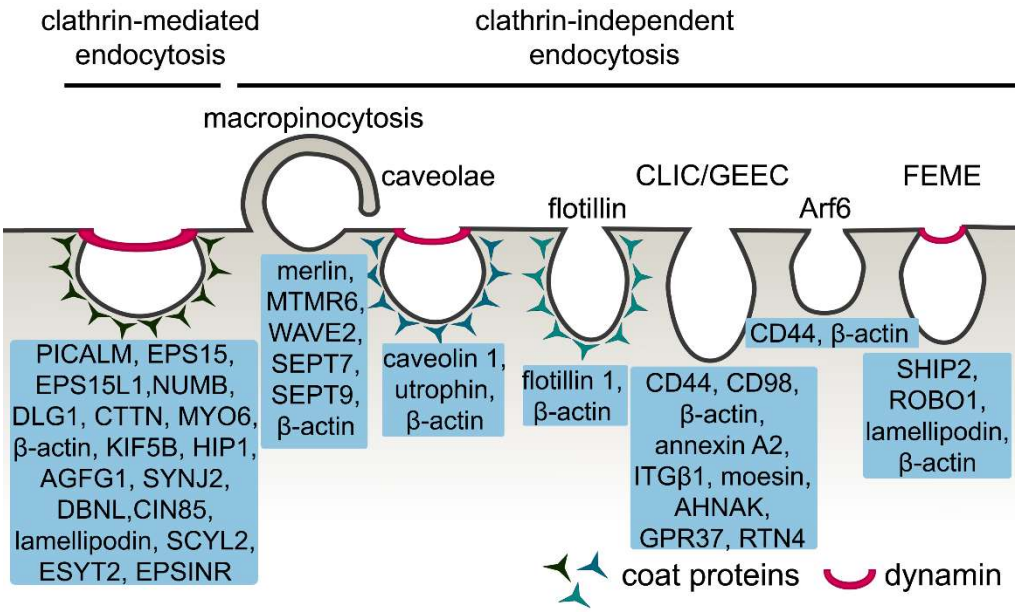

Fig. 4.19 Endocytic pathways potentially contributing to AXL endocytosis
The scheme presents clathrin-mediated and clathrin-independent endocytic routes along with their regulators identified by BioID as AXL proximity interactors.

4.4.1 Clathrin-mediated endocytosis (CME) in AXL internalization

BioID data revealed that AXL possibly interacts with multiple proteins involved in CME which implied the contribution of this pathway to AXL endocytosis. To verify this hypothesis, the colocalization between AXL and clathrin light chain (CLC) or PICALM was investigated. The total internal reflection fluorescence (TIRF) analysis of living LN229 cells expressing AXL-EGFP and mRFP-CLC or mCherry-PICALM fusion proteins showed colocalization between AXL and CLC or PICALM that was progressively increasing with

time of GAS6 stimulation (Fig. 4.20A-B). These data support the hypothesis that CME contributes to the internalization of AXL.

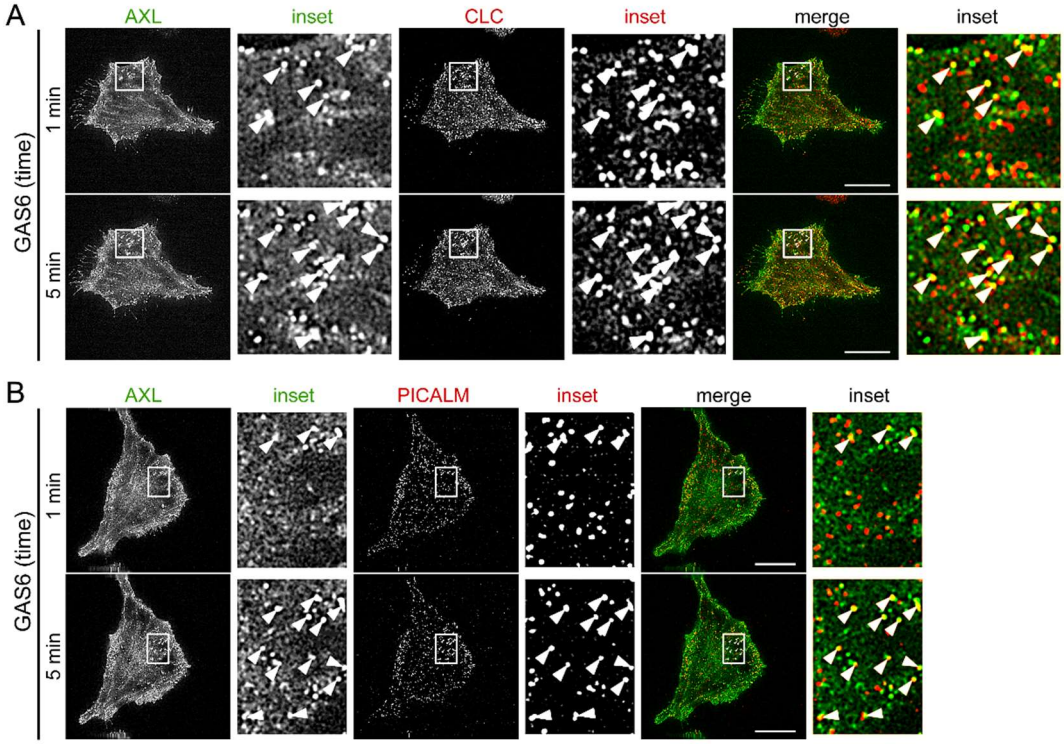

Fig. 4.20 Increased colocalization of AXL with CLC and PICALM upon GAS6 stimulation

A, B Total internal reflection fluorescence (TIRF) analysis of living LN229 cells which express AXL-EGFP (green) and mRFP-CLC (red) (A) or mCherry-PICALM (red) (B). Arrowheads indicate structures positive for both AXL and CLC (A) or PICALM (B). Serum-starved cells were stimulated with GAS6 and imaged every 20 s up to 10 min after ligand addition. Pictures show selected frames from recorded movies. Insets in presented images show magnified views of boxed regions in the main images. Scale bars: 20 μm. GAS6-GAS6-stimulated cells.

Results obtained by Dr. Daria Zdżalik-Bielecka during her short-term fellowship at the Institute for Cancer Research, Oslo University Hospital, Norway.

Next, since the identified AXL interactome showed that AXL may interact with EPS15, EPS15L1 and NUMB (Fig 4.19, Table 4.1, Table S1 and S2 in supplementary materials), which serve as alternative clathrin adaptors [386, 387], their involvement in GAS6-AXL endocytosis was verified. To test this hypothesis, internalization of GAS6-AXL complexes was measured in LN229 cells with CRISPR-Cas9-mediated knockout of *EPS15*, *EPS15L1* or *NUMB* (Fig. 4.21A). As shown in Fig. 4.21B-D, depletion of none of these proteins affected the endocytosis of GAS6 and AXL.

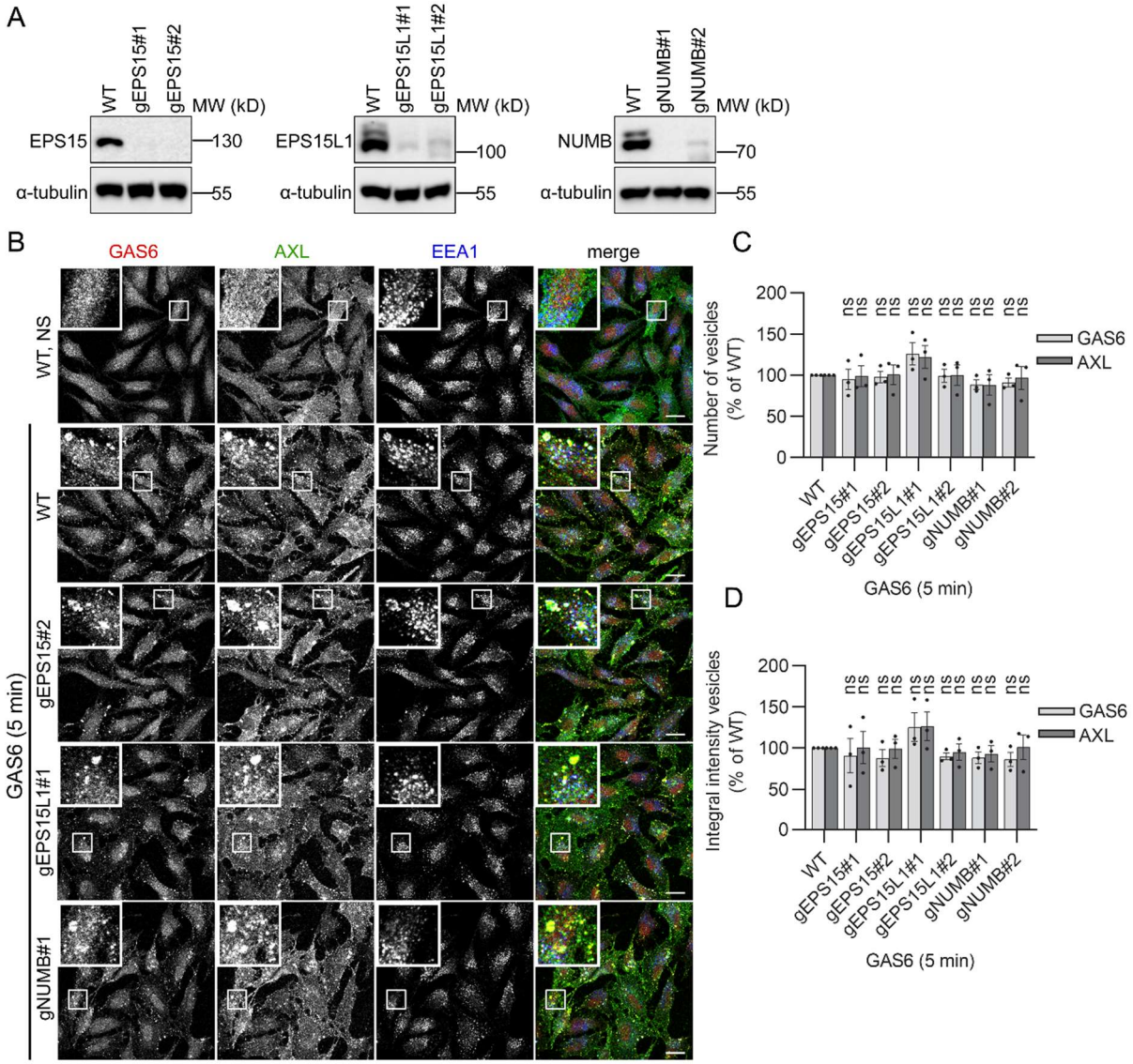

Fig. 4.21 The lack of effect of CRISPR-Cas9-mediated knockout of *EPS15*, *EPS15L1* or *NUMB* on endocytosis of GAS6-AXL complexes

A Western blot showing the efficiency of CRISPR-Cas9-mediated KO of *EPS15*, *EPS15L1* or *NUMB*. Two gRNAs targeting *EPS15* (gEPS15#1 and gEPS15#2), *EPS15L1* (gEPS15L1#1 and gEPS15L1#2) and *NUMB* (gNUMB#1 and NUMB#2) were used to generate CRISPR-Cas9-edited cell lines. Cells were lysed and immunoblotted against the indicated proteins. α-tubulin was used as a loading control. **B** Confocal images showing GAS6-induced accumulation of GAS6- and AXL- positive vesicles in cells depleted of EPS15, EPS15L1 or NUMB. WT and KO LN229 cells were serum-starved and stimulated with GAS6 for 5 min, fixed and stained with anti-Myc (red) to visualize GAS6, anti-AXL (green) and anti-EEA1 (blue) antibodies. Insets in confocal images show magnified views of boxed regions in the main images. Scale bars: 20 μm. NS- non-stimulated cells, GAS6- GAS6-stimulated cells. **C, D** Quantification of number (C) and integral fluorescence intensity (D) of GAS6- and AXL-positive vesicles in LN229 cells (representative confocal images shown in B), n=4. Each dot represents data from one independent experiment whereas bars represent the means ± SEM from n experiments. Student's one sample t-test, ns – non-significant ($p>0.05$). GAS6- GAS6-stimulated cells.

Since downregulation of alternative clathrin adaptors did not affect the endocytosis of GAS6 and AXL, the involvement of clathrin, an indispensable regulator of CME, in AXL internalization was investigated. Due to the contribution of clathrin to various cellular

processes essential for cell survival [388], the inactivation of *CLTC*, a gene encoding clathrin heavy chain (CHC), by the CRISPR-Cas9 method was ineffective. Therefore, to transiently deplete clathrin, siRNA-mediated silencing was used. To ensure efficient silencing, LN229 cells were transfected twice, with 72 h break between transfections (Fig. 4.22A). Confocal microscopy imaging revealed that clathrin depletion did not decrease endocytosis of GAS6-AXL complexes after 5 min (Fig. 4.22B-D) and 10 min (Fig. 4.23A, C and D) of GAS6 stimulation. In contrast, internalization of transferrin, a well-established cargo internalized through CME, was significantly reduced (Fig. 4.23B-D).

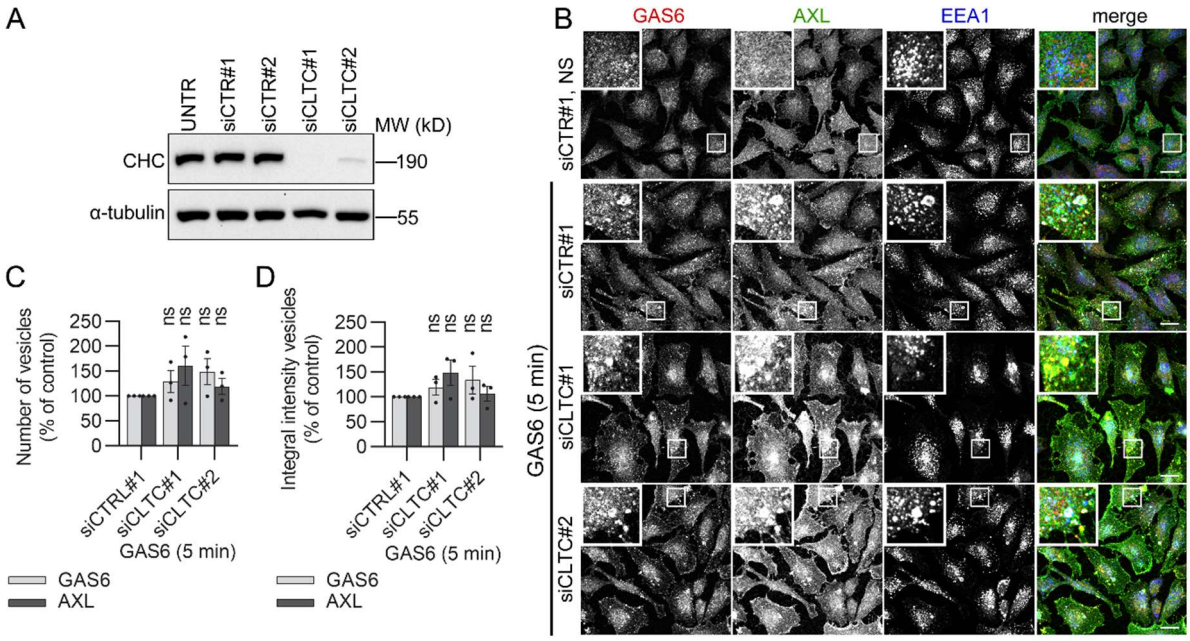

Fig. 4.22 The effect of *CLTC* silencing on GAS6-AXL endocytosis
A Western blot showing the efficiency of CHC depletion. LN229 cells were transfected twice with non-targeting (siCTR#1 and siCTR#2) and *CHC*-targeting (siCHC#1 and siCHC#2) siRNA with 72 h interval between transfections. Next, 72 h after second transfection, cells were lysed and immunoblotted against CHC. α-tubulin was used as a loading control. **B** Confocal images showing the internalization of GAS6-AXL complexes after depletion of CHC as described in A. Seventy two h after the second transfection serum-starved LN229 cells were stimulated with GAS6 for 5 min, fixed and stained with anti-Myc (red) to visualize GAS6, anti-AXL (green) and anti-EEA1 (blue) antibodies. Insets in confocal images show magnified views of boxed regions in the main images. Scale bars: 20 µm. NS- non-stimulated cells, GAS6- GAS6-stimulated cells. **C, D** Quantification of number (C) and integral fluorescence intensity (D) of GAS6- and AXL-positive vesicles in LN229 cells (representative confocal images shown in A), n=3. Each dot represents data from one independent experiment whereas bars represent the means ± SEM from n experiments. Student's one sample t-test, ns - non-significant ($p>0.05$). GAS6- GAS6-stimulated cells.

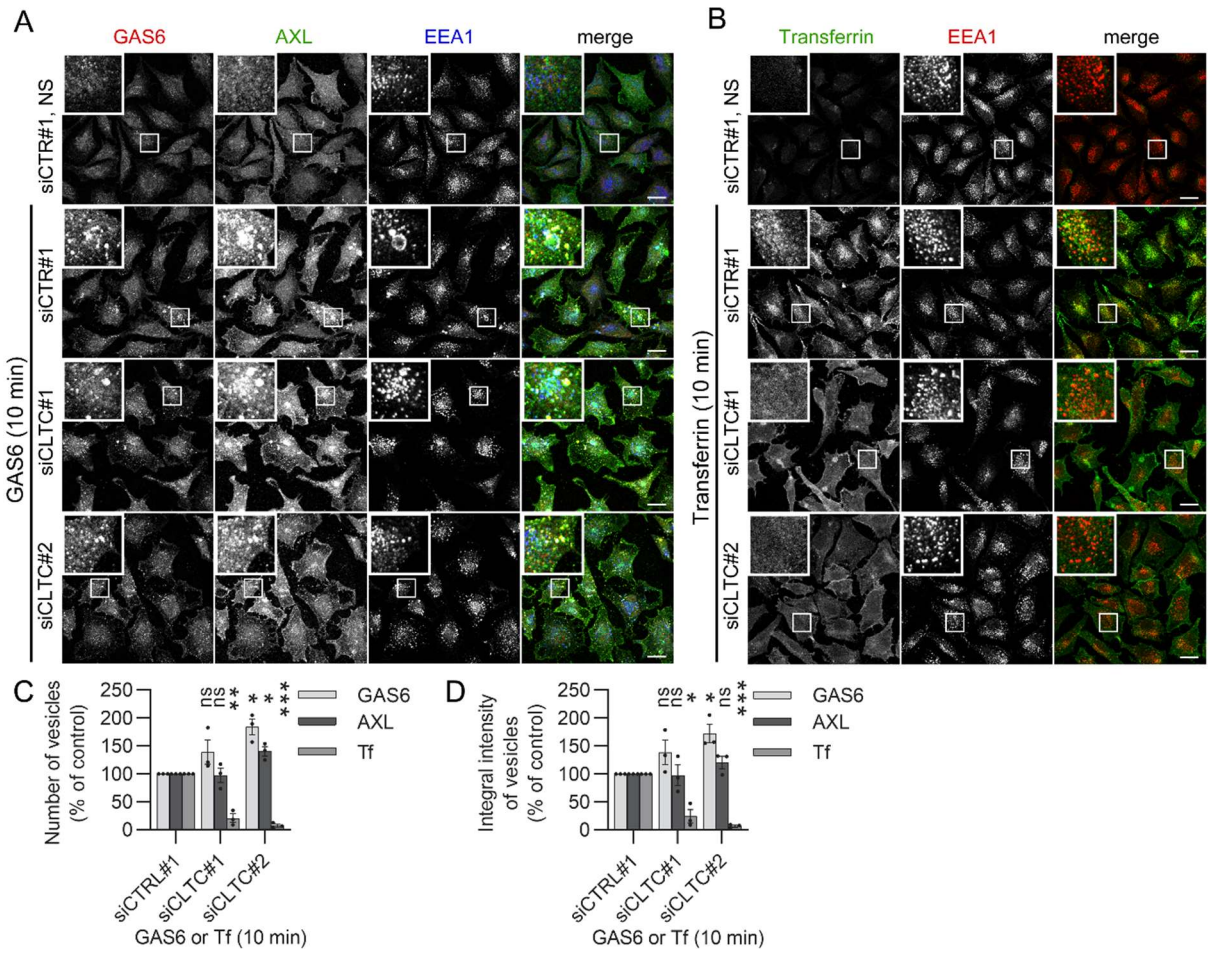

Fig. 4.23 The effect of *CLTC* silencing on GAS6-AXL endocytosis in comparison to the uptake of transferrin

A, B Confocal images showing the internalization of GAS6-AXL complexes (A) or fluorescently-labelled transferrin (Tf) (B) after depletion of CHC. LN229 cells were transfected twice with non-targeting (siCTR#1 and siCTR#2) and *CHC*-targeting (siCHC#1 and siCHC#2) siRNA with 72 h interval between transfections. Next, 72 h after the second transfection, cells were stimulated with GAS6 (A) or Tf (B) for 10 min, fixed and stained with anti-Myc (red) to visualize GAS6, anti-AXL (green) and anti-EEA1 (blue) antibodies for GAS6-stimulated cells (A) or anti-EEA1 (red) antibodies for Tf-stimulated (green) cells (B). Insets in confocal images show magnified views of boxed regions in the main images. Scale bars: 20 µm. NS- non-stimulated cells, GAS6- GAS6-stimulated cells, Transferrin/Tf- transferrin-stimulated cells. **C, D** Quantification of number (C) and integral fluorescence intensity (D) of GAS6-, AXL- and transferrin (Tf)-positive vesicles in LN229 cells (representative confocal images shown in A and B), n=3. Each dot represents data from one independent experiment whereas bars represent the means ± SEM from n experiments. Student's one sample t-test, *p≤0.05, **p≤0.01, ***p≤0.001, ns - non-significant (p>0.05). GAS6 or Tf- GAS6- or Tf- stimulated cells.

Additionally, other results obtained in our laboratory showed that, similarly do *CLTC* silencing, CRISPR-Cas9 mediated knockout of dynamin 2 (DNM2), another key regulator of CME, did not affect endocytosis of GAS6-AXL complexes. As a control, internalization of transferrin was significantly decreased under these conditions (manuscript under revision).

Altogether, despite a substantial representation of CME-related proteins in AXL proximity interactome, depletion of CME regulators did not decrease GAS6-AXL

endocytosis. However, the increased colocalization of AXL with CLC and PICALM after GAS6 stimulation suggests that at least a fraction of AXL can be internalized via CME. This may imply that in the absence of CME, AXL internalization may be compensated by the involvement of other, clathrin-independent endocytic pathways.

4.4.2 Clathrin-independent endocytosis (CIE) in the uptake of AXL

The identified AXL interactome contained various proteins implicated in CIE (Table 4.1, Fig. 4.19). Among them were regulators of macropinocytosis, caveolae-, flotillin- or ARF6-dependent endocytosis, and the CLIC/GEEC pathway (Fig. 4.19). Thus, their participation in AXL internalization was investigated.

4.4.2.1 The involvement of macropinocytosis in AXL internalization

Macropinocytosis is manifested by the formation of big vesicular structures, macropinosomes, and their emergence requires actin cytoskeleton rearrangements [122]. Since AXL interactome contained proteins implicated both in actin remodeling and macropinocytosis, the involvement of this pathway in AXL internalization was investigated. Confocal microscopy revealed that GAS6 triggered the formation of such vesicles (Fig. 4.24) and both, GAS6 and AXL, were present on the macropinosome membrane stained with EEA1 (Fig. 4.24A) and Rabankyrin-5 (Fig. 4.24B), markers of early endosomes and macropinosomes [389], respectively. Moreover, other results obtained in our group showed that AXL colocalized with high molecular mass dextran, a well-established cargo of macropinocytosis, which additionally confirmed the contribution of this pathway to AXL internalization [89].

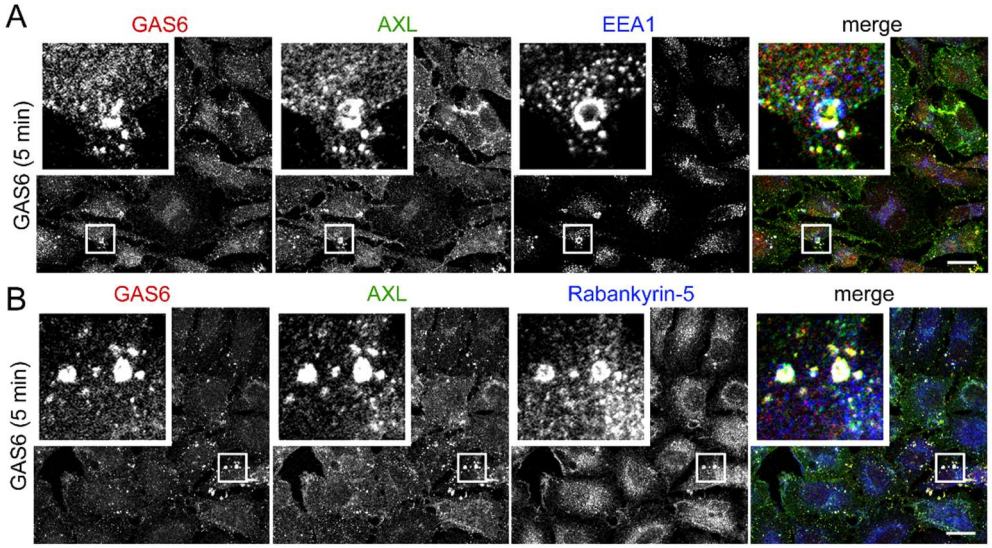

Fig. 4.24 Macropinocytosis in the uptake of GAS6-AXL complexes
A, B Confocal images showing the accumulation of GAS6 and AXL on macropinosomes. LN229 cells were stimulated with GAS6, fixed and stained with anti-Myc (red) to visualize GAS6, anti-AXL (green) and anti-EEA1 (A) or Rabankyrin-5 (B) (blue). Insets in confocal

images show magnified views of boxed regions in the main images. Scale bars: 20 μm. GAS6- GAS6-stimulated cells.

4.4.2.2 The influence of caveolin 1 or flotillin 1 depletion on AXL endocytosis

Among AXL proximity interactors were caveolin 1 (CAV1) and flotillin 1 (FLOT1), two proteins regulating caveolae- and flotillin-dependent CIE pathways, respectively [390]. Therefore, their involvement in AXL internalization was investigated. To this end, LN229 cells depleted of CAV1 or FLOT1 (Fig. 4.25A) by the CRISPR-Cas9 approach were stimulated with GAS6. As shown in Fig. 4.25, inactivation of neither CAV1 nor FLOT1 reduced the GAS6-AXL internalization. In turn, knockout of *CAV1* slightly increased the endocytosis of ligand-receptor complexes (Fig. 4.25B-D). The obtained results indicate that CAV1 and FLOT1 are either dispensable for GAS6-AXL endocytosis, or these proteins may contribute to AXL uptake, but in their absence ligand-receptor complexes are internalized by some compensatory mechanisms.

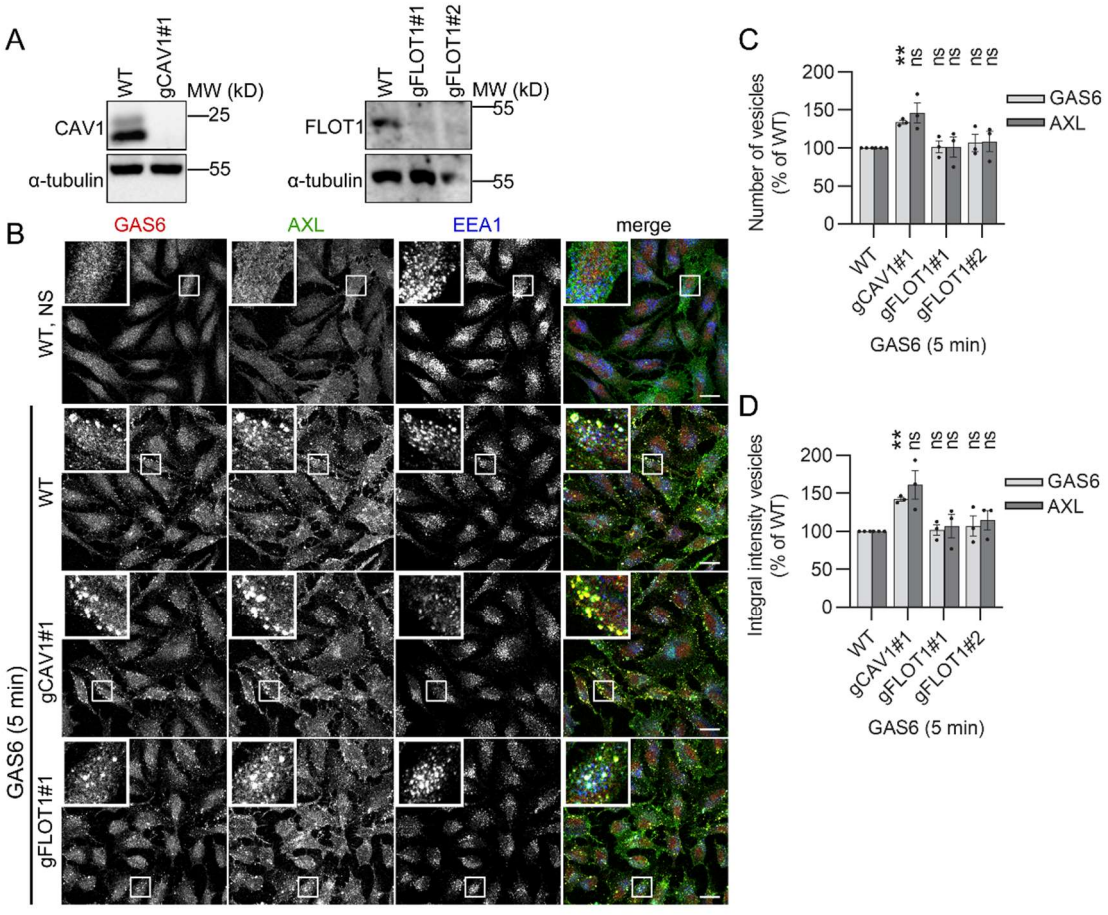

Fig. 4.25 GAS6-AXL complexes endocytosis upon depletion of CAV1 or FLOT1
A Western blot showing the efficiency of CRISPR-Cas9-mediated KO of *CAV1* or *FLOT1*. One gRNA targeting *CAV1* (gCAV1#1) and two gRNAs targeting *FLOT1* (gFLOT1#1 and gFLOT1#2) were used to generate CRISPR-Cas9-edited cell lines. Cells were lysed and immunoblotted against the indicated proteins. α-tubulin was used as a loading control. **B** Confocal images showing GAS6-induced accumulation of GAS6- and AXL- positive endosomes in cells depleted of CAV1 or FLOT1. WT and KO LN229 cells were serum-starved and stimulated with GAS6 for 5 min, fixed and stained with anti-Myc (red) to

visualize GAS6, anti-AXL (green) and anti-EEA1 (blue). Insets in confocal images show magnified views of boxed regions in the main images. Scale bars: 20 µm. NS- non-stimulated cells, GAS6- GAS6-stimulated cells. **C, D** Quantification of number (C) and integral fluorescence intensity (D) of GAS6- and AXL-positive vesicles in LN229 cells depleted of CAV1 or FLOT1 (representative confocal images shown in B), n=4. Student's one sample t-test, **p≤0.01, ns - non-significant (p>0.05). Each dot represents data from one independent experiment whereas bars represent the means ± SEM from n experiments. GAS6- GAS6-stimulated cells.

4.4.2.3 The contribution of the CLIC/GEEC pathway to GAS6-AXL endocytic uptake

Several proteins found in this thesis work as AXL proximity interactors through BioID were previously reported as components of clathrin independent carriers (CLIC). These are: β-actin, annexin A2, ITGβ1, moesin, AHNAK, GPR37, RTN4, CD44 or CD98 [179]. Importantly, the latter two are considered as typical cargos internalized via the CLIC/GEEC pathway [179, 391]. Thus, to verify the involvement of CLIC/GEEC in AXL endocytosis, LN229 cells were stimulated with GAS6 and anti-CD44 agonistic antibodies. The obtained results showed that AXL displays up to 50% colocalization with CD44 after 5 min of cell stimulation (Fig. 4.26A and B).

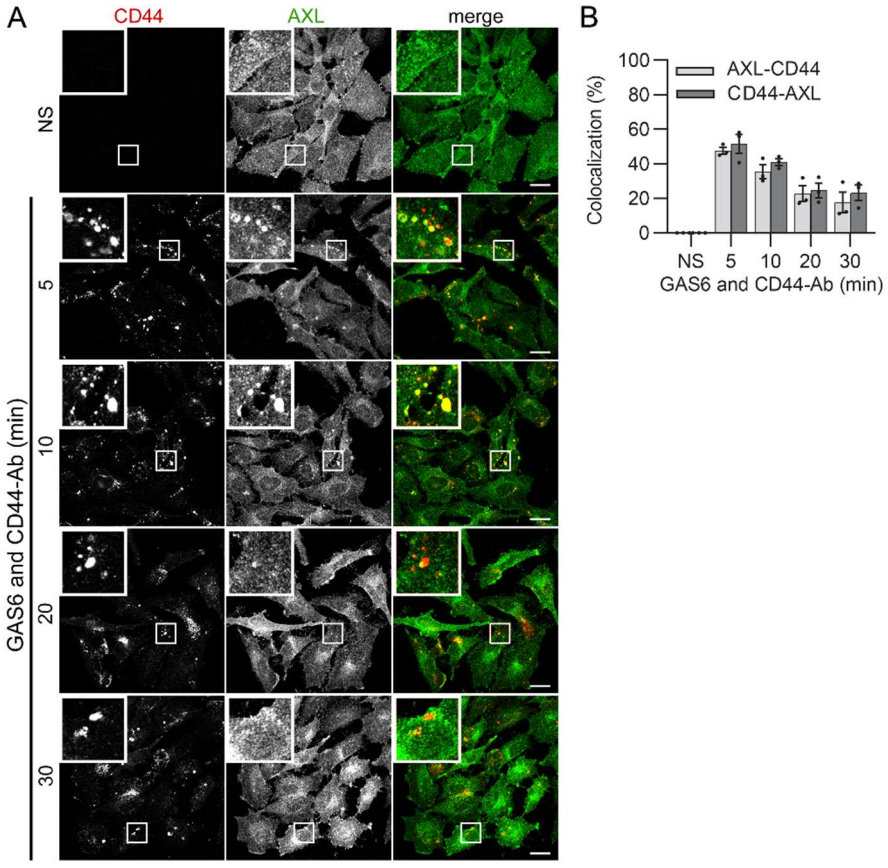

Fig. 4.26 The colocalization of AXL and CD44
A Confocal images showing colocalization between AXL and CD44. Serum-starved LN229 cells were stimulated with GAS6 and anti-CD44 agonistic antibody (CD44-Ab) for increasing time periods, fixed and immunostained with anti-AXL (green) antibodies. For visualization of CD44 (red) only secondary antibodies were used for staining. Insets in confocal images show magnified views of boxed regions in the main images. Scale bars: 20 µm. NS- non-stimulated

cells; GAS6 and CD44-Ab- cells stimulated with GAS6 and CD44-Ab. **B** Quantification of colocalization between AXL- and CD44-Ab-positive vesicles (representative confocal images shown in A) n=3. AXL-CD44- percentage of AXL-positive vesicles overlapping with CD44-positive vesicles, CD44-AXL- percentage of CD44-positive vesicles overlapping with AXL-positive vesicles. Each dot represents data from one independent experiment whereas bars represent the means ± SEM from n experiments. GAS6 and CD44-Ab- cells stimulated with GAS6 and CD44-Ab.

To further investigate the involvement of the CLIC/GEEC pathway in AXL endocytosis, genes encoding CDC42 or GRAF1, key regulators of the CLIC/GEEC pathway [175-177, 390], were silenced by siRNAs in LN229 cells (Fig. 4.27A and B). As shown in Fig. 4.27C-F, depletion of these proteins decreased GAS6-induced endocytosis of GAS6-AXL complexes. These results suggest that the CLIC/GEEC pathway mediates the internalization of GAS6 and AXL. This conclusion is additionally supported by the notion that a large fraction of AXL traffics together with internalized CD44.

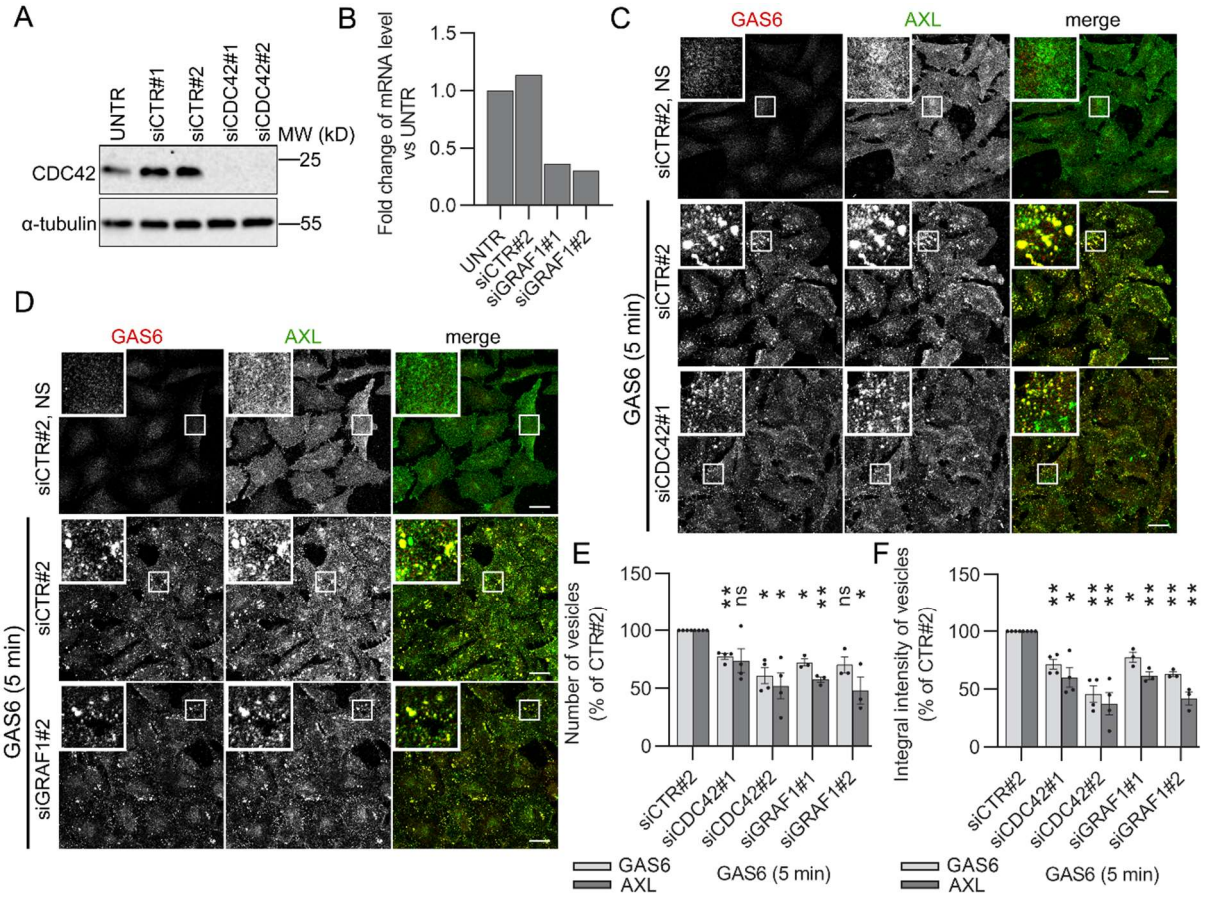

Fig. 4.27 The CLIC/GEEC pathway-mediated internalization of GAS6-AXL complexes
A Western blot showing the efficiency of CDC42 depletion. LN229 cells were transfected with non-targeting (siCTR#1 and siCTR#2) and *CDC42*-targeting (siCDC42#1 and siCDC42#2) siRNA. Seventy two h after transfection, cells were lysed and immunoblotted against CDC42. α-tubulin was used as a loading control. **B** Graph showing silencing efficiency of GRAF1. LN229 cells were depleted of GRAF1 using siRNAs (siGRAF1#1 and siGRAF1#2), along with non-targeting (siCTR#2) siRNA and analyzed by real-time quantitative PCR (RT-qPCR) after 72 h post transfection. Values are presented as a fold change versus non-transfected cells (UNTR), set as 1. **C, D** Confocal images showing GAS6-

induced accumulation of GAS6- and AXL-positive endosomes in cells depleted of CDC42 (C) or GRAF1 (D). Cells were transfected as described in A and B. Seventy two h after transfection serum-starved LN229 cells were stimulated with GAS6 for 5 min, fixed and stained with anti-Myc (red) to visualize GAS6 and anti-AXL (green) antibodies. Insets in confocal images show magnified views of boxed regions in the main images. Scale bars: 20 µm. NS- non-stimulated cells, GAS6- GAS6-stimulated cells. **E, F** Quantification of number (E) and integral fluorescence intensity (F) of GAS6- and AXL-positive vesicles in LN229 cells depleted of CDC42 (n=4) or GRAF1 (n=3), representative confocal images shown in C and D. Student's one sample t-test, *p≤0.05, **p≤0.01, ns - non-significant (p>0.05). Each dot represents data from one independent experiment whereas bars represent the means ± SEM from n experiments. GAS6- GAS6-stimulated cells.

4.4.2.4 The impact of downregulation of ARF6 for the uptake of GAS6-AXL complexes

CD44 has been also described to be internalized via ARF6- dependent endocytosis [186, 391]. Therefore, since CD44 and AXL displayed up to 50% of colocalization (Fig. 4.26B), the involvement of ARF6 in GAS6-induced AXL endocytosis was investigated in LN229 cells. To this end, GAS6-AXL internalization was analyzed in cells depleted of ARF6. The obtained results showed that inactivation of ARF6 reduced the uptake of GAS6-AXL complexes, similarly to depletion of CDC42 and GRAF1. These data indicate that along with the CLIC/GEEC pathway, AXL can be internalized in ARF6-dependent manner (Fig. 4.28A-D).

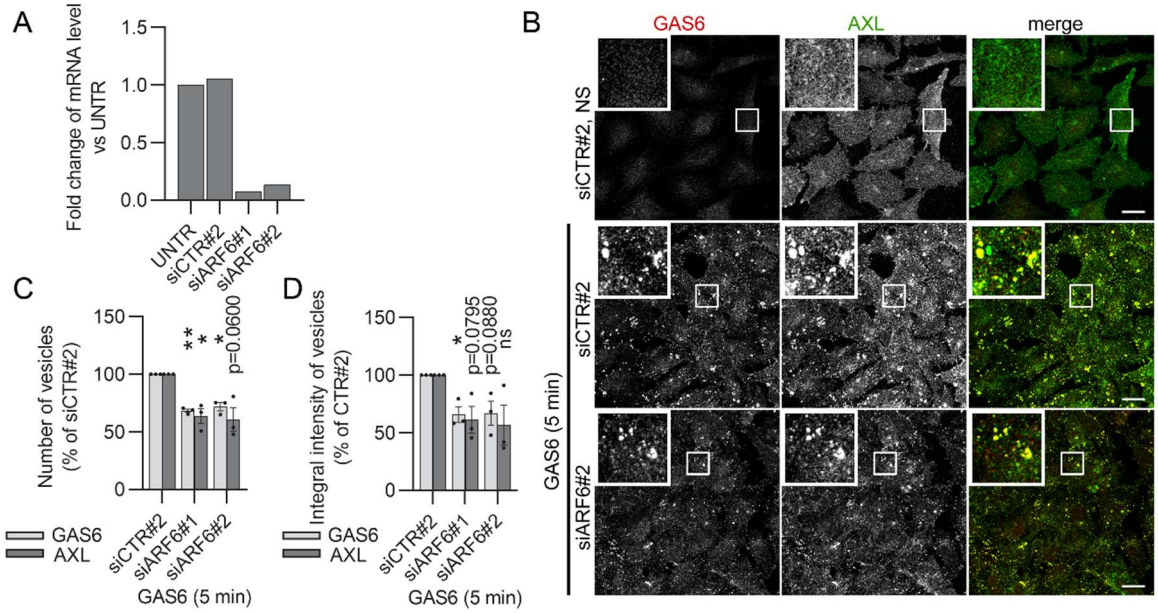

Fig. 4.28 The influence of siRNA-mediated silencing of *ARF6* on GAS6-AXL endocytosis
A Graph showing silencing efficiency of ARF6. LN229 cells were transfected with non-targeting (siCTR#2) and *ARF6*-targeting (siARF6#1 and siARF6#2) siRNA and analyzed by RT-qPCR 72 h after transfection. Values are presented as a fold change versus non-transfected cells (UNTR), set as 1. **B** Confocal images showing GAS6-induced accumulation of GAS6- and AXL- positive endosomes in cells depleted of ARF6. Cells were transfected with non-targeting siRNA (siCTR#2) and siRNA targeting *ARF6* (siARF6#1 and siARF6#2). Seventy two h after transfection serum-starved LN229 cells were stimulated with GAS6 for 5 min, fixed and stained with anti-Myc (red) to visualize GAS6 and anti-AXL (green) antibodies. Insets in confocal images show magnified views of boxed regions in the main

images. Scale bars: 20 μm. NS- non-stimulated cells, GAS6- GAS6-stimulated cells. **C, D** Quantification of number (C) and integral fluorescence intensity (D) of GAS6- and AXL-positive vesicles in LN229 cells depleted of ARF6 (representative confocal images shown in B), n=4. Student's one sample t-test, *p≤0.05, **p≤0.01, ns - non-significant (p>0.05). Each dot represents data from one independent experiment whereas bars represent the means ± SEM from n experiments. GAS6- GAS6-stimulated cells.

Summarizing all results on endocytic pathways mediating uptake of GAS6-induced AXL, the data imply that a fraction of AXL can be internalized via CME, however depletion of key regulators of this route does not affect GAS6-AXL endocytosis, suggesting that CIE pathways compensate for the endocytic uptake of AXL in the absence of functional CME. In line with that, the results described in this thesis confirmed the involvement of several CIE routes, specifically macropinocytosis, CLIC/GEEC and ARF6-dependent pathways, in GAS6-AXL internalization.

4.5 The fate of internalized AXL receptor

Upon internalization receptors reach early endosomes from which they are targeted for degradation, via late endosomes and lysosomes, or are recycled back to the plasma membrane [392]. The most commonly used marker of early endosomes is EEA1, whereas late endosomes and lysosomes are typically marked with lysosomal-associated membrane protein 1 (LAMP1).

4.5.1 Limited colocalization between AXL and EEA1

To check whether AXL traffics through EEA1-positive population of early endosomes, the colocalization of GAS6 or AXL with EEA1 was calculated. The obtained results showed that the maximal colocalization (below 40%) was observed after 5 min of stimulation, which implied that the majority of GAS6-AXL complexes did not traffic through EEA1-positive vesicles (Fig. 4.16A and 4.29A). In contrast, up to 80% colocalization of EGFR with EEA1 was observed after 10 min of stimulation with EGF (Fig. 4.29B and C). These results, together with limited colocalization between AXL and EGF shown in Fig. 4.17D, suggested that AXL and EGFR were predominantly trafficked through different populations of endosomes.

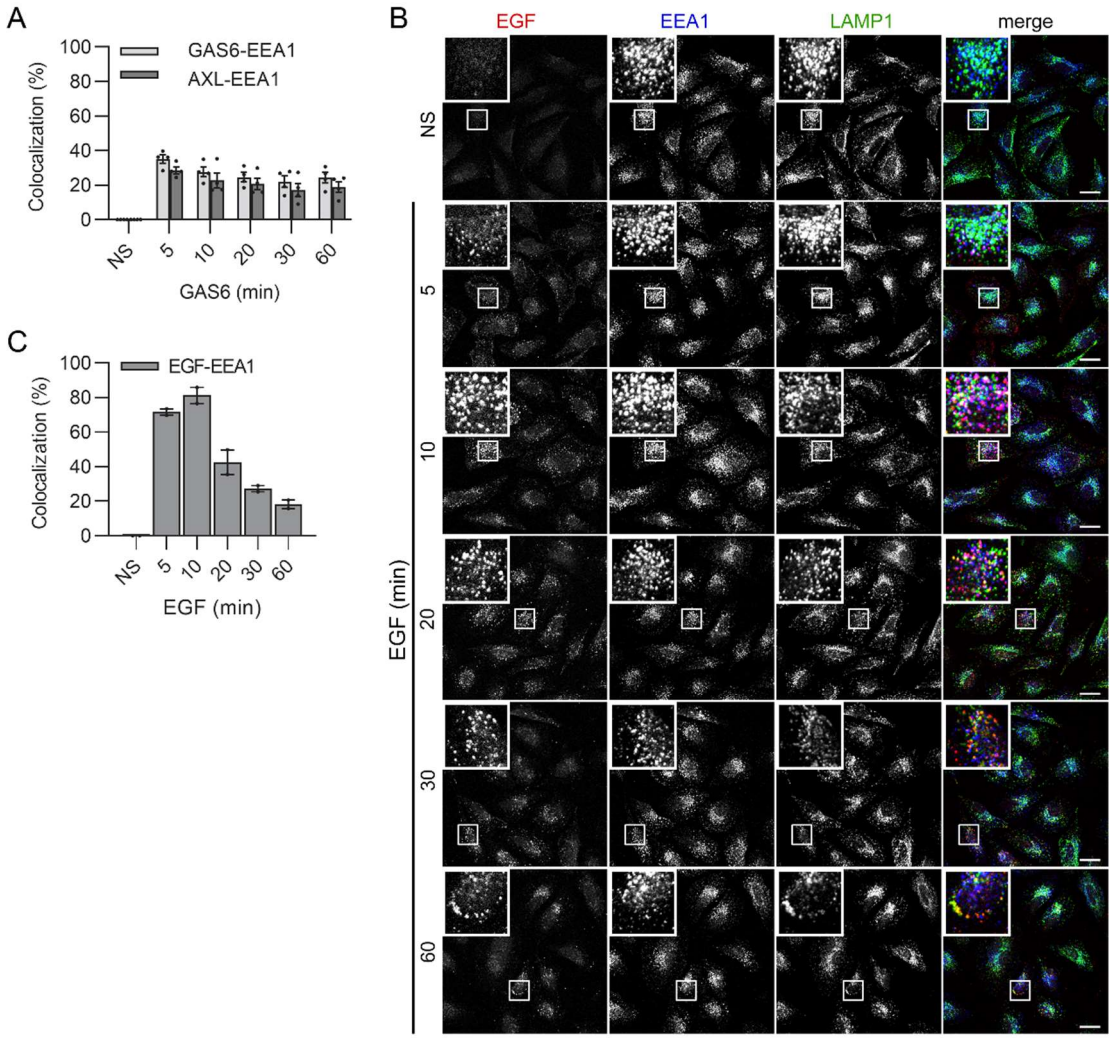

Fig. 4.29 The comparison of the colocalization between AXL, GAS6 or EGF with EEA1
A Quantification of the colocalization of GAS6 and AXL with EEA1 in LN229 cells after stimulation with GAS6 (representative confocal images shown in Fig. 4.16A), n=4. Each dot represents data from one independent experiment whereas bars represent the means ± SEM from n experiments. NS- non-stimulated cells, GAS6- GAS6-stimulated cells. **B** Confocal images showing endosomal accumulation of EGF and colocalization of EGF with EEA1 and LAMP1. Serum-starved LN229 cells were stimulated with EGF for increasing time periods, fixed and stained with anti-EGF (red), anti-EEA1 (blue) and anti-LAMP1 (green) antibodies. Insets in confocal images show magnified views of boxed regions in the main images. Scale bars: 20 µm. NS- non-stimulated cells, EGF- EGF-stimulated cells. **C** Quantification of the colocalization between EGF and EEA1 in LN229 cells after stimulation with EGF (representative confocal images shown in B), n=2. Each dot represents data from one independent experiment whereas bars represent the means ± SEM from n experiments. NS- non-stimulated cells, EGF- EGF-stimulated cells.

4.5.2 The colocalization between AXL, GAS6 or EGF with LAMP1

Colocalization of internalized RTKs with LAMP1 is considered as a hallmark of receptor degradation. Thus, to check whether internalized AXL is sorted to the endo-lysosomal system for degradation, its colocalization with LAMP1 was calculated. As shown in Fig. 4.30A and B, GAS6 and AXL were not found in LAMP1-positive endosomes, even at late time points of GAS6 stimulation. In contrast, EGFR, which was previously shown to be sorted for degradation in lysosomes after stimulation with high concentrations of EGF [393],

displayed up to 65% colocalization with LAMP1, as early as after 20 min of EGF stimulation (Fig. 4.30B). These results suggested that, unlike EGFR, internalized AXL is not primarily targeted for lysosomal degradation.

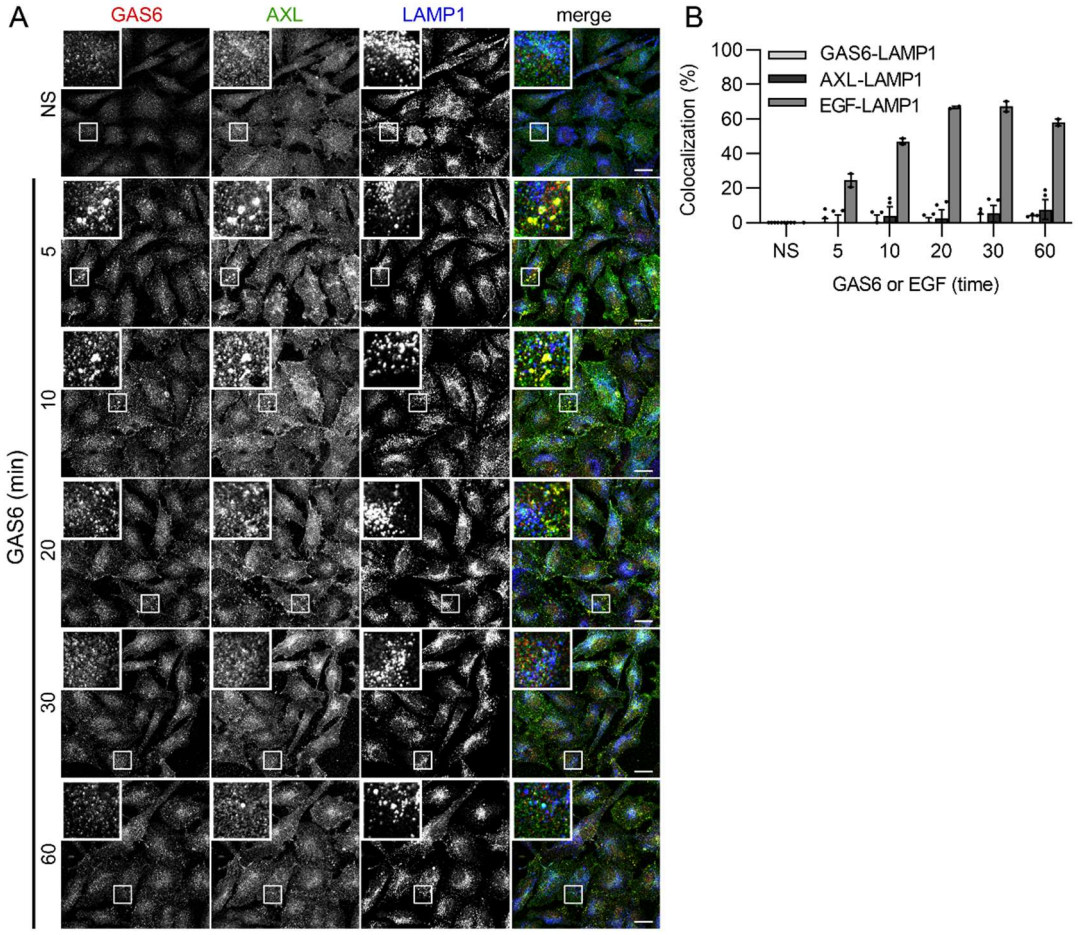

Fig. 4.30 The comparison of the colocalization between AXL, GAS6 or EGF with LAMP1

A Confocal images showing colocalization of GAS6 and AXL with LAMP1. Serum-starved LN229 cells were stimulated with GAS6 for increasing time periods, fixed and stained with anti-Myc (red) to visualize GAS6, anti-AXL (green) and anti-LAMP1 (blue). Insets in confocal images show magnified views of boxed regions in the main images. Scale bars: 20 µm. NS- non-stimulated cells, GAS6- GAS6-stimulated cells. **B** Quantification of the colocalization between GAS6, AXL or EGF with LAMP1 in LN229 cells after stimulation with GAS6 (representative images shown in A) or EGF (representative confocal images shown in Fig. 4.29B), for GAS6 and AXL n=4, for EGF n=2. Each dot represents data from one independent experiment whereas bars represent the means ± SEM from n experiments. NS- non-stimulated cells, GAS6 or EGF- GAS6- or EGF-stimulated cells.

4.5.3 The protein level of AXL upon GAS6 stimulation

To corroborate whether fast decrease in the endosomal accumulation of AXL (Fig. 4.16A-C) is not a result of its degradation, as implied by the lack of colocalization between GAS6 or AXL with LAMP1, the total level of the receptor was analyzed after stimulation with GAS6. Cells were incubated with cycloheximide (CHX), to prevent *de novo* synthesis of proteins, and next stimulated with the AXL ligand. WB analysis showed that the level of AXL was stable up to 60 min of GAS6 stimulation (Fig. 4.31A and B). These results

indicated that, in contrast to EGFR, which was described to be degraded after stimulation with high concentrations of EGF [393], endocytosed AXL is not degraded, but probably is recycled back to the plasma membrane.

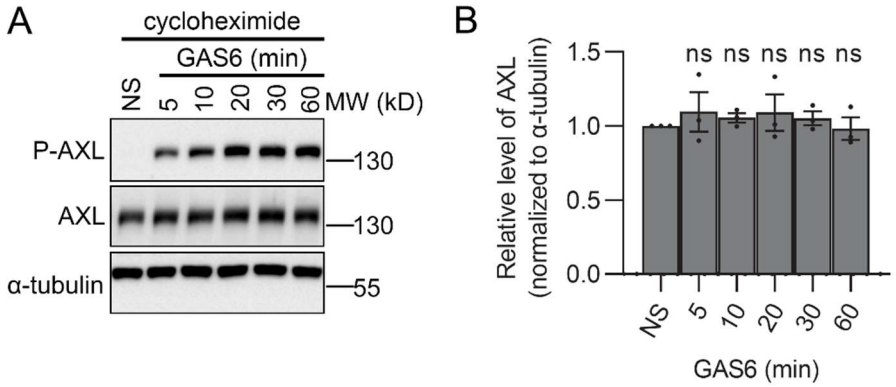

Fig. 4.31 The protein level of AXL upon GAS6 stimulation
A Western blot showing GAS6-induced phosphorylation of AXL (P-AXL, Y702) and the total level of AXL after stimulation with GAS6. Serum-starved LN229 cells were stimulated with GAS6 for the indicated time periods, lysed and immunoblotted against P-AXL and AXL. α-tubulin was used as a loading control. NS- non-stimulated cells, GAS6- GAS6-stimulated cells. **B** Graph showing the densitometric analysis of AXL levels shown in (A), normalized to α-tubulin, n=3. Student's one sample t-test, ns - non-significant ($p>0.05$). Each dot represents data from one independent experiment whereas bars represent the means ± SEM from n experiments. NS- non-stimulated cells, GAS6- GAS6-stimulated cells.

4.5.4 Prolonged phosphorylation of AKT upon GAS6-mediated activation of AXL

Degradation or recycling of receptors terminates or sustains the RTK-mediated signaling, respectively [392]. Thus, the status of ligand-induced activation of AXL and EGFR, as well as phosphorylation of their downstream effectors was investigated. WB analysis revealed that GAS6-stimulated activation of AXL was visible up to 8 h after stimulation, whereas EGF-induced EGFR phosphorylation was detected only up to 1 h after stimulation. As a consequence, activation of AXL, but not EGFR, caused long-lasting activation of AKT (P-AKT, S473), which was detected up to 8 h after stimulation (Fig. 4.32A and B). This effect was specific for AKT, as no notable changes in ERK1/2 activation were observed.

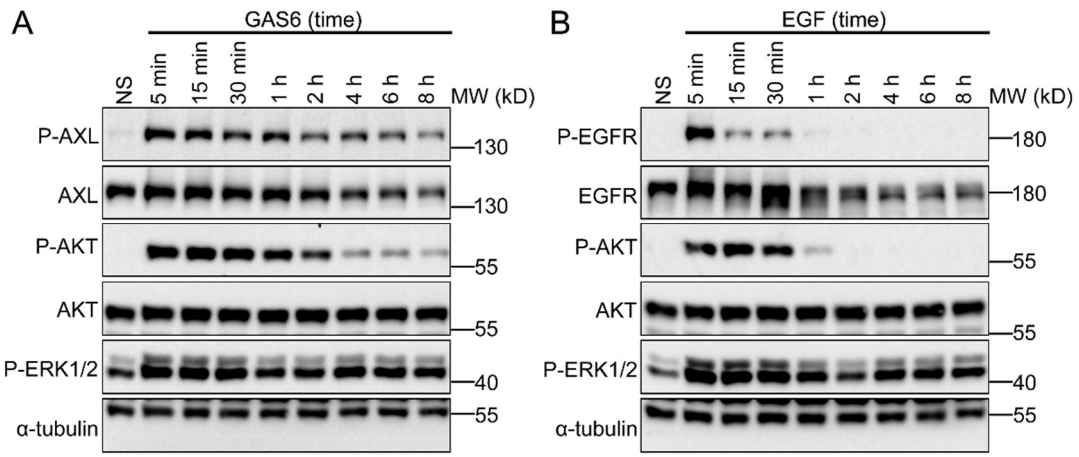

Fig. 4.32 The comparison of AKT phosphorylation upon ligand-stimulated activation of AXL or EGFR

A, B Western blot showing phosphorylation of AXL (P-AXL, Y702) (A) and EGFR (P-EGFR, Y1173) (B) and their downstream effectors, AKT (P-AKT, S473) and ERK1/2 (P-ERK, T202/T204). Serum-starved LN229 cells were stimulated with GAS6 (A) or EGF (B) for increasing time periods, lysed and immunoblotted against the indicated phosphorylated or total proteins. α-tubulin was used as a loading control. NS-non stimulated cells.

Cumulatively, these findings suggest that AXL traffics through different populations of endosomes than EGFR. Additionally, in contrast to EGFR, the majority of internalized AXL molecules are not degraded but probably recycled back to the plasma membrane, that prolongs AXL phosphorylation and activation of its downstream effector AKT.

5. Discussion

Numerous studies have linked AXL and its signaling with pathogenesis of different types of cancers as well as viral infections [24, 112]. However, AXL-driven molecular mechanisms regulating these processes at the cellular level have remained largely uncharacterized. Therefore, to shed light on the biological roles of AXL, the proximity interactome of AXL has been identified in this thesis. The obtained results showed that AXL interacts with proteins implicated in various cellular processes including actin remodeling and endocytic trafficking, among others.

Endocytosis is an important regulator of RTK function as it controls the availability of these receptors at the cell surface, their fate upon internalization, as well as RTK-mediated signaling [124-126]. The abundance of endocytic proteins among the identified AXL interactome suggests that endocytosis plays an important role in the regulation of AXL biology. Importantly, neither AXL nor other members of TAM receptor subfamily have been so far studied with respect to their endocytosis. Given this, a detailed characterization of AXL internalization has been described in this thesis. The studies performed here showed that GAS6, a ligand for AXL, induces rapid internalization of GAS6-AXL complexes, which requires the kinase activity of AXL receptor and operates via both CME and CIE pathways. Interestingly, blocking a single endocytic pathway, except for CLIC/GEEC and ARF6-dependent route, was not sufficient to efficiently reduce endocytosis of GAS6-AXL complexes. Additionally, in comparison to other RTKs, such as EGFR or PDGFRβ, endocytosis of AXL proceeded faster. Moreover, in contrast to ligated EGFR, the majority of internalized AXL was not degraded, but probably sorted for recycling back to the plasma membrane. The latter was reflected by the sustained phosphorylation of AXL and its downstream effector AKT (Fig. 5.1). Finally, the results presented in this thesis showed that depletion of AXL was sufficient to block GAS6 internalization, which supports a notion that AXL is a primary receptor for GAS6, in agreement with previous reports from our laboratory [89, 394].

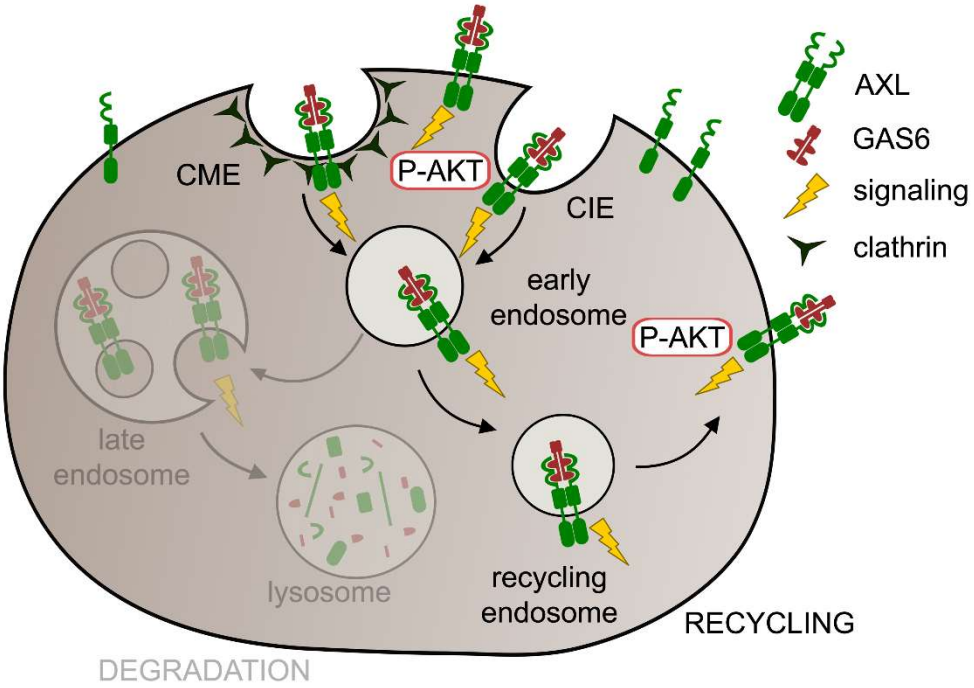

Fig. 5.1 A model showing GAS6-induced AXL endocytosis and the fate of internalized AXL receptor

GAS6 stimulation triggers internalization of AXL via CME and CIE pathways. AXL endocytosis does not promote receptor degradation, but most probably triggers its recycling back to the plasma membrane, which altogether results in sustained phosphorylation of AXL and its downstream effector AKT.

5.1 BioID as a tool for characterization of biological processes regulated by AXL

Since its development in 2012, BioID has been widely used as a tool for identification of cellular functions of various proteins, including RTKs [227, 395-398]. This method allows identification of potential interacting partners and proteins located in the close proximity of a protein of interest (Fig. 4.1). Additionally, in comparison to conventional methods such as co-immunoprecipitation, BioID allows identification of weak and transient interactions as well as mapping constituents of a certain subcellular compartment [227, 395]. For BioID, generation of cell lines with stable expression of a protein of interest fused with modified biotin ligase BirA* is recommended. In contrast to transient transfections, such conditions ensure similar levels of a protein of interest in all cells in the population [227].

Therefore, to identify an interactome of AXL, BioID has been performed in two cell lines, HEK293 and LN229, both stably expressing AXL-BirA* proteins (Fig. 4.3-4.7). HEK293 cells are commonly used for BioID [227-229], but they do not express AXL endogenously. Thus, to ensure identification of AXL interactome in a biologically- and cancer-relevant model, LN229 cells expressing this receptor were also used. Nevertheless, despite using different cell lines, the results obtained by BioID were similar. Firstly, the congruency between the two cell lines was observed with respect to the number of identified interactors with 116 and 114 proteins identified in samples from non-stimulated HEK293 and

LN229 cells, respectively, and 151 proteins identified in samples from HEK293 and 147 from LN229 cells stimulated with GAS6 (Fig. 4.8). Secondly, the identified proteins were implicated in similar cellular functions and pointed to the involvement of AXL in the regulation of axonogenesis, cell junction organization, receptor-mediated endocytosis, endosomal transport, signaling and actin dynamics, among others (Fig. 4.8-4.10) [89]. Thus, even though HEK293 cells do not express AXL endogenously, in contrast to LN229 cells, both cell lines turned out to be suitable for the identification of AXL proximity interactome.

Characterization of AXL interactome in the presence or absence of GAS6 aimed to distinguish between AXL functions in GAS6-stimulated vs basal conditions, respectively. In both cell lines more interactors were identified in cells after GAS6 stimulation in comparison to non-stimulated cells, specifically 151 vs 116 in HEK293 cells and 147 vs 114 in LN229 cells (Fig. 4.8). This was also reflected in the GO analyses of biological processes, which showed that the majority of them require activated receptor (Fig. 4.9). Notably, among identified AXL interactors, several typical adaptors and effectors for RTK signaling were present [399, 400], such as GAB1, GAB2, p85 subunits of PI3K, NCK2, SHC1, STAT2, STAT3, and the majority of them were specifically identified upon GAS6 stimulation (Table S1 and S2 in supplementary materials). Thus, despite the fact that AXL signaling occurs within several minutes, a relatively long-lasting BioID assay was a very useful tool to characterize GAS6-dependent AXL processes. Specifically, in GAS6-stimulated cells the ligand was constantly present in the medium for 24 h, which allowed multiple cycles of AXL activation and, in turn, accumulation of the biotinylated proximal proteins interacting with the activated receptor. Importantly, 95 out of 147 AXL proximity interactors identified in GAS6-stimulated LN229 cells were also found by Abu-Thuraia *et al.* in one of the recently published AXL phosphoproteomes, identified in Hs578T cells after 5, 10 and 20 min of GAS6 stimulation [75]. Such significant overlap between the two datasets provides an independent validation of the BioID results presented here and justifies the selection of BioID method to study GAS6-induced AXL processes. Of note, these datasets, as well as another AXL phophoproteomic study by Wu *et al.* [401], highlighted the involvement of this receptor in the regulation of actin dynamics. In line with that, results published by our laboratory confirmed the contribution of AXL to the regulation of actin-related processes. Our data showed that GAS6-mediated AXL activation promoted actin cytoskeleton rearrangements manifested by formation of circular dorsal ruffles (CDRs) and peripheral ruffles (PRs), macropinocytosis and focal adhesion (FA) turnover, which altogether contributed to invasion of cancer cells [89].

BioID allows also obtaining clues about intracellular localization of proteins and the GO analysis of cellular components of AXL proximity interactors indicated the potential compartments occupied by AXL receptor. For example, some identified AXL interactors are known to reside on the plasma membrane, a typical AXL localization site, but also on leading edges of cells, lamellipodium, FAs or endosomes (Fig. 4.10B). The more profound analysis of AXL interactors revealed a broad representation of proteins implicated in endocytosis and suggested involvement of several endocytic pathways in AXL intracellular trafficking, which was further validated experimentally in this dissertation (Fig. 4.11-4.32). By comparison, a proximity interactome of FGFR4 identified by BioID was previously used for mapping of the intracellular trafficking of FGF1-activated FGFR4 [398]. In turn, in case of insulin-like growth factor 1 receptor (IGF1R), BioID allowed identification of SNX6 as a new interactor of IGF1R and a regulator of its signaling [396]. Given this, based on the data presented here and studies by others, BioID can be considered as a useful strategy to study the localization and the biology of RTKs both under basal and ligand-stimulated conditions [89, 396-398].

5.2 Multitude of routes of GAS6-induced AXL internalization

Endocytosis is considered as one of major regulators of RTK function, and these receptors were shown to be internalized via multiple endocytic pathways, both CME and CIE. Existence of such distinct mechanisms of internalization ensures the precise regulation of endocytic uptake of receptors, which affects their fate and, in turn, regulates RTK-mediated signaling and cellular responses [121, 126]. Furthermore, exploitation of multiple endocytic pathways by a given receptor ensures its efficient uptake, even if one of them is perturbed [121, 126]. Therefore, since the identified AXL interactome contained multiple proteins implicated in endocytosis, the mechanisms of GAS6-induced endocytic uptake of AXL receptor have been investigated in this thesis. The obtained results showed that upon GAS6 stimulation, GAS6-AXL complexes are rapidly internalized into the cells (Fig. 4.12 and 4.16) via both CME and CIE pathways (Fig. 4.19-4.28).

The results presented here showed that AXL colocalizes with CME regulators, such as CLC and PICALM, which points towards the involvement of CME in AXL endocytosis (Fig. 4.20). However, inactivation of key regulators of CME, including efficient depletion of CHC, did not reduce AXL internalization (Fig. 4.21-4.23). In the literature, impairment of CME was shown to affect endocytosis and signaling outputs of other RTKs, such as EGFR or PDGFRβ [124, 181, 209]. Specifically, siRNA-mediated depletion of CHC or AP2μ2 significantly decreased internalization of EGFR or PDGFRβ [181, 209, 402]. Additionally, uptake of these receptors was also reduced upon depletion of DNM2 [181, 403]. In contrast, as shown by Kamila Kozik, a master student in our laboratory, AXL endocytosis was not perturbed even

upon efficient knockout of DNM2, despite involvement of this protein in both CME as well as some CIE pathways (manuscript under revision). These results may indicate that, as opposed to EGFR or PDGFRβ [181, 402], the internalization pathways of AXL are largely interchangeable, and in the absence of functional CME other, clathrin-independent, pathways mediate compensatory uptake of AXL receptor.

Differences in AXL internalization in comparison to the endocytic uptake of other RTKs were also manifested by the kinetics of these processes. The results presented here showed that GAS6-induced internalization of AXL occurs faster than the uptake of ligated EGFR or PDGFRβ, in cancer cells or in normal human fibroblasts, respectively (Fig. 4.16-4.18). Such dissimilarities may suggest that AXL endocytosis is predominantly mediated via fast CIE pathways, and AXL interactome suggested that several CIE routes are implicated in AXL endocytosis. The common feature of CIE is their strong dependency on actin polymerization [137]. Thus, the involvement of CIE in the uptake of GAS6-AXL complexes is consistent with our findings, showing that AXL activation induces remodeling of actin cytoskeleton [89]. Specifically, GAS6 triggered intense membrane ruffling manifested by appearance of PRs and CDRs, which in turn promoted formation of big endosomal structures, macropinosomes, and facilitated uptake of GAS6-AXL complexes via macropinocytosis (Fig. 4.24) [89]. Furthermore, the identified AXL interactome contained proteins involved also in other CIE pathways, such as caveolae-, flotillin-, ARF6-dependent, CLIC/GEEC or FEME routes. Some of these fast endocytic pathways play a critical role in processes that require quick redistribution of RTKs from one cellular compartment to another, for example during cell spreading, migration and invasion [404, 405]. In line with that, CLIC/GEEC and FEME pathways were reported to function at the leading edges of migrating cells [179, 189] and, as shown by Zajac *et al.* and our group, AXL localizes to these structures [89, 406]. Thus, fast endocytosis may contribute to the regulation of AXL localization and signaling during cancer cell migration and invasion [89].

The involvement of CIE routes in AXL internalization has been further elaborated in this thesis (Fig. 4.19, 4.25-4.28). The obtained results showed that AXL endocytosis was decreased only upon downregulation of CLIC/GEEC or ARF6-dependent pathways (Fig. 4.27-4.28), suggesting a predominant role of these two endocytic routes in the internalization of GAS6-AXL complexes. Interestingly, both CLIC/GEEC and ARF6-dependent pathways are known to regulate internalization of CD44 [179, 186], a protein considered as typical CLIC/GEEC cargo and one of identified AXL proximity interactors. Thus, colocalization of both proteins was analyzed in LN229 cells stimulated with GAS6 and anti-CD44 agonistic antibodies, showing up to 50% of colocalization between these two proteins (Fig. 4.26).

Interestingly, CD44 was already shown to modulate signaling and function of RTKs such as MET, VEGFR, FGFR, EGFR or PDGFR [407], thus, the results obtained here suggest that CD44 might act as a co-receptor for AXL participating in its internalization. Nevertheless, this hypothesis requires further experimental examination.

Based on AXL proximity interactome, caveolae-dependent endocytosis was also considered to be involved in AXL endocytosis. However, experiments showed that downregulation of caveolin 1, a main regulator of the pathway, did not decrease AXL endocytosis. In turn, it unexpectedly caused a significant increase in the internalization of GAS6-AXL complexes (Fig. 4.25). This upregulation of AXL endocytic uptake may result from the fact that caveolin 1 and cavin 1 (another regulator of caveolae-mediated endocytosis) were shown to modulate other endocytic pathways, specifically the CLIC/GEEC route [245, 408]. Increased expression of both proteins reduced CLIC/GEEC endocytosis by affecting PM distribution of CDC42, a main Rho GTPase involved in the formation and maturation of CLICs [175, 245]. Additionally, caveolin 1 was shown to bind CDC42 in its GDP-bound state, thus maintaining it in its inactive form [408]. Therefore, the observed increase in AXL endocytosis in the absence of caveolin 1 may result from the CLIC/GEEC pathway operating more efficiently.

Overall, the obtained data showed that AXL endocytosis may be facilitated by both CME and CIE pathways, the latter being macropinocytosis, CLIC/GEEC and ARF6-dependent endocytosis. However, downregulation of a single endocytic route, except for CLIC/GEEC and ARF6-dependent endocytosis, did not decrease internalization of GAS6-AXL complexes. Additionally, experiments regarding the involvement of CME in AXL internalization showed that, despite AXL colocalization with CLC and PICALM, downregulation of key regulators of CME did not reduce cellular uptake of AXL (Fig. 4.20-4.23). Therefore, these results argue that the colocalization studies may serve as a better approach to investigate the contribution of a particular endocytic pathway to RTK endocytosis, than inactivation of specific endocytic regulators.

5.3 The role of endocytosis in the regulation of the fate of internalized receptors

After internalization, RTKs accumulate on early endosomes, from where they are either targeted for degradation in lysosomes or recycled back to the plasma membrane [124]. Both processes are mediated by different populations of endosomes, thus analysis of the colocalization of their markers with a given RTK may give insights into the fate of internalized receptor.

The results presented in this thesis showed that, in contrast to EGFR, AXL displays only limited colocalization with early endosomes marked with EEA1 (Fig. 4.29). Thus, a

different population of early endosomes must be predominantly responsible for endocytic trafficking and sorting of internalized AXL receptor. APPL1-positive vesicles may represent one such population [205]. For example, in cells expressing mutated p53, APPL1 endosomes located in the cell periphery were responsible for fast recycling of EGFR and β1 integrins, increased turnover of FAs and increased migration and invasion of cancer cells [409]. Since AXL triggers an invasive phenotype also through regulation of FA dynamics [75, 89] and most probably undergoes fast recycling, it is possible that this receptor traffics through APPL1-positive endosomes, however the latter requires further verification.

Despite the fact that AXL and EGFR were shown to heterodimerize [38, 410], they displayed limited colocalization (Fig. 4.17), which indicates that these receptors traffic mostly through different populations of endosomes. Consequently, in contrast to ligated EGFR, GAS6-AXL complexes did not colocalize with LAMP1 (Fig. 4.30), a marker of late endosomes and lysosomes. Accordingly, GAS6 stimulation did not trigger degradation of AXL receptor (Fig. 4.31). Of note, limited colocalization of AXL with EEA1 already suggested that the majority of endocytosed AXL is not degraded, since the recent study by Kamentseva *et al.* postulated that EEA1-positive vesicles may serve as pre-existing compartments of the degradative pathway [411].

AXL interactome contained a broad representation of proteins implicated in endocytic recycling (Table 1, Table S1 and S2 in supplementary materials), which suggests that internalized AXL is most probably recycled back to the plasma membrane. The fast delivery of AXL back to the plasma membrane might be responsible for the observed here sustained activation of AKT (Fig. 4.32). Consequently, this prolonged AXL-mediated AKT phosphorylation might be important for AXL-regulated cancer cell migration and invasion [409, 412, 413], especially that the plasma membrane is a major site of activation of this downstream effector kinase [414, 415]. In contrast, EGFR-mediated phosphorylation of AKT was transient and disappeared after 1 h of ligand stimulation, which most probably resulted from termination of EGFR signaling due to degradation of this receptor (Fig. 4.32). Such differences between AXL- and EGFR-induced signaling may further affect cellular responses triggered by these receptors. For example, a comparison of the phosphoproteomic studies of AXL and EGFR has already indicated distinct roles of these receptors in cancer cell migration and invasion, suggesting that EGFR modulates adherens junction disassembly, whereas AXL is important for FA turnover [75].

As shown by Abu-Thuraia *et al*., AXL not only regulates turnover of FAs but also localizes to these structures [75]. Additionally, a recent study by Revach *et al*. showed that AXL localizes also to invadopodia and regulates function of these actin-rich invasive

protrusions in melanoma cells [416]. Thus, AXL localization to FAs and invadopodia might be crucial for the regulation of dynamics of these structures and, in turn, promote AXL-mediated migration and invasion of cancer cells. How AXL localizes to these structures remains unknown, however it has been shown for adhesion molecules, such as integrins as well as RTKs, that recycling can mediate their translocation between distinct plasma membrane regions to facilitate migration and invasion of cancer cells [417, 418]. Given this, it is possible that rapid uptake of AXL and its subsequent recycling might be required for the delivery of this receptor to both FAs and invadopodia, therefore linking AXL intracellular trafficking to AXL-dependent invasion. Importantly, a very recent study of Smith *et al.* showed that also signaling from recycling endosomes can affect RTK-mediated cellular responses. Specifically, the authors showed that recycling-dependent FGFR signaling promoted phosphorylation of EGFR, which in turn altered trafficking of the two receptors and stimulated FGFR-induced cell proliferation [419]. Thus, since upon internalization AXL undergoes recycling, and its heterodimerization with EGFR has been already shown [38, 410], it is plausible that both receptors can mutually affect their signaling and perhaps also their intracellular trafficking.

Based on the results presented here, AXL internalization and subsequent recycling can be mediated by several pathways. Nevertheless, finding the link between particular mechanisms of AXL internalization and AXL-mediated cellular responses remains difficult. With the exception of CLIC/GEEC and ARF6-dependent endocytosis, downregulation of any other single endocytic pathway did not decrease AXL internalization (Fig. 4.21-4.28). A similar problem may occur with the characterization of AXL recycling routes. The identified AXL interactome contained multiple proteins implicated in diverse recycling pathways. For example, it included SNX1, SNX2 and SNX6, members of the sorting nexin family involved in endosomal cargo sorting [420]; GGA3, which was already shown to regulate signaling from activated MET or TrkA receptors through their recycling [285, 286] or RAB11FIPs, effector proteins associated with the widely studied recycling route through RAB11 endosomes [328, 331, 334], among others. Therefore, it is plausible that AXL recycling, similarly to its internalization, is mediated by multiple, potentially overlapping mechanisms. Additionally, main molecular players regulating endocytic uptake and recycling of AXL may have pleiotropic cellular functions, which hampers finding a direct link between endocytic or recycling events and a particular cellular response.

5.4 The role of GAS6 in the activation of TAM receptors

Previous studies implied that GAS6 can bind and activate all three TAMs [9, 378-381]. However, the data recently published by our group questioned the involvement of GAS6 in the activation of TYRO3 or MER, since depletion of AXL, but not of TYRO3, blocked GAS6-induced processes such as membrane ruffling, macropinocytosis, cell invasion and phosphorylation of downstream effectors [89, 394]. This dissertation provides yet another piece of evidence supporting the predominant role of GAS6 in the activation of AXL but not other TAM receptors. The results presented here showed that GAS6 stimulation specifically triggers internalization of AXL, since depletion of AXL but not of TYRO3 (MER, a third TAM receptor, is not expressed in LN229 cells used in the study), completely abolished intracellular accumulation of the ligand on endosomes (Fig. 4.13 and 4.14). Altogether, this thesis and previous studies performed by our group provide evidence that AXL is a primary receptor for GAS6 [89, 394].

Since GAS6 simulation triggers endocytosis but also phosphorylation of AXL, the involvement of AXL tyrosine kinase domain activity in the internalization of GAS6-AXL complexes has been investigated. In case of EGFR, multiple studies have shown that the induction of its kinase activity is required for the endocytic uptake of EGFR [382, 421-426]. However, there are studies that question the link between the activation of EGFR kinase domain and receptor internalization [383, 427]. The results obtained in this dissertation showed that treatment of cells with AXL kinase inhibitors prevented endocytosis of GAS6-AXL complexes (Fig. 4.15), providing evidence that activation of AXL kinase domain is indispensable for the internalization of this RTK.

5.5 Consequences of AXL endocytosis – the role in viral entry

Since endocytosis serves as a mechanism for viral infection, and AXL was described as an entry receptor for several viruses, including Zika virus and SARS-CoV-2 [110, 111, 428], a detailed characterization of AXL internalization is of particular importance. Studies on Ebola virus and Lassa virus showed that AXL specifically increases their cellular entry through macropinocytosis [108, 429], and the results obtained within this dissertation, as well as in the article recently published by our group [89], revealed that GAS6 triggers AXL-mediated membrane ruffling and macropinocytosis. On the other hand, AXL-dependent Zika virus entry requires clathrin-mediated endocytosis [110, 430], which was also identified here as one of internalization pathways mediating uptake of AXL. Additionally, a recent study of Wang *et al*. showed that SARS-CoV-2 colocalized with AXL in H1299 cells within intracellular compartments positive for several endocytic markers such as CHC, EEA1 or CAV1 [111].

The abovementioned reports indicate that AXL-mediated viral entry may be facilitated via multiple routes of endocytosis. In line with that, the results obtained in this thesis showed that AXL can utilize several endocytic pathways to enter cells, but the downregulation of one of them had only moderate effect on AXL internalization. In turn, GAS6-mediated AXL endocytosis was completely abolished upon inhibition of its kinase activity (Fig. 4.15). Accordingly, AXL-dependent entry of Lassa virus, Ebola virus, Zika virus and SARS-CoV-2 has been reported to rely on AXL kinase activity [108, 110, 111, 429]. Thus, based on the data presented in this study and reports of other researchers, inhibition of AXL kinase domain can be considered as a more effective strategy for antiviral therapy in comparison to targeting a given endocytic pathway. Importantly, R428 (bemcentinib), one of AXL inhibitors, was suggested as a promising drug against COVID-19 and is currently being tested in clinical trials [118-120]. Thus, the results presented within this dissertation, as well as the study recently published by our group [89], provide a rationale for the use of AXL inhibitors in antiviral therapies. Specifically, a previously observed decrease in viral infection upon pharmacological inhibition of AXL kinase activity [108, 110, 111, 429] can be mechanistically explained by the fact that AXL endocytosis was completely abolished in cells treated with AXL inhibitors.

6. Conclusions

The data presented in this dissertation provide new insights into the cellular processes regulated by AXL receptor as well as endocytic trafficking of this receptor. Specifically, the results argue that:

1. BioID is a useful tool for the identification of AXL interactome and the characterization of AXL-dependent cellular processes.
2. AXL interacts with proteins implicated in various actin-related processes, axonogenesis, cell junction organization, signaling, regulation of GTPase activity, cell-substrate adhesion, receptor-mediated endocytosis and endosomal transport, among others. Importantly, the presence of several proteins implicated in endocytic trafficking among proximity interactors of AXL indicates that endocytosis is an important process regulating the function of AXL.
3. Upon ligand binding, GAS6-AXL complexes are rapidly internalized via clathrin-mediated endocytosis as well as several clathrin-independent routes, namely: macropinocytosis, CLIC/GEEC and ARF6-dependent pathways.
4. AXL is a primary receptor for GAS6 and the activation of AXL tyrosine kinase domain is indispensable for endocytosis of GAS6-AXL complexes.
5. GAS6-induced AXL endocytosis is a faster process than ligand-stimulated internalization of other RTKs, such as EGFR or PDGFRβ.
6. The majority of GAS6-AXL complexes traffics through different populations of endosomes than ligand-bound EGFR.
7. Internalized AXL is not sorted towards degradation in lysosomes but most probably recycled back to the plasma membrane, which correlates with prolonged activation of AXL and its downstream effector AKT.

7. Future prospects

The results presented in this dissertation provided the first comprehensive analysis of AXL interactome that shed light on the cellular processes regulated by this receptor and pointed towards the involvement of AXL in the regulation of actin dynamics. Moreover, the numerous representation of endocytic proteins among AXL proximity interactome suggested that endocytosis plays an important role in the regulation of AXL function. Thus, since AXL endocytosis has not been studied so far, the characterization of this process has been performed in this thesis, showing the involvement of several endocytic pathways in AXL internalization, and suggesting that the majority of internalized receptor is recycled back to the plasma membrane. However, several aspects of AXL biology still remain to be addressed.

The most obvious question concerns the mechanisms of AXL endocytic recycling. Since AXL interactome suggests a potential involvement of several recycling pathways in AXL trafficking, it would be important to analyze their contribution. Based on the experience from studies on AXL endocytosis, depletion of specific regulators of a particular recycling route may not be the best approach, since it may result in compensatory recycling mediated by other pathways. Given this, the colocalization experiments may serve as a better methodology to characterize this process. For this purpose, immunofluorescence analyses of cells stained with anti-AXL antibodies together with antibodies recognizing proteins regulating endocytic recycling could be applied. If specific antibodies are not available, an alternative approach may include tagging of recycling regulators with fluorescent tags (e.g. GFP, mCherry). Ideally, CRISPR-Cas9-mediated knock-in of a given fluorescent tag should be introduced to allow labeling of endogenous proteins and avoid overload of cells with a tagged protein, which is often a side effect of overexpression. Additionally, fluorescent tag labeling would also enable to monitor AXL endocytic trafficking in living cells.

Another aspect that requires further studies refers to the fate of internalized AXL receptor and its dependency on a particular endocytic pathway. The results presented in this thesis showed that after internalization the majority of AXL is not degraded but most probably recycled back to the plasma membrane (Fig. 4.30 and 4.31). This was further correlated with sustained phosphorylation of AXL and its downstream effector AKT (Fig. 4.32). Thus, it would be interesting to check whether depletion of AXL trafficking regulators (both for endocytosis and recycling) would affect the fate of internalized receptor, its half-life, duration of its activation and subsequent phosphorylation of its downstream effectors. To address this question, western blot analysis of cells depleted of proteins regulating specific intracellular trafficking routes should be applied. On the other hand, CD44, a cargo of the CLIC/GEEC pathway, that was identified as a potential AXL interacting partner (Table 4.1)

and traffics together with AXL (Fig. 4.26), was found to reduce lysosome-mediated EGFR degradation resulting in sustained downstream activation of AKT [412]. Thus, the association of AXL with CD44 might be also responsible for attenuation of AXL degradation and observed prolonged activation of the receptor and AKT (Fig. 4.32). To verify this potential relationship, degradation of AXL and the phosphorylation status of AXL and AKT should be monitored in cells depleted of CD44.

Another remarkable area for further studies includes finding the link between intracellular trafficking and cellular processes regulated by AXL. Specifically, since numerous studies linked AXL signaling with metastasis and tumor progression [13, 24, 52, 62], it would be interesting to check whether perturbation of AXL trafficking would affect AXL-driven cancer cell invasion. Importantly, the results recently published by our group showed that GAS6 triggers turnover of FAs as well as cell elongation and spreading, which in turn leads to invasion of cancer cells measured by the growth of spheroids in Matrigel [89]. Additionally, studies by Revach *et al.* revealed that AXL localizes to and induces formation of invadopodia, invasive protrusions capable of degradation of ECM components [416]. Thus, analysis of these processes in cells depleted of various endocytic regulators would help to link particular intracellular trafficking routes with AXL-induced invasive phenotype. To start with, it would be reasonable to check the contribution of CLIC/GEEC and ARF6-dependent pathways to AXL-driven invasion, as their downregulation reduced the level of internalized AXL (Fig. 4.27 and 4.28). For this purpose, generation of cell lines bearing CRISPR-Cas9-mediated KO of genes encoding CDC42, GRAF1 or ARF6, main regulators of these pathways, is required, especially for long-lasting spheroid invasion assay. However, it is possible that uptake of GAS6-AXL complexes via a particular endocytic pathway, other than CLIC/GEEC or ARF6-dependent, is crucial for triggering specific cellular responses, even if the total level of internalized AXL receptor was not affected. Given this, testing of the implication of other endocytic pathways in the regulation of AXL-induced cellular processes should also be included.

Finally, additional analyses of the identified AXL interactome may indicate further scientific directions. It could perhaps help to identify unknown functions of this receptor or reveal molecular mechanisms of already known AXL-driven biological processes. One such example is macropinocytosis. As already mentioned, the results recently published by our group showed that GAS6-AXL signaling triggers macropinocytosis that facilitates the uptake of albumin to support cancer cell growth under glutamine deprivation [89]. Interestingly, a comparison of the described here proximity interactors of AXL with regulators of RAS-induced macropinocytosis identified in a genome-wide RNAi screen [431] revealed a partial

overlap between the analyzed datasets. This suggests that among AXL interactors are proteins that possibly regulate AXL-induced macropinocytosis. Thus, verification of their contribution to these processes would help to reveal the molecular mechanisms underlying AXL-driven macropinocytic uptake of nutrients that supports cancer cell growth. In line with that, in a recently received grant, Laboratory of Cell Biology at IIMCB will further investigate the role of AXL and its proximity interactors in macropinocytic nutrient scavenging and subsequent contribution of this process to AXL-driven growth and drug resistance of cancer cells (OPUS grant from the National Science Center, DEC-2020/39/B/NZ3/03429).

8. Literature

1. Lemmon MA, Schlessinger J: Cell signaling by receptor tyrosine kinases. *Cell* 2010, 141(7):1117-1134.
2. Lapraz F, Rottinger E, Duboc V, Range R, Duloquin L, Walton K, Wu SY, Bradham C, Loza MA, Hibino T *et al*: RTK and TGF-beta signaling pathways genes in the sea urchin genome. *Dev Biol* 2006, 300(1):132-152.
3. Satou Y, Sasakura Y, Yamada L, Imai KS, Satoh N, Degnan B: A genomewide survey of developmentally relevant genes in Ciona intestinalis. V. Genes for receptor tyrosine kinase pathway and Notch signaling pathway. *Dev Genes Evol* 2003, 213(5-6):254-263.
4. Manning G, Plowman GD, Hunter T, Sudarsanam S: Evolution of protein kinase signaling from yeast to man. *Trends Biochem Sci* 2002, 27(10):514-520.
5. Manning G, Whyte DB, Martinez R, Hunter T, Sudarsanam S: The protein kinase complement of the human genome. *Science* 2002, 298(5600):1912-1934.
6. Lemke G, Rothlin CV: Immunobiology of the TAM receptors. *Nat Rev Immunol* 2008, 8(5):327-336.
7. Lemke G: Biology of the TAM receptors. *Cold Spring Harb Perspect Biol* 2013, 5(11):a009076.
8. Rothlin CV, Carrera-Silva EA, Bosurgi L, Ghosh S: TAM receptor signaling in immune homeostasis. *Annu Rev Immunol* 2015, 33:355-391.
9. Stitt TN, Conn G, Gore M, Lai C, Bruno J, Radziejewski C, Mattsson K, Fisher J, Gies DR, Jones PF *et al*: The anticoagulation factor protein S and its relative, Gas6, are ligands for the Tyro 3/Axl family of receptor tyrosine kinases. *Cell* 1995, 80(4):661-670.
10. Caberoy NB, Zhou Y, Li W: Tubby and tubby-like protein 1 are new MerTK ligands for phagocytosis. *EMBO J* 2010, 29(23):3898-3910.
11. Caberoy NB, Alvarado G, Bigcas JL, Li W: Galectin-3 is a new MerTK-specific eat-me signal. *J Cell Physiol* 2012, 227(2):401-407.
12. Burstyn-Cohen T, Maimon A: TAM receptors, Phosphatidylserine, inflammation, and Cancer. *Cell Commun Signal* 2019, 17(1):156.
13. Graham DK, DeRyckere D, Davies KD, Earp HS: The TAM family: phosphatidylserine sensing receptor tyrosine kinases gone awry in cancer. *Nat Rev Cancer* 2014, 14(12):769-785.
14. Burstyn-Cohen T: TAM receptor signaling in development. *Int J Dev Biol* 2017, 61(3-4-5):215-224.
15. Manfioletti G, Brancolini C, Avanzi G, Schneider C: The protein encoded by a growth arrest-specific gene (gas6) is a new member of the vitamin K-dependent proteins related to protein S, a negative coregulator in the blood coagulation cascade. *Mol Cell Biol* 1993, 13(8):4976-4985.
16. Lemke G: Phosphatidylserine Is the Signal for TAM Receptors and Their Ligands. *Trends Biochem Sci* 2017, 42(9):738-748.
17. Scott RS, McMahon EJ, Pop SM, Reap EA, Caricchio R, Cohen PL, Earp HS, Matsushima GK: Phagocytosis and clearance of apoptotic cells is mediated by MER. *Nature* 2001, 411(6834):207-211.
18. Lemke G, Burstyn-Cohen T: TAM receptors and the clearance of apoptotic cells. *Ann N Y Acad Sci* 2010, 1209:23-29.
19. Nguyen KQ, Tsou WI, Kotenko S, Birge RB: TAM receptors in apoptotic cell clearance, autoimmunity, and cancer. *Autoimmunity* 2013, 46(5):294-297.
20. Rothlin CV, Ghosh S, Zuniga EI, Oldstone MB, Lemke G: TAM receptors are pleiotropic inhibitors of the innate immune response. *Cell* 2007, 131(6):1124-1136.
21. Caraux A, Lu Q, Fernandez N, Riou S, Di Santo JP, Raulet DH, Lemke G, Roth C: Natural killer cell differentiation driven by Tyro3 receptor tyrosine kinases. *Nat Immunol* 2006, 7(7):747-754.
22. Liu E, Hjelle B, Bishop JM: Transforming genes in chronic myelogenous leukemia. *Proc Natl Acad Sci U S A* 1988, 85(6):1952-1956.
23. Linger RM, Keating AK, Earp HS, Graham DK: TAM receptor tyrosine kinases: biologic functions, signaling, and potential therapeutic targeting in human cancer. *Adv Cancer Res* 2008, 100:35-83.
24. Zhu C, Wei Y, Wei X: AXL receptor tyrosine kinase as a promising anti-cancer approach: functions, molecular mechanisms and clinical applications. *Mol Cancer* 2019, 18(1):153.

25. Faust M, Ebensperger C, Schulz AS, Schleithoff L, Hameister H, Bartram CR, Janssen JW: The murine ufo receptor: molecular cloning, chromosomal localization and in situ expression analysis. *Oncogene* 1992, 7(7):1287-1293.
26. Axelrod H, Pienta KJ: Axl as a mediator of cellular growth and survival. *Oncotarget* 2014, 5(19):8818-8852.
27. Lu Q, Gore M, Zhang Q, Camenisch T, Boast S, Casagranda F, Lai C, Skinner MK, Klein R, Matsushima GK *et al*: Tyro-3 family receptors are essential regulators of mammalian spermatogenesis. *Nature* 1999, 398(6729):723-728.
28. Lu Q, Lemke G: Homeostatic regulation of the immune system by receptor tyrosine kinases of the Tyro 3 family. *Science* 2001, 293(5528):306-311.
29. Schoumacher M, Burbridge M: Key Roles of AXL and MER Receptor Tyrosine Kinases in Resistance to Multiple Anticancer Therapies. *Curr Oncol Rep* 2017, 19(3):19.
30. Sasaki T, Knyazev PG, Clout NJ, Cheburkin Y, Gohring W, Ullrich A, Timpl R, Hohenester E: Structural basis for Gas6-Axl signalling. *EMBO J* 2006, 25(1):80-87.
31. Bellosta P, Costa M, Lin DA, Basilico C: The receptor tyrosine kinase ARK mediates cell aggregation by homophilic binding. *Mol Cell Biol* 1995, 15(2):614-625.
32. Burchert A, Attar EC, McCloskey P, Fridell YW, Liu ET: Determinants for transformation induced by the Axl receptor tyrosine kinase. *Oncogene* 1998, 16(24):3177-3187.
33. Konishi A, Aizawa T, Mohan A, Korshunov VA, Berk BC: Hydrogen peroxide activates the Gas6-Axl pathway in vascular smooth muscle cells. *J Biol Chem* 2004, 279(27):28766-28770.
34. Valverde P: Effects of Gas6 and hydrogen peroxide in Axl ubiquitination and downregulation. *Biochem Biophys Res Commun* 2005, 333(1):180-185.
35. Brown JE, Krodel M, Pazos M, Lai C, Prieto AL: Cross-phosphorylation, signaling and proliferative functions of the Tyro3 and Axl receptors in Rat2 cells. *PLoS One* 2012, 7(5):e36800.
36. Seitz HM, Camenisch TD, Lemke G, Earp HS, Matsushima GK: Macrophages and dendritic cells use different Axl/Mertk/Tyro3 receptors in clearance of apoptotic cells. *J Immunol* 2007, 178(9):5635-5642.
37. Sinha S, Boysen J, Nelson M, Warner SL, Bearss D, Kay NE, Ghosh AK: Axl activates fibroblast growth factor receptor pathway to potentiate survival signals in B-cell chronic lymphocytic leukemia cells. *Leukemia* 2016, 30(6):1431-1436.
38. Vouri M, Croucher DR, Kennedy SP, An Q, Pilkington GJ, Hafizi S: Axl-EGFR receptor tyrosine kinase hetero-interaction provides EGFR with access to pro-invasive signalling in cancer cells. *Oncogenesis* 2016, 5(10):e266.
39. Antony J, Tan TZ, Kelly Z, Low J, Choolani M, Recchi C, Gabra H, Thiery JP, Huang RY: The GAS6-AXL signaling network is a mesenchymal (Mes) molecular subtype-specific therapeutic target for ovarian cancer. *Sci Signal* 2016, 9(448):ra97.
40. Salian-Mehta S, Xu M, Wierman ME: AXL and MET crosstalk to promote gonadotropin releasing hormone (GnRH) neuronal cell migration and survival. *Mol Cell Endocrinol* 2013, 374(1-2):92-100.
41. Morioka S, Maueroder C, Ravichandran KS: Living on the Edge: Efferocytosis at the Interface of Homeostasis and Pathology. *Immunity* 2019, 50(5):1149-1162.
42. Duncan JL, LaVail MM, Yasumura D, Matthes MT, Yang H, Trautmann N, Chappelow AV, Feng W, Earp HS, Matsushima GK *et al*: An RCS-like retinal dystrophy phenotype in mer knockout mice. *Invest Ophthalmol Vis Sci* 2003, 44(2):826-838.
43. D'Cruz PM, Yasumura D, Weir J, Matthes MT, Abderrahim H, LaVail MM, Vollrath D: Mutation of the receptor tyrosine kinase gene Mertk in the retinal dystrophic RCS rat. *Hum Mol Genet* 2000, 9(4):645-651.
44. Zagorska A, Traves PG, Lew ED, Dransfield I, Lemke G: Diversification of TAM receptor tyrosine kinase function. *Nat Immunol* 2014, 15(10):920-928.
45. Vago JP, Amaral FA, van de Loo FAJ: Resolving inflammation by TAM receptor activation. *Pharmacol Ther* 2021, 227:107893.
46. Park IK, Giovenzana C, Hughes TL, Yu J, Trotta R, Caligiuri MA: The Axl/Gas6 pathway is required for optimal cytokine signaling during human natural killer cell development. *Blood* 2009, 113(11):2470-2477.

47. Bassyouni IH, El-Wakd MM, Azab NA, Bassyouni RH: Diminished soluble levels of growth arrest specific protein 6 and tyrosine kinase receptor Axl in patients with rheumatoid arthritis. *Int J Rheum Dis* 2017, 20(1):53-59.
48. Orme JJ, Du Y, Vanarsa K, Mayeux J, Li L, Mutwally A, Arriens C, Min S, Hutcheson J, Davis LS *et al*: Heightened cleavage of Axl receptor tyrosine kinase by ADAM metalloproteases may contribute to disease pathogenesis in SLE. *Clin Immunol* 2016, 169:58-68.
49. Ekman C, Linder A, Akesson P, Dahlback B: Plasma concentrations of Gas6 (growth arrest specific protein 6) and its soluble tyrosine kinase receptor sAxl in sepsis and systemic inflammatory response syndromes. *Crit Care* 2010, 14(4):R158.
50. Stalder G, Que YA, Calzavarini S, Burnier L, Kosinski C, Ballabeni P, Roger T, Calandra T, Duchosal MA, Liaudet L *et al*: Study of Early Elevated Gas6 Plasma Level as a Predictor of Mortality in a Prospective Cohort of Patients with Sepsis. *PLoS One* 2016, 11(10):e0163542.
51. Weinger JG, Omari KM, Marsden K, Raine CS, Shafit-Zagardo B: Up-regulation of soluble Axl and Mer receptor tyrosine kinases negatively correlates with Gas6 in established multiple sclerosis lesions. *Am J Pathol* 2009, 175(1):283-293.
52. Rankin EB, Giaccia AJ: The Receptor Tyrosine Kinase AXL in Cancer Progression. *Cancers (Basel)* 2016, 8(11).
53. Vajkoczy P, Knyazev P, Kunkel A, Capelle HH, Behrndt S, von Tengg-Kobligk H, Kiessling F, Eichelsbacher U, Essig M, Read TA *et al*: Dominant-negative inhibition of the Axl receptor tyrosine kinase suppresses brain tumor cell growth and invasion and prolongs survival. *Proc Natl Acad Sci U S A* 2006, 103(15):5799-5804.
54. Zhang Y, Tang YJ, Man Y, Pan F, Li ZH, Jia LS: Knockdown of AXL receptor tyrosine kinase in osteosarcoma cells leads to decreased proliferation and increased apoptosis. *Int J Immunopathol Pharmacol* 2013, 26(1):179-188.
55. Sainaghi PP, Castello L, Bergamasco L, Galletti M, Bellosta P, Avanzi GC: Gas6 induces proliferation in prostate carcinoma cell lines expressing the Axl receptor. *J Cell Physiol* 2005, 204(1):36-44.
56. Paccez JD, Vasques GJ, Correa RG, Vasconcellos JF, Duncan K, Gu X, Bhasin M, Libermann TA, Zerbini LF: The receptor tyrosine kinase Axl is an essential regulator of prostate cancer proliferation and tumor growth and represents a new therapeutic target. *Oncogene* 2013, 32(6):689-698.
57. Demarchi F, Verardo R, Varnum B, Brancolini C, Schneider C: Gas6 anti-apoptotic signaling requires NF-kappa B activation. *J Biol Chem* 2001, 276(34):31738-31744.
58. Lee WP, Wen Y, Varnum B, Hung MC: Akt is required for Axl-Gas6 signaling to protect cells from E1A-mediated apoptosis. *Oncogene* 2002, 21(3):329-336.
59. Hong CC, Lay JD, Huang JS, Cheng AL, Tang JL, Lin MT, Lai GM, Chuang SE: Receptor tyrosine kinase AXL is induced by chemotherapy drugs and overexpression of AXL confers drug resistance in acute myeloid leukemia. *Cancer Lett* 2008, 268(2):314-324.
60. Keating AK, Kim GK, Jones AE, Donson AM, Ware K, Mulcahy JM, Salzberg DB, Foreman NK, Liang X, Thorburn A *et al*: Inhibition of Mer and Axl receptor tyrosine kinases in astrocytoma cells leads to increased apoptosis and improved chemosensitivity. *Mol Cancer Ther* 2010, 9(5):1298-1307.
61. Linger RM, Cohen RA, Cummings CT, Sather S, Migdall-Wilson J, Middleton DH, Lu X, Baron AE, Franklin WA, Merrick DT *et al*: Mer or Axl receptor tyrosine kinase inhibition promotes apoptosis, blocks growth and enhances chemosensitivity of human non-small cell lung cancer. *Oncogene* 2013, 32(29):3420-3431.
62. Tanaka M, Siemann DW: Gas6/Axl Signaling Pathway in the Tumor Immune Microenvironment. *Cancers (Basel)* 2020, 12(7).
63. Tanaka M, Siemann DW: Axl signaling is an important mediator of tumor angiogenesis. *Oncotarget* 2019, 10(30):2887-2898.
64. Fridell YW, Villa J, Jr., Attar EC, Liu ET: GAS6 induces Axl-mediated chemotaxis of vascular smooth muscle cells. *J Biol Chem* 1998, 273(12):7123-7126.
65. Holland SJ, Powell MJ, Franci C, Chan EW, Friera AM, Atchison RE, McLaughlin J, Swift SE, Pali ES, Yam G *et al*: Multiple roles for the receptor tyrosine kinase axl in tumor formation. *Cancer Res* 2005, 65(20):9294-9303.

66. Goyette MA, Duhamel S, Aubert L, Pelletier A, Savage P, Thibault MP, Johnson RM, Carmeliet P, Basik M, Gaboury L *et al*: The Receptor Tyrosine Kinase AXL Is Required at Multiple Steps of the Metastatic Cascade during HER2-Positive Breast Cancer Progression. *Cell Rep* 2018, 23(5):1476-1490.
67. Singh A, Settleman J: EMT, cancer stem cells and drug resistance: an emerging axis of evil in the war on cancer. *Oncogene* 2010, 29(34):4741-4751.
68. Nieto MA, Huang RY, Jackson RA, Thiery JP: Emt: 2016. *Cell* 2016, 166(1):21-45.
69. Sun BO, Fang Y, Li Z, Chen Z, Xiang J: Role of cellular cytoskeleton in epithelial-mesenchymal transition process during cancer progression. *Biomed Rep* 2015, 3(5):603-610.
70. Wilson C, Ye X, Pham T, Lin E, Chan S, McNamara E, Neve RM, Belmont L, Koeppen H, Yauch RL *et al*: AXL inhibition sensitizes mesenchymal cancer cells to antimitotic drugs. *Cancer Res* 2014, 74(20):5878-5890.
71. Gjerdrum C, Tiron C, Hoiby T, Stefansson I, Haugen H, Sandal T, Collett K, Li S, McCormack E, Gjertsen BT *et al*: Axl is an essential epithelial-to-mesenchymal transition-induced regulator of breast cancer metastasis and patient survival. *Proc Natl Acad Sci U S A* 2010, 107(3):1124-1129.
72. Koorstra JB, Karikari CA, Feldmann G, Bisht S, Rojas PL, Offerhaus GJ, Alvarez H, Maitra A: The Axl receptor tyrosine kinase confers an adverse prognostic influence in pancreatic cancer and represents a new therapeutic target. *Cancer Biol Ther* 2009, 8(7):618-626.
73. Asiedu MK, Beauchamp-Perez FD, Ingle JN, Behrens MD, Radisky DC, Knutson KL: AXL induces epithelial-to-mesenchymal transition and regulates the function of breast cancer stem cells. *Oncogene* 2014, 33(10):1316-1324.
74. Cichon MA, Szentpetery Z, Caley MP, Papadakis ES, Mackenzie IC, Brennan CH, O'Toole EA: The receptor tyrosine kinase Axl regulates cell-cell adhesion and stemness in cutaneous squamous cell carcinoma. *Oncogene* 2014, 33(32):4185-4192.
75. Abu-Thuraia A, Goyette MA, Boulais J, Delliaux C, Apcher C, Schott C, Chidiac R, Bagci H, Thibault MP, Davidson D *et al*: AXL confers cell migration and invasion by hijacking a PEAK1-regulated focal adhesion protein network. *Nat Commun* 2020, 11(1):3586.
76. Hong J, Peng D, Chen Z, Sehdev V, Belkhiri A: ABL regulation by AXL promotes cisplatin resistance in esophageal cancer. *Cancer Res* 2013, 73(1):331-340.
77. Brand TM, Iida M, Stein AP, Corrigan KL, Braverman CM, Coan JP, Pearson HE, Bahrar H, Fowler TL, Bednarz BP *et al*: AXL Is a Logical Molecular Target in Head and Neck Squamous Cell Carcinoma. *Clin Cancer Res* 2015, 21(11):2601-2612.
78. Giles KM, Kalinowski FC, Candy PA, Epis MR, Zhang PM, Redfern AD, Stuart LM, Goodall GJ, Leedman PJ: Axl mediates acquired resistance of head and neck cancer cells to the epidermal growth factor receptor inhibitor erlotinib. *Mol Cancer Ther* 2013, 12(11):2541-2558.
79. Taniguchi H, Yamada T, Wang R, Tanimura K, Adachi Y, Nishiyama A, Tanimoto A, Takeuchi S, Araujo LH, Boroni M *et al*: AXL confers intrinsic resistance to osimertinib and advances the emergence of tolerant cells. *Nat Commun* 2019, 10(1):259.
80. Muller J, Krijgsman O, Tsoi J, Robert L, Hugo W, Song C, Kong X, Possik PA, Cornelissen-Steijger PD, Geukes Foppen MH *et al*: Low MITF/AXL ratio predicts early resistance to multiple targeted drugs in melanoma. *Nat Commun* 2014, 5:5712.
81. Elkabets M, Pazarentzos E, Juric D, Sheng Q, Pelossof RA, Brook S, Benzaken AO, Rodon J, Morse N, Yan JJ *et al*: AXL mediates resistance to PI3Kalpha inhibition by activating the EGFR/PKC/mTOR axis in head and neck and esophageal squamous cell carcinomas. *Cancer Cell* 2015, 27(4):533-546.
82. Debruyne DN, Bhatnagar N, Sharma B, Luther W, Moore NF, Cheung NK, Gray NS, George RE: ALK inhibitor resistance in ALK(F1174L)-driven neuroblastoma is associated with AXL activation and induction of EMT. *Oncogene* 2016, 35(28):3681-3691.
83. Byers LA, Diao L, Wang J, Saintigny P, Girard L, Peyton M, Shen L, Fan Y, Giri U, Tumula PK *et al*: An epithelial-mesenchymal transition gene signature predicts resistance to EGFR and PI3K inhibitors and identifies Axl as a therapeutic target for overcoming EGFR inhibitor resistance. *Clin Cancer Res* 2013, 19(1):279-290.
84. Hugo W, Zaretsky JM, Sun L, Song C, Moreno BH, Hu-Lieskovan S, Berent-Maoz B, Pang J, Chmielowski B, Cherry G *et al*: Genomic and Transcriptomic Features of Response to Anti-PD-1 Therapy in Metastatic Melanoma. *Cell* 2016, 165(1):35-44.

85. Kasikara C, Kumar S, Kimani S, Tsou WI, Geng K, Davra V, Sriram G, Devoe C, Nguyen KN, Antes A *et al*: Phosphatidylserine Sensing by TAM Receptors Regulates AKT-Dependent Chemoresistance and PD-L1 Expression. *Mol Cancer Res* 2017, 15(6):753-764.
86. Lucibello G, Mograbi B, Milano G, Hofman P, Brest P: PD-L1 regulation revisited: impact on immunotherapeutic strategies. *Trends Mol Med* 2021, 27(9):868-881.
87. Tsukita Y, Fujino N, Miyauchi E, Saito R, Fujishima F, Itakura K, Kyogoku Y, Okutomo K, Yamada M, Okazaki T *et al*: Axl kinase drives immune checkpoint and chemokine signalling pathways in lung adenocarcinomas. *Mol Cancer* 2019, 18(1):24.
88. Di Stasi R, De Rosa L, D'Andrea LD: Therapeutic aspects of the Axl/Gas6 molecular system. *Drug Discov Today* 2020, 25(12):2130-2148.
89. Zdzalik-Bielecka D, Poswiata A, Kozik K, Jastrzebski K, Schink KO, Brewinska-Olchowik M, Piwocka K, Stenmark H, Miaczynska M: The GAS6-AXL signaling pathway triggers actin remodeling that drives membrane ruffling, macropinocytosis, and cancer-cell invasion. *Proc Natl Acad Sci U S A* 2021, 118(28).
90. Onken J, Torka R, Korsing S, Radke J, Krementeskaia I, Nieminen M, Bai X, Ullrich A, Heppner F, Vajkoczy P: Inhibiting receptor tyrosine kinase AXL with small molecule inhibitor BMS-777607 reduces glioblastoma growth, migration, and invasion in vitro and in vivo. *Oncotarget* 2016, 7(9):9876-9889.
91. Jeon JY, Buelow DR, Garrison DA, Niu M, Eisenmann ED, Huang KM, Zavorka Thomas ME, Weber RH, Whatcott CJ, Warner SL *et al*: TP-0903 is active in models of drug-resistant acute myeloid leukemia. *JCI Insight* 2020, 5(23).
92. Sinha S, Boysen J, Nelson M, Secreto C, Warner SL, Bearss DJ, Lesnick C, Shanafelt TD, Kay NE, Ghosh AK: Targeted Axl Inhibition Primes Chronic Lymphocytic Leukemia B Cells to Apoptosis and Shows Synergistic/Additive Effects in Combination with BTK Inhibitors. *Clin Cancer Res* 2015, 21(9):2115-2126.
93. Holland SJ, Pan A, Franci C, Hu Y, Chang B, Li W, Duan M, Torneros A, Yu J, Heckrodt TJ *et al*: R428, a selective small molecule inhibitor of Axl kinase, blocks tumor spread and prolongs survival in models of metastatic breast cancer. *Cancer Res* 2010, 70(4):1544-1554.
94. Jimbo T, Hatanaka M, Komatsu T, Taira T, Kumazawa K, Maeda N, Suzuki T, Ota M, Haginoya N, Isoyama T *et al*: DS-1205b, a novel selective inhibitor of AXL kinase, blocks resistance to EGFR-tyrosine kinase inhibitors in a non-small cell lung cancer xenograft model. *Oncotarget* 2019, 10(50):5152-5167.
95. Myers SH, Brunton VG, Unciti-Broceta A: AXL Inhibitors in Cancer: A Medicinal Chemistry Perspective. *J Med Chem* 2016, 59(8):3593-3608.
96. ClinicalTrials.gov [https://clinicaltrials.gov]
97. Sheridan C: First Axl inhibitor enters clinical trials. *Nat Biotechnol* 2013, 31(9):775-776.
98. Kimani SG, Kumar S, Bansal N, Singh K, Kholodovych V, Comollo T, Peng Y, Kotenko SV, Sarafianos SG, Bertino JR *et al*: Small molecule inhibitors block Gas6-inducible TAM activation and tumorigenicity. *Sci Rep* 2017, 7:43908.
99. Cerchia L, Esposito CL, Camorani S, Rienzo A, Stasio L, Insabato L, Affuso A, de Franciscis V: Targeting Axl with an high-affinity inhibitory aptamer. *Mol Ther* 2012, 20(12):2291-2303.
100. Kanlikilicer P, Ozpolat B, Aslan B, Bayraktar R, Gurbuz N, Rodriguez-Aguayo C, Bayraktar E, Denizli M, Gonzalez-Villasana V, Ivan C *et al*: Therapeutic Targeting of AXL Receptor Tyrosine Kinase Inhibits Tumor Growth and Intraperitoneal Metastasis in Ovarian Cancer Models. *Mol Ther Nucleic Acids* 2017, 9:251-262.
101. Moody G, Belmontes B, Masterman S, Wang W, King C, Murawsky C, Tsuruda T, Liu S, Radinsky R, Beltran PJ: Antibody-mediated neutralization of autocrine Gas6 inhibits the growth of pancreatic ductal adenocarcinoma tumors in vivo. *Int J Cancer* 2016, 139(6):1340-1349.
102. Kariolis MS, Miao YR, Jones DS, 2nd, Kapur S, Mathews, II, Giaccia AJ, Cochran JR: An engineered Axl 'decoy receptor' effectively silences the Gas6-Axl signaling axis. *Nat Chem Biol* 2014, 10(11):977-983.
103. Ye X, Li Y, Stawicki S, Couto S, Eastham-Anderson J, Kallop D, Weimer R, Wu Y, Pei L: An anti-Axl monoclonal antibody attenuates xenograft tumor growth and enhances the effect of multiple anticancer therapies. *Oncogene* 2010, 29(38):5254-5264.

104. Duan Y, Luo L, Qiao C, Li X, Wang J, Liu H, Zhou T, Shen B, Lv M, Feng J: A novel human anti-AXL monoclonal antibody attenuates tumour cell migration. *Scand J Immunol* 2019, 90(2):e12777.
105. Leconet W, Chentouf M, du Manoir S, Chevalier C, Sirvent A, Ait-Arsa I, Busson M, Jarlier M, Radosevic-Robin N, Theillet C *et al*: Therapeutic Activity of Anti-AXL Antibody against Triple-Negative Breast Cancer Patient-Derived Xenografts and Metastasis. *Clin Cancer Res* 2017, 23(11):2806-2816.
106. Koopman LA, Terp MG, Zom GG, Janmaat ML, Jacobsen K, Gresnigt-van den Heuvel E, Brandhorst M, Forssmann U, de Bree F, Pencheva N *et al*: Enapotamab vedotin, an AXL-specific antibody-drug conjugate, shows preclinical antitumor activity in non-small cell lung cancer. *JCI Insight* 2019, 4(21).
107. Meertens L, Carnec X, Lecoin MP, Ramdasi R, Guivel-Benhassine F, Lew E, Lemke G, Schwartz O, Amara A: The TIM and TAM families of phosphatidylserine receptors mediate dengue virus entry. *Cell Host Microbe* 2012, 12(4):544-557.
108. Fedeli C, Torriani G, Galan-Navarro C, Moraz ML, Moreno H, Gerold G, Kunz S: Axl Can Serve as Entry Factor for Lassa Virus Depending on the Functional Glycosylation of Dystroglycan. *J Virol* 2018, 92(5).
109. Shimojima M, Takada A, Ebihara H, Neumann G, Fujioka K, Irimura T, Jones S, Feldmann H, Kawaoka Y: Tyro3 family-mediated cell entry of Ebola and Marburg viruses. *J Virol* 2006, 80(20):10109-10116.
110. Meertens L, Labeau A, Dejarnac O, Cipriani S, Sinigaglia L, Bonnet-Madin L, Le Charpentier T, Hafirassou ML, Zamborlini A, Cao-Lormeau VM *et al*: Axl Mediates ZIKA Virus Entry in Human Glial Cells and Modulates Innate Immune Responses. *Cell Rep* 2017, 18(2):324-333.
111. Wang S, Qiu Z, Hou Y, Deng X, Xu W, Zheng T, Wu P, Xie S, Bian W, Zhang C *et al*: AXL is a candidate receptor for SARS-CoV-2 that promotes infection of pulmonary and bronchial epithelial cells. *Cell Res* 2021, 31(2):126-140.
112. Wang ZY, Wang PG, An J: The Multifaceted Roles of TAM Receptors during Viral Infection. *Virol Sin* 2020.
113. Morizono K, Xie Y, Olafsen T, Lee B, Dasgupta A, Wu AM, Chen IS: The soluble serum protein Gas6 bridges virion envelope phosphatidylserine to the TAM receptor tyrosine kinase Axl to mediate viral entry. *Cell Host Microbe* 2011, 9(4):286-298.
114. Sun B, Qi N, Shang T, Wu H, Deng T, Han D: Sertoli cell-initiated testicular innate immune response through toll-like receptor-3 activation is negatively regulated by Tyro3, Axl, and mer receptors. *Endocrinology* 2010, 151(6):2886-2897.
115. Grabiec AM, Goenka A, Fife ME, Fujimori T, Hussell T: Axl and MerTK receptor tyrosine kinases maintain human macrophage efferocytic capacity in the presence of viral triggers. *Eur J Immunol* 2018, 48(5):855-860.
116. Brindley MA, Hunt CL, Kondratowicz AS, Bowman J, Sinn PL, McCray PB, Jr., Quinn K, Weller ML, Chiorini JA, Maury W: Tyrosine kinase receptor Axl enhances entry of Zaire ebolavirus without direct interactions with the viral glycoprotein. *Virology* 2011, 415(2):83-94.
117. Liu S, DeLalio LJ, Isakson BE, Wang TT: AXL-Mediated Productive Infection of Human Endothelial Cells by Zika Virus. *Circ Res* 2016, 119(11):1183-1189.
118. Tutusaus A, Mari M, Ortiz-Perez JT, Nicolaes GAF, Morales A, Garcia de Frutos P: Role of Vitamin K-Dependent Factors Protein S and GAS6 and TAM Receptors in SARS-CoV-2 Infection and COVID-19-Associated Immunothrombosis. *Cells* 2020, 9(10).
119. Bouhaddou M, Memon D, Meyer B, White KM, Rezelj VV, Correa Marrero M, Polacco BJ, Melnyk JE, Ulferts S, Kaake RM *et al*: The Global Phosphorylation Landscape of SARS-CoV-2 Infection. *Cell* 2020, 182(3):685-712 e619.
120. Wilkinson T, Dixon R, Page C, Carroll M, Griffiths G, Ho LP, De Soyza A, Felton T, Lewis KE, Phekoo K *et al*: ACCORD: A Multicentre, Seamless, Phase 2 Adaptive Randomisation Platform Study to Assess the Efficacy and Safety of Multiple Candidate Agents for the Treatment of COVID-19 in Hospitalised Patients: A structured summary of a study protocol for a randomised controlled trial. *Trials* 2020, 21(1):691.
121. Doherty GJ, McMahon HT: Mechanisms of endocytosis. *Annu Rev Biochem* 2009, 78:857-902.

122. Sigismund S, Confalonieri S, Ciliberto A, Polo S, Scita G, Di Fiore PP: Endocytosis and signaling: cell logistics shape the eukaryotic cell plan. *Physiol Rev* 2012, 92(1):273-366.
123. Palm W, Thompson CB: Nutrient acquisition strategies of mammalian cells. *Nature* 2017, 546(7657):234-242.
124. Goh LK, Sorkin A: Endocytosis of receptor tyrosine kinases. *Cold Spring Harb Perspect Biol* 2013, 5(5):a017459.
125. Miaczynska M: Effects of membrane trafficking on signaling by receptor tyrosine kinases. *Cold Spring Harb Perspect Biol* 2013, 5(11):a009035.
126. Thottacherry JJ, Sathe M, Prabhakara C, Mayor S: Spoiled for Choice: Diverse Endocytic Pathways Function at the Cell Surface. *Annu Rev Cell Dev Biol* 2019, 35:55-84.
127. Villasenor R, Kalaidzidis Y, Zerial M: Signal processing by the endosomal system. *Curr Opin Cell Biol* 2016, 39:53-60.
128. Pearse BM: Coated vesicles from pig brain: purification and biochemical characterization. *J Mol Biol* 1975, 97(1):93-98.
129. McMahon HT, Boucrot E: Molecular mechanism and physiological functions of clathrin-mediated endocytosis. *Nat Rev Mol Cell Biol* 2011, 12(8):517-533.
130. Mettlen M, Chen PH, Srinivasan S, Danuser G, Schmid SL: Regulation of Clathrin-Mediated Endocytosis. *Annu Rev Biochem* 2018, 87:871-896.
131. Kaksonen M, Roux A: Mechanisms of clathrin-mediated endocytosis. *Nat Rev Mol Cell Biol* 2018, 19(5):313-326.
132. Henne WM, Boucrot E, Meinecke M, Evergren E, Vallis Y, Mittal R, McMahon HT: FCHo proteins are nucleators of clathrin-mediated endocytosis. *Science* 2010, 328(5983):1281-1284.
133. Kelly BT, Graham SC, Liska N, Dannhauser PN, Honing S, Ungewickell EJ, Owen DJ: Clathrin adaptors. AP2 controls clathrin polymerization with a membrane-activated switch. *Science* 2014, 345(6195):459-463.
134. Miller SE, Mathiasen S, Bright NA, Pierre F, Kelly BT, Kladt N, Schauss A, Merrifield CJ, Stamou D, Honing S *et al*: CALM regulates clathrin-coated vesicle size and maturation by directly sensing and driving membrane curvature. *Dev Cell* 2015, 33(2):163-175.
135. Ma L, Umasankar PK, Wrobel AG, Lymar A, McCoy AJ, Holkar SS, Jha A, Pradhan-Sundd T, Watkins SC, Owen DJ *et al*: Transient Fcho1/2Eps15/RAP-2 Nanoclusters Prime the AP-2 Clathrin Adaptor for Cargo Binding. *Dev Cell* 2016, 37(5):428-443.
136. Santolini E, Puri C, Salcini AE, Gagliani MC, Pelicci PG, Tacchetti C, Di Fiore PP: Numb is an endocytic protein. *J Cell Biol* 2000, 151(6):1345-1352.
137. Hinze C, Boucrot E: Local actin polymerization during endocytic carrier formation. *Biochem Soc Trans* 2018, 46(3):565-576.
138. Pucadyil TJ, Schmid SL: Real-time visualization of dynamin-catalyzed membrane fission and vesicle release. *Cell* 2008, 135(7):1263-1275.
139. Milosevic I, Giovedi S, Lou X, Raimondi A, Collesi C, Shen H, Paradise S, O'Toole E, Ferguson S, Cremona O *et al*: Recruitment of endophilin to clathrin-coated pit necks is required for efficient vesicle uncoating after fission. *Neuron* 2011, 72(4):587-601.
140. Soulet F, Yarar D, Leonard M, Schmid SL: SNX9 regulates dynamin assembly and is required for efficient clathrin-mediated endocytosis. *Mol Biol Cell* 2005, 16(4):2058-2067.
141. Daumke O, Roux A, Haucke V: BAR domain scaffolds in dynamin-mediated membrane fission. *Cell* 2014, 156(5):882-892.
142. Romer W, Pontani LL, Sorre B, Rentero C, Berland L, Chambon V, Lamaze C, Bassereau P, Sykes C, Gaus K *et al*: Actin dynamics drive membrane reorganization and scission in clathrin-independent endocytosis. *Cell* 2010, 140(4):540-553.
143. Ferreira APA, Boucrot E: Mechanisms of Carrier Formation during Clathrin-Independent Endocytosis. *Trends Cell Biol* 2018, 28(3):188-200.
144. Sandvig K, Kavaliauskiene S, Skotland T: Clathrin-independent endocytosis: an increasing degree of complexity. *Histochem Cell Biol* 2018, 150(2):107-118.
145. Renard HF, Boucrot E: Unconventional endocytic mechanisms. *Curr Opin Cell Biol* 2021, 71:120-129.
146. Stow JL, Hung Y, Wall AA: Macropinocytosis: Insights from immunology and cancer. *Curr Opin Cell Biol* 2020, 65:131-140.

147. Kim SM, Nguyen TT, Ravi A, Kubiniok P, Finicle BT, Jayashankar V, Malacrida L, Hou J, Robertson J, Gao D *et al*: PTEN Deficiency and AMPK Activation Promote Nutrient Scavenging and Anabolism in Prostate Cancer Cells. *Cancer Discov* 2018, 8(7):866-883.
148. Commisso C, Davidson SM, Soydaner-Azeloglu RG, Parker SJ, Kamphorst JJ, Hackett S, Grabocka E, Nofal M, Drebin JA, Thompson CB *et al*: Macropinocytosis of protein is an amino acid supply route in Ras-transformed cells. *Nature* 2013, 497(7451):633-637.
149. Jayashankar V, Edinger AL: Macropinocytosis confers resistance to therapies targeting cancer anabolism. *Nat Commun* 2020, 11(1):1121.
150. West MA, Bretscher MS, Watts C: Distinct endocytotic pathways in epidermal growth factor-stimulated human carcinoma A431 cells. *J Cell Biol* 1989, 109(6 Pt 1):2731-2739.
151. Schmees C, Villasenor R, Zheng W, Ma H, Zerial M, Heldin CH, Hellberg C: Macropinocytosis of the PDGF beta-receptor promotes fibroblast transformation by H-RasG12V. *Mol Biol Cell* 2012, 23(13):2571-2582.
152. Mercer J, Helenius A: Virus entry by macropinocytosis. *Nat Cell Biol* 2009, 11(5):510-520.
153. Kerr MC, Teasdale RD: Defining macropinocytosis. *Traffic* 2009, 10(4):364-371.
154. Parton RG, del Pozo MA: Caveolae as plasma membrane sensors, protectors and organizers. *Nat Rev Mol Cell Biol* 2013, 14(2):98-112.
155. Drab M, Verkade P, Elger M, Kasper M, Lohn M, Lauterbach B, Menne J, Lindschau C, Mende F, Luft FC *et al*: Loss of caveolae, vascular dysfunction, and pulmonary defects in caveolin-1 gene-disrupted mice. *Science* 2001, 293(5539):2449-2452.
156. Galbiati F, Engelman JA, Volonte D, Zhang XL, Minetti C, Li M, Hou H, Jr., Kneitz B, Edelmann W, Lisanti MP: Caveolin-3 null mice show a loss of caveolae, changes in the microdomain distribution of the dystrophin-glycoprotein complex, and t-tubule abnormalities. *J Biol Chem* 2001, 276(24):21425-21433.
157. Hill MM, Bastiani M, Luetterforst R, Kirkham M, Kirkham A, Nixon SJ, Walser P, Abankwa D, Oorschot VM, Martin S *et al*: PTRF-Cavin, a conserved cytoplasmic protein required for caveola formation and function. *Cell* 2008, 132(1):113-124.
158. Parton RG: Caveolae: Structure, Function, and Relationship to Disease. *Annu Rev Cell Dev Biol* 2018, 34:111-136.
159. Anderson HA, Chen Y, Norkin LC: Bound simian virus 40 translocates to caveolin-enriched membrane domains, and its entry is inhibited by drugs that selectively disrupt caveolae. *Mol Biol Cell* 1996, 7(11):1825-1834.
160. Shogomori H, Futerman AH: Cholera toxin is found in detergent-insoluble rafts/domains at the cell surface of hippocampal neurons but is internalized via a raft-independent mechanism. *J Biol Chem* 2001, 276(12):9182-9188.
161. Herreros J, Ng T, Schiavo G: Lipid rafts act as specialized domains for tetanus toxin binding and internalization into neurons. *Mol Biol Cell* 2001, 12(10):2947-2960.
162. Gleizes PE, Noaillac-Depeyre J, Dupont MA, Gas N: Basic fibroblast growth factor (FGF-2) is addressed to caveolae after binding to the plasma membrane of BHK cells. *Eur J Cell Biol* 1996, 71(2):144-153.
163. Dittmann K, Mayer C, Kehlbach R, Rodemann HP: Radiation-induced caveolin-1 associated EGFR internalization is linked with nuclear EGFR transport and activation of DNA-PK. *Mol Cancer* 2008, 7:69.
164. D'Alessio A, Al-Lamki RS, Bradley JR, Pober JS: Caveolae participate in tumor necrosis factor receptor 1 signaling and internalization in a human endothelial cell line. *Am J Pathol* 2005, 166(4):1273-1282.
165. Sinha B, Koster D, Ruez R, Gonnord P, Bastiani M, Abankwa D, Stan RV, Butler-Browne G, Vedie B, Johannes L *et al*: Cells respond to mechanical stress by rapid disassembly of caveolae. *Cell* 2011, 144(3):402-413.
166. Bickel PE, Scherer PE, Schnitzer JE, Oh P, Lisanti MP, Lodish HF: Flotillin and epidermal surface antigen define a new family of caveolae-associated integral membrane proteins. *J Biol Chem* 1997, 272(21):13793-13802.
167. Lang DM, Lommel S, Jung M, Ankerhold R, Petrausch B, Laessing U, Wiechers MF, Plattner H, Stuermer CA: Identification of reggie-1 and reggie-2 as plasmamembrane-associated proteins which cocluster with activated GPI-anchored cell adhesion molecules in non-caveolar micropatches in neurons. *J Neurobiol* 1998, 37(4):502-523.

168. Glebov OO, Bright NA, Nichols BJ: Flotillin-1 defines a clathrin-independent endocytic pathway in mammalian cells. *Nat Cell Biol* 2006, 8(1):46-54.
169. Frick M, Bright NA, Riento K, Bray A, Merrified C, Nichols BJ: Coassembly of flotillins induces formation of membrane microdomains, membrane curvature, and vesicle budding. *Curr Biol* 2007, 17(13):1151-1156.
170. Ait-Slimane T, Galmes R, Trugnan G, Maurice M: Basolateral internalization of GPI-anchored proteins occurs via a clathrin-independent flotillin-dependent pathway in polarized hepatic cells. *Mol Biol Cell* 2009, 20(17):3792-3800.
171. Meister M, Tikkanen R: Endocytic trafficking of membrane-bound cargo: a flotillin point of view. *Membranes (Basel)* 2014, 4(3):356-371.
172. Solis GP, Schrock Y, Hulsbusch N, Wiechers M, Plattner H, Stuermer CA: Reggies/flotillins regulate E-cadherin-mediated cell contact formation by affecting EGFR trafficking. *Mol Biol Cell* 2012, 23(10):1812-1825.
173. Yamamoto H, Umeda D, Matsumoto S, Kikuchi A: LDL switches the LRP6 internalization route from flotillin dependent to clathrin dependent in hepatic cells. *J Cell Sci* 2017, 130(20):3542-3556.
174. Fekri F, Abousawan J, Bautista S, Orofiamma L, Dayam RM, Antonescu CN, Karshafian R: Targeted enhancement of flotillin-dependent endocytosis augments cellular uptake and impact of cytotoxic drugs. *Sci Rep* 2019, 9(1):17768.
175. Sabharanjak S, Sharma P, Parton RG, Mayor S: GPI-anchored proteins are delivered to recycling endosomes via a distinct cdc42-regulated, clathrin-independent pinocytic pathway. *Dev Cell* 2002, 2(4):411-423.
176. Chadda R, Howes MT, Plowman SJ, Hancock JF, Parton RG, Mayor S: Cholesterol-sensitive Cdc42 activation regulates actin polymerization for endocytosis via the GEEC pathway. *Traffic* 2007, 8(6):702-717.
177. Lundmark R, Doherty GJ, Howes MT, Cortese K, Vallis Y, Parton RG, McMahon HT: The GTPase-activating protein GRAF1 regulates the CLIC/GEEC endocytic pathway. *Curr Biol* 2008, 18(22):1802-1808.
178. Kirkham M, Fujita A, Chadda R, Nixon SJ, Kurzchalia TV, Sharma DK, Pagano RE, Hancock JF, Mayor S, Parton RG: Ultrastructural identification of uncoated caveolin-independent early endocytic vehicles. *J Cell Biol* 2005, 168(3):465-476.
179. Howes MT, Kirkham M, Riches J, Cortese K, Walser PJ, Simpson F, Hill MM, Jones A, Lundmark R, Lindsay MR *et al*: Clathrin-independent carriers form a high capacity endocytic sorting system at the leading edge of migrating cells. *J Cell Biol* 2010, 190(4):675-691.
180. Lakshminarayan R, Wunder C, Becken U, Howes MT, Benzing C, Arumugam S, Sales S, Ariotti N, Chambon V, Lamaze C *et al*: Galectin-3 drives glycosphingolipid-dependent biogenesis of clathrin-independent carriers. *Nat Cell Biol* 2014, 16(6):595-606.
181. Jastrzebski K, Zdzalik-Bielecka D, Maminska A, Kalaidzidis Y, Hellberg C, Miaczynska M: Multiple routes of endocytic internalization of PDGFRbeta contribute to PDGF-induced STAT3 signaling. *J Cell Sci* 2017, 130(3):577-589.
182. Sztul E, Chen PW, Casanova JE, Cherfils J, Dacks JB, Lambright DG, Lee FS, Randazzo PA, Santy LC, Schurmann A *et al*: ARF GTPases and their GEFs and GAPs: concepts and challenges. *Mol Biol Cell* 2019, 30(11):1249-1271.
183. Van Acker T, Tavernier J, Peelman F: The Small GTPase Arf6: An Overview of Its Mechanisms of Action and of Its Role in Host(-)Pathogen Interactions and Innate Immunity. *Int J Mol Sci* 2019, 20(9).
184. Radhakrishna H, Donaldson JG: ADP-ribosylation factor 6 regulates a novel plasma membrane recycling pathway. *J Cell Biol* 1997, 139(1):49-61.
185. Naslavsky N, Weigert R, Donaldson JG: Convergence of non-clathrin- and clathrin-derived endosomes involves Arf6 inactivation and changes in phosphoinositides. *Mol Biol Cell* 2003, 14(2):417-431.
186. Eyster CA, Higginson JD, Huebner R, Porat-Shliom N, Weigert R, Wu WW, Shen RF, Donaldson JG: Discovery of new cargo proteins that enter cells through clathrin-independent endocytosis. *Traffic* 2009, 10(5):590-599.
187. Naslavsky N, Weigert R, Donaldson JG: Characterization of a nonclathrin endocytic pathway: membrane cargo and lipid requirements. *Mol Biol Cell* 2004, 15(8):3542-3552.

188. Kumari S, Mayor S: ARF1 is directly involved in dynamin-independent endocytosis. *Nat Cell Biol* 2008, 10(1):30-41.
189. Boucrot E, Ferreira AP, Almeida-Souza L, Debard S, Vallis Y, Howard G, Bertot L, Sauvonnet N, McMahon HT: Endophilin marks and controls a clathrin-independent endocytic pathway. *Nature* 2015, 517(7535):460-465.
190. Verstreken P, Kjaerulff O, Lloyd TE, Atkinson R, Zhou Y, Meinertzhagen IA, Bellen HJ: Endophilin mutations block clathrin-mediated endocytosis but not neurotransmitter release. *Cell* 2002, 109(1):101-112.
191. Casamento A, Boucrot E: Molecular mechanism of Fast Endophilin-Mediated Endocytosis. *Biochem J* 2020, 477(12):2327-2345.
192. Chan Wah Hak L, Khan S, Di Meglio I, Law AL, Lucken-Ardjomande Hasler S, Quintaneiro LM, Ferreira APA, Krause M, McMahon HT, Boucrot E: FBP17 and CIP4 recruit SHIP2 and lamellipodin to prime the plasma membrane for fast endophilin-mediated endocytosis. *Nat Cell Biol* 2018, 20(9):1023-1031.
193. Renard HF, Simunovic M, Lemiere J, Boucrot E, Garcia-Castillo MD, Arumugam S, Chambon V, Lamaze C, Wunder C, Kenworthy AK *et al*: Endophilin-A2 functions in membrane scission in clathrin-independent endocytosis. *Nature* 2015, 517(7535):493-496.
194. Ferreira APA, Casamento A, Carrillo Roas S, Halff EF, Panambalana J, Subramaniam S, Schutzenhofer K, Chan Wah Hak L, McGourty K, Thalassinos K *et al*: Cdk5 and GSK3beta inhibit fast endophilin-mediated endocytosis. *Nat Commun* 2021, 12(1):2424.
195. Genet G, Boye K, Mathivet T, Ola R, Zhang F, Dubrac A, Li J, Genet N, Henrique Geraldo L, Benedetti L *et al*: Endophilin-A2 dependent VEGFR2 endocytosis promotes sprouting angiogenesis. *Nat Commun* 2019, 10(1):2350.
196. Irannejad R, Tsvetanova NG, Lobingier BT, von Zastrow M: Effects of endocytosis on receptor-mediated signaling. *Curr Opin Cell Biol* 2015, 35:137-143.
197. Sadowski L, Pilecka I, Miaczynska M: Signaling from endosomes: location makes a difference. *Exp Cell Res* 2009, 315(9):1601-1609.
198. Di Guglielmo GM, Baass PC, Ou WJ, Posner BI, Bergeron JJ: Compartmentalization of SHC, GRB2 and mSOS, and hyperphosphorylation of Raf-1 by EGF but not insulin in liver parenchyma. *EMBO J* 1994, 13(18):4269-4277.
199. Grimes ML, Zhou J, Beattie EC, Yuen EC, Hall DE, Valletta JS, Topp KS, LaVail JH, Bunnett NW, Mobley WC: Endocytosis of activated TrkA: evidence that nerve growth factor induces formation of signaling endosomes. *J Neurosci* 1996, 16(24):7950-7964.
200. Wang Y, Pennock SD, Chen X, Kazlauskas A, Wang Z: Platelet-derived growth factor receptor-mediated signal transduction from endosomes. *J Biol Chem* 2004, 279(9):8038-8046.
201. Vieira AV, Lamaze C, Schmid SL: Control of EGF receptor signaling by clathrin-mediated endocytosis. *Science* 1996, 274(5295):2086-2089.
202. Pennock S, Wang Z: Stimulation of cell proliferation by endosomal epidermal growth factor receptor as revealed through two distinct phases of signaling. *Mol Cell Biol* 2003, 23(16):5803-5815.
203. Cosker KE, Segal RA: Neuronal signaling through endocytosis. *Cold Spring Harb Perspect Biol* 2014, 6(2).
204. Kermorgant S, Parker PJ: Receptor trafficking controls weak signal delivery: a strategy used by c-Met for STAT3 nuclear accumulation. *J Cell Biol* 2008, 182(5):855-863.
205. Miaczynska M, Christoforidis S, Giner A, Shevchenko A, Uttenweiler-Joseph S, Habermann B, Wilm M, Parton RG, Zerial M: APPL proteins link Rab5 to nuclear signal transduction via an endosomal compartment. *Cell* 2004, 116(3):445-456.
206. Lin DC, Quevedo C, Brewer NE, Bell A, Testa JR, Grimes ML, Miller FD, Kaplan DR: APPL1 associates with TrkA and GIPC1 and is required for nerve growth factor-mediated signal transduction. *Mol Cell Biol* 2006, 26(23):8928-8941.
207. Zoncu R, Perera RM, Balkin DM, Pirruccello M, Toomre D, De Camilli P: A phosphoinositide switch controls the maturation and signaling properties of APPL endosomes. *Cell* 2009, 136(6):1110-1121.
208. Sigismund S, Woelk T, Puri C, Maspero E, Tacchetti C, Transidico P, Di Fiore PP, Polo S: Clathrin-independent endocytosis of ubiquitinated cargos. *Proc Natl Acad Sci U S A* 2005, 102(8):2760-2765.

209. Sigismund S, Argenzio E, Tosoni D, Cavallaro E, Polo S, Di Fiore PP: Clathrin-mediated internalization is essential for sustained EGFR signaling but dispensable for degradation. *Dev Cell* 2008, 15(2):209-219.
210. De Donatis A, Comito G, Buricchi F, Vinci MC, Parenti A, Caselli A, Camici G, Manao G, Ramponi G, Cirri P: Proliferation versus migration in platelet-derived growth factor signaling: the key role of endocytosis. *J Biol Chem* 2008, 283(29):19948-19956.
211. Saraon P, Pathmanathan S, Snider J, Lyakisheva A, Wong V, Stagljar I: Receptor tyrosine kinases and cancer: oncogenic mechanisms and therapeutic approaches. *Oncogene* 2021, 40(24):4079-4093.
212. Mellman I, Yarden Y: Endocytosis and cancer. *Cold Spring Harb Perspect Biol* 2013, 5(12):a016949.
213. Schmid SL: Reciprocal regulation of signaling and endocytosis: Implications for the evolving cancer cell. *J Cell Biol* 2017, 216(9):2623-2632.
214. Han W, Zhang T, Yu H, Foulke JG, Tang CK: Hypophosphorylation of residue Y1045 leads to defective downregulation of EGFRvIII. *Cancer Biol Ther* 2006, 5(10):1361-1368.
215. Porther N, Barbieri MA: The role of endocytic Rab GTPases in regulation of growth factor signaling and the migration and invasion of tumor cells. *Small GTPases* 2015, 6(3):135-144.
216. Muller PA, Caswell PT, Doyle B, Iwanicki MP, Tan EH, Karim S, Lukashchuk N, Gillespie DA, Ludwig RL, Gosselin P *et al*: Mutant p53 drives invasion by promoting integrin recycling. *Cell* 2009, 139(7):1327-1341.
217. Muller PA, Trinidad AG, Timpson P, Morton JP, Zanivan S, van den Berghe PV, Nixon C, Karim SA, Caswell PT, Noll JE *et al*: Mutant p53 enhances MET trafficking and signalling to drive cell scattering and invasion. *Oncogene* 2013, 32(10):1252-1265.
218. Palacios F, Tushir JS, Fujita Y, D'Souza-Schorey C: Lysosomal targeting of E-cadherin: a unique mechanism for the down-regulation of cell-cell adhesion during epithelial to mesenchymal transitions. *Mol Cell Biol* 2005, 25(1):389-402.
219. Doench JG, Fusi N, Sullender M, Hegde M, Vaimberg EW, Donovan KF, Smith I, Tothova Z, Wilen C, Orchard R *et al*: Optimized sgRNA design to maximize activity and minimize off-target effects of CRISPR-Cas9. *Nat Biotechnol* 2016, 34(2):184-191.
220. Roux KJ, Kim DI, Burke B: BioID: a screen for protein-protein interactions. *Curr Protoc Protein Sci* 2013, 74:19 23 11-19 23 14.
221. Walther TC, Mann M: Mass spectrometry-based proteomics in cell biology. *J Cell Biol* 2010, 190(4):491-500.
222. Perez-Riverol Y, Csordas A, Bai J, Bernal-Llinares M, Hewapathirana S, Kundu DJ, Inuganti A, Griss J, Mayer G, Eisenacher M *et al*: The PRIDE database and related tools and resources in 2019: improving support for quantification data. *Nucleic Acids Res* 2019, 47(D1):D442-D450.
223. Yu G, Wang LG, Han Y, He QY: clusterProfiler: an R package for comparing biological themes among gene clusters. *OMICS* 2012, 16(5):284-287.
224. Rink J, Ghigo E, Kalaidzidis Y, Zerial M: Rab conversion as a mechanism of progression from early to late endosomes. *Cell* 2005, 122(5):735-749.
225. Collinet C, Stoter M, Bradshaw CR, Samusik N, Rink JC, Kenski D, Habermann B, Buchholz F, Henschel R, Mueller MS *et al*: Systems survey of endocytosis by multiparametric image analysis. *Nature* 2010, 464(7286):243-249.
226. Sneeggen M, Pedersen NM, Campsteijn C, Haugsten EM, Stenmark H, Schink KO: WDFY2 restrains matrix metalloproteinase secretion and cell invasion by controlling VAMP3-dependent recycling. *Nat Commun* 2019, 10(1):2850.
227. Roux KJ, Kim DI, Raida M, Burke B: A promiscuous biotin ligase fusion protein identifies proximal and interacting proteins in mammalian cells. *J Cell Biol* 2012, 196(6):801-810.
228. Lambert JP, Tucholska M, Go C, Knight JD, Gingras AC: Proximity biotinylation and affinity purification are complementary approaches for the interactome mapping of chromatin-associated protein complexes. *J Proteomics* 2015, 118:81-94.
229. Cendrowski J, Kaczmarek M, Mazur M, Kuzmicz-Kowalska K, Jastrzebski K, Brewinska-Olchowik M, Kominek A, Piwocka K, Miaczynska M: Splicing variation of BMP2K balances abundance of COPII assemblies and autophagic degradation in erythroid cells. *Elife* 2020, 9.

230. Grassart A, Cheng AT, Hong SH, Zhang F, Zenzer N, Feng Y, Briner DM, Davis GD, Malkov D, Drubin DG: Actin and dynamin2 dynamics and interplay during clathrin-mediated endocytosis. *J Cell Biol* 2014, 205(5):721-735.
231. Pryor PR, Jackson L, Gray SR, Edeling MA, Thompson A, Sanderson CM, Evans PR, Owen DJ, Luzio JP: Molecular basis for the sorting of the SNARE VAMP7 into endocytic clathrin-coated vesicles by the ArfGAP Hrb. *Cell* 2008, 134(5):817-827.
232. Chaineau M, Danglot L, Proux-Gillardeaux V, Galli T: Role of HRB in clathrin-dependent endocytosis. *J Biol Chem* 2008, 283(49):34365-34373.
233. Tong J, Sydorskyy Y, St-Germain JR, Taylor P, Tsao MS, Moran MF: Odin (ANKS1A) modulates EGF receptor recycling and stability. *PLoS One* 2013, 8(6):e64817.
234. Lee H, Noh H, Mun J, Gu C, Sever S, Park S: Anks1a regulates COPII-mediated anterograde transport of receptor tyrosine kinases critical for tumorigenesis. *Nat Commun* 2016, 7:12799.
235. White IJ, Bailey LM, Aghakhani MR, Moss SE, Futter CE: EGF stimulates annexin 1-dependent inward vesiculation in a multivesicular endosome subpopulation. *EMBO J* 2006, 25(1):1-12.
236. Morel E, Gruenberg J: Annexin A2 binding to endosomes and functions in endosomal transport are regulated by tyrosine 23 phosphorylation. *J Biol Chem* 2009, 284(3):1604-1611.
237. de Graauw M, Cao L, Winkel L, van Miltenburg MH, le Devedec SE, Klop M, Yan K, Pont C, Rogkoti VM, Tijsma A *et al*: Annexin A2 depletion delays EGFR endocytic trafficking via cofilin activation and enhances EGFR signaling and metastasis formation. *Oncogene* 2014, 33(20):2610-2619.
238. Chapuy B, Tikkanen R, Muhlhausen C, Wenzel D, von Figura K, Honing S: AP-1 and AP-3 mediate sorting of melanosomal and lysosomal membrane proteins into distinct post-Golgi trafficking pathways. *Traffic* 2008, 9(7):1157-1172.
239. Nishimura N, Plutner H, Hahn K, Balch WE: The delta subunit of AP-3 is required for efficient transport of VSV-G from the trans-Golgi network to the cell surface. *Proc Natl Acad Sci U S A* 2002, 99(10):6755-6760.
240. Gong L, Bates S, Li J, Qiao D, Glass K, Wei W, Hsu VW, Zhou X, Silverman EK: Connecting COPD GWAS Genes: FAM13A Controls TGFbeta2 Secretion by Modulating AP-3 Transport. *Am J Respir Cell Mol Biol* 2021, 65(5):532-543.
241. Hehnly H, Longhini KM, Chen JL, Stamnes M: Retrograde Shiga toxin trafficking is regulated by ARHGAP21 and Cdc42. *Mol Biol Cell* 2009, 20(20):4303-4312.
242. Barral DC, Garg S, Casalou C, Watts GF, Sandoval JL, Ramalho JS, Hsu VW, Brenner MB: Arl13b regulates endocytic recycling traffic. *Proc Natl Acad Sci U S A* 2012, 109(52):21354-21359.
243. Inoue H, Ha VL, Prekeris R, Randazzo PA: Arf GTPase-activating protein ASAP1 interacts with Rab11 effector FIP3 and regulates pericentrosomal localization of transferrin receptor-positive recycling endosome. *Mol Biol Cell* 2008, 19(10):4224-4237.
244. Jiang N, Yang Y, Zhao G, Yuan Q, Liu Z, Wang X, Geng Z, Jia M, Zheng J, Lu X *et al*: Knockout of ASAP1 induces autophagy in papillary thyroid carcinoma by inhibiting the mTOR signaling pathway. *Pathol Res Pract* 2020, 216(6):152950.
245. Chaudhary N, Gomez GA, Howes MT, Lo HP, McMahon KA, Rae JA, Schieber NL, Hill MM, Gaus K, Yap AS *et al*: Endocytic crosstalk: cavins, caveolins, and caveolae regulate clathrin-independent endocytosis. *PLoS Biol* 2014, 12(4):e1001832.
246. Soubeyran P, Kowanetz K, Szymkiewicz I, Langdon WY, Dikic I: Cbl-CIN85-endophilin complex mediates ligand-induced downregulation of EGF receptors. *Nature* 2002, 416(6877):183-187.
247. Jacob M, Todd L, Sampson MF, Pure E: Dual role of Cbl links critical events in BCR endocytosis. *Int Immunol* 2008, 20(4):485-497.
248. Wee P, Wang Z: Regulation of EGFR Endocytosis by CBL During Mitosis. *Cells* 2018, 7(12).
249. Weng L, Enomoto A, Miyoshi H, Takahashi K, Asai N, Morone N, Jiang P, An J, Kato T, Kuroda K *et al*: Regulation of cargo-selective endocytosis by dynamin 2 GTPase-activating protein girdin. *EMBO J* 2014, 33(18):2098-2112.
250. Gauthier NC, Monzo P, Gonzalez T, Doye A, Oldani A, Gounon P, Ricci V, Cormont M, Boquet P: Early endosomes associated with dynamic F-actin structures are required for late trafficking of H. pylori VacA toxin. *J Cell Biol* 2007, 177(2):343-354.

251. Lynch DK, Winata SC, Lyons RJ, Hughes WE, Lehrbach GM, Wasinger V, Corthals G, Cordwell S, Daly RJ: A Cortactin-CD2-associated protein (CD2AP) complex provides a novel link between epidermal growth factor receptor endocytosis and the actin cytoskeleton. *J Biol Chem* 2003, 278(24):21805-21813.
252. Cormont M, Meton I, Mari M, Monzo P, Keslair F, Gaskin C, McGraw TE, Le Marchand-Brustel Y: CD2AP/CMS regulates endosome morphology and traffic to the degradative pathway through its interaction with Rab4 and c-Cbl. *Traffic* 2003, 4(2):97-112.
253. Saint-Pol A, Yelamos B, Amessou M, Mills IG, Dugast M, Tenza D, Schu P, Antony C, McMahon HT, Lamaze C *et al*: Clathrin adaptor epsinR is required for retrograde sorting on early endosomal membranes. *Dev Cell* 2004, 6(4):525-538.
254. Mills IG, Praefcke GJ, Vallis Y, Peter BJ, Olesen LE, Gallop JL, Butler PJ, Evans PR, McMahon HT: EpsinR: an AP1/clathrin interacting protein involved in vesicle trafficking. *J Cell Biol* 2003, 160(2):213-222.
255. Hirst J, Edgar JR, Borner GH, Li S, Sahlender DA, Antrobus R, Robinson MS: Contributions of epsinR and gadkin to clathrin-mediated intracellular trafficking. *Mol Biol Cell* 2015, 26(17):3085-3103.
256. Aridor M, Bannykh SI, Rowe T, Balch WE: Sequential coupling between COPII and COPI vesicle coats in endoplasmic reticulum to Golgi transport. *J Cell Biol* 1995, 131(4):875-893.
257. Bonifacino JS, Lippincott-Schwartz J: Coat proteins: shaping membrane transport. *Nat Rev Mol Cell Biol* 2003, 4(5):409-414.
258. Futatsumori M, Kasai K, Takatsu H, Shin HW, Nakayama K: Identification and characterization of novel isoforms of COP I subunits. *J Biochem* 2000, 128(5):793-801.
259. Takatsu H, Futatsumori M, Yoshino K, Yoshida Y, Shin HW, Nakayama K: Similar subunit interactions contribute to assembly of clathrin adaptor complexes and COPI complex: analysis using yeast three-hybrid system. *Biochem Biophys Res Commun* 2001, 284(4):1083-1089.
260. Bulgakova NA, Brown NH: Drosophila p120-catenin is crucial for endocytosis of the dynamic E-cadherin-Bazooka complex. *J Cell Sci* 2016, 129(3):477-482.
261. Cao H, Orth JD, Chen J, Weller SG, Heuser JE, McNiven MA: Cortactin is a component of clathrin-coated pits and participates in receptor-mediated endocytosis. *Mol Cell Biol* 2003, 23(6):2162-2170.
262. Sauvonnet N, Dujeancourt A, Dautry-Varsat A: Cortactin and dynamin are required for the clathrin-independent endocytosis of gammac cytokine receptor. *J Cell Biol* 2005, 168(1):155-163.
263. Connert S, Wienand S, Thiel C, Krikunova M, Glyvuk N, Tsytsyura Y, Hilfiker-Kleiner D, Bartsch JW, Klingauf J, Wienands J: SH3P7/mAbp1 deficiency leads to tissue and behavioral abnormalities and impaired vesicle transport. *EMBO J* 2006, 25(8):1611-1622.
264. Kessels MM, Engqvist-Goldstein AE, Drubin DG, Qualmann B: Mammalian Abp1, a signal-responsive F-actin-binding protein, links the actin cytoskeleton to endocytosis via the GTPase dynamin. *J Cell Biol* 2001, 153(2):351-366.
265. Walch L: Emerging role of the scaffolding protein Dlg1 in vesicle trafficking. *Traffic* 2013, 14(9):964-973.
266. Yu A, Rual JF, Tamai K, Harada Y, Vidal M, He X, Kirchhausen T: Association of Dishevelled with the clathrin AP-2 adaptor is required for Frizzled endocytosis and planar cell polarity signaling. *Dev Cell* 2007, 12(1):129-141.
267. Dupuis N, Fafouri A, Bayot A, Kumar M, Lecharpentier T, Ball G, Edwards D, Bernard V, Dournaud P, Drunat S *et al*: Dymeclin deficiency causes postnatal microcephaly, hypomyelination and reticulum-to-Golgi trafficking defects in mice and humans. *Hum Mol Genet* 2015, 24(10):2771-2783.
268. Moreno-Layseca P, Jantti NZ, Godbole R, Sommer C, Jacquemet G, Al-Akhrass H, Conway JRW, Kronqvist P, Kallionpaa RE, Oliveira-Ferrer L *et al*: Cargo-specific recruitment in clathrin- and dynamin-independent endocytosis. *Nat Cell Biol* 2021, 23(10):1073-1084.
269. Wang P, Liu H, Wang Y, Liu O, Zhang J, Gleason A, Yang Z, Wang H, Shi A, Grant BD: RAB-10 Promotes EHBP-1 Bridging of Filamentous Actin and Tubular Recycling Endosomes. *PLoS Genet* 2016, 12(6):e1006093.
270. Shi A, Chen CC, Banerjee R, Glodowski D, Audhya A, Rongo C, Grant BD: EHBP-1 functions with RAB-10 during endocytic recycling in Caenorhabditis elegans. *Mol Biol Cell* 2010, 21(16):2930-2943.

271. Guilherme A, Soriano NA, Bose S, Holik J, Bose A, Pomerleau DP, Furcinitti P, Leszyk J, Corvera S, Czech MP: EHD2 and the novel EH domain binding protein EHBP1 couple endocytosis to the actin cytoskeleton. *J Biol Chem* 2004, 279(11):10593-10605.
272. Nakajo A, Yoshimura S, Togawa H, Kunii M, Iwano T, Izumi A, Noguchi Y, Watanabe A, Goto A, Sato T *et al*: EHBP1L1 coordinates Rab8 and Bin1 to regulate apical-directed transport in polarized epithelial cells. *J Cell Biol* 2016, 212(3):297-306.
273. Deroyer C, Renert AF, Merville MP, Fillet M: New role for EMD (emerin), a key inner nuclear membrane protein, as an enhancer of autophagosome formation in the C16-ceramide autophagy pathway. *Autophagy* 2014, 10(7):1229-1240.
274. Chi S, Cao H, Chen J, McNiven MA: Eps15 mediates vesicle trafficking from the trans-Golgi network via an interaction with the clathrin adaptor AP-1. *Mol Biol Cell* 2008, 19(8):3564-3575.
275. Chi S, Cao H, Wang Y, McNiven MA: Recycling of the epidermal growth factor receptor is mediated by a novel form of the clathrin adaptor protein Eps15. *J Biol Chem* 2011, 286(40):35196-35208.
276. Carbone R, Fre S, Iannolo G, Belleudi F, Mancini P, Pelicci PG, Torrisi MR, Di Fiore PP: eps15 and eps15R are essential components of the endocytic pathway. *Cancer Res* 1997, 57(24):5498-5504.
277. Liu H, Wang S, Hang W, Gao J, Zhang W, Cheng Z, Yang C, He J, Zhou J, Chen J *et al*: LET-413/Erbin acts as a RAB-5 effector to promote RAB-10 activation during endocytic recycling. *J Cell Biol* 2018, 217(1):299-314.
278. Progida C, Bakke O: Bidirectional traffic between the Golgi and the endosomes - machineries and regulation. *J Cell Sci* 2016, 129(21):3971-3982.
279. Monier S, Jollivet F, Janoueix-Lerosey I, Johannes L, Goud B: Characterization of novel Rab6-interacting proteins involved in endosome-to-TGN transport. *Traffic* 2002, 3(4):289-297.
280. Ohara-Imaizumi M, Ohtsuka T, Matsushima S, Akimoto Y, Nishiwaki C, Nakamichi Y, Kikuta T, Nagai S, Kawakami H, Watanabe T *et al*: ELKS, a protein structurally related to the active zone-associated protein CAST, is expressed in pancreatic beta cells and functions in insulin exocytosis: interaction of ELKS with exocytotic machinery analyzed by total internal reflection fluorescence microscopy. *Mol Biol Cell* 2005, 16(7):3289-3300.
281. Fourriere L, Kasri A, Gareil N, Bardin S, Bousquet H, Pereira D, Perez F, Goud B, Boncompain G, Miserey-Lenkei S: RAB6 and microtubules restrict protein secretion to focal adhesions. *J Cell Biol* 2019, 218(7):2215-2231.
282. Jean S, Mikryukov A, Tremblay MG, Baril J, Guillou F, Bellenfant S, Moss T: Extended-synaptotagmin-2 mediates FGF receptor endocytosis and ERK activation in vivo. *Dev Cell* 2010, 19(3):426-439.
283. Nozima BH, Mendes TB, Pereira G, Araldi RP, Iwamura ESM, Smaili SS, Carvalheira GMG, Cerutti JM: FAM129A regulates autophagy in thyroid carcinomas in an oncogene-dependent manner. *Endocr Relat Cancer* 2019, 26(1):227-238.
284. Solis GP, Hulsbusch N, Radon Y, Katanaev VL, Plattner H, Stuermer CA: Reggies/flotillins interact with Rab11a and SNX4 at the tubulovesicular recycling compartment and function in transferrin receptor and E-cadherin trafficking. *Mol Biol Cell* 2013, 24(17):2689-2702.
285. Parachoniak CA, Luo Y, Abella JV, Keen JH, Park M: GGA3 functions as a switch to promote Met receptor recycling, essential for sustained ERK and cell migration. *Dev Cell* 2011, 20(6):751-763.
286. Li X, Lavigne P, Lavoie C: GGA3 mediates TrkA endocytic recycling to promote sustained Akt phosphorylation and cell survival. *Mol Biol Cell* 2015, 26(24):4412-4426.
287. Tisdale EJ, Talati NK, Artalejo CR, Shisheva A: GAPDH binds Akt to facilitate cargo transport in the early secretory pathway. *Exp Cell Res* 2016, 349(2):310-319.
288. Yang JS, Hsu JW, Park SY, Li J, Oldham WM, Beznoussenko GV, Mironov AA, Loscalzo J, Hsu VW: GAPDH inhibits intracellular pathways during starvation for cellular energy homeostasis. *Nature* 2018, 561(7722):263-267.
289. Koreishi M, Gniadek TJ, Yu S, Masuda J, Honjo Y, Satoh A: The golgin tether giantin regulates the secretory pathway by controlling stack organization within Golgi apparatus. *PLoS One* 2013, 8(3):e59821.

290. Metzler M, Legendre-Guillemin V, Gan L, Chopra V, Kwok A, McPherson PS, Hayden MR: HIP1 functions in clathrin-mediated endocytosis through binding to clathrin and adaptor protein 2. *J Biol Chem* 2001, 276(42):39271-39276.
291. Legendre-Guillemin V, Metzler M, Charbonneau M, Gan L, Chopra V, Philie J, Hayden MR, McPherson PS: HIP1 and HIP12 display differential binding to F-actin, AP2, and clathrin. Identification of a novel interaction with clathrin light chain. *J Biol Chem* 2002, 277(22):19897-19904.
292. Nimmervoll B, Chtcheglova LA, Juhasz K, Cremades N, Aprile FA, Sonnleitner A, Hinterdorfer P, Vigh L, Preiner J, Balogi Z: Cell surface localised Hsp70 is a cancer specific regulator of clathrin-independent endocytosis. *FEBS Lett* 2015, 589(19 Pt B):2747-2753.
293. Nakatsu F, Messa M, Nandez R, Czapla H, Zou Y, Strittmatter SM, De Camilli P: Sac2/INPP5F is an inositol 4-phosphatase that functions in the endocytic pathway. *J Cell Biol* 2015, 209(1):85-95.
294. Zhuang G, Hunter S, Hwang Y, Chen J: Regulation of EphA2 receptor endocytosis by SHIP2 lipid phosphatase via phosphatidylinositol 3-Kinase-dependent Rac1 activation. *J Biol Chem* 2007, 282(4):2683-2694.
295. Ni YX, Zhou N, Xue WQ, Rong L, Yung WH, Lin RZ, Kao RY, Duan ZG, Sun HT, Gong HR *et al*: A new role of anterograde motor Kif5b in facilitating large clathrin-coated vesicle mediated endocytosis via regulating clathrin uncoating. *Cell Discov* 2018, 4:65.
296. Silver KE, Harrison RE: Kinesin 5B is necessary for delivery of membrane and receptors during FcgammaR-mediated phagocytosis. *J Immunol* 2011, 186(2):816-825.
297. Martinez Jaramillo C, Trujillo-Vargas CM: LRBA in the endomembrane system. *Colomb Med (Cali)* 2018, 49(3):236-243.
298. Yang H, Wang X, Sumners C, Raizada MK: Obligatory role of protein kinase Cbeta and MARCKS in vesicular trafficking in living neurons. *Hypertension* 2002, 39(2 Pt 2):567-572.
299. Su R, Han ZY, Fan JP, Zhang YL: A possible role of myristoylated alanine-rich C kinase substrate in endocytic pathway of Alzheimer's disease. *Neurosci Bull* 2010, 26(4):338-344.
300. Sharma M, Giridharan SS, Rahajeng J, Naslavsky N, Caplan S: MICAL-L1 links EHD1 to tubular recycling endosomes and regulates receptor recycling. *Mol Biol Cell* 2009, 20(24):5181-5194.
301. Rahajeng J, Giridharan SS, Cai B, Naslavsky N, Caplan S: MICAL-L1 is a tubular endosomal membrane hub that connects Rab35 and Arf6 with Rab8a. *Traffic* 2012, 13(1):82-93.
302. Abou-Zeid N, Pandjaitan R, Sengmanivong L, David V, Le Pavec G, Salamero J, Zahraoui A: MICAL-like1 mediates epidermal growth factor receptor endocytosis. *Mol Biol Cell* 2011, 22(18):3431-3441.
303. Barroso-Gonzalez J, Machado JD, Garcia-Exposito L, Valenzuela-Fernandez A: Moesin regulates the trafficking of nascent clathrin-coated vesicles. *J Biol Chem* 2009, 284(4):2419-2434.
304. Nomachi A, Yoshinaga M, Liu J, Kanchanawong P, Tohyama K, Thumkeo D, Watanabe T, Narumiya S, Hirata T: Moesin controls clathrin-mediated S1PR1 internalization in T cells. *PLoS One* 2013, 8(12):e82590.
305. Muriel O, Tomas A, Scott CC, Gruenberg J: Moesin and cortactin control actin-dependent multivesicular endosome biogenesis. *Mol Biol Cell* 2016, 27(21):3305-3316.
306. Maekawa M, Terasaka S, Mochizuki Y, Kawai K, Ikeda Y, Araki N, Skolnik EY, Taguchi T, Arai H: Sequential breakdown of 3-phosphorylated phosphoinositides is essential for the completion of macropinocytosis. *Proc Natl Acad Sci U S A* 2014, 111(11):E978-987.
307. Vergne I, Roberts E, Elmaoued RA, Tosch V, Delgado MA, Proikas-Cezanne T, Laporte J, Deretic V: Control of autophagy initiation by phosphoinositide 3-phosphatase Jumpy. *EMBO J* 2009, 28(15):2244-2258.
308. Miserey-Lenkei S, Chalancon G, Bardin S, Formstecher E, Goud B, Echard A: Rab and actomyosin-dependent fission of transport vesicles at the Golgi complex. *Nat Cell Biol* 2010, 12(7):645-654.
309. Almeida CG, Yamada A, Tenza D, Louvard D, Raposo G, Coudrier E: Myosin 1b promotes the formation of post-Golgi carriers by regulating actin assembly and membrane remodelling at the trans-Golgi network. *Nat Cell Biol* 2011, 13(7):779-789.

310. Buss F, Arden SD, Lindsay M, Luzio JP, Kendrick-Jones J: Myosin VI isoform localized to clathrin-coated vesicles with a role in clathrin-mediated endocytosis. *EMBO J* 2001, 20(14):3676-3684.
311. Osterweil E, Wells DG, Mooseker MS: A role for myosin VI in postsynaptic structure and glutamate receptor endocytosis. *J Cell Biol* 2005, 168(2):329-338.
312. Pietiainen V, Vassilev B, Blom T, Wang W, Nelson J, Bittman R, Back N, Zelcer N, Ikonen E: NDRG1 functions in LDL receptor trafficking by regulating endosomal recycling and degradation. *J Cell Sci* 2013, 126(Pt 17):3961-3971.
313. Bloomfield G, Traynor D, Sander SP, Veltman DM, Pachebat JA, Kay RR: Neurofibromin controls macropinocytosis and phagocytosis in Dictyostelium. *Elife* 2015, 4.
314. Ghoshal P, Singla B, Lin H, Cherian-Shaw M, Tritz R, Padgett CA, Hudson F, Zhang H, Stansfield BK, Csanyi G: Loss of GTPase activating protein neurofibromin stimulates paracrine cell communication via macropinocytosis. *Redox Biol* 2019, 27:101224.
315. Chiasson-MacKenzie C, Morris ZS, Liu CH, Bradford WB, Koorman T, McClatchey AI: Merlin/ERM proteins regulate growth factor-induced macropinocytosis and receptor recycling by organizing the plasma membrane:cytoskeleton interface. *Genes Dev* 2018, 32(17-18):1201-1214.
316. Hennigan RF, Moon CA, Parysek LM, Monk KR, Morfini G, Berth S, Brady S, Ratner N: The NF2 tumor suppressor regulates microtubule-based vesicle trafficking via a novel Rac, MLK and p38(SAPK) pathway. *Oncogene* 2013, 32(9):1135-1143.
317. Maitra S, Kulikauskas RM, Gavilan H, Fehon RG: The tumor suppressors Merlin and Expanded function cooperatively to modulate receptor endocytosis and signaling. *Curr Biol* 2006, 16(7):702-709.
318. Tokumitsu H, Hatano N, Yokokura S, Sueyoshi Y, Nozaki N, Kobayashi R: Phosphorylation of Numb regulates its interaction with the clathrin-associated adaptor AP-2. *FEBS Lett* 2006, 580(24):5797-5801.
319. Bogdanovic O, Delfino-Machin M, Nicolas-Perez M, Gavilan MP, Gago-Rodrigues I, Fernandez-Minan A, Lillo C, Rios RM, Wittbrodt J, Martinez-Morales JR: Numb/Numbl-Opo antagonism controls retinal epithelium morphogenesis by regulating integrin endocytosis. *Dev Cell* 2012, 23(4):782-795.
320. Gulino A, Di Marcotullio L, Screpanti I: The multiple functions of Numb. *Exp Cell Res* 2010, 316(6):900-906.
321. Zhou T, Lu Y, Xu C, Wang R, Zhang L, Lu P: Occludin protects secretory cells from ER stress by facilitating SNARE-dependent apical protein exocytosis. *Proc Natl Acad Sci U S A* 2020, 117(9):4758-4769.
322. Fredriksson K, Van Itallie CM, Aponte A, Gucek M, Tietgens AJ, Anderson JM: Proteomic analysis of proteins surrounding occludin and claudin-4 reveals their proximity to signaling and trafficking networks. *PLoS One* 2015, 10(3):e0117074.
323. Tebar F, Bohlander SK, Sorkin A: Clathrin assembly lymphoid myeloid leukemia (CALM) protein: localization in endocytic-coated pits, interactions with clathrin, and the impact of overexpression on clathrin-mediated traffic. *Mol Biol Cell* 1999, 10(8):2687-2702.
324. Carroll KS, Hanna J, Simon I, Krise J, Barbero P, Pfeffer SR: Role of Rab9 GTPase in facilitating receptor recruitment by TIP47. *Science* 2001, 292(5520):1373-1376.
325. Orsel JG, Sincock PM, Krise JP, Pfeffer SR: Recognition of the 300-kDa mannose 6-phosphate receptor cytoplasmic domain by 47-kDa tail-interacting protein. *Proc Natl Acad Sci U S A* 2000, 97(16):9047-9051.
326. Choi E, Kikuchi S, Gao H, Brodzik K, Nassour I, Yopp A, Singal AG, Zhu H, Yu H: Mitotic regulators and the SHP2-MAPK pathway promote IR endocytosis and feedback regulation of insulin signaling. *Nat Commun* 2019, 10(1):1473.
327. Hampton KK, Craven RJ: Pathways driving the endocytosis of mutant and wild-type EGFR in cancer. *Oncoscience* 2014, 1(8):504-512.
328. Lindsay AJ, Hendrick AG, Cantalupo G, Senic-Matuglia F, Goud B, Bucci C, McCaffrey MW: Rab coupling protein (RCP), a novel Rab4 and Rab11 effector protein. *J Biol Chem* 2002, 277(14):12190-12199.
329. Jing J, Junutula JR, Wu C, Burden J, Matern H, Peden AA, Prekeris R: FIP1/RCP binding to Golgin-97 regulates retrograde transport from recycling endosomes to the trans-Golgi network. *Mol Biol Cell* 2010, 21(17):3041-3053.

330. Carson BP, Del Bas JM, Moreno-Navarrete JM, Fernandez-Real JM, Mora S: The rab11 effector protein FIP1 regulates adiponectin trafficking and secretion. *PLoS One* 2013, 8(9):e74687.
331. Cullis DN, Philip B, Baleja JD, Feig LA: Rab11-FIP2, an adaptor protein connecting cellular components involved in internalization and recycling of epidermal growth factor receptors. *J Biol Chem* 2002, 277(51):49158-49166.
332. Lindsay AJ, McCaffrey MW: Rab11-FIP2 functions in transferrin recycling and associates with endosomal membranes via its COOH-terminal domain. *J Biol Chem* 2002, 277(30):27193-27199.
333. Schonteich E, Wilson GM, Burden J, Hopkins CR, Anderson K, Goldenring JR, Prekeris R: The Rip11/Rab11-FIP5 and kinesin II complex regulates endocytic protein recycling. *J Cell Sci* 2008, 121(Pt 22):3824-3833.
334. Prekeris R, Klumperman J, Scheller RH: A Rab11/Rip11 protein complex regulates apical membrane trafficking via recycling endosomes. *Mol Cell* 2000, 6(6):1437-1448.
335. Sugawara K, Shibasaki T, Mizoguchi A, Saito T, Seino S: Rab11 and its effector Rip11 participate in regulation of insulin granule exocytosis. *Genes Cells* 2009, 14(4):445-456.
336. Vehlow A, Soong D, Vizcay-Barrena G, Bodo C, Law AL, Perera U, Krause M: Endophilin, Lamellipodin, and Mena cooperate to regulate F-actin-dependent EGF-receptor endocytosis. *EMBO J* 2013, 32(20):2722-2734.
337. de Vreede G, Schoenfeld JD, Windler SL, Morrison H, Lu H, Bilder D: The Scribble module regulates retromer-dependent endocytic trafficking during epithelial polarization. *Development* 2014, 141(14):2796-2802.
338. Piguel NH, Fievre S, Blanc JM, Carta M, Moreau MM, Moutin E, Pinheiro VL, Medina C, Ezan J, Lasvaux L *et al*: Scribble1/AP2 complex coordinates NMDA receptor endocytic recycling. *Cell Rep* 2014, 9(2):712-727.
339. Duwel M, Ungewickell EJ: Clathrin-dependent association of CVAK104 with endosomes and the trans-Golgi network. *Mol Biol Cell* 2006, 17(10):4513-4525.
340. Wendeler MW, Paccaud JP, Hauri HP: Role of Sec24 isoforms in selective export of membrane proteins from the endoplasmic reticulum. *EMBO Rep* 2007, 8(3):258-264.
341. Mancias JD, Goldberg J: Structural basis of cargo membrane protein discrimination by the human COPII coat machinery. *EMBO J* 2008, 27(21):2918-2928.
342. Traikov S, Stange C, Wassmer T, Paul-Gilloteaux P, Salamero J, Raposo G, Hoflack B: Septin6 and Septin7 GTP binding proteins regulate AP-3- and ESCRT-dependent multivesicular body biogenesis. *PLoS One* 2014, 9(11):e109372.
343. Song K, Russo G, Krauss M: Septins As Modulators of Endo-Lysosomal Membrane Traffic. *Front Cell Dev Biol* 2016, 4:124.
344. Diesenberg K, Beerbaum M, Fink U, Schmieder P, Krauss M: SEPT9 negatively regulates ubiquitin-dependent downregulation of EGFR. *J Cell Sci* 2015, 128(2):397-407.
345. Molfetta R, Belleudi F, Peruzzi G, Morrone S, Leone L, Dikic I, Piccoli M, Frati L, Torrisi MR, Santoni A *et al*: CIN85 regulates the ligand-dependent endocytosis of the IgE receptor: a new molecular mechanism to dampen mast cell function. *J Immunol* 2005, 175(7):4208-4216.
346. Petrelli A, Gilestro GF, Lanzardo S, Comoglio PM, Migone N, Giordano S: The endophilin-CIN85-Cbl complex mediates ligand-dependent downregulation of c-Met. *Nature* 2002, 416(6877):187-190.
347. Lin DH, Yue P, Pan CY, Sun P, Zhang X, Han Z, Roos M, Caplan M, Giebisch G, Wang WH: POSH stimulates the ubiquitination and the clathrin-independent endocytosis of ROMK1 channels. *J Biol Chem* 2009, 284(43):29614-29624.
348. Alroy I, Tuvia S, Greener T, Gordon D, Barr HM, Taglicht D, Mandil-Levin R, Ben-Avraham D, Konforty D, Nir A *et al*: The trans-Golgi network-associated human ubiquitin-protein ligase POSH is essential for HIV type 1 production. *Proc Natl Acad Sci U S A* 2005, 102(5):1478-1483.
349. Song M, Giza J, Proenca CC, Jing D, Elliott M, Dincheva I, Shmelkov SV, Kim J, Schreiner R, Huang SH *et al*: Slitrk5 Mediates BDNF-Dependent TrkB Receptor Trafficking and Signaling. *Dev Cell* 2015, 33(6):690-702.
350. Raynaud F, Homburger V, Seveno M, Vigy O, Moutin E, Fagni L, Perroy J: SNAP23-Kif5 complex controls mGlu1 receptor trafficking. *J Mol Cell Biol* 2018, 10(5):423-436.

351. Williams KC, McNeilly RE, Coppolino MG: SNAP23, Syntaxin4, and vesicle-associated membrane protein 7 (VAMP7) mediate trafficking of membrane type 1-matrix metalloproteinase (MT1-MMP) during invadopodium formation and tumor cell invasion. *Mol Biol Cell* 2014, 25(13):2061-2070.
352. Suh YH, Terashima A, Petralia RS, Wenthold RJ, Isaac JT, Roche KW, Roche PA: A neuronal role for SNAP-23 in postsynaptic glutamate receptor trafficking. *Nat Neurosci* 2010, 13(3):338-343.
353. Rotem-Yehudar R, Galperin E, Horowitz M: Association of insulin-like growth factor 1 receptor with EHD1 and SNAP29. *J Biol Chem* 2001, 276(35):33054-33060.
354. Morelli E, Ginefra P, Mastrodonato V, Beznoussenko GV, Rusten TE, Bilder D, Stenmark H, Mironov AA, Vaccari T: Multiple functions of the SNARE protein Snap29 in autophagy, endocytic, and exocytic trafficking during epithelial formation in Drosophila. *Autophagy* 2014, 10(12):2251-2268.
355. Rapaport D, Lugassy Y, Sprecher E, Horowitz M: Loss of SNAP29 impairs endocytic recycling and cell motility. *PLoS One* 2010, 5(3):e9759.
356. Carlton J, Bujny M, Peter BJ, Oorschot VM, Rutherford A, Mellor H, Klumperman J, McMahon HT, Cullen PJ: Sorting nexin-1 mediates tubular endosome-to-TGN transport through coincidence sensing of high- curvature membranes and 3-phosphoinositides. *Curr Biol* 2004, 14(20):1791-1800.
357. Rojas R, Kametaka S, Haft CR, Bonifacino JS: Interchangeable but essential functions of SNX1 and SNX2 in the association of retromer with endosomes and the trafficking of mannose 6-phosphate receptors. *Mol Cell Biol* 2007, 27(3):1112-1124.
358. Zhong Q, Lazar CS, Tronchere H, Sato T, Meerloo T, Yeo M, Songyang Z, Emr SD, Gill GN: Endosomal localization and function of sorting nexin 1. *Proc Natl Acad Sci U S A* 2002, 99(10):6767-6772.
359. Ogi S, Fujita H, Kashihara M, Yamamoto C, Sonoda K, Okamoto I, Nakagawa K, Ohdo S, Tanaka Y, Kuwano M *et al*: Sorting nexin 2-mediated membrane trafficking of c-Met contributes to sensitivity of molecular-targeted drugs. *Cancer Sci* 2013, 104(5):573-583.
360. Wassmer T, Attar N, Bujny MV, Oakley J, Traer CJ, Cullen PJ: A loss-of-function screen reveals SNX5 and SNX6 as potential components of the mammalian retromer. *J Cell Sci* 2007, 120(Pt 1):45-54.
361. Simonetti B, Paul B, Chaudhari K, Weeratunga S, Steinberg F, Gorla M, Heesom KJ, Bashaw GJ, Collins BM, Cullen PJ: Molecular identification of a BAR domain-containing coat complex for endosomal recycling of transmembrane proteins. *Nat Cell Biol* 2019, 21(10):1219-1233.
362. Hong Z, Yang Y, Zhang C, Niu Y, Li K, Zhao X, Liu JJ: The retromer component SNX6 interacts with dynactin p150(Glued) and mediates endosome-to-TGN transport. *Cell Res* 2009, 19(12):1334-1349.
363. Malecz N, McCabe PC, Spaargaren C, Qiu R, Chuang Y, Symons M: Synaptojanin 2, a novel Rac1 effector that regulates clathrin-mediated endocytosis. *Curr Biol* 2000, 10(21):1383-1386.
364. Tao T, Sun J, Peng Y, Li Y, Wang P, Chen X, Zhao W, Zheng YY, Wei L, Wang W *et al*: Golgi-resident TRIO regulates membrane trafficking during neurite outgrowth. *J Biol Chem* 2019, 294(28):10954-10968.
365. Roboti P, Sato K, Lowe M: The golgin GMAP-210 is required for efficient membrane trafficking in the early secretory pathway. *J Cell Sci* 2015, 128(8):1595-1606.
366. Kanai Y, Wang D, Hirokawa N: KIF13B enhances the endocytosis of LRP1 by recruiting LRP1 to caveolae. *J Cell Biol* 2014, 204(3):395-408.
367. Riggs KA, Hasan N, Humphrey D, Raleigh C, Nevitt C, Corbin D, Hu C: Regulation of integrin endocytic recycling and chemotactic cell migration by syntaxin 6 and VAMP3 interaction. *J Cell Sci* 2012, 125(Pt 16):3827-3839.
368. Hu C, Hardee D, Minnear F: Membrane fusion by VAMP3 and plasma membrane t-SNAREs. *Exp Cell Res* 2007, 313(15):3198-3209.
369. Kuijpers M, Yu KL, Teuling E, Akhmanova A, Jaarsma D, Hoogenraad CC: The ALS8 protein VAPB interacts with the ER-Golgi recycling protein YIF1A and regulates membrane delivery into dendrites. *EMBO J* 2013, 32(14):2056-2072.

370. Dong R, Saheki Y, Swarup S, Lucast L, Harper JW, De Camilli P: Endosome-ER Contacts Control Actin Nucleation and Retromer Function through VAP-Dependent Regulation of PI4P. *Cell* 2016, 166(2):408-423.
371. Sun P, Yamamoto H, Suetsugu S, Miki H, Takenawa T, Endo T: Small GTPase Rah/Rab34 is associated with membrane ruffles and macropinosomes and promotes macropinosome formation. *J Biol Chem* 2003, 278(6):4063-4071.
372. Basquin C, Trichet M, Vihinen H, Malarde V, Lagache T, Ripoll L, Jokitalo E, Olivo-Marin JC, Gautreau A, Sauvonnet N: Membrane protrusion powers clathrin-independent endocytosis of interleukin-2 receptor. *EMBO J* 2015, 34(16):2147-2161.
373. Tai G, Lu L, Wang TL, Tang BL, Goud B, Johannes L, Hong W: Participation of the syntaxin 5/Ykt6/GS28/GS15 SNARE complex in transport from the early/recycling endosome to the trans-Golgi network. *Mol Biol Cell* 2004, 15(9):4011-4022.
374. Gross JC, Chaudhary V, Bartscherer K, Boutros M: Active Wnt proteins are secreted on exosomes. *Nat Cell Biol* 2012, 14(10):1036-1045.
375. Gordon DE, Chia J, Jayawardena K, Antrobus R, Bard F, Peden AA: VAMP3/Syb and YKT6 are required for the fusion of constitutive secretory carriers with the plasma membrane. *PLoS Genet* 2017, 13(4):e1006698.
376. Breusegem SY, Seaman MNJ: Genome-wide RNAi screen reveals a role for multipass membrane proteins in endosome-to-golgi retrieval. *Cell Rep* 2014, 9(5):1931-1945.
377. Seet LF, Hong W: Endofin recruits clathrin to early endosomes via TOM1. *J Cell Sci* 2005, 118(Pt 3):575-587.
378. Nagata K, Ohashi K, Nakano T, Arita H, Zong C, Hanafusa H, Mizuno K: Identification of the product of growth arrest-specific gene 6 as a common ligand for Axl, Sky, and Mer receptor tyrosine kinases. *J Biol Chem* 1996, 271(47):30022-30027.
379. Mark MR, Chen J, Hammonds RG, Sadick M, Godowsk PJ: Characterization of Gas6, a member of the superfamily of G domain-containing proteins, as a ligand for Rse and Axl. *J Biol Chem* 1996, 271(16):9785-9789.
380. Chen J, Carey K, Godowski PJ: Identification of Gas6 as a ligand for Mer, a neural cell adhesion molecule related receptor tyrosine kinase implicated in cellular transformation. *Oncogene* 1997, 14(17):2033-2039.
381. Lew ED, Oh J, Burrola PG, Lax I, Zagorska A, Traves PG, Schlessinger J, Lemke G: Differential TAM receptor-ligand-phospholipid interactions delimit differential TAM bioactivities. *Elife* 2014, 3.
382. Lamaze C, Schmid SL: Recruitment of epidermal growth factor receptors into coated pits requires their activated tyrosine kinase. *J Cell Biol* 1995, 129(1):47-54.
383. Wang Q, Villeneuve G, Wang Z: Control of epidermal growth factor receptor endocytosis by receptor dimerization, rather than receptor kinase activation. *EMBO Rep* 2005, 6(10):942-948.
384. Rogers MA, Fantauzzo KA: The emerging complexity of PDGFRs: activation, internalization and signal attenuation. *Biochem Soc Trans* 2020, 48(3):1167-1176.
385. Caldieri G, Malabarba MG, Di Fiore PP, Sigismund S: EGFR Trafficking in Physiology and Cancer. *Prog Mol Subcell Biol* 2018, 57:235-272.
386. Traub LM: Sorting it out: AP-2 and alternate clathrin adaptors in endocytic cargo selection. *J Cell Biol* 2003, 163(2):203-208.
387. Maldonado-Baez L, Wendland B: Endocytic adaptors: recruiters, coordinators and regulators. *Trends Cell Biol* 2006, 16(10):505-513.
388. Royle SJ, Bright NA, Lagnado L: Clathrin is required for the function of the mitotic spindle. *Nature* 2005, 434(7037):1152-1157.
389. Schnatwinkel C, Christoforidis S, Lindsay MR, Uttenweiler-Joseph S, Wilm M, Parton RG, Zerial M: The Rab5 effector Rabankyrin-5 regulates and coordinates different endocytic mechanisms. *PLoS Biol* 2004, 2(9):E261.
390. Mayor S, Parton RG, Donaldson JG: Clathrin-independent pathways of endocytosis. *Cold Spring Harb Perspect Biol* 2014, 6(6).
391. Maldonado-Baez L, Williamson C, Donaldson JG: Clathrin-independent endocytosis: a cargo-centric view. *Exp Cell Res* 2013, 319(18):2759-2769.
392. Cullen PJ, Steinberg F: To degrade or not to degrade: mechanisms and significance of endocytic recycling. *Nat Rev Mol Cell Biol* 2018, 19(11):679-696.

393. Levkowitz G, Waterman H, Zamir E, Kam Z, Oved S, Langdon WY, Beguinot L, Geiger B, Yarden Y: c-Cbl/Sli-1 regulates endocytic sorting and ubiquitination of the epidermal growth factor receptor. *Genes Dev* 1998, 12(23):3663-3674.
394. Zdzalik-Bielecka D, Kozik K, Poswiata A, Jastrzebski K, Jakubik M, Miaczynska M: Bemcentinib and Gilteritinib Inhibit Cell Growth and Impair the Endo-Lysosomal and Autophagy Systems in an AXL-Independent Manner. *Mol Cancer Res* 2021.
395. Sears RM, May DG, Roux KJ: BioID as a Tool for Protein-Proximity Labeling in Living Cells. *Methods Mol Biol* 2019, 2012:299-313.
396. Bareja A, Hodgkinson CP, Soderblom E, Waitt G, Dzau VJ: The proximity-labeling technique BioID identifies sorting nexin 6 as a member of the insulin-like growth factor 1 (IGF1)-IGF1 receptor pathway. *J Biol Chem* 2018, 293(17):6449-6459.
397. Perez White BE, Ventrella R, Kaplan N, Cable CJ, Thomas PM, Getsios S: EphA2 proteomics in human keratinocytes reveals a novel association with afadin and epidermal tight junctions. *J Cell Sci* 2017, 130(1):111-118.
398. Haugsten EM, Sorensen V, Kunova Bosakova M, de Souza GA, Krejci P, Wiedlocha A, Wesche J: Proximity Labeling Reveals Molecular Determinants of FGFR4 Endosomal Transport. *J Proteome Res* 2016, 15(10):3841-3855.
399. Schlessinger J: Cell signaling by receptor tyrosine kinases. *Cell* 2000, 103(2):211-225.
400. Luo LY, Hahn WC: Oncogenic Signaling Adaptor Proteins. *J Genet Genomics* 2015, 42(10):521-529.
401. Wu X, Wang L, Pearson NA, Renuse S, Cheng R, Liang Y, Mun DG, Madugundu AK, Xu Y, Gill PS *et al*: Quantitative Tyrosine Phosphoproteome Profiling of AXL Receptor Tyrosine Kinase Signaling Network. *Cancers (Basel)* 2021, 13(16).
402. Huang F, Khvorova A, Marshall W, Sorkin A: Analysis of clathrin-mediated endocytosis of epidermal growth factor receptor by RNA interference. *J Biol Chem* 2004, 279(16):16657-16661.
403. Sousa LP, Lax I, Shen H, Ferguson SM, De Camilli P, Schlessinger J: Suppression of EGFR endocytosis by dynamin depletion reveals that EGFR signaling occurs primarily at the plasma membrane. *Proc Natl Acad Sci U S A* 2012, 109(12):4419-4424.
404. Maritzen T, Schachtner H, Legler DF: On the move: endocytic trafficking in cell migration. *Cell Mol Life Sci* 2015, 72(11):2119-2134.
405. Gu Z, Noss EH, Hsu VW, Brenner MB: Integrins traffic rapidly via circular dorsal ruffles and macropinocytosis during stimulated cell migration. *J Cell Biol* 2011, 193(1):61-70.
406. Zajac O, Leclere R, Nicolas A, Meseure D, Marchio C, Vincent-Salomon A, Roman-Roman S, Schoumacher M, Dubois T: AXL Controls Directed Migration of Mesenchymal Triple-Negative Breast Cancer Cells. *Cells* 2020, 9(1).
407. Orian-Rousseau V, Sleeman J: CD44 is a multidomain signaling platform that integrates extracellular matrix cues with growth factor and cytokine signals. *Adv Cancer Res* 2014, 123:231-254.
408. Nevins AK, Thurmond DC: Caveolin-1 functions as a novel Cdc42 guanine nucleotide dissociation inhibitor in pancreatic beta-cells. *J Biol Chem* 2006, 281(28):18961-18972.
409. Lakoduk AM, Roudot P, Mettlen M, Grossman HM, Schmid SL, Chen PH: Mutant p53 amplifies a dynamin-1/APPL1 endosome feedback loop that regulates recycling and migration. *J Cell Biol* 2019, 218(6):1928-1942.
410. Meyer AS, Miller MA, Gertler FB, Lauffenburger DA: The receptor AXL diversifies EGFR signaling and limits the response to EGFR-targeted inhibitors in triple-negative breast cancer cells. *Sci Signal* 2013, 6(287):ra66.
411. Kamentseva R, Kosheverova V, Kharchenko M, Zlobina M, Salova A, Belyaeva T, Nikolsky N, Kornilova E: Functional cycle of EEA1-positive early endosome: Direct evidence for pre-existing compartment of degradative pathway. *PLoS One* 2020, 15(5):e0232532.
412. Wang W, Zhang H, Liu S, Kim CK, Xu Y, Hurley LA, Nishikawa R, Nagane M, Hu B, Stegh AH *et al*: Internalized CD44s splice isoform attenuates EGFR degradation by targeting Rab7A. *Proc Natl Acad Sci U S A* 2017, 114(31):8366-8371.
413. Crupi MJF, Maritan SM, Reyes-Alvarez E, Lian EY, Hyndman BD, Rekab AN, Moodley S, Antonescu CN, Mulligan LM: GGA3-mediated recycling of the RET receptor tyrosine kinase contributes to cell migration and invasion. *Oncogene* 2020, 39(6):1361-1377.

414. Ebner M, Lucic I, Leonard TA, Yudushkin I: PI(3,4,5)P3 Engagement Restricts Akt Activity to Cellular Membranes. *Mol Cell* 2017, 65(3):416-431 e416.
415. Siess KM, Leonard TA: Lipid-dependent Akt-ivity: where, when, and how. *Biochem Soc Trans* 2019, 47(3):897-908.
416. Revach OY, Sandler O, Samuels Y, Geiger B: Cross-Talk between Receptor Tyrosine Kinases AXL and ERBB3 Regulates Invadopodia Formation in Melanoma Cells. *Cancer Res* 2019, 79(10):2634-2648.
417. Wilson BJ, Allen JL, Caswell PT: Vesicle trafficking pathways that direct cell migration in 3D matrices and in vivo. *Traffic* 2018, 19(12):899-909.
418. Paul NR, Jacquemet G, Caswell PT: Endocytic Trafficking of Integrins in Cell Migration. *Curr Biol* 2015, 25(22):R1092-1105.
419. Smith MP, Ferguson HR, Ferguson J, Zindy E, Kowalczyk KM, Kedward T, Bates C, Parsons J, Watson J, Chandler S *et al*: Reciprocal priming between receptor tyrosine kinases at recycling endosomes orchestrates cellular signalling outputs. *EMBO J* 2021, 40(14):e107182.
420. Gallon M, Cullen PJ: Retromer and sorting nexins in endosomal sorting. *Biochem Soc Trans* 2015, 43(1):33-47.
421. Glenney JR, Jr., Chen WS, Lazar CS, Walton GM, Zokas LM, Rosenfeld MG, Gill GN: Ligand-induced endocytosis of the EGF receptor is blocked by mutational inactivation and by microinjection of anti-phosphotyrosine antibodies. *Cell* 1988, 52(5):675-684.
422. Wilde A, Beattie EC, Lem L, Riethof DA, Liu SH, Mobley WC, Soriano P, Brodsky FM: EGF receptor signaling stimulates SRC kinase phosphorylation of clathrin, influencing clathrin redistribution and EGF uptake. *Cell* 1999, 96(5):677-687.
423. Sorkina T, Huang F, Beguinot L, Sorkin A: Effect of tyrosine kinase inhibitors on clathrin-coated pit recruitment and internalization of epidermal growth factor receptor. *J Biol Chem* 2002, 277(30):27433-27441.
424. Schmidt MHH, Furnari FB, Cavenee WK, Bogler O: Epidermal growth factor receptor signaling intensity determines intracellular protein interactions, ubiquitination, and internalization. *Proc Natl Acad Sci U S A* 2003, 100(11):6505-6510.
425. Heukers R, Vermeulen JF, Fereidouni F, Bader AN, Voortman J, Roovers RC, Gerritsen HC, van Bergen En Henegouwen PM: Endocytosis of EGFR requires its kinase activity and N-terminal transmembrane dimerization motif. *J Cell Sci* 2013, 126(Pt 21):4900-4912.
426. Pinilla-Macua I, Grassart A, Duvvuri U, Watkins SC, Sorkin A: EGF receptor signaling, phosphorylation, ubiquitylation and endocytosis in tumors in vivo. *Elife* 2017, 6:e31993.
427. Felder S, Miller K, Moehren G, Ullrich A, Schlessinger J, Hopkins CR: Kinase activity controls the sorting of the epidermal growth factor receptor within the multivesicular body. *Cell* 1990, 61(4):623-634.
428. Grove J, Marsh M: The cell biology of receptor-mediated virus entry. *J Cell Biol* 2011, 195(7):1071-1082.
429. Hunt CL, Kolokoltsov AA, Davey RA, Maury W: The Tyro3 receptor kinase Axl enhances macropinocytosis of Zaire ebolavirus. *J Virol* 2011, 85(1):334-347.
430. Persaud M, Martinez-Lopez A, Buffone C, Porcelli SA, Diaz-Griffero F: Infection by Zika viruses requires the transmembrane protein AXL, endocytosis and low pH. *Virology* 2018, 518:301-312.
431. Ramirez C, Hauser AD, Vucic EA, Bar-Sagi D: Plasma membrane V-ATPase controls oncogenic RAS-induced macropinocytosis. *Nature* 2019, 576(7787):477-481.

9. Publications by Agata Poświata

1. Zdzalik-Bielecka D, **Poswiata A**, Kozik K, Jastrzebski K, Schink KO, Brewinska-Olchowik M, Piwocka K, Stenmark H, Miaczynska M: The GAS6-AXL signaling pathway triggers actin remodeling that drives membrane ruffling, macropinocytosis, and cancer-cell invasion. *Proceedings of the National Academy of Sciences of the United States of America (PNAS)* 2021, 118(28), doi:10.1073/pnas.2024596118.
2. Zdzalik-Bielecka D, Kozik K, **Poswiata A**, Jastrzebski K, Jakubik M, Miaczynska M: Bemcentinib and Gilteritinib Inhibit Cell Growth and Impair the Endo-Lysosomal and Autophagy Systems in an AXL-Independent Manner. *Molecular Cancer Research* 2022, 20(3): 446-455, doi: 10.1158/1541-7786.MCR-21-0444
3. **Poswiata A**, Kozik K, Miaczynska M, Zdzalik-Bielecka D: Endocytic trafficking of GAS6-AXL complexes is associated with sustained AKT activation *Cellular and Molecular Life Sciences* (under revision)

10. Supplementary materials

Supplementary Table S1 and S2 are available on the included CD, or online as supplementary information for the publication by Zdzalik-Bielecka *et al.* [89].